THE UNIVERSITY OF MANITOBA

NUMERICAL ANALYSIS OF FULLY DEVELOPED LAMINAR FLOW IN TUBES WITH LONGITUDINALLY TWISTED FULL FINS

by

KALIKA RANJAN SAMANT

A THESIS

SUBMITTED TO THE FACULTY OF GRADUATE STUDIES IN PARTIAL FULFILLMENT OF THE REQUIREMENTS FOR THE DEGREE OF

MASTER OF SCIENCE

Department of Mechanical Engineering

Winnipeg, Manitoba

June, 1981

NUMERICAL ANALYSIS OF FULLY DEVELOPED LAMINAR FLOW IN TUBES WITH LONGITUDINALLY TWISTED FULL FINS

BY

KALIKA RANJAN SAMANT

A thesis submitted to the Faculty of Graduate Studies of the University of Manitoba in partial fulfillment of the requirements of the degree of

MASTER OF SCIENCE

ABSTRACT

A numerical study of fully-developed, laminar, incompressible viscous flow in tubes with internal spiral fins was conducted. An existing vorticity based numerical procedure was used to solve the governing continuity and momentum equations for the limiting case where the fins extend to the center of the tube. The effects of twist ratio and Reynolds number on predicted momentum transfer characteristics of the flow were investigated for 4, 8, and 12 number of fins with a fixed half fin angle of $\pi/60$ radians. The friction factor values and the distributions of axial velocity, resultant secondary velocity, and local wall shear stress showed strong dependence on twist ratio and Reynolds number as separate parameters. Since the flow in the axial direction was guided by the fins, the circumferential velocity was in the direction of fin twisting everywhere in the flow field. The flow, therefore, did not represent recirculation. The magnitudes of the secondary velocities increased with twist ratio and Reynolds number. The axial velocity distribution became increasingly flatter and asymmetric about the central plane as the twist ratio or, Reynolds number, was increased. The distributions of local wall shear stress on the fin surfaces (and in some cases (notably high twist ratio and Reynolds number) also on the tube wall) showed asymmetric behaviour. At a Reynolds number of 1000, friction factor increased over values for tubes with straight fins by about 14% to 130% depending on the value of twist ratio and the number of fins whereas at a Reynolds number of 10, the enhancement in friction factor was within 81% of the values for straight finned tubes. For fixed fin number and twist ratio, the

effect of Reynolds number on friction factor ratio was significant only for Re > ~ 100. Empirical correlations for predicting friction factor values were developed.

TABLE OF CONTENTS

	Page
ABSTRACT	i
TABLE OF CONTENTS	iii
LIST OF TABLES	v
LIST OF FIGURES	vi
NOMENCLATURE	x
1.0 INTRODUCTION	1
1.1 Motivation	1
1.2 Scope of the Present Work	2
2.0 LITERATURE REVIEW	3
2.1 Experimental	3
2.2 Analytical	6
3.0 MATHEMATICAL FORMULATION	12
3.1 The Geometry	12
3.2 The Coordinate System	13
3.3 The Governing Equations	15
3.4 Generalized Representation of the Governing Equations	22
3.5 Boundary Conditions	24
4.0 METHOD OF SOLUTION	25
4.1 Finite Difference Solution	25
4.2 Vorticity Boundary Condition	26
4.3 The Computational Procedure	27

		Page
5.0	PRELIMINARY STUDIES	35
	5.1 Straight Finned Tubes	35
	5.2 Tubes with Twisted Tape Inserts	35
6.0	RESULTS AND DISCUSSION	38
	6.1 Axial Velocity Profiles	38
	6.2 Secondary Velocity Profiles	41
	6.3 Distribution of Local Wall Shear Stress.	42
	6.4 Friction Factor	44
	6.5 Empirical Correlations for Friction Factor	45
7.0	CONCLUDING REMARKS	47
8.0	RECOMMENDATIONS FOR FUTURE EXTENSION WORK	49
9.0	ACKNOWLEDGEMENTS	50
10.0	REFERENCES	51
APPENDIX A:	Formulation of Local Wall Shear Stress and Mean Pressure Gradient	53
APPENDIX B:	Derivation of Finite Difference Equation . . .	58
APPENDIX C:	Finite Difference Representation of Derivatives	65
APPENDIX D:	Derivation of Boundary Condition for Vorticity .	69
APPENDIX E:	Flow Chart and Listing of the Computer Programme	72
APPENDIX F:	Implicit Formulation of Vorticity Boundary Condition	99
TABLES		103
FIGURES		136

LIST OF TABLES

Table		Page
1	Effect of Grid Size on Predicted Values of Friction Factor for Straight and Spiral Finned Tubes	103
2	Effect of Twist Ratio and Reynolds Number on the Rate of Convergence for M = 4	104
3	Effect of Twist Ratio and Reynolds Number on the Rate of Convergence for M = 8	105
4	Effect of Twist Ratio and Reynolds Number on the Rate of Convergence for M = 12	106
5	Friction Factor Values for Tubes with Straight Fins	107
6	Characteristics of the Flow for M = 4	108
7	Characteristics of the Flow for M = 8	110
8	Characteristics of the Flow for M = 12	112
9	Predicted Values of the Ratio f/f_o for M = 4	114
10	Predicted Values of the Ratio f/f_o for M = 8	115
11	Predicted Values of the Ratio f/f_0 for M = 12	116
12	Local Values of Axial Velocity and Resultant Secondary Velocity for Selected Values of M, α, and Re	117

LIST OF FIGURES

Figure		Page
1	Internally Finned Tube Geometry and Coordinate System	136
2	Illustration of the Twisted Fin Inside a Tube	137
3	Twisted Control Volume and its Projection on the r' - θ' Plane	138
4	Domain of Interest	139
5	Illustration of the Finite-Difference Grid; the Dotted Lines Enclose the Control Volume	140
6	Comparison of Velocity Distribution at the Axis of Symmetry for M = 4 and α = 0	141
7	Comparison of Velocity Distribution at the Axis of Symmetry for M = 8 and α = 0	142
8	Comparison of Velocity Distribution at the Axis of Symmetry for M = 12 and α = 0	143
9	Comparison of Friction Factor Values for M = 2, β = 0, and α = 0.1	144
10	Comparison of Friction Factor Values for M = 2, β = 0, and α = 0.3	145
11	Comparison of Friction Factor Values for M = 2, β = 0, and α = 0.5	146
12	Comparison of Resultant Secondary Velocity Distribution at the Central Plane for M = 2, β = 0, α = 0.5, and Re = 515	147
13	Comparison of Axial Velocity Profiles for M = 2, β = 0, α = 0.5, and Re = 700	148
14	Predicted Axial Velocity Profiles for M = 4, α = 0.1, and Re = 1000	149
15	Predicted Axial Velocity Profiles for M = 4, α = 0.3, and Re = 1000	150
16	Predicted Axial Velocity Profiles for M = 4, α = 0.5, and Re = 1000	151

Figure		Page
17	Predicted Axial Velocity Profiles for M = 4, α = 0.4, and Re = 100	152
18	Predicted Axial Velocity Profiles for M = 4, α = 0.4, and Re = 500	153
19	Predicted Axial Velocity Profiles for M = 4, α = 0.4, and Re = 1000	154
20	Effect of Twist Ratio (α = 0, 0.1) on Predicted Axial Velocity Profiles at M = 8 and Re = 1000	155
21	Effect of Twist Ratio (α = 0.3, 0.5) on Predicted Axial Velocity Profiles at M = 8 and Re = 1000	156
22	Effect of Reynolds Number (Re = 10,100) on Predicted Axial Velocity Profiles at M = 8 and α = 0.4	157
23	Effect of Reynolds Number (Re = 400,1000) on Predicted Axial Velocity Profiles at M = 8 and α = 0.4	158
24	Effect of Twist Ratio on Predicted Axial Velocity Profiles at M = 12 and Re = 1000	159
25	Effect of Reynolds Number on Predicted Axial Velocity Profiles at M = 12 and α = 0.4	160
26	Predicted Resultant Secondary Velocity Distribution for M = 4, α = 0.5 and Re = 1000	161
27	Predicted Resultant Secondary Velocity Distribution for M = 8, α = 0.5 and Re = 1000	162
28	Distribution of Wall Shear Stress for M = 4, α = 0.1, and Re = 1000	163
29	Distribution of Wall Shear Stress for M = 4, α = 0.3, and Re = 1000	164
30	Distribution of Wall Shear Stress for M = 4, α = 0.5, and Re = 1000	165
31	Distribution of Wall Shear Stress for M = 4, α = 0.4, and Re = 100	166
32	Distribution of Wall Shear Stress for M = 4, α = 0.4, and Re = 500	167
33	Distribution of Wall Shear Stress for M = 4, α = 0.4, and Re = 1000	168

Figure		Page
34	Distribution of Wall Shear Stress for M_o = 8, α = 0.1, and Re = 1000	169
35	Distribution of Wall Shear Stress for M = 8, α = 0.3, and Re = 1000	170
36	Distribution of Wall Shear Stress for M = 8, α = 0.5, and Re = 1000	171
37	Distribution of Wall Shear Stress for M = 8, α = 0.1, and Re = 50	172
38	Distribution of Wall Shear Stress for M = 8, α = 0.5, and Re = 50	173
39	Distribution of Wall Shear Stress for M = 8, α = 0.5, and Re = 500	174
40	Distribution of Wall Shear Stress for M = 12, α = 0.1, and Re = 1000	175
41	Distribution of Wall Shear Stress for M = 12, α = 0.3, and Re = 1000	176
42	Distribution of Wall Shear Stress for M = 12, α = 0.5, and Re = 1000	177
43	Distribution of Wall Shear Stress for M = 12, α = 0.4, and Re = 100	178
44	Distribution of Wall Shear Stress for M = 12, α = 0.4, and Re = 500	179
45	Distribution of Wall Shear Stress for M = 12, α = 0.4, and Re = 1000	180
46	Effect of Twist Ratio on Friction Factor for M = 4	181
47	Effect of Twist Ratio on Friction Factor for M = 8	182
48	Effect of Twist Ratio on Friction Factor for M = 12	183

Figure		Page
49	Effect of Reynolds Number on Friction Factor for M = 4	184
50	Effect of Reynolds Number on Friction Factor for M = 8	185
51	Effect of Reynolds Number on Friction Factor for M = 12	186

NOMENCLATURE

a, b_1, b_2,	coefficients in the general partial
c, d	differential equation
a_1, a_2, a_3	coefficients in the empirical relations for f/f_o
A_c	total surface area for dz' length of the finned tube
A_E, A_W, A_N, A_S	convection terms
A_{f_a}	actual flow cross-sectional area
A_o	total surface area per unit length of the tube with straight fins
A_α	total surface area per unit length of the tube with spiral fins
B_E, B_W, B_N, B_S	diffusion terms
C_1, C_2, C_3	coefficients in the vorticity boundary condition
cc	convergence criterion
C_E, C_W, C_N, C_S	coefficients in the successive-substitution formula
$d\ell$	actual length of the fin in dz' length of the tube
$d\dot{m}_{r'}$, $d\dot{m}_{\theta'}$	radial and circumferential mass flow rates through an elemental control volume
dr', dθ', dz'	elemental distances in r', θ' and z' directions, respectively
f	friction factor for a tube with spiral fins, $\frac{\pi 2\rho r_o^{\,5}}{\dot{m}^2}\left(-\frac{d\bar{p}}{dz'}\right)$
f_o	friction factor for a tube with straight fins
F(Vz)	function of axial velocity
H	dimensionless fin height

he, hw, hn, hs, h, h'	distances in the finite-difference representation of derivatives
I, J	indices for the finite-difference grid corresponding to the r' and θ' directions, respectively
K	fin conductance parameter, $\beta k_s/k_f$
k_f	thermal conductivity of fin
k_s	thermal conductivity of fluid
$\dot{m}$	mass flow rate
M	number of fins
n	distance between the wall grid node and the adjacent node
Nu	Nusselt number
$P(r', \theta', z')$	pressure at a point (r', θ', z') in the flow
$\bar{P}(z')$	mean pressure at a cross-section
$P_o(r', \theta')$	variable pressure
r_o	inside radius of the tube
r_i	radius at the tip of the fin
r, θ, z	cylindrical polar coordinates
r', θ', z'	coordinates of a rotating coordinate system
Re	Reynolds number based on actual mass flow rate, $2\dot{m}/\pi r_o \mu$
S	pitch for 180° rotation of the root of the fin
V_P	integral in the source term
V_r, V_θ, V_z	velocity components in r, θ, and z directions respectively
V_s	Resultant secondary velocity

Greek Letters

α	twist ratio, $\pi r_o/s$
β	half fin angle
$\Delta 1$, $\Delta 2$, Δ	distance in the finite-difference representation of derivatives
γ	angle made by the root of the fin with the tube axis
μ	dynamic viscosity
ω	vorticity
ϕ	angular rotation of the root of the fin in an axial distance z. Also used to designate a dependent variable
ρ	density
ψ	stream function
τ_{av}	average wall shear stress over the cross-section
τ_{abc}	average wall shear stress over the tube wall
τ_{cd}, τ_{ao}	average wall shear stress on fin surfaces
τ_{rr}, $\tau_{\theta\theta}$, τ_{zz}, $\tau_{r\theta}$, $\tau_{\theta r}$, $\tau_{\theta z}$, $\tau_{z\theta}$, τ_{zr}, τ_{rz}	stress tensor
τ_{tz}	local axial shear stress

Subscripts

m or mean	mean value over the cross-section
o	wall grid node
no	near-wall grid node
max	maximum value

Superscripts

N	Nth iteration
ref	reference value
ω	vorticity
Ψ	stream function

1.0 INTRODUCTION

In recent years, the internally finned tube geometry (Figure 1) has received considerable research interest as it offers an efficient and compact means of heat transfer augmentation. Both experimental and analytical techniques have been employed by various investigators to study the momentum and heat transfer for flow through such tubes. Various degrees of heat transfer enhancement have been reported in the literature depending on the flow condition (laminar, turbulent), tube geometry (number of fins, fin height, fin thickness, and twist ratio), fluid properties and thermal boundary conditions (constant heat flux, constant surface temperature). However, these increases in heat transfer have been accompanied by increases in pumping power, hence optimization is required in order to select the best configuration for a specific situation.

1.1 Motivation

The problem considered here is the laminar momentum transfer in tubes with internal spiral fins where the fins extend to the center of the tube. The motivation of a study of this problem arises from the superior performances of spiral finned tubes compared to straight finned tubes as reported by various investigators [1, 2] based on their experimental studies. However, only limited theoretical study concerning flow in such tubes have been reported. These have either involved various simplifying assumptions or have been extremely limited in scope. Date [3] has computed laminar and turbulent flow

characteristics in tubes with twisted tape inserts (i.e. two opposing full fins) whereas Ivanovic's [4] laminar flow results are valid only for small twist ratios ($\alpha \leq 0.3$) and negligible fin thickness. The need for a rigourous analysis of the problem is, therefore, obvious.

1.2 Scope of the Present Work

The objective of the present work is to study numerically the characteristics of the flow in tubes with internal spiral fins without any restriction on the value of the twist ratio. A number of characteristics that are typical of such flow have been revealed and are discussed at a later stage. At the same time, results have been successfully predicted for twist ratio up to 0.5. The present investigation should, therefore, be viewed as an important first step towards solving the problem of finite length fins. Future research must also seek heat transfer solutions for the two fundamental boundary conditions, namely, the constant heat flux and constant wall temperature conditions.

2.0 LITERATURE REVIEW

The affluence of literature available on fluid flow and heat transfer for internally finned tubes can be broadly classified according to the method employed to study the phenomena, viz. experimental and analytical (including numerical analysis). Only the literature dealing with laminar flow condition is reviewed, in the order of mention, unless a particular work involves other flow conditions as well.

2.1 Experimental

Experimental results were reported by Vasil'Chenko and Barbaritskaya [5,6] for laminar and turbulent flow of transformer oil in tubes with straight fins of trapezoidal cross-section under nonisothermal condition (cooling). In the range of parameters considered (M = 0,4, 6,8; H = 0,0.36, 0.41, 0.565, 0.6; $\beta \approx 4.4°$ to 5.5°), they observed significant improvement in friction factor and Nusselt number over the values for finless tubes. The influence on friction factor due to viscosity variations with cooling of transformer oil was found to be considerably greater with laminar flow than with turbulent flow. They also noticed that for short fins, transition to turbulent flow occurred well before the usual critical value of Reynolds number ($\approx$ 2300) was reached.

Watkinson et al [1] presented isothermal friction factor and Nusselt number data for a motor oil in the laminar and transition regions based on their experimental investigation. Eighteen internally

finned tubes were tested to cover a wide range of parameters including twist ratio. At a Reynolds number of 500, heat transfer was enhanced over smooth tube values by 8 to 224% depending on the tube geometry. For example, at M = 8, H = 0.298, and α = 0.470 the enhancement was 224% while a combination of M = 16, H = 0.168, and α = 0.525 yielded an increase of 156%. However, at the same Reynolds number, the associated increase in friction factor was, in general, within 100%. An analysis based on constant pumping power requirement further recommended use of the spiral finned tube (M = 8, H = 0.298, α = 0.470). Correlating equations for heat transfer and friction factor were also presented for both straight and spiral finned tubes. The transition from laminar flow occurred at lower Reynolds number than the critical value for smooth tube and appeared to be a strong function of fin height to equivalent diameter ratio.

Soliman and Feingold [7] performed experiments to compare the performance of a quintuplex spiral finned tube with the performances of a single spiral finned tube and a smooth tube (M = 16, H $\approx$ 0.17, $\alpha \approx$ 0.525 for each finned tube) with almost the same inside diameter. They concluded that the increase in heat transfer was offset by the associated increase in pumping power required for the quintuplex finned tube and consequently recommended use of such tubes where the size of heat exchanger was the major concern. When considered on the basis of the minimum pumping power required to transfer a given amount of heat, the single finned tube proved to be the best choice.

Marner and Bergles [2] studied the effect of different thermal conditions on friction factor and Nusselt number during a series of experiments with twisted tape inserts, static-mixer inserts and finned tubes (straight and spiral) using different working fluids (water, motor oil, ethylene glycol) mainly under laminar flow conditions. Under constant heat flux condition, Nusselt numbers for twisted-tape inserts were independent of tube length but varied with tape twist ratio, Reynolds number, and Prandtl number. A correlating equation for Nusselt number as a function of these parameters was reported. Improvements in Nusselt number for straight finned tube was found to be highly dependent on Prandtl number while water data showed a length effect. Very high heat transfer coefficients were obtained with Koch mixer inserts but these were accompanied by large isothermal pressure drops. They found twisted tape inserts and finned tubes to yield substantial enhancement in heat transfer for a given increase in pressure drop, and selected these geometries for further investigation. Twisted tape inserts yielded greater friction factor as compared to spiral fins and, unlike the latter, showed significant effect of heating or cooling on friction factor results. Mean Nusselt number results and constant pumping power performance analysis further showed distinct superiority of spiral fins to twisted tape inserts under both heating and cooling with constant wall temperature conditions.

2.2 Analytical

The first analytical solution for momentum and heat transfer in internally finned tubes was reported by Hu and Chang [8]. They neglected the thickness of the fins and assumed a constant and uniform heat flux on internal cylindrical surface and on each fin. The governing momentum and energy equations including the effects of viscous dissipation and heat generation but neglecting any variation of fluid properties, were solved by using Green's function. The reported friction factor and Nusselt number results covered a range of $0 \leq M \leq 32$, and $0 \leq H \leq 1.0$. The effect of dissipation function was found to be negligible in all cases. The optimum Nusselt number was found to be 86.82 at $M = 22$ and $H = 0.795$ with no heat generation, and at $M = 16$ and $H = 0.8$ with heat generation. They noticed that for short fins of any number and long fins of very large number, the Nusselt number was below the value for a finless tube. This may be due to the unrealistic assumption of uniform heat flux on the fin surfaces. Equivelocity lines and isotherms were also reported and the presence of so-called primary loops (occurring at the center of the tube) and secondary loops (between the fins) was noticed.

Nandakumar and Masliyah [9, 10] included the effect of finite thickness of the fins by assuming a fin shape of triangular cross-section. The finite element method was used to solve the momentum and energy equations for the case of no axial conduction and no viscous dissipation. They assumed axially uniform heat flux and peripherally uniform temperature on the tube surface and uniform temperature

(equal to the tube wall temperature) along the fin. Friction factor and Nusselt number values values were reported for $4 \leq M \leq 24$, $0.1 \leq H \leq 0.8$, and $0 \leq \beta \leq 3°$. Friction factor results were also included for $0 \leq \beta \leq 6°$ and a correlation for fRe was included. The reported friction factor results are higher than the experimental correlation given by Watkinson et al [1] for $0.57 < De/Di < 0.68$ (De = equivalent hydraulic diameter, Di = tube internal diameter).

A fin profile very close to real fin configurations was considered by Soliman and Feingold [11]. The fin profile was defined by two radial flanks encompassing a variable angle and having a variable height. The tip of the fin was a circular arc concentric with the tube. The solution for velocity distribution and friction factor was presented in terms of an infinite series. Sufficient accuracy was attainable with only about 15 terms included in the series solution. The friction factor results were presented for a wide range of parameters ($0 \leq M \leq 32$; $0.05 \leq H \leq 1.0$; $0 \leq \beta \leq 3°$). Contrary to Hu and Chang [8], who reported that for short fins the secondary loops did not exist, it was found that there was a critical fin height above which secondary loops were found, and for fixed fin thickness, this critical fin height decreased with an increase in the number of fins. The effect of fin thickness was found to be more pronounced for longer fins than it was for shorter fins.

Soliman and Feingold later [12] extended the technique developed in [11] to obtain analytical solution for temperature distribution and

Nusselt number for the constant heat flux condition (constant heat input per unit length, and a peripherally uniform temperature along the inner surface of the tube including the fins). Axial conduction and viscous dissipation were neglected and fluid properties were assumed to be constant. For all combinations of H and β, Nu increased with an increase of M upto a critical value and thereafter decreased to reach the value for a smooth tube when the fins filled the perimeter of the tube completely. The location of the peak value of Nu depended on the fin height. The effect of number of fins and fin height on the dimensionless temperature distribution was also discussed.

Soliman [13] investigated the effect of fin conductance on heat transfer by assuming circumferentially uniform but radially variable temperature distribution within each fin. He concluded that the heat transfer characteristics were influenced by a single parameter K, defined as $(\beta k_s/k_f)$. In general, the effect of finite conductance of fin material was to lower the dimensionless temperature distribution within the fluid and consequently the Nusselt number as compared to the corresponding values for the ideal case of $K = \infty$. These effects were significant only for long fins ($H \geq 0.4$). K had no noticeable effect on the location of the peak value of Nu for short fins, and only a small effect was associated with long fins.

Local and average heat transfer results were reported by Soliman et al [14] for a wide range of parameters ($4 \leq M \leq 32$, $0.2 \leq H \leq 0.8$,

and $\beta = 3°$) for the case of uniform outside wall temperature. The influence of fin conductance was considered while viscous dissipation and fluid property variations were neglected in solving the momentum and energy equations by finite difference method. Reported average Nusselt number data showed considerable enhancement above values for finless tubes, particularly at $M = 16$ and $H = 0.8$. The effect of fin conductance was significant for $M \leq 16$ and $H \geq 0.6$; the distribution of local heat flux at the side of the fin and along the tube wall was found to be strongly dependent on the values of M and H. For short fins ($H \leq 0.2$), the local heat flux was zero at the base and a maximum at the tip of the fin and showed noticeable effect of K only for low values of M. For long fins ($H \geq 0.8$), the peak of local heat flux occurred almost midway along the fin, and again, the K-effect was not noticeable at large values of M. The distribution of local heat flux on the tube wall was also found to be non-uniform except at $M = 24$ and $H = 0.8$. For a given tube (fixed M and H), the dimensionless temperature distribution showed strong dependence on K and formed closed loops for long fins.

Analytical data for momentum and heat transfer in tubes with spiral fins are scarce. Date [3] employed the concept of a rotating coordinate system to eliminate the axial dependence of the flow in a tube with twisted tape insert. He then solved the resulting conservation equations to predict friction factor and Nusselt number values for laminar and turbulent flows neglecting the thickness of

the tape and assuming insignificant viscous dissipation and axial conduction. The reported laminar friction factor and Nusselt number data indicate enhancements over corresponding values for straight semi-circular duct but are lower than the experimental values produced later by Marner and Bergles [2]. For turbulent flow, the predicted friction factor and Nusselt number data were about 30 percent lower than the experimental results available. Date [3] attributed this discrepancy to the inadequacy of the effective-viscosity concept in modelling turbulent stresses in twisted-tape flow.

Ivanovic [4] predicted momentum and heat transfer (constant heat flux condition) characteristics for laminar flow in tubes with internal spiral fins of zero thickness. He assumed that the contribution of the secondary pressure gradient, $\partial P_o/\partial \theta'$, in the axial momentum equation was insignificant and showed that the theoretical dependence of the flow characteristics on α and Re can be replaced by a single dependence on the product αRe at low twist ratios ($\alpha \leq 0.3$). The friction factor normalized by the corresponding value for the tube with straight fin increased nonlinearly with αRe for $\alpha Re \geq 50$, the increase being significant for tubes with a small number of long fins (for example, $M = 4$, $H = 0.8$). For large number of fins ($M \geq 18$), the increase was minor irrespective of the fin height. A qualitatively similar dependence of the Nusselt number (normalized by the corresponding value for $\alpha = 0$ case) on αRe was noticed. For long fins, the

distribution of local heat transfer coefficient on the fin surface indicated a peak located approximately at 0.3 of the fin height. For short fins, the local heat transfer coefficient increased monotonically from zero at the base to a maximum at the tip of the fin.

3.0 MATHEMATICAL FORMULATION

Fully developed laminar flow of a constant property fluid is considered. Body forces are assumed to be negligible. The problem is formulated for the general case of spiral fins of finite thickness and finite length. The conservation equations describing the fluid flow are developed first. Then the boundary conditions are specified for the limiting case where the fins extend to the centerline of the tube.

3.1 The Geometry

The cross-section of the tube geometry under consideration is shown schematically in Figure 1. The fin profile is defined by two radial flanks encompassing an angle of 6° and having a variable height. The tips of the fins are circular arcs concentric with the tube. The fins are equally spaced along the periphery of the tube and are twisted in the longitudinal direction. The root of the fin rotates through 180° in an axial distance S (Figure 2). The twist ratio (α) is defined as:

$$\alpha = \tan\gamma = \frac{\pi r_o}{S} \tag{3.1}$$

where γ is the angle made by the root of the fin with tube axis (see Figure 1).

3.2 The Coordinate System

A fully developed flow is characterized by the axial invariance of the velocity distribution. For example, in the case of fully developed laminar flow in tubes with straight fins, the velocity distribution is identical at every cross-section and the only velocity component is in the axial direction. However, when the fins are twisted, the fluid particles move in a helical path because the main flow in the axial direction is guided by the fins. Consequently, the velocity vector has radial and circumferential components in addition to the axial component and the stream lines are not straight in the axial direction. Therefore, if the customary cylindrical polar coordinate system is used to describe the flow, the axial dependence of variables can not be removed and the problem must be treated as three dimensional. However, if it is recognized that the velocity distribution will be identical at points that are similarly located with respect to the surface of the fin as one moves downstream, the axial dependence can be removed by measuring the circumferential distance always from the surface of the fin (see Figure 1). The flow can now be treated as two dimensional with one obvious difference; i.e. points with identical flow characteristics will appear rotated as one moves axially. The relationship between the new coordinate system (designated by r', θ', z') and the customary coordinate system (r, θ, z) can be derived by referring to Figure 2. A point 'A' located on the fin surface moves an axial distance z and a circumferential distance

ϕr in arriving at the point 'B'*. Thus,

$$\phi = \frac{\pi}{S} z \quad . \tag{3.2}$$

Therefore, the new coordinate system is related to the customary one by the following equations:

$$r' = r \ , \tag{3.3a}$$

$$\theta' = \theta + \frac{\pi}{S} z, \tag{3.3b}$$

and

$$z' = z \ . \tag{3.3c}$$

Equations (3.3) imply that when the fins are twisted in the anti-clockwise direction and z and z' are measured in the direction of axial flow, one has to move through a distance corresponding to $\theta' = \theta + \pi z/S$ in order to follow a particular particle.

As a consequence of equations (3.3), the following relations may be written:

$$\frac{\partial}{\partial r} = \frac{\partial}{\partial r'} \ , \tag{3.4a}$$

$$\frac{\partial}{\partial \theta} = \frac{\partial}{\partial \theta'} \ , \tag{3.4b}$$

and

$$\frac{\partial}{\partial z} = \frac{\partial}{\partial z'} + \frac{\pi}{S} \frac{\partial}{\partial \theta'} \ . \tag{3.4c}$$

*Points A, B and C may be located on the surface of the fin at any radius r although they are shown in Figure 2 to correspond to the locations $r = r_o$.

In the fully developed region the dependence on the new axial coordinate z' will be taken to be zero. Mathematically, this is expressed as:

$$\frac{\partial}{\partial z'} = 0. \tag{3.5}$$

It should be noted that, due to twisting, the actual length of the fin contained in an axial distance dz' is greater than that of a corresponding straight fin. In view of equation (3.2) and the discussion preceding it, the actual length of the fin in an axial distance dz' is:

$$d\ell = [(dz')^2 + (r'\, d\phi)^2]^{\frac{1}{2}}, \text{ hence}$$

$$d\ell = [1 + (\alpha \frac{r'}{r_o})^2]^{\frac{1}{2}}\, dz' \quad . \tag{3.6}$$

3.3 The Governing Equations

The governing equations are the continuity and the momentum equations. For a constant property fluid in steady laminar flow, these equations in the (r, θ, z) coordinate system are (e.g. see [15]):

Continuity Equation

$$\rho \left\{\frac{1}{r} \frac{\partial}{\partial r} (rV_r) + \frac{1}{r} \frac{\partial V_\theta}{\partial \theta} + \frac{\partial V_z}{\partial z}\right\} = 0 \ , \tag{3.7}$$

Axial Momentum Equation

$$\rho \left\{V_z \frac{\partial V_z}{\partial z} + \frac{V_\theta}{r} \frac{\partial V_z}{\partial \theta} + V_r \frac{\partial V_z}{\partial r}\right\}$$

$$= - \frac{\partial P}{\partial z} + \mu \left\{\frac{1}{r} \frac{\partial}{\partial r} \left(r \frac{\partial V_z}{\partial r}\right) + \frac{1}{r^2} \frac{\partial^2 V_z}{\partial \theta^2} + \frac{\partial^2 V_z}{\partial z^2}\right\} \ , \tag{3.8}$$

Circumferential Momentum Equation

$$\rho \left\{V_r \frac{\partial V_\theta}{\partial r} + \frac{V_\theta}{r} \frac{\partial V_\theta}{\partial \theta} + \frac{V_r V_\theta}{r} + V_z \frac{\partial V_\theta}{\partial z}\right\}$$

$$= - \frac{1}{r} \frac{\partial P}{\partial \theta} + \mu \left\{\frac{\partial}{\partial r} \left(\frac{1}{r} \frac{\partial}{\partial r} (rV_\theta)\right) + \frac{1}{r^2} \frac{\partial^2 V_\theta}{\partial \theta^2} + \frac{2}{r^2} \frac{\partial V_r}{\partial \theta} + \frac{\partial^2 V_\theta}{\partial z^2}\right\} \ , \tag{3.9}$$

Radial Momentum Equation

$$\rho \left\{V_r \frac{\partial V_r}{\partial r} + \frac{V_\theta}{r} \frac{\partial V_r}{\partial \theta} - \frac{V_{\theta^2}}{r} + V_z \frac{\partial V_r}{\partial z}\right\}$$

$$= - \frac{\partial P}{\partial r} + \mu \left\{\frac{\partial}{\partial r} \left(\frac{1}{r} \frac{\partial}{\partial r} (rV_r)\right) + \frac{1}{r^2} \frac{\partial^2 V_r}{\partial \theta^2} - \right.$$

$$\left. - \frac{2}{r^2} \frac{\partial V_\theta}{\partial \theta} + \frac{\partial^2 V_r}{\partial z^2}\right\} \ . \tag{3.10}$$

Equations (3.3), (3.4), and (3.5) are now used to transform the governing equations to the new coordinate system (r', θ', z'). It is assumed that the pressure at any point in the flow consists of two parts as follows:

1. A mean pressure, $\bar{P}(z')$, which is constant over the cross-section; the axial force due to the axial gradient of $\bar{P}(z')$ is balanced by that due to the shear stresses on the tube wall and the fin surfaces.

2. A varying component, $P_o(r', \theta')$, which is induced in the flow due to twisting of the fin.

Thus,

$$P(r', \theta', z') = \bar{P}(z') + P_o(r', \theta') \quad . \tag{3.11}$$

Equation (3.5) holds for all dependent variables except for the mean pressure $\bar{P}(z')$; $d\bar{P}/dz'$ is a constant for fully developed flow and can be expressed in terms of wall shear stresses (see Appendix A). The final form of the governing equations in (r', θ', z') coordinate system is:

Continuity Equation

$$\rho \left\{\frac{1}{r'} \frac{\partial}{\partial r'}(r'V_r) + \frac{1}{r'} \frac{\partial}{\partial \theta'} (V_\theta + \alpha \frac{r'}{r_o} V_z)\right\} = 0 \quad , \tag{3.12}$$

Axial Momentum Equation

$$\rho \{V_r \frac{\partial V_z}{\partial r'} + (\frac{V_\theta}{r'} + \frac{\alpha}{r_o} V_z) \frac{\partial V_z}{\partial \theta'}\}$$

$$= - \{\frac{d\bar{P}}{dz'} + \frac{\alpha}{r_o} \frac{\partial P_o}{\partial \theta'}\} + \mu \{\frac{1}{r'} \frac{\partial}{\partial r'} (r' \frac{\partial V_z}{\partial r'}) +$$

$$+ (1 + \frac{\alpha^2 r'^2}{r_o^2}) \frac{1}{r'^2} \frac{\partial^2 V_z}{\partial \theta'^2}\} \quad , \tag{3.13}$$

Circumferential Momentum Equation

$$\rho \{V_r \frac{\partial V_\theta}{\partial r'} + (\frac{V_\theta}{r'} + \frac{\alpha}{r_o} V_z) \frac{\partial V_\theta}{\partial \theta'} + \frac{V_r V_\theta}{r'}\}$$

$$= - \frac{1}{r'} \frac{\partial P_o}{\partial \theta'} + \mu \{\frac{\partial}{\partial r'} (\frac{1}{r'} \frac{\partial}{\partial r'} (r' V_\theta)) + \frac{2}{r'^2} \frac{\partial V_r}{\partial \theta'} +$$

$$+ (1 + \frac{\alpha^2 r'^2}{r_o^2}) \frac{\partial^2 V_\theta}{r'^2 \partial \theta'^2}\} \quad , \tag{3.14}$$

Radial Momentum Equation

$$\rho \{V_r \frac{\partial V_r}{\partial r'} + (\frac{V_\theta}{r'} + \frac{\alpha}{r_o} V_z) \frac{\partial V_r}{\partial \theta'} - \frac{V_{\theta^2}}{r'}\}$$

$$= - \frac{\partial P_o}{\partial r'} + \mu \{\frac{\partial}{\partial r'} (\frac{1}{r'} \frac{\partial}{\partial r'} (r' V_r)) - \frac{2}{r'^2} \frac{\partial V_\theta}{\partial \theta'} +$$

$$+ (1 + \frac{\alpha^2 r'^2}{r_o^2}) \frac{\partial^2 V_r}{r'^2 \partial \theta'^2}\} \quad . \tag{3.15}$$

It should be noted that although the governing equations have been transformed in the (r', θ', z') coordinate system, the velocity components V_r, V_θ, and V_z themselves are in the original r, θ, and z direction respectively.

Following Gosman et al [16], axial vorticity (ω) and stream function (Ψ) are now introduced as main independent variables. This allows representation of circumferential and radial momentum equations by a single equation for vorticity. Axial vorticity is defined as:

$$\omega = \frac{1}{r'} \left\{ \frac{\partial V_r}{\partial \theta'} - \frac{\partial}{\partial r'} (r' V_\theta) \right\} \quad . \tag{3.16}$$

To derive the vorticity equation, the radial momentum equation is differentiated with respect to θ' and the circumferential momentum equation with respect to r', and the second equation is subtracted from the first. Using the definition of vorticity, the following final form of vorticity equation is obtained: -

The Vorticity Equation

$$\rho \left\{ V_r \frac{\partial \omega}{\partial r'} + \left(\frac{V_\theta}{r'} + \frac{\alpha}{r_o} V_z \right) \frac{\partial \omega}{\partial \theta'} \right\} -$$

$$- \frac{\mu}{r'} \frac{\partial}{\partial r'} \left(r' \frac{\partial \omega}{\partial r'} \right) - \mu \left(1 + \frac{\alpha^2 r'^2}{r_o^2} \right) \frac{1}{r'^2} \frac{\partial^2 \omega}{\partial \theta'^2} +$$

$$+ \rho \frac{\alpha}{r_o} \left\{ \frac{1}{r'} \frac{\partial V_z}{\partial \theta'} \frac{\partial}{\partial r'} (r' V_\theta) - \frac{\partial V_z}{\partial r'} \frac{\partial V_\theta}{\partial \theta'} \right\} = 0 \quad . \tag{3.17}$$

The stream function is now defined as follows such that the continuity equation is implicitly satisfied:

$$\frac{\partial \Psi}{\partial r'} = \rho \left(V_\theta + \frac{\alpha r'}{r_o} V_z\right) \quad , \tag{3.18a}$$

$$\frac{\partial \Psi}{\partial \theta'} = - \rho r' V_r \ . \tag{3.18b}$$

Substitution of V_θ and V_r from equations (3.18) into the definition of vorticity, equation (3.16), results in the stream function equation which is as follows:

The Stream Function Equation

$$\left\{\frac{1}{r'} \frac{\partial}{\partial r'} \left(r' \frac{\partial \Psi}{\partial r'}\right) + \frac{1}{r'^2} \frac{\partial^2 \Psi}{\partial \theta'^2}\right\} +$$

$$+\rho \left\{\omega - \frac{\alpha}{r_o r'} \frac{\partial}{\partial r'} \left(V_z r'^2\right)\right\} = 0 \ . \tag{3.19}$$

The physical significance of the definition of stream function can be appreciated by referring to Figure 3 which shows a control volume twisted in the longitudinal direction and its projection on the r' - θ' plane. The projection of longitudinal twisted faces ADD'A' and BCC'B' is represented by crossed-hatched areas. Faces ABB'A' and DCC'D' are crossed by the radial velocity component V_r. Thus, the

mass flow rate through these faces is:

$$d\dot{m}_{r'} = \rho r' V_r d\theta' dz' \tag{3.20a}$$

where $r'd\theta'dz'$ is the elemental area normal to the flow.

The side faces ADD'A' and BCC'B' are not only crossed by the circumferential velocity component V_θ, but because of twisting, these faces are also exposed to the axial velocity component V_z. The total mass flow rate through these faces is, therefore, the sum of the two contributions. Thus,

$$d\dot{m}_{\theta'} = \rho V_\theta \text{ (area of face ADD'A') } +$$

$$+ \rho V_z \text{ (projected area of face ADD'A' on r' - } \theta' \text{ plane)}$$

$$= \rho V_\theta (dr'dz') + PV_z (dr'r'd\phi) .$$

Substituting $d\phi$ from equation (3.2),

$$d\dot{m}_{\theta'} = \rho(V_\theta + \frac{\alpha}{r_o} r'Vz)\, dr'dz' . \tag{3.20b}$$

The definition of stream function via equations (3.18) thus represents the actual mass flow rates through the faces of the control volume and $(V_\theta + \frac{\alpha r'}{r_o} V_z)$ may be viewed as the effective velocity in the circumferential direction. When there is no twisting ($\alpha = 0$), equation (3.12) takes its usual form.

3.4 Generalized Representation of the Governing Equations

The equations to be solved are equation (3.17) for vorticity, equation (3.19) for stream function and equation (3.13) for axial velocity. As described in Gosman et al [16], these equations can be put in standard elliptic form by replacing $(\frac{V_\theta}{r'} + \frac{\alpha}{r_o} V_z)$ and V_r appearing on the left hand sides of (3.13) and (3.17) by stream function via equations (3.18). The resulting general elliptical equation for any dependent variable ϕ is of the form:

$$a\left\{\frac{\partial}{\partial\theta'}\left(\phi\,\frac{\partial\Psi}{\partial r'}\right) - \frac{\partial}{\partial r'}\left(\phi\,\frac{\partial\Psi}{\partial\theta'}\right)\right\} -$$

$$\longleftarrow \quad \text{Convection Terms} \quad \longrightarrow$$

$$-\frac{\partial}{\partial\theta'}\left\{b_1\,\frac{\partial}{\partial\theta'}(c\phi)\right\} - \frac{\partial}{\partial r'}\left\{b_2\,\frac{\partial}{\partial r'}(c\phi)\right\} +$$

$$\longleftarrow \quad \text{Diffusion Terms} \quad \longrightarrow$$

$$+ \qquad d = 0 \qquad \text{(3.21)}$$

Source Terms

where a, b_1, b_2, c, and d for each dependent variable are as follows:

ϕ	a	b_1	b_2	c	d
Ψ	0	$1/\rho r'$	r'/ρ	1	$r' \{\frac{\alpha}{r_o}(r' \frac{\partial Vz}{\partial r'} + 2V_z) - \omega\}$
ω	1	$\mu(\frac{1}{r'} + \frac{\alpha^2 r'}{r_o^2})$	$\mu r'$	1	d^ω
Vz	1	$\mu(\frac{1}{r'} + \frac{\alpha^2}{r_o^2} r')$	$\mu r'$	1	$r' \{\frac{d\bar{P}}{dz'} + \frac{\alpha}{r_o} \frac{\partial P_o}{\partial \theta'}\}$

where

$$d^\omega = \rho \frac{\alpha}{r_o} r' \left[\frac{1}{r'} \frac{\partial V_z}{\partial \theta'} \left\{\frac{1}{\rho}\left(\frac{\partial \Psi}{\partial r'} + r' \frac{\partial^2 \Psi}{\partial r'^2}\right) - \right.\right.$$

$$\left. - \frac{\alpha}{r_o}(2r'V_z + r'^2 \frac{\partial V_z}{\partial r'})\right\} - r' \frac{\partial V_z}{\partial r'}\left(\frac{1}{\rho} \frac{\partial^2 \Psi}{r' \partial r' \partial \theta'} - \right.$$

$$\left. - \frac{\alpha}{r_o} \frac{\partial V_z}{\partial \theta'}\right)\Big] \quad . \tag{3.22}$$

The term $\frac{\partial p_o}{\partial \theta'}$ appearing in the source term of the axial momentum equation can be obtained from equation (3.14) as follows:

$$\frac{\partial P_o}{\partial \theta'} = \mu r' \left\{\frac{1}{r'} \frac{\partial V_\theta}{\partial r'} - \frac{V_\theta}{r'^2} + \frac{\partial^2 V_\theta}{\partial r'^2} + \frac{2}{r'^2} \frac{\partial V_r}{\partial \theta'} + \right.$$

$$\left. + \left(1 + \frac{\alpha^2}{r_o^2} r'^2\right) \frac{1}{r'^2} \frac{\partial^2 V_\theta}{\partial \theta'^2}\right\} - \rho \left\{r' V_r \frac{\partial V_\theta}{\partial r'} + \right.$$

$$\left. + \left(V_\theta + \frac{\alpha r'}{r_o} V_z\right) \frac{\partial V_\theta}{\partial \theta'} + V_r V_\theta\right\} \quad , \tag{3.23}$$

where V_r and V_θ are evaluated from equations (3.18).

3.5 Boundary Conditions

The equations given by (3.21) must be supplemented with suitable boundary conditions to completely define the problem. Boundary conditions are now developed for the limiting case where the fins extend to the centerline of the tube, thus dividing the cross-section of the tube into a number of passages as shown in Figure 4. Due to symmetry, only one such passage need be considered. It should be noted that because of twisting, the flow is not symmetrical about the central plane O-B.

In view of the no-slip condition, the velocities are all zero on solid walls and the stream function assumes a constant value. In the present study, stream function was assigned zero value on the solid walls. Thus, the values of velocities and stream function on the four boundaries, viz. fin surface O-A, tube wall A-B-C, fin surface C-D, and the center node D-O are zero. The boundary condition for vorticity is discussed in Section 4.2.

4.0 METHOD OF SOLUTION

In Section 3.0, a set of elliptic partial differential equations describing the momentum transfer in fully developed laminar flow in a tube with twisted fins was derived from the conservation equations. The governing equations are coupled and non-linear in nature. A closed form analytical solution is, therefore, not possible and one has to resort to numerical techniques such as the finite-difference method used here.

4.1 Finite Difference Solution

The starting point in solving a set of partial differential equation using a finite difference method is to convert these equations into a set of finite difference equations at discrete points (called the grid nodes*) in the flow field. The process of arriving at the finite difference equation is described in detail by Gosman et al [16] and is summarized in Appendix B. Basically, it involves integration of partial differential equations over control volumes surrounding grid nodes with assumptions concerning the distributions of the variables between the nodes of the grid. A cross-section of one such control volume is shown in Figure 5 by the cross-hatched area. The final outcome of this analysis is the following successive substitution formula:

$$\phi_p = C_E\phi_E + C_W\phi_W + C_N\phi_N + C_S\phi_S + D \ , \qquad (4.1)$$

*See Figure 5 for illustration.

where the C coefficients represent convection and diffusion of variable ϕ whereas D represents its source.

Source terms usually contained first and higher order derivatives of the ϕ variables (see Section 3.4). These derivatives were put in finite difference form using well known central difference formulae. Forward and backward difference formulae were used to evaluate the local wall shear stresses which involved first derivative of velocities at the solid walls (see Appendix A). A review of finite difference representation of derivatives is given in Appendix C.

4.2 Vorticity Boundary Condition

The boundary conditions for axial velocity and stream function have already been indicated in Section 3.5. The boundary condition for vorticity can be derived by assuming suitable shapes of velocity profiles in the near-wall region. The vorticity boundary conditions applicable to the four boundaries are (see Figure 5):

Fin Surfaces O-A and C-D

$$\omega_o = 3 \frac{(\Psi_o - \Psi_{no})}{\rho n^2} - \frac{1}{2} \omega_{no} \quad . \tag{4.2}$$

Tube Wall A-B-C

$$\omega_o = \frac{6(3n - 2r_o)}{(5n - 4r_o)} \frac{(\Psi_o - \Psi_{no})}{\rho n^2} - \frac{2(n - r_o)}{(5n - 4r_o)} \omega_{no} -$$

$$- \frac{\alpha}{r_o} \frac{(3r_o - 2n)(3n - 2r_o)}{n(5n - 4r_o)} V_{z,no} \quad . \qquad (4.3)$$

Center Node D-O

$$\omega_o = \frac{36}{5} \frac{(\Psi_o - \Psi_{no})}{\rho n^2} - \frac{4}{5} \omega_{no} + \frac{\alpha}{r_o} \frac{12}{5} V_{zno} \quad . \qquad (4.4)$$

The derivation of vorticity boundary condition can be found in Appendix D.

4.3 The Computational Procedure

Equation (4.1) can be written for each variable ϕ at every interior node of the domain of interest and the ϕ conditions can be specified at the boundaries. Thus the set of finite difference equations is a solvable one. However, since the C coefficients and the source term D in equation (4.1) are themselves function of ϕ, an iterative solution procedure is needed. The Gauss-Seidel iterative technique described by Gosman et al [16] was used to solve the finite difference equations. The following range of parameters was covered (with $\beta = \pi/60$ radians):

$$4 \leq M \leq 12$$

$$10 \leq Re \leq 1000$$

$$0 \leq \alpha \leq 0.5 \quad .$$

Here, comments on the upper limit of Reynolds number and twist ratio are in order. There is sufficient evidence in the literature based on experimental results [1, 2] to believe that for Re > 1000, the flow through twisted geometries may be near transition or already in transition. Thus, a value of 1000 appears to be a suitable limit on the Reynolds number to ensure laminar flow conditions. The maximum value of the twist ratio commonly used fall in the vicinity of 0.5. Eleven out of the thirteen spiral finned tubes tested by Watkinson et al [1] had twist ratios less than 0.5 while the remaining two had twist ratio values of 0.52 and 0.53. Thus, the range of the present investigation covers the majority of applications.

A flow chart and listing of the computer programme is given in Appendix E. The principle features of the computational procedure are summarized below:

a) Iteration Scheme

One complete iteration cycle consisted of three sub-cycles, one for each of the three variables. In each sub-cycle, the field was scanned row by row, and a single variable was updated using equation (4.1). A significant advantage of this type of scanning was that the newly computed ϕ-values were used as soon as they became available thus accelerating the convergence. When all the sub-cycles had been completed, vorticity values were calculated on the boundaries (boundary conditions of axial velocity and stream function did not require iteration), and the axial velocity field was re-adjusted so that the

mean axial velocity corresponded to the known Reynolds number. A new* iteration cycle began and the procedure was repeated until the changes in the values of the variables between successive iterations became acceptably small. The term $\partial P_o/\partial\theta'$ appearing in the source term of the axial velocity was updated periodically to ensure stability of the iteration process. After a solution had converged, the following parameters were calculated:

(i) Friction Factor

Reynolds number and friction factor were defined on the basis of actual mass flow rate. Thus:

$$Re = \frac{2\dot{m}}{\pi r_o \mu} , \tag{4.5}$$

and

$$f = \frac{\pi^2 \rho r_o^5}{\dot{m}^2} \left(-\frac{d\bar{P}}{dz'}\right) , \tag{4.6}$$

where

$$\dot{m} = \rho A_{fa} V_{z,m} \tag{4.7}$$

$$A_{fa} = r_o^2 \{\pi - M\beta (2H - H^2)\} \tag{4.8}$$

and

$$V_{z,m} = \frac{1}{A_{fa}} \int_{r=0}^{r_o} \int_{\theta'=0}^{\theta_o} V_z \, r' \, dr' \, d\theta' \tag{4.9}$$

*The term $d\bar{P}/dz'$ was evaluated for each iteration via wall shear stresses using the relations developed in Appendix A.

(ii) Resultant Secondary Velocity

Resultant secondary velocity (V_s) was defined as:

$$V_s = \sqrt{V_r^2 + V_\theta^2} \quad . \tag{4.10}$$

Thus, the direction of V_s relative to that of V_θ was given by Tan^{-1} (V_r/V_θ). The mean value $(V_{s,m})$ was calculated from equation (4.9) with V_z replaced by V_s. Simpson's 1/3 rule was used to evaluate the double integral in equation (4.9).

(iii) Local Wall Shear Stress

Local wall shear stresses were calculated using the relations derived in Appendix A, namely:

$$\tau_{tz} = \mu \frac{\partial V_z}{\partial r'} \qquad \text{(Tube Wall)} \tag{4.11}$$

$$\tau_{tz} = \frac{\mu}{r'} \left(1 + 2 \frac{\alpha}{r_o} r'\right) \frac{\partial V_z}{\partial \theta'} + \mu \frac{\alpha}{r_o} \left(\frac{\partial V_\theta}{\partial \theta'} + \frac{\partial V_r}{\partial \theta'}\right) \quad \text{(Fin Surfaces)} \tag{4.12}$$

b) Grid Size

The effect of grid size on the predicted values of friction factor was investigated, both for straight and spiral finned tubes. Four different grid sizes (11 x 11, 13 x 13, 15 x 15 and 17 x 17) were used for this purpose. The predicted values of $f_o Re$ (for straight finned tubes) and f/f_o (for spiral finned tubes) are listed in Table 1 for

M = 4, 8, 12; α = 0.3, 0.4, 0.5; and Re = 1000. For straight finned tubes, the effect of increasing grid size was to bring the predicted $f_o Re$ value increasingly closer to the exact solution due to Soliman and Feingold [11]. The increase in grid size, however, resulted in increased computational cost. Hence, the 15 x 15 grid size was chosen as a compromise between accuracy and economy.

As can be seen from Table 1, the 15 x 15 grid size gave sufficient numerical accuracy for spiral finned tubes as well*.

c) Initial Conditions

Initial conditions needed were the number of fins, twist ratio, Reynolds number, and the distributions of velocity components, vorticity, and stream function. The axial velocity field was initialized with the mean axial velocity corresponding to the Reynolds number; the remaining variables were initialized with zero everywhere.

d) Convergence Criterion

An iterative procedure is said to have converged when the values of variables between successive iteration cycles are acceptably small. The convergence criterion was expressed as:

*There were exceptions to this trend, e.g., M = 12, α = 0.5, and Re = 1000. (See Table 1). Nevertheless, the 15 x 15 grid size was chosen for all predictions.

$$cc = \left| \frac{\phi^N - \phi^{N-1}}{\phi^{ref}} \right|_{max} . \qquad (4.13)$$

ϕ^{ref} was assigned the value ϕ^N for axial velocity. For vorticity and stream function, ϕ^N was nearly zero in certain regions of the flow and cc became large even though $\phi^N - \phi^{N-1}$ was small. To avoid this, ϕ^{ref} was defined as follows:

$$\phi^{ref} = [|\phi_N| + |\phi_S| + |\phi_E| + |\phi_W|]/4 \qquad (4.14)$$

The solution was declared to have converged when cc became less than 0.001 for all three variables.

e) Relaxation Factor

In general, no relaxation was necessary to achieve convergence in the majority of cases. However, for high twist ratio and/or high Reynolds number (usually such cases occurred when the product αRe exceeded 300), the process failed to converge of its own and it became necessary to under-relax the variations of the values of stream function and vorticity between successive iterations. Values of relaxation factors for stream function and vorticity were typically 0.6 and 0.4 respectively.

f) Stability

An iterative procedure is stable if the changes in the values of the variables between successive iterations diminish monotonically. The present computational procedure became unstable under the following circumstances:

(i) When the spacing between the grid lines in the radial direction was small (<1/14), the wall vorticities calculated from equations (4.3) and (4.4) became unrealistically very large and instability occurred. To avoid this difficulty, the wall vorticities were removed from the substitution formulae for the near-wall nodes by once-for-all algebraic elimination. The implicit formulation of vorticity boundary condition is given in Appendix F and was used for all predictions.

(ii) At high twist ratio and/or high Reynolds number (usually $\alpha Re > 300$), the source term of vorticity equation became very large causing the value of vorticity to alter greatly from the previous iteration. This caused the stream function to change greatly as vorticity appeared in the source term of the stream function equation. The greatly altered stream function perturbed the flow further. Date [3] has used the so-called multi-point circulation adjustment procedure to cure the instability. In the present analysis, the more conventional procedure of under-relaxing the stream function and vorticity equations proved equally effective.

Tables 2 through 4 list the number of iterations needed for convergence [with initial conditions as described in Section 4.3c)] and the maximum residuals for the dependent variables for M = 4, 8, and 12 respectively at several values of α and Re. The number of iterations to convergence increased rapidly as (i) α increases at a fixed Re, or (ii) Re increases at a fixed α, indicating the instability due to stream function-vorticity linkage discussed earlier. Convergence was also affected by the value of M, and in some cases (notably high α and Re) rapid rates of convergence were noticed as the value of M increased from 8 to 12. In all cases, convergence was governed by the stream function-vorticity linkage; axial velocity consistently behaved well.

5.0 PRELIMINARY STUDIES

5.1 Straight Finned Tubes

Series solutions for friction factor and velocity distributions for laminar flow in tubes with internal straight fins are available due to Soliman and Feingold [11]. Computations were performed to compare the results of the present investigation with those of [11]. As indicated in Table 5, the agreement on friction factor values is within 1.3%. The computed velocity distributions at the axis of symmetry ($\theta' = \theta_0/2$) are plotted in Figures 6-8 along with the results of [11] for M = 4, 8 and 12. As can be seen the agreement is very good.

5.2 Tubes with Twisted Tape Inserts

The geometry of a twisted tape insert in a tube is equivalent to that of a tube with two opposing full fins of zero thickness. In Figures 9-11, friction factor results are compared with those of Date [3]. At $\alpha = 0.1$, the agreement is within 8.3%, but the agreement becomes somewhat worse at higher values of α. Date [3] has reported that at low Reynolds number ($Re \lesssim 100$), the friction factor data converge on the value for a straight circular duct irrespective of the value of the twist ratio. In the present investigation, friction factor approached almost a constant value at low Reynolds number ($Re \lesssim 50$), but always remained greater than the value for the $\alpha = 0$ case. To

explore the probable cause of the discrepency, computations were performed at α = 0.5 and Re = 515 and 700. The distribution of resultant secondary velocity as reported by Date [17] for α = 0.5 and Re = 515 shows certain anomalies. Physically, $V_s/V_{z,m}$ should increase linearly with radius to reach a maximum value near the tube wall; and, on solid walls, $V_s/V_{z,m}$ should be zero in view of the no slip condition. This type of pattern was obtained in the present computation (Figure 12). Qualitatively similar distribution was also reported in [18] for turbulent flow in tubes with twisted tape inserts. On the contrary, Date's [17] results indicate a trend whereby $V_s/V_{z,m}$ is largest near the center node (See Figure 12). In addition, Date's secondary velocity data indicates that $V_s/V_{z,m}$ is higher near tape surface O-A than it is near C-D which is unrealistic.

In Figure 13, the equivelocity lines $[V_z/V_{z,m}]$ are compared with [17] for α = 0.5 and Re = 700. The effect of twisting in the asymmetric pattern of velocity profiles is more pronounced in the present prediction.

The aforementioned anomalies in Date's [3, 17] predictions may be mainly due to the error in his formulation of vorticity source term which is reproduced here: [also see equation (3.22)]

$$d^{\omega} = \frac{\pi r'}{S}\left[\frac{\partial V_z}{\partial \theta'}\left\{\frac{1}{r'}\frac{\partial}{\partial r'}\left(r'\frac{\partial \psi}{\partial r'}\right) - \frac{\rho \pi r'}{S}\frac{\partial}{\partial r'}\left(V_z r'^2\right)\right\} - \right.$$

$$\left. - \frac{\partial V_z}{\partial r'}\left\{\frac{\partial^2 \psi}{\partial r' \partial \theta'} - \frac{\rho \pi r'}{S}\frac{\partial V_z}{\partial \theta'}\right\}\right] .$$

Besides, his implicit formulation for vorticity boundary condition is inconsistent with the successive substitution formula, equation (4.1), from which it has been derived. In addition, Date's [17] method for removing instability due to stream function-vorticity linkage appears to be in error due to omission of density (ρ) throughout the analysis.

Since Date's work, experimental isothermal friction factor results have become available through Marner and Bergles [2] for laminar flow in a tube with twisted tape insert. Their results for $\alpha = 0.5$ are indicated in Figure 11 and compare well with the present predictions based on $\beta = 0$*.

In view of the above, it was concluded that the prediction scheme (as developed) was performing satisfactorily. The main predictions involving $M \geq 4$ were then undertaken, and the results are presented and discussed in the next section.

---

*The test section used in [2] corresponds to $\beta \approx 2.58°$. However, with $M = 2$ the effect of finite thickness will be minor. Also, since f and Re are independent of the fluid properties, the present predictions are directly comparable with the results of [2].

6.0 RESULTS AND DISCUSSION

Selected samples of the distributions of axial velocity, resultant secondary velocity, and local wall shear stress are presented in Figures 14-45. The effects of twist ratio and Reynolds number on predicted friction factor values are shown in Figures 46-51. Certain characteristics of the flow are given in Tables 6-8 and the friction factor data are listed in Tables 9-11. Local values of axial velocity and resultant secondary velocity are given in Table 12 for several values of M, α, and Re.

6.1 Axial Velocity Profiles

The effect of increasing α from 0.1 to 0.5 at Re = 1000 on the axial velocity distribution is shown in Figures 14-16 for M = 4. At α = 0.1 (Figure 14), the equivelocity lines are almost symmetrical about the central plane and the effect of twisting is noticeable only as a relatively small shift of the peak of the axial velocity in the direction opposite to the fin twisting. This is due to the small magnitudes of secondary velocities generated; the mean resultant secondary velocity, $V_{s,m}$, being only 6.5% of the mean axial velocity, $V_{z,m}$ (See Table 6). As the twist ratio is increased, the secondary velocities generated become increasingly significant ($[V_s/V_{z,m}]_{mean}$ = 20.4% at α = 0.3 and 34.4% at α = 0.5) causing the flow path to become increasingly helical. The axial velocity distribution, consequently, becomes increasingly asymmetric about the central plane and the peak

is shifted increasingly away from the central plane in the direction opposite to fin twisting (See Figures 15-16). Because of the helical nature of the flow, the fluid particles with greater velocities move outwardly towards the solid walls thus increasing the velocity gradients near the walls. For a constant mass flow rate, continuity can only be satisfied by a relatively flatter velocity profiles. This fact is evidenced in Table 6 where a decrease in $[V_z/V_{z,m}]_{max}$ is noticed as α increases; the decrease being more significant at higher Re due to larger secondary velocities generated. For example, for an increase in α from 0.1 to 0.5, the flattening (decrease in $[V_z/V_{z,m}]_{max}$) is 0.91% at Re = 10 as compared to 11.49% at Re = 600 and 13.10% at Re = 1000.

The effect of increasing Re from 100 to 1000 at α = 0.4 on the axial velocity distribution is shown in Figures 17-19 for M = 4. At Re = 100 (Figure 17), the effect of twisting is negligible; the equivelocity lines are essentially symmetric about the central plane where the peak of the axial velocity (differing insignificantly from the value for α = 0 case) is also located. The effect of twisting is, however, apparent at Re = 500 and Re = 1000 (See Figures 18-19). It is seen that as the Reynolds number is increased, the profiles again become increasingly asymmetric and the peak of the axial velocity is shifted increasingly away from the central plane. As can be seen from Table 6, flattening with Reynolds number is greater at a higher twist ratio viz., for an increase in Re from 10 to 600, the decrease in $[V_z/V_{z,m}]_{max}$ is 2.40% at α = 0.1 and 12.82% at α = 0.5. Similarly,

the decrease is 9.00% at α = 0.2 against 14.65% at α = 0.4 when Re is increased from 10 to 1000.

The effects of α and Re on the axial velocity distribution are shown in Figures 20-25 for M = 8 and 12. As can be seen, the affects are qualitatively similar to those described above for M = 4. At small α or small Re (Figures 20, 22, 24-25), the effect of twisting is minor. However, as α (at fixed Re) or Re (at fixed α) is increased, the profiles again become asymmetric and flatter. The shift in the location of $[V_z/V_{z,m}]_{max}$ is less for M = 8 and 12 as compared to that for M = 4 due to relatively smaller flow area. In general, flattening with Re decreases as M increases. For example, at α = 0.3 the decrease in $[V_z/V_{z,m}]_{max}$ is 13.03% for M = 4, 10.01% for M = 8, and 6.71% for M = 12 as Re increases from 10 to 1000. Flattening with α shows no distinct pattern as M is increased. At Re = 10, flattening is 0.91% for M = 4, 2.67% for M = 8, and 3.33% for M = 12 when α increases from 0.1 to 0.5 whereas the corresponding increase in flattening remains almost constant with M at Re = 1000 (13.1% at M = 4, 14.01% at M = 8, and 13.86% at M = 12).

In Tables 6-8, the maximum value of $\frac{\alpha}{r_o}\left[\frac{\partial P_o/\partial\theta'}{d\bar{P}/dz'}\right]$ is listed at several values of α, Re, and M to indicate the significance of the term $\frac{\alpha}{r_o}\frac{\partial P_o}{\partial\theta'}$ in the axial momentum equation (3.21) relative to the axial pressure gradient, $\frac{d\bar{P}}{dz'}$. The magnitude of the term $\frac{\alpha}{r_o}\left[\frac{\partial P_o/\partial\theta'}{d\bar{P}/dz'}\right]$ increases with α and Re irrespective of the value of M.

Date [3] has reported that for flow in tubes with twisted tape inserts, the axial velocity distribution shows two peaks at high twist ratio (α = 0.7) and high Reynolds number (Re $\approx$ 1200). From the axial velocity profiles presented here, occurrence of two peaks seems likely for M = 4 at $\alpha \geq 0.7$ and Re = 1000. For M > 4, such peaks may not exist due to smaller inter-fin spacings. However, in view of Date's [3, 17] errors as mentioned in Section 5.2, no conclusive statement can be made in this regard.

6.2 Secondary Velocity Profiles

Secondary velocities are generated due to twisting of the fins. Since the flow is guided by the fins, the flow is in the direction of fin twisting everywhere in the flow field. This fact is evidenced in Figures 26-27 where the resultant secondary velocity vectors normalized by the mean axial velocity value are plotted for M = 4 and 8 respectively at α = 0.5 and Re = 1000. Length, direction, and tail of the arrows respectively represent magnitude, direction, and location of the resultant secondary velocity ($[V_s/V_{z,m}]$) vectors. The magnitude of resultant secondary velocity increases with radius to reach a maximum value near the tube wall whereafter it decreases to become zero on the wall. The distribution of velocity components are asymmetrical about the central plane (See also Table 12). As can be seen from Tables 6-8, the magnitudes of secondary velocities increase with twist ratio indicating that the flow becomes increasingly helical

as the twist ratio is increased. The magnitudes also increase with Reynolds number as the helical flow speeds up although, as expected, the ratio $[V_s/V_{z,m}]_{mean}$ remains almost constant. At a given twist ratio and Reynolds number, $[V_s/V_{z,m}]_{mean}$ increases with M due to increasingly smaller flow areas involved. In the present investigation the mean value of $V_s/V_{z,m}$ was found to lie between 0.062 to 0.365.

6.3 Distribution of Local Wall Shear Stress

The variation of local wall shear stress normalized by the average value over the entire cross-section is shown in Figures 28-45 where the left distribution corresponds to fin surface O-A and right distribution to C-D as per Figure 4. Table 6-8 include average values of shear stresses along the tube wall, fin surfaces, and over the entire cross-section based on r_o = 0.02 m and air as the working fluid. Figures 28-30 deal with M = 4 and Re = 1000. At α = 0.1 (Figure 28), the distributions along the fin surfaces are only slightly asymmetric (τ_{oa} = 0.3313 x 10^{-2} N/m^2 and τ_{cd} = 0.3921 x 10^{-2}) while along the tube wall (τ_{abc} = 0.3960 x 10^{-2} N/m^2), the distribution is almost symmetric with a peak occurring midway between the fins. This was expected in view of the small secondary velocities generated and the distribution of axial velocity already discussed. At α = 0.3 (Figure 29), the distributions on the fins become asymmetric. These shear stress distributions along the fin surfaces are characterized by a terrace like shape along the fin surface O-A with a peak value that

is about 33% lower than that for fin surface C-D. The distribution along the tube wall also becomes somewhat asymmetric with the peak shifted in the direction opposite to the fin twisting. Average shear stress along fin surface C-D is higher than that along fin surface O-A by $0.1745 \times 10^{-2} N/m^2$. A further increase in α to 0.5 causes the shear stress distribution (Figure 30) to become more asymmetric, both along the fin surface and the tube wall ($\tau_{oa} = 0.6423 \times 10^{-2}$ N/m^2, $\tau_{cd} = 0.8795 \times 10^{-2}$ N/m^2 and $\tau_{abc} = 0.6373 \times 10^{-2}$ N/m^2) as the secondary velocities generated become significant ($[V_s/V_{z,m}]_{mean} = 34.4\%$). As can be seen from Table 6, the effect of increasing twist ratio on the distributions of wall shear stress is significant only at higher Reynolds number; at low Reynolds number, e.g. Re = 10, the average wall shear stresses on both fin surfaces are almost the same.

The effect of increasing Reynolds number from 100 to 1000 at $\alpha = 0.4$ on the distributions of wall shear stress is shown in Figures 31-33 for M = 4 and is the same as already discussed; asymmetry is significant only at $Re \geq 500$ and $\alpha \geq 0.2$ (see also Table 6). However, it should be noted from Tables 6-8, that even at very low Re and α, e.g. Re = 10 and $\alpha = 0.1$, the average wall shear stresses are somewhat greater than the $\alpha = 0$ case due to which friction factor is always greater than for the $\alpha = 0$ case. This point is discussed further in the next sub-section.

Similar affects are associated with the distribution of shear stress for M = 8 and 12 (See Figure 34-45) with the following exceptions:

(i) The distribution along the tube wall is almost symmetric even at high α and high Re, e.g., M = 8, α = 0.5, and Re = 1000 (Figure 36).

(ii) For M = 12, the terrace like shape as discussed in connection with M = 4 is not found (Figures 40-45).

Both (i) and (ii) above are due to the relatively smaller flow area available for M = 8 and 12.

6.4 Friction Factor

For a tube with straight fins the product f_0Re depends on M, H, and β and is a constant for a given combination of these parameters. However, with finite twisting fRe becomes additionally dependent on α and Re. The ratio of predicted friction factor (f) to the value (f_0) for a tube with straight fins is listed in Tables 9-11 for several combinations of M, α, and Re. Computed values of f_0Re along with those due to [11] are given in Table 5 for M = 4, 8, and 12. In Figures 46-48, the variation of f/f_0 with α is plotted at several Reynolds number for M = 4, 8 and 12 respectively. In general, f/f_0 increases non-linearly from 1.0 (at α = 0) to a maximum value (at α = 0.5) which depends on the combination of M and Re. For example, at M = 4 and Re = 1000 the maximum value of f/f_0 is 2.297 indicating an increase of 129.7% in friction factor over the value for a tube with straight fins while the corresponding increases are 118.6% for M = 8 and 103.8% for M = 12. At low twist ratios ($\approx$ 0.05 for M = 4, 0.1 for M = 8,

and 0.2 for M = 12), f/f_o is somewhat independent of Reynolds number. This is due to the small magnitudes of secondary velocities generated; consequently, the contribution of the gradients of secondary velocities towards the pressure drop is insignificant (See equation (4.12)). However, due to the additional term involving the derivative of the axial velocity and the fact that $A_\alpha/A_o > 1$ (See Tables 6-8), f/f_o always remains greater than unity.

The effect of Reynolds number on predicted values of f/f_o is shown in Figures 49-51 for M = 4, 8 and 12 respectively. At low Reynolds number (up to Re $\approx$ 100), the increase is insignificant due to small secondary velocities generated and the consequences thereof as discussed earlier. A further increase in Re causes f/f_o to increase in a somewhat exponential fashion. A lower value of M yields a greater increase in f/f_o value in the latter region. For example, the associated increase in f/f_o for an increase in Re from 10 to 1000 at α = 0.5 is about 61% for M = 4 while at M = 12, the corresponding increase is only about 13%. This is due to the reason that at higher values of M, the increase in f/f_o is governed by the mere presence of fins and the secondary flows generated due to twisting become of minor significance.

6.5 Empirical Correlations for Friction Factor

The dependence of f/f_o on α and Re can be described by the following empirical formulae:

$$\frac{f}{f_o} = 1 + \alpha^{a_1} \; Re^{a_2} \qquad \text{for} \qquad Re \leq 100$$

$$= (100)^{a_2} \; \alpha^{a_1} + \exp[a_3 \alpha \; (Re - 100)] \quad \text{for } 100 < Re \leq 1000$$

where the coefficients a_1, a_2, and a_3 depend on the value of M and are given below along with the standard deviations and maximum (absolute) errors:

M	a_1	a_2	a_3	Standard Deviation	Maximum Error (absolute)
4	1.19	0.040	0.00140	2.397	4.469
8	1.05	0.060	0.00090	2.907	7.493
12	1.02	0.118	0.00020	3.691	9.710

Standard deviation and maximum (absolute) error were defined, respectively, as:

Standard Deviation

$$= \frac{\left[\sum_1^N \{(f/f_o)_{correlated} - (f/f_0)_{predicted}\}^2/N\right]^{\frac{1}{2}}}{\text{Average } (f/f_o)_{correlated}} \times 100$$

Maximum (Absolute) Error

$$= \left| \frac{(f/f_o)_{correlated} - (f/f_o)_{predicted}}{(f/f_o)_{correlated}} \right|_{max} \times 100$$

7.0 CONCLUDING REMARKS

The following conclusions can be drawn from the results of the present investigation:

1) The axial velocity distribution becomes increasingly flatter and asymmetric about the central plane as the twist ratio or Reynolds number is increased.

2) The main flow in the axial direction is guided by the fins. Secondary velocities are, therefore, present due to twisting of the fins, and they increase in magnitude as (i) twist ratio is increased causing the flow to become increasingly helical; (ii) Reynolds number is increased causing the helical flow to speed up.

3) The circumferential velocity is in the direction of fin twisting everywhere in the flow field. Thus, the flow does not represent recirculation.

4) The magnitudes of local wall shear stresses increase with twist ratio and Reynolds number as the axial velocity distribution becomes flatter and the magnitudes of secondary velocities generated become significant.

5) The distributions of local wall shear stress on the fin surfaces and, in some cases (notably high twist ratio and Reynolds number) on the tube wall, are highly asymmetric. The average wall shear stress on fin surface C-D is higher than on O-A (See Tables 6-8).

6) Friction factor increases non-linearly with twist ratio and Reynolds number and is always greater than the value for a tube with straight fins. The effect of Reynolds number is, however, noticeable only for Re > ~ 100.

8.0 RECOMMENDATION FOR FUTURE EXTENSION WORK

Several extensions of the present work are possible. A few topics are listed below:

i) Momentum transfer characteristics for fully developed laminar flow in tubes with spiral fins of finite thickness and finite length. This will require specification of boundary conditions for vorticity, stream function, and axial velocity on $r' = 0$, $0 \leq \theta' \leq \theta_o$; $\theta' = 0$, $0 < r' < r_i$; and $\theta' = \theta_o$, $0 < r' < r_i$ (See Figure 1). Efforts are already underway to predict friction factor characteristics for this case.

ii) Heat transfer characteristics for fully developed laminar flow in tubes with spiral fins of finite thickness and finite length for constant heat flux and constant wall temperature boundary conditions including the effect of finite fin conductance.

iii) Laminar fluid flow and heat transfer characteristics for flow through annuli with internal spiral fins.

9.0 ACKNOWLEDGEMENTS

The author is grateful to Dr. A.C. Trupp for the guidance and encouragement he received during the course of this investigation. The financial assistance provided by the University of Manitoba and the National Research Council of Canada are gratefully acknowledged.

10.0 REFERENCES

1. Watkinson, A.P., Miletti, D.L., and Kubanek, G.R., "Heat Transfer and Pressure Drop of Internally Finned Tubes in Laminar Oil Flow", ASME Paper No. 77-HT-41, 1977.

2. Marner, W.J., and Bergles, A.E., "Augmentation of Tubeside Laminar Flow Heat Transfer by Means of Twisted-Tape Inserts, Static-mixer Inserts and Internally Finned Tubes", Proceedings of the Sixth International Heat Transfer Conference, 1978, Vol. 2, pp. 583-588.

3. Date, A.W., "Prediction of Fully Developed Flow in a Tube Containing a Twisted-Tape", Int. J. Heat Mass Transfer, Vol. 17, 1974, pp. 845-859.

4. Ivanovic, M., "Prediction of Flow and Heat Transfer in Internally Finned Tubes", Ph.D. Thesis, University of Minnesota, July, 1978.

5. Vasilchenko, Y.A., and Barbaritskaya, M.S., "Resistance with Non-isothermal Fluid Flow in Tubes with Longitudinal Fins", Thermal Engineering, Vol. 16, 1969, No. 1, pp. 28-35.

6. Vasilchenko, Y.A., and Barbaritskaya, M.S., "Heat Transfer in Tubes with Longitudinal Fins", Thermal Engineering, Vol. 16, 1969, No. 5, pp. 105-109.

7. Soliman, H.M., and Feingold, A., "Heat Transfer, Pressure Drop, and Performance Evaluation of a Quintuplex Internally Finned Tube", ASME Paper No. 77-HT-46, 1977.

8. Hu, M.H., and Chang, Y.P., "Optimization of Finned Tubes for Heat Transfer in Laminar Flow", ASME Journal of Heat Transfer, Vol. 95, 1973, pp. 332-338.

9. Nandakumar,K., and Masliyah, J.H., "Fully Developed Viscous Flow in Internally Finned Tubes", The Chemical Engineering Journal, Vol. 10, 1975, pp. 113-120.

10. Masliyah, J.H., and Nandakumar, K., "Heat Transfer in Internally Finned Tubes", ASME Journal of Heat Transfer, Vol. 96, 1976, pp. 257-261.

11. Soliman, H.M., and Feingold, A., "Analysis of Fully Developed Laminar Flow in Longitudinal Internally Finned Tubes", "The Chemical Engineering Journal", Vol. 14, 1977, pp. 119-128.

12. Soliman, H.M., and Feingold, A., "Analysis of Heat Transfer in Internally Finned Tubes under Laminar Flow Conditions", Proceedings of the Sixth International Heat Transfer Conference, 1978, Vol. 2, pp. 571-576.

13. Soliman, H.M., "The Effect of Fin Conductance on Laminar Heat Transfer Characteristics of Internally Finned Tubes", To appear in Can. J. of Chem. Eng., 1981.

14. Soliman, H.M., Chau, T.S., and Trupp, A.C., "Analysis of Laminar Heat Transfer in Internally Finned Tubes with Uniform Outside Wall Temperature", ASME Journal of Heat Transfer, Vol. 102, 1980, pp. 598-604.

15. Bird, R.B., Stewart, W.E., and Lightfoot, E.N., "Transport Phenomena", John Wiley, New York, 1960.

16. Gosman, A.D., Pun, W.M., Runchal, A.K., Spalding, D.B., and Wolfstein, M., "Heat and Mass Transfer in Recirculating Flows", Academic Press, London, 1969.

17. Date, A.W., "Prediction of Friction Factor and Heat Transfer Characteristics of Flow in a Tube with Twisted Tape", Ph.D. Thesis, Imperial College of Science and Technology, January 1973.

18. Smithberg, E., and Landis, F., "Friction and Heat Transfer Characteristics in Tubes with Twisted Tape Swirl Generators", ASME Journal of Heat Transfer, Vol. 86, 1964, pp. 39-49.

19. Trupp, A.C., and Soliman, H.M., "Performance Optimization of Internally Finned Tubes for Laminar Flow Heat Exchangers", Rep. No. ER25.29, Dept. of Mech. Eng'g., University of Manitoba, November 1980.

APPENDIX A

FORMULATION OF LOCAL WALL SHEAR STRESS AND THE MEAN PRESSURE GRADIENT

The stress tensor in (r, θ, z) corrdinate system is [15]:

$$\left.\begin{aligned}
\tau_{rr} &= \mu \{2\frac{\partial V_r}{\partial r} - \frac{2}{3}(\vec{\nabla}\cdot\vec{V})\} \\
\tau_{\theta\theta} &= \mu \{2(\frac{1}{r}\frac{\partial V_\theta}{\partial \theta} + \frac{V_r}{r}) - \frac{2}{3}(\vec{\nabla}\cdot\vec{V})\} \\
\tau_{zz} &= \mu \{2\frac{\partial V_z}{\partial z} - \frac{2}{3}(\vec{\nabla}\cdot\vec{V})\} \\
\tau_{r\theta} &= \tau_{\theta r} = \mu \{r\frac{\partial}{\partial r}(\frac{V_\theta}{r}) + \frac{1}{r}\frac{\partial V_r}{\partial \theta}\} \\
\tau_{\theta z} &= \tau_{z\theta} = \mu \{\frac{\partial V_\theta}{\partial z} + \frac{1}{r}\frac{\partial V_z}{\partial \theta}\} \\
\tau_{zr} &= \tau_{rz} = \mu \{\frac{\partial V_z}{\partial r} + \frac{\partial V_r}{\partial z}\}
\end{aligned}\right\} \qquad (A.1)$$

where $\vec{\nabla}\cdot\vec{V} = \frac{1}{r}\frac{\partial}{\partial r}(rV_r) + \frac{1}{r}\frac{\partial V_\theta}{\partial \theta} + \frac{\partial V_z}{\partial z}$.

These stresses are transformed in (r', θ', z') coordinate system using the condition of fully developed flow and noting that $\vec{\nabla}\cdot\vec{V}$ is zero in view of the continuity equation.

$$\left.\begin{aligned}
\tau_{rr} &= 2\mu \quad \frac{\partial V_r}{\partial r'} \\
\tau_{\theta\theta} &= 2\mu \quad \left(\frac{1}{r'} \quad \frac{\partial V_\theta}{\partial \theta'} + \frac{V_r}{r'}\right) \\
\tau_{zz} &= 2\mu \quad \frac{\alpha}{r_o} \quad \frac{\partial V_z}{\partial \theta'} \\
\tau_{r\theta} &= \tau_{\theta r} = \mu \left\{r' \quad \frac{\partial}{\partial r'} \left(\frac{V_\theta}{r'}\right) + \frac{1}{r'} \quad \frac{\partial V_r}{\partial \theta'}\right\} \\
\tau_{\theta z} &= \tau_{z\theta} = \mu \quad \left(\frac{\alpha}{r_o} \frac{\partial V_\theta}{\partial \theta'} + \frac{1}{r'} \frac{\partial V_z}{\partial \theta'}\right) \\
\tau_{zr} &= \tau_{rz} = \mu \left(\frac{\partial V_z}{\partial r'} + \frac{\alpha}{r_o} \frac{\partial V_r}{\partial \theta'}\right)
\end{aligned}\right\} \qquad (A.2)$$

The total axial shear stress is, therefore:

$$\begin{aligned}
\tau_{tz} &= \tau_{zz} + \tau_{\theta z} + \tau_{rz} \\
&= \frac{\mu}{r'} \left(1 + 2 \frac{\alpha}{r_o} r'\right) \frac{\partial V_z}{\partial \theta'} + \mu \frac{\alpha}{r_o} \frac{\partial V_\theta}{\partial \theta'} + \mu \left(\frac{\partial V_z}{\partial r'} + \frac{\alpha}{r_o} \frac{\partial V_r}{\partial \theta'}\right) \quad . \qquad (A.3)
\end{aligned}$$

In view of the no-slip condition, the expression for local axial wall shear stress is simplified as follows:

Tube Wall

$$\tau_{tz} = \mu \frac{\partial V_z}{\partial r'} \qquad (A.4)$$

Fin Surfaces

$$\tau_{tz} = \frac{\mu}{r'}\left(1 + 2\frac{\alpha}{r_o}r'\right)\frac{\partial V_z}{\partial \theta'} + \mu\frac{\alpha}{r_o}\left(\frac{\partial V_\theta}{\partial \theta'} + \frac{\partial V_r}{\partial \theta'}\right) \quad . \tag{A.5}$$

The average wall shear stress can now be obtained by evaluating the following integral numerically:

$$\tau_{av} = \frac{1}{A_c}\int_{A_c} \tau_{tz}\, dA_c \quad . \tag{A.6}$$

Where A_c is the total surface area of the tube and fins in an axial length dz' of the tube and is evaluated as follows:

$$A_c = \int_{A_c} dA_c \tag{A.7}$$

where,

$$dA_c = r_o d\theta' dz' + 2\left\{1 + \alpha^2(r'/r_o)^2\right\}^{\frac{1}{2}} dr'dz' +$$

Tube Wall Fin Surfaces

$$\left\{1 + \alpha^2 (r_i/r_o)^2\right\}^{\frac{1}{2}} r_i d\theta' dz' \tag{A.8}$$

Fin Arc

$$\text{Thus, } A_c = r_o dz' \int_0^{2\pi} d\theta' + 2Mdz' \int_{r_1}^{r_o} \{1 + \alpha^2 (r_i/r_o)^2\}^{\frac{1}{2}} dr' +$$

Tube Wall — Fin Surfaces

$$+ M \{1 + \alpha^2 (r_i/r_o)^2\}^{\frac{1}{2}} r_i dz' \int_{-\beta}^{\beta} d\theta'$$

Fin Arc

$$= 2Mr_o \{\frac{\pi}{M} - \beta(1+\alpha^2)^{\frac{1}{2}}\} dz' +$$

Tube Wall

$$+ M [r_o (1 + \alpha^2)^{\frac{1}{2}} - r_i (1+\alpha^2 \frac{r_i}{r_o})^{\frac{1}{2}} + \frac{r_o}{\alpha} \{\ell n(\alpha+(1+\alpha^2)^{\frac{1}{2}}) - \ell n(\alpha \frac{r_i}{r_o} +$$

$$+ (1 + \alpha^2 \frac{r_i^2}{r_o^2})^{\frac{1}{2}})\}] dz' +$$

Fin Surfaces

$$+ 2Mr_i \beta (1 + \alpha^2 \frac{r_i^2}{r_o^2})^{\frac{1}{2}} dz' \quad , \text{ for } \alpha > 0 \qquad \text{(A.9)}$$

Fin Arc

For $\alpha = o$,

$$A_c = r_o dz' \int_0^{2\pi} d\theta' + 2Mdz' \int_{r_i}^{r_o} dr' + Mr_i dz' \int_{-\beta}^{\beta} d\theta'$$

Tube Wall — Fin Surfaces — Fin Arc

$$= 2Mr_o\left(\frac{\pi}{M} - \beta\right) dz' + 2M(r_o - r_i)\, dz' + 2Mr_i\beta\, dz'$$

Tube Wall Fin Surfaces Fin Arc (A.10)

A force balance over a control volume of length dz' yields:

$$\frac{d\bar{P}}{dz'}\, dz'\, A_{fa} = \tau_{av}\, A_c ,$$

thus,

$$\frac{d\bar{P}}{dz'} = \frac{\tau_{av}\, A_c}{dz'\, A_{fa}} , \qquad (A.11)$$

where

$$A_{fa} = r_o^2\, \{\pi - M\beta(2H - H^2)\} \qquad (A.12)$$

APPENDIX B

DERIVATION OF FINITE DIFFERENCE EQUATION

The general elliptic partial differential equation for any dependent variable ϕ is:

$$a_\phi \left\{\frac{\partial}{\partial\theta'}\left(\phi\,\frac{\partial\Psi}{\partial r'}\right) - \frac{\partial}{\partial r'}\left(\phi\,\frac{\partial\Psi}{\partial\theta'}\right)\right\} -$$

Convection Terms

$$- \frac{\partial}{\partial\theta'}\left\{b_1\,\frac{\partial}{\partial\theta'}\,(c\phi)\right\} - \frac{\partial}{\partial r'}\left\{b_2\,\frac{\partial}{\partial r'}\,(c\phi)\right\} + \qquad \text{(B.1)}$$

Diffusion Terms

$$+ d = o$$

Source Terms

The integration of equation (B.1) is performed over the control volume, shown in Figure 5 in cross-section, which enclosed the node P. The sides of the control volume are supposed to lie mid-way between the neighbouring grid lines. The integral to be evaluated is:

$$\int_{r'_s}^{r'_n} \int_{\theta'_\omega}^{\theta'_e} a_\phi \left\{\frac{\partial}{\partial\theta'}\left(\phi \frac{\partial\Psi}{\partial r'}\right) - \frac{\partial}{\partial r'}\left(\phi \frac{\partial\Psi}{\partial\theta'}\right)\right\} dr' d\theta' -$$

Convection Terms

$$- \int_{r'_s}^{r'_n} \int_{\theta'_\omega}^{\theta'_e} \left[\frac{\partial}{\partial\theta'}\left\{b_1 \frac{\partial}{\partial\theta'}(c\phi)\right\} - \frac{\partial}{\partial r'}\left\{b_2 \frac{\partial}{\partial r'}(c\phi)\right\}\right] dr'd\theta' +$$

Diffusion Terms

$$+ \int_{r'_s}^{r'_n} \int_{\theta'_\omega}^{\theta'_e} d \; dr'd\theta' = o \qquad \text{(B.2)}$$

Source Terms

Convection Terms (Icon)

$$\text{Icon} = a_\phi \int_{r'_s}^{r'_n} \left\{\phi_e \left(\frac{\partial\Psi}{\partial r'}\right)_e - \phi_w \left(\frac{\partial\Psi}{\partial r'}\right)_w\right\} dr' -$$

$$- a_\phi \int_{\theta'_\omega}^{\theta'_e} \left\{\phi_n \left(\frac{\partial\Psi}{\partial\theta'}\right)_n - \phi_s \left(\frac{\partial\Psi}{\partial\theta'}\right)_s\right\} d\theta' \qquad \text{(B.3)}$$

where a_ϕ is a constant.

Here only one of the four integrals in the equation (B.3) will be evaluated.

Let,

$$Ic_1 = a_\phi \int_{r'_s}^{r'_n} \phi_e \left(\frac{\partial \Psi}{\partial r'}\right)_e dr'$$

For well behaved functions ϕ and Ψ, there exists an average value of ϕ_e, denoted by $\bar{\phi}_e$, such that

$$\bar{\phi}_e = \frac{\int_{r'_s}^{r'_n} \phi_e \left(\frac{\partial \Psi}{\partial r'}\right)_e dr'}{\int_{r'_s}^{r'_n} \left(\frac{\partial \Psi}{\partial r'}\right)_e dr'}$$

$$= \frac{Ic_1}{a_\phi (\Psi_{ne} - \Psi_{se})}$$

thus $$Ic_1 = a_\phi \bar{\phi}_e (\Psi_{ne} - \Psi_{se}) \quad . \tag{B.4}$$

Following the upwind-difference scheme described by Gosman et al [16], Ic_1 is expressed as

$$Ic_1 = a_\phi \left[\phi_E \left\{\frac{(\Psi_{ne} - \Psi_{se}) - |\Psi_{ne} - \Psi_{se}|}{2}\right\} + \right.$$

$$\left. + \phi_P \left\{\frac{(\Psi_{ne} - \Psi_{se}) + |\Psi_{ne} - \Psi_{se}|}{2}\right\}\right] \quad . \tag{B.5}$$

The value of stream function at a particular corner of the control volume is assumed to be equal to the average of the value on the four neighbouring nodes. For example:

$$\Psi_{se} \approx \frac{1}{4} (\Psi_{SE} + \Psi_E + \Psi_P + \Psi_S) \tag{B.6}$$

Similar expressions can be obtained for other integrals in equation (B.3). After minor re-arrangements, the final expression for convection term is

$$\text{Icon} = A_E (\phi_P - \phi_E) + A_W (\phi_P - \phi_W) + A_N (\phi_P - \phi_N) + \\ + A_S (\phi_P - \phi_S) \tag{B.7}$$

where

$$A_E = \frac{a_\phi}{8} \{(\Psi_{SE} + \Psi_S - \Psi_{NE} - \Psi_N) + |\Psi_{SE} + \Psi_S - \Psi_{NE} - \Psi_N|\} ,$$

$$A_W = \frac{a_\phi}{8} (\Psi_{NW} + \Psi_N - \Psi_{SW} - \Psi_S) + |\Psi_{NW} + \Psi_N - \Psi_{SW} - \Psi_S|\} ,$$

$$A_N = \frac{a_\phi}{8} (\Psi_{NE} + \Psi_E - \Psi_{NW} - \Psi_W) + |\Psi_{NE} + \Psi_E - \Psi_{NW} - \Psi_W|\} ,$$

and

$$A_S = \frac{a_\phi}{8} (\Psi_{SW} + \Psi_W - \Psi_{SE} - \Psi_E) + |\Psi_{SW} + \Psi_W - \Psi_{SE} - \Psi_E|\} . \tag{B.8}$$

Diffusion Terms (I_{DIFF})

$$I_{DIFF} = \int_{r'_s}^{r'_n} \left[\{ b_1 \frac{\partial}{\partial \theta'} (c\phi) \}_e - \{ b_1 \frac{\partial}{\partial \theta'} (c\phi) \}_\omega \right] dr' +$$

$$+ \int_{\theta'_\omega}^{\theta'_e} \left[\{ b_2 \frac{\partial}{\partial r'} (c\phi) \}_n - \{ b_2 \frac{\partial}{\partial r'} (c\phi) \}_s \right] d\theta' \quad . \qquad (B.9)$$

Let $I_{D1} = \int_{r'_s}^{r'_n} \{ b_1 \frac{\partial}{\partial \theta'} (c\phi) \}_e \, dr'$.

The following assumptions are made:

$$b_{1,e} = (b_{1,P} + b_{1,E})/2 \ ,$$

and

$$\left[\frac{\partial}{\partial \theta'} (c\phi) \right]_e = \frac{c,E \ \phi_E - c,P \ \phi_P}{\theta'_E - \theta'_P} \quad .$$

Thus $I_{D1} = \frac{1}{4} (b_{1,P} + b_{1,E}) \ (c,E \ \phi_E - c,P \ \phi_P) \ \frac{(r'_N - r'_S)}{(\theta'_E - \theta'_P)}$. (B.10)

Evaluating the remaining integrals in equation (B.9) along the same lines, the following expression for diffusion terms is obtained:

$$I_{DIFF} = B_E\,(c,E\;\phi_E - c,P\;\phi_P) + B_W\,(c,W\;\phi_W - c,P\;\phi_P) +$$

$$+ B_N\,(c,N\;\phi_N - c,P\;\phi_P) + B_S\,(c,S\;\phi_S - c,P\;\phi_P), \qquad \text{(B.11)}$$

where

$$\left.\begin{aligned} B_E &= \frac{1}{4}\,(b_{i,P} + b_{1,E})\;\frac{(r'_N - r'_S)}{(\theta'_E - \theta'_P)}\;, \\ B_W &= \frac{1}{4}\,(b_{1,P} + b_{1,W})\;\frac{(r'_N - r'_S)}{(\theta'_P - \theta'_W)}\;, \\ B_N &= \frac{1}{4}\,(b_{2,N} + b_{2,P})\;\frac{(\theta'_E - \theta'_W)}{(r'_N - r'_P)}\;, \\ B_S &= \frac{1}{4}\,(b_{2,S} + B_{2,P})\;\frac{(\theta'_E - \theta'_W)}{(r'_P - r'_S)}\;. \end{aligned}\right\} \qquad \text{(B.12)}$$

Source Terms (I_{SOR})

$$I_{SOR} = \int_{r'_s}^{r'_n}\int_{\theta'_\omega}^{\theta'_e} d\;dr'd\theta' \quad .$$

It is assumed that d is uniform over the control volume and takes on the value at node P. Thus, the following can be approximated:

$$I_{SOR} \approx d,P \quad V_P \;, \qquad \text{(B.13)}$$

where

$$V_P = \frac{1}{4} (\theta'_E - \theta'_W) \quad (r'_N - r'_S) \quad .$$

Combining the convection, diffusion and source terms, one obtains:

$$\phi_P = C_E\phi_E + C_W\phi_W + C_N\phi_N + C_S\phi_S + D, \tag{B.14}$$

where

$$\left.\begin{aligned} C_E &= (A_E + B_E\ c,E)/\Sigma_{AB} \ , \\ C_W &= (A_W + B_W\ c,W)/\Sigma_{AB} \ , \\ C_N &= (A_N + B_N\ c,N)/\Sigma_{AB} \ , \\ C_S &= (A_S + B_S\ c,S)/\Sigma_{AB} \ , \\ D &= d,p \cdot Vp/\Sigma_{AB} \ , \end{aligned}\right\} \tag{B.15}$$

and

$$\Sigma_{AB} = A_E + A_W + A_N + A_S + c,P\ (B_E + B_W + B_N + B_S) \quad .$$

APPENDIX C

FINITE DIFFERENCE REPRESENTATION OF DERIVATIVES

1) First Derivatives

First derivatives of a general variable ϕ with respect to spatial variables r' and θ', at the node P, can be put in central difference form as:

$$\left(\frac{\partial\phi}{\partial r'}\right)_P = \frac{(h_s/h_n)(\phi_N-\phi_P) + (h_n/h_s)(\phi_P-\phi_S)}{(h_s+h_n)} , \tag{C.1}$$

and

$$\left(\frac{1}{r'}\ \frac{\partial\phi}{\partial\theta'}\right)_P = \frac{(h_w/h_e)(\phi_E-\phi_P) + (h_e/h_w)(\phi_P-\phi_W)}{(h_e+h_w)} ,$$

where h_e, h_w, h_n, and h_s are the distances shown in Figure C1.

When the grids are uniformly spaced, the above relations reduce to:

$$\left(\frac{\partial\phi}{\partial r'}\right)_P = \frac{\phi_N-\phi_S}{2h} ,$$

and

$$\left(\frac{1}{r'}\ \frac{\partial\phi}{\partial\theta'}\right)_P = \frac{\phi_E-\phi_W}{2h'} , \tag{C.2}$$

where

$$h = h_s = h_n$$

and

$$h' = h_e = h_w .$$

Sometimes it is not possible to express the derivatives in the central difference form as the values of the variables on both sides of a node (see Figures C2 and C3) are not available. In such cases, the derivatives can be expressed in forward or backward difference as follows:

Forward Difference

$$\left(\frac{\partial\phi}{\partial r'}\right)_1 = \phi_2 \frac{\Delta 1+\Delta 2}{\Delta 1\ \Delta 2} - \phi_3 \frac{\Delta 1}{\Delta 2(\Delta 1+\Delta 2)} - \phi_1 \frac{2\Delta 1+\Delta 2}{\Delta 1(\Delta 1+\Delta 2)} \quad . \tag{C.3}$$

Backward Difference

$$\left(\frac{\partial\phi}{\partial r'}\right)_1 = \phi_1 \frac{\Delta 2+2\Delta 1}{\Delta 1(\Delta 1+\Delta 2)} - \phi_2 \frac{\Delta 1+\Delta 2}{\Delta 1\Delta 2} + \phi_3 \frac{\Delta 1}{\Delta 2(\Delta 1+\Delta 2)} \quad . \tag{C.4}$$

For uniformly spaced grids, $\Delta 1=\Delta=\Delta 2$. Thus equations (C.3) and (C.4) reduce to:

$$\left(\frac{\partial\phi}{\partial r'}\right)_1 = \frac{2\phi_2}{\Delta} - \frac{\phi_3}{2\Delta} - \frac{3}{2}\frac{\phi_1}{\Delta}, \tag{C.5}$$

and

$$\left(\frac{\partial\phi}{\partial r'}\right)_1 = \frac{3}{2}\ \frac{\phi_1}{\Delta} - \frac{2}{\Delta}\phi_2 + \frac{1}{2}\frac{\phi_3}{\Delta}, \quad \text{respectively.} \tag{C.6}$$

Equations (C.3) through (C.6) are also valid for derivatives with respect to θ' provided Δ's represents distances in the θ'-direction.

2) Second Derivatives

Second derivatives can be represented in finite difference form by using the formulae for first derivatives already developed in this Appendix. For example:

$$\left(\frac{\partial^2\phi}{\partial r'^2}\right)_P = \frac{(h_s/h_n)\ \{\left(\frac{\partial\phi}{\partial r'}\right)_N - \left(\frac{\partial\phi}{\partial r'}\right)_P\} + (h_n/h_s)\ \{\left(\frac{\partial\phi}{\partial r'}\right)_P - \left(\frac{\partial\phi}{\partial r'}\right)_s\}}{(h_s + h_n)} \quad . \tag{C.7}$$

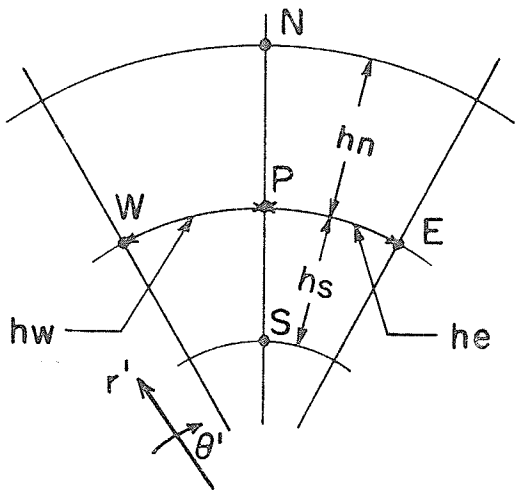

Figure C.1: Central Difference

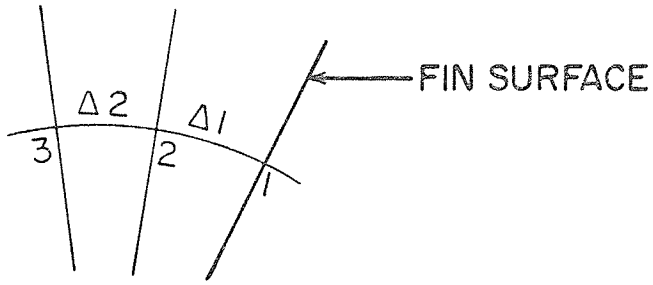

Figure C.2: Forward Difference

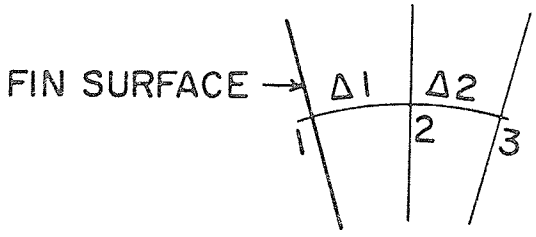

Figure C.3: Backward Difference

APPENDIX D

DERIVATION OF BOUNDARY CONDITIONS FOR VORTICITY

Tube Wall

Following Date [17], in the near wall region, the following velocity profiles are assumed:

$$V_\theta = ay + by^2$$

$$V_r = 0 \qquad (D.1)$$

and

$$V_z = cy$$

where a, b, and c are constants and y is the distance from the wall (see Figure 5). Thus the definition of vorticity, equation (3.15), gives:

$$\omega = (a + 2by) - \frac{(ay + by^2)}{(r_o - y)} \qquad (D.2)$$

and the definition of stream function, equation (3.17a), gives

$$\frac{\partial \Psi}{\partial y} = - \rho \{ay + by^2 + \frac{\alpha}{r_o} c (r_o y - y^2)\} \qquad (D.3)$$

where

$$c = V_{z,no/n}$$

From equation (D.2), the vorticity at y=o and y=n are:

$$\omega_o = a, \text{ and} \tag{D.4}$$

$$\omega_{no} = \omega_o \frac{(r_o-2n)}{(r_o-n)} + bn \frac{(2r_o-3n)}{(r_o-n)} \quad , \text{ respectively.}$$

Integrating equation (D.3) from y=o to y=n and substituting the values of a, b, and c, the following expression for ω_o is obtained after some algebraic manipulations

$$\omega_o = \frac{6(3n - 2r_o)}{(5n - 4r_o)} \frac{(\Psi_o - \Psi_{no})}{\rho n^2} - \frac{2(n - r_o)}{(5n - 4r_o)} \omega_{no} -$$

$$- \frac{\alpha}{r_o} \frac{(3r_o - 2n)}{n(5n - 4r_o)} \frac{(3n - 2r_o)}{} V_{z,no} \cdot \tag{D.5}$$

Fin Surface

The following velocity profiles are assumed in the near wall region:

$$V_\theta = 0$$

$$V_r = ay + by^2 \tag{D.6}$$

$$V_z = cy$$

where

$$y = r'\theta' \quad .$$

Following an analysis paralleling that for the tube wall, one obtains:

$$\omega_o = \frac{3\,(\Psi_o - \Psi_{no})}{\rho n^2} - \frac{1}{2}\,\omega_{no} \quad . \tag{D.7}$$

Center Node

This boundary is treated as one of zero radius. The following velocity profiles are assumed in the region near the center node:

$$\begin{aligned} V_\theta &= ar' + br'^2 \\ V_{r'} &= 0 \\ V_z &= cr' \end{aligned} \quad . \tag{D.8}$$

An analysis similar to those for the tube wall and fin surfaces finally yields:

$$\omega_o = \frac{36}{5}\,\frac{(\Psi_o - \Psi_{no})}{\rho n^2} - \frac{4}{5}\,\omega_{no} + \frac{\alpha}{r_o}\,\frac{12}{5}\,V_{z,no} \tag{D.9}$$

APPENDIX E

FLOW CHART AND LISTING

OF THE COMPUTER PROGRAMME

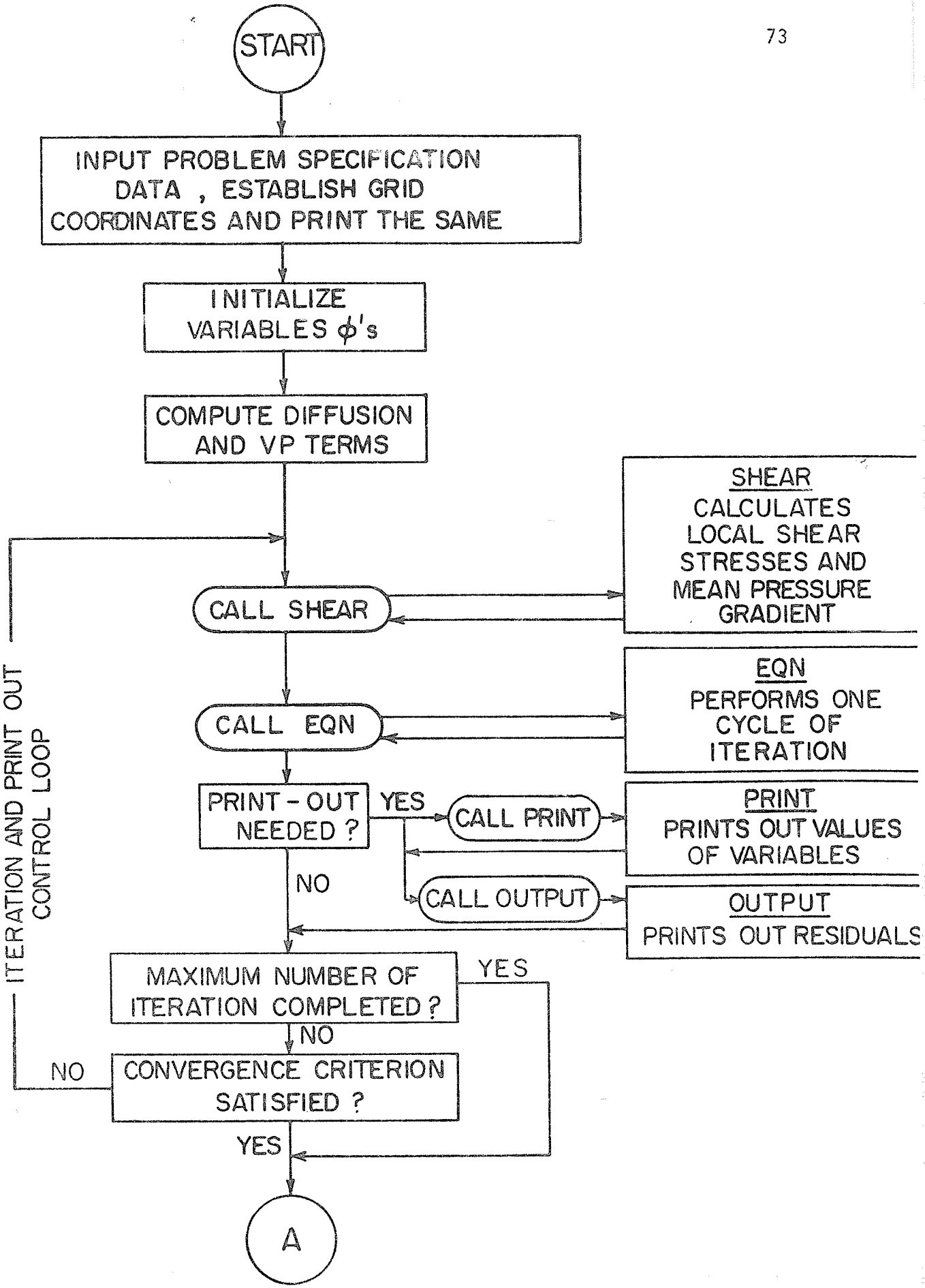
START
INPUT PROBLEM SPECIFICATION DATA , ESTABLISH GRID COORDINATES AND PRINT THE SAME
INITIALIZE VARIABLES φ's
COMPUTE DIFFUSION AND VP TERMS
CALL SHEAR
SHEAR
CALCULATES LOCAL SHEAR STRESSES AND MEAN PRESSURE GRADIENT
CALL EQN
EQN
PERFORMS ONE CYCLE OF ITERATION
PRINT - OUT NEEDED ?
YES
CALL PRINT
PRINT
PRINTS OUT VALUES OF VARIABLES
NO
CALL OUTPUT
OUTPUT
PRINTS OUT RESIDUALS
ITERATION AND PRINT OUT CONTROL LOOP
MAXIMUM NUMBER OF ITERATION COMPLETED ?
YES
NO
NO
CONVERGENCE CRITERION SATISFIED ?
YES
A

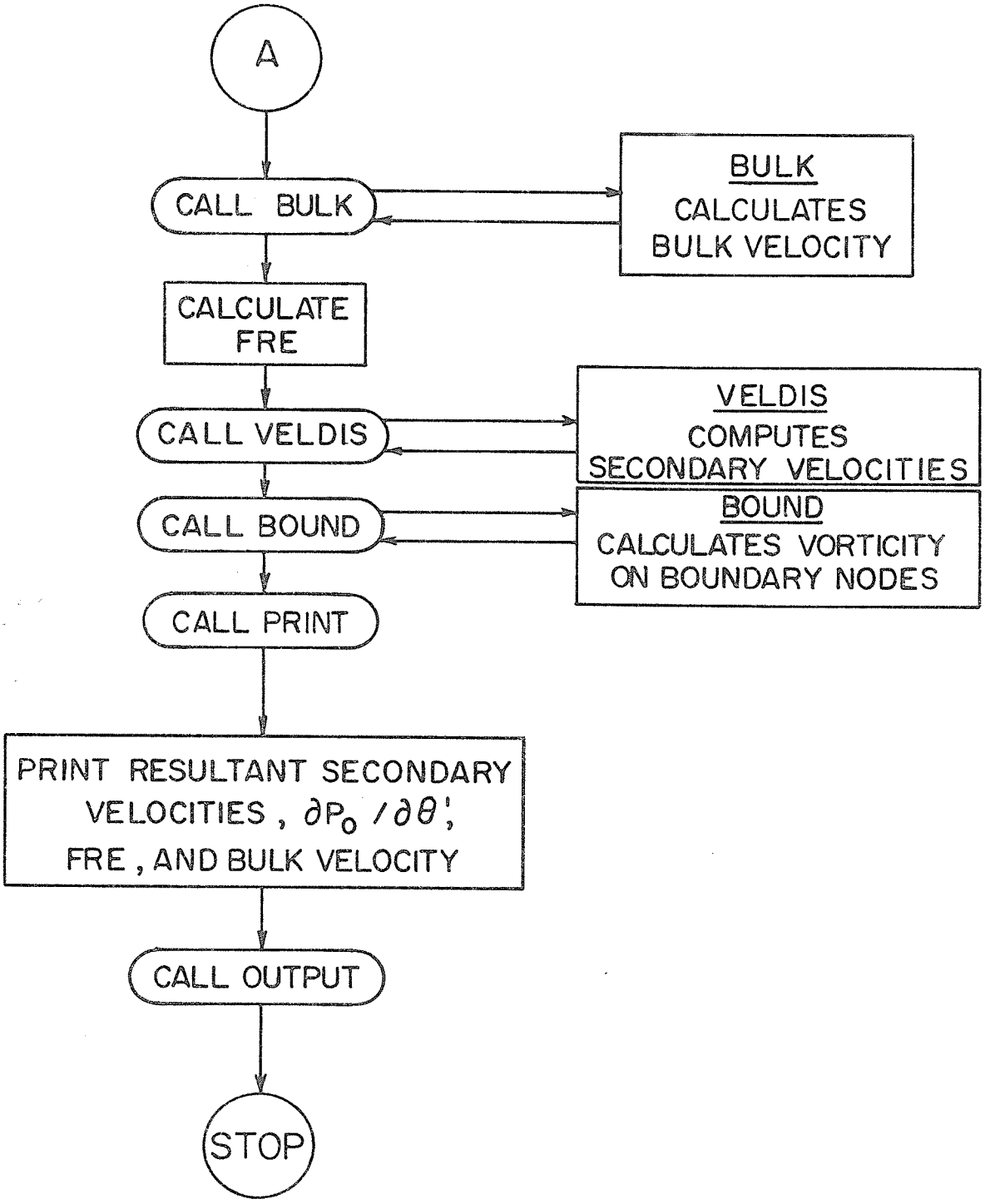
A
CALL BULK
BULK
CALCULATES
BULK VELOCITY
CALCULATE
FRE
CALL VELDIS
VELDIS
COMPUTES
SECONDARY VELOCITIES
CALL BOUND
BOUND
CALCULATES VORTICITY
ON BOUNDARY NODES
CALL PRINT
PRINT RESULTANT SECONDARY
VELOCITIES , $\partial P_0 / \partial \theta$,
FRE , AND BULK VELOCITY
CALL OUTPUT
STOP

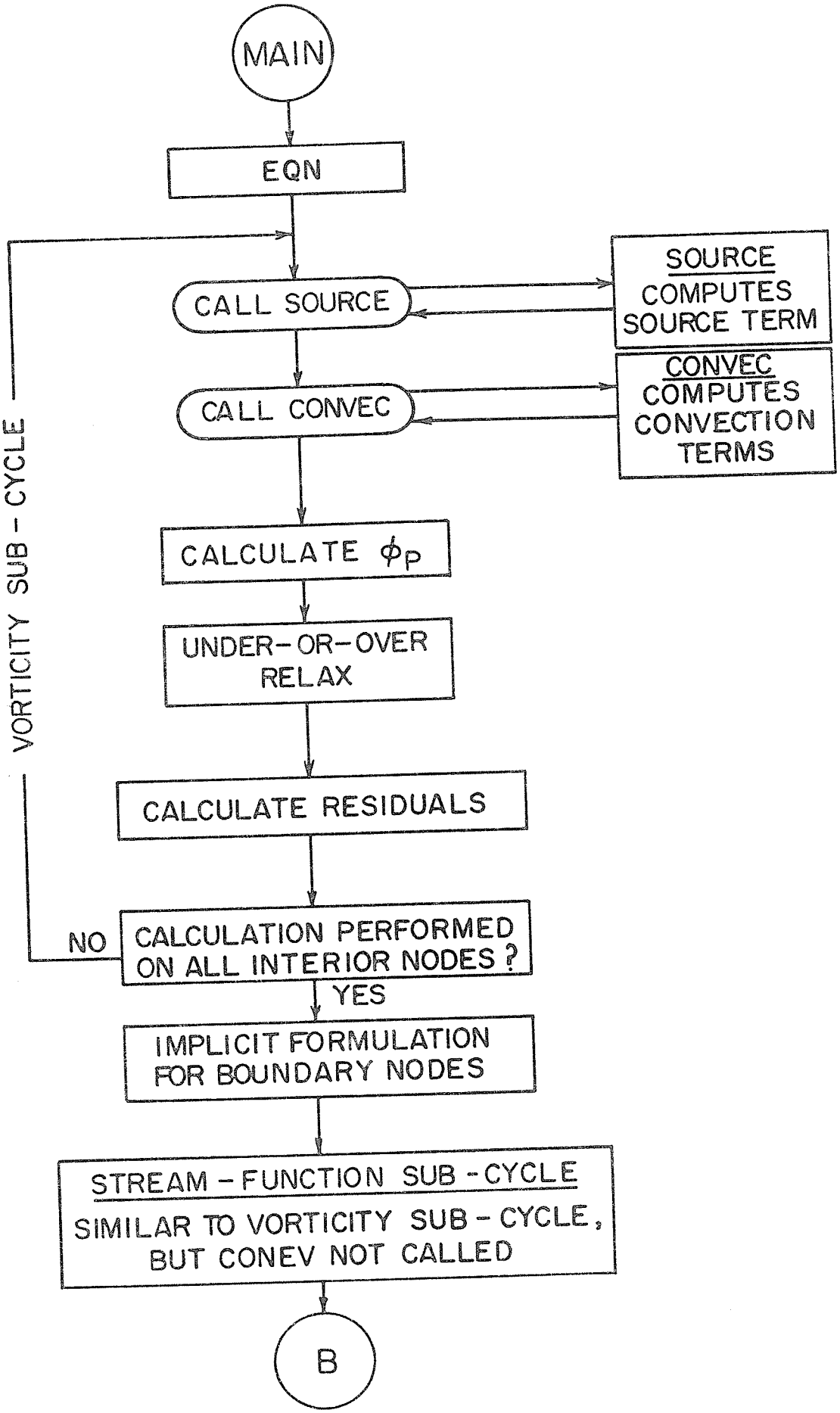
MAIN
EQN
CALL SOURCE
SOURCE
COMPUTES
SOURCE TERM
CALL CONVEC
CONVEC
COMPUTES
CONVECTION
TERMS
CALCULATE ϕ_P
UNDER-OR-OVER
RELAX
CALCULATE RESIDUALS
NO
CALCULATION PERFORMED
ON ALL INTERIOR NODES ?
YES
IMPLICIT FORMULATION
FOR BOUNDARY NODES
STREAM - FUNCTION SUB - CYCLE
SIMILAR TO VORTICITY SUB - CYCLE,
BUT CONEV NOT CALLED
B
VORTICITY SUB - CYCLE

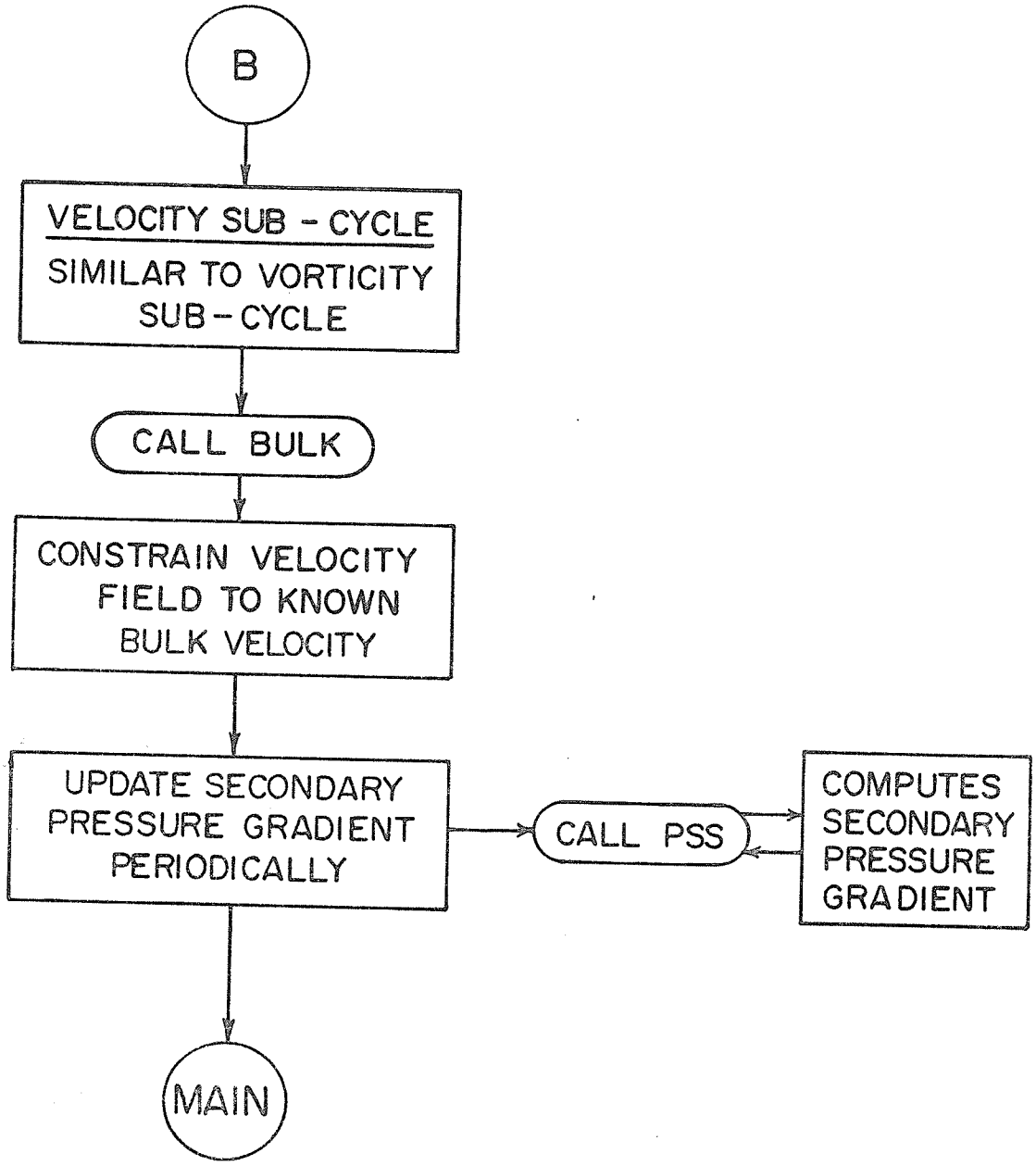
B
VELOCITY SUB - CYCLE
SIMILAR TO VORTICITY SUB - CYCLE
CALL BULK
CONSTRAIN VELOCITY FIELD TO KNOWN BULK VELOCITY
UPDATE SECONDARY PRESSURE GRADIENT PERIODICALLY
CALL PSS
COMPUTES SECONDARY PRESSURE GRADIENT
MAIN

```
      IMPLICIT REAL (A-H,O-Z)
      DIMENSION A(20,20,5),VZVM(20,20),DPDTHA(20,20),RSDU(3),
     * RES(3),CC(3),RP(3),VSVM(20,20),DUDR(20),DUDT1(20),DUDT2(20),
     * STREAM(20,20),DIREC(20,20)
      COMMON /CG/ X1(20),X2(20),VP(20,20)
      COMMON /CB/ BE(20,20,3),BW(20,20,3),BN(20,20,3),BS(20,20,3)
      COMMON /CP/ RSS(20,20,3),UB
      COMMON /CR/ NNF,FH,R0,AF,PS,AL,ROW,AMEW,NITER,BETA
      COMMON /CX/ AREA,AVG,SUM1,SUM2,SUM3,AREA1,AREA2,AREA3,AVG1,AVG2,
     * AVG3
CC    ************************************************************
CC    SPIRAL FINS OF FINITE THICKNESS AND FULL LENGTH
CC    DIMENSIONAL FORMULATION
CC    ************************************************************
      DATA IN,JN,KN /20,20,5/
      DATA NW,NF,NVZ,NV1,NV2 /1,2,3,4,5/
      DATA IEN,IV /3,5/
      DATA RSDU /3*0.0/
      DATA DPDTHA /400*0.0/
      DATA VSVM /400*0.0/
      DATA STREAM /400*0.0/
      NMAX=1
      NPRINT=3000
      NP=25
      NOP=1
      NOT=1
CC    CONVERGENCE CRITERION
      CC(NW)=0.001
      CC(NF)=0.001
      CC(NVZ)=0.001
CC    RELAXATION PARAMETERS
      RP(NW)=1.0
      RP(NF)=1.0
      RP(NVZ)=1.0
CC    DIMENSIONLESS FIN HIGHT
      H=1.0
CC    TUBE RADIUS ( METERS )
      R0=0.02
CC    FIN HIGHT ( METER )
      FH=H*R0
CC    RADIUS AT THE TIP OF THE FIN ( METER )
      RI=R0-FH
CC    NUMBER OF FINS
      NNF=8
CC    HALF FIN ANGLE
      PI=3.14159
      BETAD=3.0
      BETA=BETAD*PI/180.
CC    TOTAL FLOW AREA ( SQ. METERS )
      AF=R0*R0*(PI-NNF*BETA*(2.*H-H*H))
CC    TWIST RATIO
      AL=0.3
      IF(AL.EQ.0.0)CC(NVZ)=0.00001
      PS=AL/R0
```

```
CC      DENSITY OF AIR ( KG/CU. METER )
        ROW=1.204
CC      VISCOSITY OF AIR ( KG/M-S )
        AMEW=1.817 E-05
CC      REYNOLDS NUMBER
        RE=1000.
CC      MASS FLOW RATE
        FRATE=RE*PI*RO*AMEW/2.
CC      BULK VELOCITY
        UB=FRATE/(ROW*AF)
CC      COMPUTE GRID COORDINATES
CC      CIRCUMERENTIAL DIRECTION
        ALPHAR=2.*(PI/NNF-BETA)
        N1=15
        X1(1)=0.0
        DO 1 I=2,N1
        X1(I)=X1(I-1)+ALPHAR/(N1-1)
1       CONTINUE
CC      RADIAL DIRECTION
        N2=15
        X2(1)=0.0
        DO 2 J=2,N2
        X2(J)=X2(J-1)+RO/(N2-1)
2       CONTINUE
CC      PRINT OUT COORDINATES
        PRINT 500, (X1(I), I=1,N1)
        PRINT 510, (X2(J), J=1,N2)
        PRINT 560, NNF,FH,AL,NMAX,RE,UB
        PRINT 557, CC(NW),CC(NF),CC(NVZ)
        PRINT 570, (RP(K), K=1,IEN)
CC      INITIALIZE FLOW FIELD
        IDATA=0
        IF(IDATA .EQ. 0) GO TO 34
        DO 35 K=1,3
        DO 35 J=1,N2
        READ (1,400) (A(I,J,K), I=1,N1)
35      CONTINUE
        DO 36 J=1,N2
        READ (1,400) (DPDTHA(I,J), I=1,N1)
36      CONTINUE
        CALL  VELDIS(IN,JN,KN,A,N1,N2)
        GO TO 37
CC      AXIAL VORTICITY ( 1/SEC )
34      DO 20 I=1,N1
        DO 20 J=1,N2
        A(I,J,NW)=0.0
20      CONTINUE
CC      STREAM FUNCTION ( KG/M-S )
        DO 30 I=1,N1
        DO 30 J=1,N2
        A(I,J,NF)=0.0
30      CONTINUE
CC      AXIAL VELOCITY ( M/S )
        DO 40 I=1,N1
```

```
      DO 40 J=1,N2
      A(I,J,NVZ)=UB
      IF(I .EQ.1 .OR. I .EQ. N1 .OR. J .EQ. 1 .OR. J .EQ. N2)
     * A(I,J,NVZ)=0.
40    CONTINUE
CC    SECONDARY VELOCITIES ( M/S )
      DO 50 K=NV1,NV2
      DO 50 J=1,N2
      DO 50 I=1,N1
      A(I,J,K)=0.0
50    CONTINUE
CC    SET RESIDUAL FIELD TO ZERO
37    DO 60 K=1,3
      DO 60 I=1,N1
      DO 60 J=1,N2
      RSS(I,J,K)=0.0
60    CONTINUE
CC    COMPUTE VP TERMS
      INM=N1-1
      JNM=N2-1
      DO 70 J=2,JNM
      DO 70 I=2,INM
      VP(I,J)=0.25*(X1(I+1)-X1(I-1))*(X2(J+1)-X2(J-1))
70    CONTINUE
CC    COMPUTE DIFFUSION TERMS
      KK=NW
      IF(AL.EQ.0.0)KK=NVZ
      DO 80 K=KK,NVZ
      DO 80 J=2,JNM
      DO 80 I=2,INM
      B=X2(J+1)-X2(J-1)
      C=X1(I+1)-X1(I)
      D=X1(I)-X1(I-1)
      E=X1(I+1)-X1(I-1)
      F=X2(J+1)-X2(J)
      G=X2(J)-X2(J-1)
      RSQE=2.0*AMEW*(1.0/X2(J) + PS*PS*X2(J))
      RSQW=RSQE
      RSQN=AMEW*(X2(J+1)+X2(J))
      RSQS=AMEW*(X2(J-1)+X2(J))
      IF(K.NE.NF) GO TO 103
      RSQE=2.0/(ROW*X2(J))
      RSQW=RSQE
      RSQN=(X2(J+1)+X2(J))/ROW
      RSQS=(X2(J-1)+X2(J))/ROW
103   BE(I,J,K)=0.25*RSQE*B/C
      BW(I,J,K)=0.25*RSQW*B/D
      BN(I,J,K)=0.25*RSQN*E/F
      BS(I,J,K)=0.25*RSQS*E/G
80    CONTINUE
CC    COMPUTE BULK VELOCITY
      CALL  BULK(IN,JN,KN,A,N1,N2,UBAR)
      PRINT 558, UBAR
      PRINT 580
```

```
CC      ITERATION AND PRINT OUT CONTROL LOOP
        DO 90 NITER=1,NMAX
CC      CAUSE ONE CYCLE OF ITERATION TO BE PERFORMED
        CALL  SHEAR(IN,JN,KN,A,N1,N2,DPDZ,DUDR,DUDT1,DUDT2)
        CALL  EQN(IN,JN,KN,A,N1,N2,RP,RSDU,DPDZ,DPDTHA)
CC      TEST IF PRINT OUT TO BE PERFORMED
        IF(MOD(NITER,NPRINT).NE.0) GO TO 100
        CALL  PRINT(IN,JN,KN,A,N1,N2,1,IEN)
        CALL  OUTPUT(N1,N2,1,IEN)
100     IF(MOD(NITER,NP).NE.0) GO TO 110
        F=ABS(DPDZ)*(R0**5)*ROW*PI*PI/(FRATE**2)
        FRE=F*RE
        PRINT 590, NITER,(RSDU(K),K=1,IEN),FRE
110     RES(1)=RSDU(1)
        RES(2)=RSDU(2)
        RES(3)=RSDU(3)
        RSDU(1)=0.0
        RSDU(2)=0.0
        RSDU(3)=0.0
CC      TEST IF CONVERGENCE CRITERION IS SATISFIED
        IF(ABS(RES(1)).LE.ABS(CC(1)).AND.ABS(RES(2)).LE.ABS(CC(2))
     * .AND.ABS(RES(3)).LE.ABS(CC(3))) GO TO 120
90      CONTINUE
CC      END OF LOOP
        IF(NITER.EQ.NMAX+1) GO TO 140
120     PRINT 600, NITER
CC      CALCULATE BULK VELOCITY
        CALL  BULK(IN,JN,KN,A,N1,N2,UBAR)
CC      CALCULATE REYNOLDS NUMBER
        FRATE=ROW*AF*UBAR
        RE=2.*FRATE/(PI*R0*AMEW)
CC      CALCULATE FRICTION FACTOR
        F=ABS(DPDZ)*(R0**5)*ROW*PI*PI/(FRATE**2)
        FRE=F*RE
        IF(AL.EQ.0.0)GO TO 700
CC      OBTAIN VELOCITY COMPONENTS
        CALL  VELDIS(IN,JN,KN,A,N1,N2)
CC      CALCULATE WALL VORTICITIES
        CALL  BOUND(IN,JN,KN,A,N1,N2)
CC      FINAL PRINT OUT
        CALL  PRINT(IN,JN,KN,A,N1,N2,1,IV)
        GO TO 701
700     CALL  PRINT(IN,JN,KN,A,N1,N2,NVZ,NVZ)
701     PRINT 610, UBAR,RE,FRE
CC      AXIAL VELOCITY NORMALIZED BY BULK VELOCITY
        DO 11 J=1,N2
        DO 11 I=1,N1
        VZVM(I,J)=A(I,J,NVZ)/UBAR
11      CONTINUE
        PRINT 15
        DO 16 J=1,N2
        PRINT 17, (VZVM(I,J), I=1,N1)
        PRINT 18, J
16      CONTINUE
```

```
      IF(AL.EQ.0.0)GO TO 702
CC    DIMENSIONLESS STREAM FUNCTION
      DO 666 J=1,N2
      DO 666 I=1,N1
      STREAM(I,J)=A(I,J,NF)/AMEW
666   CONTINUE
      PRINT 27
      DO 28 J=1,N2
      PRINT 17, (DPDTHA(I,J), I=1,N1)
      PRINT 18, J
28    CONTINUE
CC    CALCULATE RESULTANT SECONDARY VELOCITY
      PRINT 55
      DO 51 J=1,N2
      DO 51 I=1,N1
      VSVM(I,J)=SQRT(A(I,J,NV1)*A(I,J,NV1)+A(I,J,NV2)*
     * A(I,J,NV2))/UBAR
51    CONTINUE
      DO 52 J=1,N2
      PRINT 17, (VSVM(I,J), I=1,N1)
      PRINT 18, J
52    CONTINUE
CC    CALCULATE DIRECTION OF RESULTANT VELOCITY
      DO 137 J=2,JNM
      DO 137 I=2,INM
      DIREC(I,J)=ATAN2(A(I,J,NV1),A(I,J,NV2))
      DIREC(I,J)=DIREC(I,J)*180./PI
137   CONTINUE
      PRINT 159
      DO 139 J=2,JNM
      PRINT 17, (DIREC(I,J), I=2,INM)
139   CONTINUE
CC    PRINT OUT RESIDUALS
      CALL  OUTPUT(N1,N1,1,IEN)
      GO TO 703
702   CALL  OUTPUT(N1,N2,NVZ,NVZ)
      GO TO 704
703   IF(NOP.EQ.1)GO TO 704
      DO 32 K=1,3
      DO 32 J=1,N2
      WRITE(2,400) (A(I,J,K), I=1,N1)
32    CONTINUE
      DO 33 J=1,N2
      WRITE(2,400) (DPDTHA(I,J), I=1,N1)
33    CONTINUE
CC    STORE VZVM
      DO 706 J=1,N2
      WRITE(2,400) (VZVM(I,J), I=1,N1)
706   CONTINUE
CC    CALCULATE LOCAL WALL SHEAR STRESSES
704   CALL SHEAR(IN,JN,KN,A,N1,N2,DPDZW,DUDR,DUDT1,DUDT2)
      PRINT 56
      PRINT 17,(DUDR(I), I=1, N1)
      PRINT 57
```

```
      PRINT 17,(DUDT1(J), J=1, N2)
      PRINT 57
      PRINT 17,(DUDT2(J), J=1, N2)
      PRINT 444, DPDZW, AVG, AREA, SUM1,SUM2,SUM3,AREA1,AREA2,AREA3,
     * AVG1,AVG2,AVG3
      CALL  BULKS(IN,JN,VSVM,N1,N2,SMEAN)
      PRINT 445, SMEAN
      IF(AL .EQ. 0.0 .OR. NOT .EQ.1) GO TO 3
CC    PUNCH CARDS
      DO 667 J=1,N2
      PUNCH 668, (VZVM(I,J), I=1,N1)
667   CONTINUE
      DO 669 J=1,N2
      PUNCH 668, (STREAM(I,J), I=1,N1)
669   CONTINUE
      GO TO 3
140   PRINT 620, NMAX
      CALL  BOUND(IN,JN,KN,A,N1,N2)
      CALL  PRINT(IN,JN,KN,A,N1,N2,1,IEN)
      CALL  OUTPUT(N1,N2,1,IEN)
      CALL  BULK(IN,JN,KN,A,N1,N2,UBAR)
      FRATE=ROW*AF*UBAR
      RE=2.*FRATE/(PI*R0*AMEW)
      PRINT 630, UBAR,RE
      CALL  SHEAR(IN,JN,KN,A,N1,N2,DPDZW,DUDR,DUDT1,DUDT2)
      PRINT 444, DPDZW, AVG, AREA, SUM1,SUM2,SUM3,AREA1,AREA2,AREA3,
     * AVG1,AVG2,AVG3
      CALL  BULKS(IN,JN,VSVM,N1,N2,SMEAN)
      PRINT 445, SMEAN
3     CONTINUE
      STOP
500   FORMAT('1',10X,'DISTANCE IN ANGULAR DIRECTION ( IN RADIANS )'/
     * /('0',4F25.6))
510   FORMAT('-'///' ',10X,'DISTANCE IN RADIAL DIRECTION ',
     * '( IN METERS )'//('0',4F25.5))
570   FORMAT('0',10X,'RELAXATION PARAMETERS FOR VORTICITY,STREAM',
     * ' FUNCTION AND AXIAL VELOCITY ARE RESPECTIVELY --'/'0',
     * 3(10X,F6.3))
560   FORMAT('-'///' ',10X,'THE INITIAL INFORMATION SUPPLIED',
     * '  IS --- , '//'0',10X,'NUMBER OF FINS,NNF=',I4/'0',10X,
     * 'FIN HIGHT,FH ( METERS )  =',F5.2/'0',10X,'TWIST RATIO',
     * ' AL =',F6.3/'0',10X,'MAXIMUM NUMBER OF ITERATIONS',
     * ',NMAX=',I6/'0',10X,'REYNOLDS NUMBER,RE=',F8.1/'0',10X,
     * 'BULK VELOCITY,UB=',E16.7///)
580   FORMAT('-'//' ',10X,'MAXIMUM RESIDUAL FOR EACH VARIABLE'/'0',
     * 10X,'NITER',6X,'VORTICITY',6X,'STREAM FUN.',6X,'AXIAL VEL'/)
590   FORMAT(' ',10X,I6,4(6X,F11.6),5X,F11.6,5X,F11.6)
600   FORMAT('-'///' ',10X,'CONVERGED SOLUTION REQUIRING ',I6,
     * ' ITERATIONS FOLLOWS'/)
620   FORMAT('0',10X,'THE PROCESS DID NOT CONVERGE IN ',I6,
     * ' ITERATIONS'/)
557   FORMAT('-',10X,'CONVERGENCE CRITERION FOR VORTICITY,CC(1)=',
     * F11.6/'0',10X,'CONVERGENCE CRITERION FOR STREAM FUNCTION,',
     * 'CC(2)=',F11.6/'0',10X,'CONVERGENCE CRITERION FOR AXIAL ',
```

```
     * 'VELOCITY,CC(3)=',F11.6//)
 558   FORMAT('-',10X,'UBAR=',E16.7//)
 610   FORMAT(' '///'0',10X,'BULK VELOCITY, UBAR=',E16.7/'0',10X,
     * 'REYNOLDS NUMBER, RE=',F11.1/'0',10X,'FRICTION FACTOR ',
     * 'TIMES REYNOLDS NUMBER, FRE=',E16.7//)
  15   FORMAT('1',30X,'AXIAL VELOCITY NORMALIZED BY BULK VELOCITY'/
     * '0',129X,'J'//)
  17   FORMAT('0',7E11.4)
  18   FORMAT('+',129X,I2)
  27   FORMAT('1',50X,'DPDTHA'/)
 400   FORMAT(' ',7E11.4)
 668   FORMAT(7E11.4)
  55   FORMAT(' '///' ',20X,'SECONDARY VELOCITY NORMALIZED BY ',
     * 'BULK VELOCITY'/)
 630   FORMAT('-',10X,'BULK VELOCITY, UBAR=',E16.7/'0',10X,
     * 'REYNOLDS NUMBER, RE=',F8.1//)
  56   FORMAT('-'//' ',10X,'LOCAL WALL SHEAR STRESSES NORMALIZED ',
     * 'BY AVERAGE WALL SHEAR STRESS'//'-',10X,'TUBE WALL'/)
  57   FORMAT('-',10X,'FIN SURFACE'/)
 444   FORMAT('-',10X,'PRESSURE GRADIENT VIA WALL SHEAR STRESS = ',
     * F10.6//' ',10X,'AVERAGE WALL SHEAR STRESS =',E16.7//' ',
     * 'SURFACE AREA PER CELL PER UNIT AXIAL LENGTH =',E16.7//'-',10X,
     * 'SUM1=',E16.7,2X,'SUM2=',E16.7,2X,'SUM3=',E16.7//'-',10X,
     * 'AREA1=',E16.7,2X,'AREA2=',E16.7,2X,'AREA3=',E16.7//'-',10X,
     * 'AVG1=',E16.7,2X,'AVG2=',E16.7,2X,'AVG3=',E16.7///)
 445   FORMAT('-',10X,'MEAN SECONDARY VELOCITY =',E11.4//)
 159   FORMAT('-',30X,'RESULTANT VELOCITY DIRECTION'//)
       END
CC     SUBROUTINE FOR CALCULATING BULK VELOCITY BY INTEGRATION
       SUBROUTINE  BULK(IN,JN,KN,A,N1,N2,UBAR)
       DIMENSION A(IN,JN,KN),SUM(20),AAA(20,20)
       COMMON /CG/ X1(20),X2(20),VP(20,20)
       COMMON /CR/ NNF,FH,RO,AF,PS,AL,ROW,AMEW,NITER,BETA
       C0=0.0
       PI=3.14159
       ALPHAR=2.*(PI/NNF-BETA)
       DR=RO/(N2-1)
       DT=ALPHAR/(N1-1)
       DO 1 I=1,N1
       DO 1 J=1,N2
       AAA(I,J)=A(I,J,3)
       IF(I.EQ.1)AAA(I,J)=C0*A(I+1,J,3)
       IF(I.EQ.N1)AAA(I,J)=C0*A(I-1,J,3)
1      CONTINUE
       DO 10 J=1,N2
       SUM(J)=0.
       DO 10 I=1,N1
       K=2
       IF(MOD(I,2).EQ.0)K=4
       IF(I.EQ.1 .OR. I.EQ.N1)K=1
       SUM(J)=SUM(J)+DT*AAA(I,J)*K/3.
10     CONTINUE
       IF(SUM(1).EQ.0.0)SUM(1)=C0*SUM(2)
       IF(SUM(N2).EQ.0.0)SUM(N2)=C0*SUM(N2-1)
```

```
      TOTAL=0.
      DO 20 J=1,N2
      K=2
      IF(MOD(J,2).EQ.0) K=4
      IF(J.EQ.1 .OR. J.EQ.N2)K=1
      TOTAL=TOTAL+DR*SUM(J)*X2(J)*K/3.
20    CONTINUE
      UBAR=TOTAL*NNF/AF
      RETURN
      END
CC    SUBROUTINE FOR CALCULATING MEAN SECONDARY VELOCITY
      SUBROUTINE  BULKS(IN,JN,VSVM,N1,N2,SMEAN)
      IMPLICIT REAL (A-H,O-Z)
      DIMENSION VSVM(20,20),SUM(20)
      COMMON /CG/ X1(20),X2(20),VP(20,20)
      COMMON /CR/ NNF,FH,RO,AF,PS,AL,ROW,AMEW,NITER,BETA
      PI=3.14159
      ALPHAR=2.*(PI/NNF-BETA)
      DR=RO/(N2-1)
      DT=ALPHAR/(N1-1)
      DO 10 J=1,N2
      SUM(J)=0.
      DO 10 I=1,N1
      K=2
      IF(MOD(I,2).EQ.0)K=4
      IF(I.EQ.1 .OR. I.EQ.N1)K=1
      SUM(J)=SUM(J)+DT*VSVM(I,J)*K/3.
10    CONTINUE
      TOTAL=0.
      DO 20 J=1,N2
      K=2
      IF(MOD(J,2).EQ.0) K=4
      IF(J.EQ.1 .OR. J.EQ.N2)K=1
      TOTAL=TOTAL+DR*SUM(J)*X2(J)*K/3.
20    CONTINUE
      SMEAN=TOTAL*NNF/AF
      RETURN
      END
CC    ITERATION SUBROUTINE
      SUBROUTINE  EQN(IN,JN,KN,A,N1,N2,RP,RSDU,DPDZ,DPDTHA)
      IMPLICIT REAL (A-H,O-Z)
      DIMENSION A(IN,JN,KN),RSDU(3),RP(3),DPDTHA(20,20),ZVZ(20,20)
      COMMON /CG/ X1(20),X2(20),VP(20,20)
      COMMON /CB/ BE(20,20,3),BW(20,20,3),BN(20,20,3),BS(20,20,3)
      COMMON /CP/ RSS(20,20,3),UB
      COMMON /CR/ NNF,FH,RO,AF,PS,AL,ROW,AMEW,NITER,BETA
      DATA NW,NF,NVZ /1,2,3/
      INM=N1-1
      JNM=N2-1
      IF(AL .EQ. 0.0) GO TO 101
CC    AXIAL VORTICITY SUBCYCLE
      INMM=INM-1
      JNMM=JNM-1
      DO 10 J=3,JNMM
```

```
      DO 20 I=3,INMM
CC    CALCULATE SOURCE TERM
      CALL  SORCE(IN,JN,KN,A,SOURCE,I,J,NW,DPDZ,DPDTHA)
CC    CALCULATE CONVECTION TERMS
      CALL  CONVEC(IN,JN,KN,A,AE,AW,AN,AS,I,J,NW)
      CE=AE+BE(I,J,NW)
      CW=AW+BW(I,J,NW)
      CN=AN+BN(I,J,NW)
      CS=AS+BS(I,J,NW)
      ANUM=CE*A(I+1,J,NW)+CW*A(I-1,J,NW)+CN*A(I,J+1,NW)+
     * CS*A(I,J-1,NW)+SOURCE
      ADNM=CE+CW+CN+CS
      IF(ANUM .EQ. 0.0 .OR. ADNM .EQ. 0.0) GO TO 20
CC    STORE OLD VALUE
      Z=A(I,J,NW)
CC    CALCULATE REFERANCE VALUE
      ZREF=(ABS(A(I,J+1,NW))+ABS(A(I,J-1,NW))+
     * ABS(A(I+1,J,NW))+ABS(A(I-1,J,NW)))/4.
CC    CALCULATE NEW VALUE
      A(I,J,NW)=ANUM/ADNM
CC    CALCULATE RESIDUAL
      IF(ZREF .EQ. 0.0)GO TO 1
      RSS(I,J,NW)=(A(I,J,NW)-Z)/ZREF
CC    UNDER OR OVER RELAX
1     A(I,J,NW)=Z+RP(NW)*(A(I,J,NW)-Z)
      IF(ABS(RSS(I,J,NW)).GT.ABS(RSDU(NW)))RSDU(NW)=RSS(I,J,NW)
20    CONTINUE
10    CONTINUE
CC    IMPLICIT FORMULATION FOR NEXT TO BOUNDARY NODES
      DR=R0-X2(N2-1)
      G1=6.*(3.*DR-2.*R0)/(5.*DR-4.*R0)
      G2=-2.*(DR-R0)/(5.*DR-4.*R0)
      G3=-PS*(3.*R0-2.*DR)*(3.*DR-2.*R0)/(DR*(5.*DR-4.*R0))
      J=JNM
      DO 30 I=3,INMM
      HN=X2(J+1)-X2(J)
      HS=X2(J)-X2(J-1)
      DVZDR=((A(I,J+1,NVZ)-A(I,J,NVZ))*HS/HN+(A(I,J,NVZ)-
     * A(I,J-1,NVZ))*HN/HS)/(HN+HS)
      FVZ=PS*X2(J)*VP(I,J)*(X2(J)*DVZDR+2.*A(I,J,NVZ))
      CF=BE(I,J,NF)+BW(I,J,NF)+BN(I,J,NF)+BS(I,J,NF)
      CALL  CONVEC(IN,JN,KN,A,AE,AW,AN,AS,I,J,NW)
      CE=AE+BE(I,J,NW)
      CW=AW+BW(I,J,NW)
      CN=AN+BN(I,J,NW)
      CS=AS+BS(I,J,NW)
      CWT=CE+CW+CN+CS
      CALL  SORCE(IN,JN,KN,A,SOURCE,I,J,NW,DPDZ,DPDTHA)
      SUM1=SOURCE+CE*A(I+1,J,NW)+CW*A(I-1,J,NW)+CS*A(I,J-1,NW)
      DEN=CWT-CN*G2+CN*G1*X2(J)*VP(I,J)/(ROW*DR*DR*CF)
      S2=(BE(I,J,NF)*A(I+1,J,NF)+BW(I,J,NF)*A(I-1,J,NF)+
     * BN(I,J,NF)*A(I,J+1,NF)+BS(I,J,NF)*A(I,J-1,NF))/CF
      SUM2=A(I,J+1,NF)-S2+FVZ/CF
      SUM3=(G1*SUM2/(ROW*DR*DR)+G3*A(I,J,NVZ))*CN
```

```
      SUM=SUM1+SUM3
      IF( DEN.EQ.0.0) GO TO 30
      Z=A(I,J,NW)
      A(I,J,NW)=SUM/DEN
      A(I,J,NW)=Z+RP(NW)*(A(I,J,NW)-Z)
30    CONTINUE
CC
CC
CC
      I=2
      G1=3.
      G2=-0.5
      DO 40 J=3,JNMM
      DT=X2(J)*X1(2)
      HN=X2(J+1)-X2(J)
      HS=X2(J)-X2(J-1)
      DVZDR=((A(I,J+1,NVZ)-A(I,J,NVZ))*HS/HN+(A(I,J,NVZ)-
     * A(I,J-1,NVZ))*HN/HS)/(HN+HS)
      FVZ=PS*X2(J)*VP(I,J)*(X2(J)*DVZDR+2.*A(I,J,NVZ))
      CF=BE(I,J,NF)+BW(I,J,NF)+BN(I,J,NF)+BS(I,J,NF)
      CALL  CONVEC(IN,JN,KN,A,AE,AW,AN,AS,I,J,NW)
      CE=AE+BE(I,J,NW)
      CW=AW+BW(I,J,NW)
      CN=AN+BN(I,J,NW)
      CS=AS+BS(I,J,NW)
      CWT=CE+CW+CN+CS
      CALL  SORCE(IN,JN,KN,A,SOURCE,I,J,NW,DPDZ,DPDTHA)
      SUM1=SOURCE+CE*A(I+1,J,NW)+CN*A(I,J+1,NW)+CS*A(I,J-1,NW)
      DEN=CWT-CW*G2+CW*G1*X2(J)*VP(I,J)/(ROW*DT*DT*CF)
      S2=(BE(I,J,NF)*A(I+1,J,NF)+BW(I,J,NF)*A(I-1,J,NF)+
     * BN(I,J,NF)*A(I,J+1,NF)+BS(I,J,NF)*A(I,J-1,NF))/CF
      SUM2=A(I-1,J,NF)-S2+FVZ/CF
      SUM3=CW*G1*SUM2/(DT*DT*ROW)
      SUM=SUM1+SUM3
      IF( DEN.EQ.0.0) GO TO 40
      Z=A(I,J,NW)
      A(I,J,NW)=SUM/DEN
      A(I,J,NW)=Z+RP(NW)*(A(I,J,NW)-Z)
40    CONTINUE
CC
CC
CC
      I=N1-1
      G1=3.
      G2=-0.5
      DO 50 J=3,JNMM
      DT=X2(J)*(X1(N1)-X1(N1-1))
      HN=X2(J+1)-X2(J)
      HS=X2(J)-X2(J-1)
      DVZDR=((A(I,J+1,NVZ)-A(I,J,NVZ))*HS/HN+(A(I,J,NVZ)-
     * A(I,J-1,NVZ))*HN/HS)/(HN+HS)
      FVZ=PS*X2(J)*VP(I,J)*(X2(J)*DVZDR+2.*A(I,J,NVZ))
      CF=BE(I,J,NF)+BW(I,J,NF)+BN(I,J,NF)+BS(I,J,NF)
      CALL  CONVEC(IN,JN,KN,A,AE,AW,AN,AS,I,J,NW)
```

```
      CE=AE+BE(I,J,NW)
      CW=AW+BW(I,J,NW)
      CN=AN+BN(I,J,NW)
      CS=AS+BS(I,J,NW)
      CWT=CE+CW+CN+CS
      CALL  SORCE(IN,JN,KN,A,SOURCE,I,J,NW,DPDZ,DPDTHA)
      SUM1=SOURCE+CW*A(I-1,J,NW)+CN*A(I,J+1,NW)+CS*A(I,J-1,NW)
      DEN=CWT-CE*G2+CE*G1*X2(J)*VP(I,J)/(ROW*DT*DT*CF)
      S2=(BE(I,J,NF)*A(I+1,J,NF)+BW(I,J,NF)*A(I-1,J,NF)+
     * BN(I,J,NF)*A(I,J+1,NF)+BS(I,J,NF)*A(I,J-1,NF))/CF
      SUM2=A(I+1,J,NF)-S2+FVZ/CF
      SUM3=CE*G1*SUM2/(ROW*DT*DT)
      SUM=SUM1+SUM3
      IF( DEN.EQ.0.0) GO TO 50
      Z=A(I,J,NW)
      A(I,J,NW)=SUM/DEN
      A(I,J,NW)=Z+RP(NW)*(A(I,J,NW)-Z)
50    CONTINUE
CC
CC
CC
      J=2
      G1=36./5.
      G2=-4./5.
      G3=PS*12./5.
      DR=X2(J)
      DO 60 I=3,INMM
      HN=X2(J+1)-X2(J)
      HS=X2(J)-X2(J-1)
      DVZDR=((A(I,J+1,NVZ)-A(I,J,NVZ))*HS/HN+(A(I,J,NVZ)-
     * A(I,J-1,NVZ))*HN/HS)/(HN+HS)
      FVZ=PS*X2(J)*VP(I,J)*(X2(J)*DVZDR+2.*A(I,J,NVZ))
      CF=BE(I,J,NF)+BW(I,J,NF)+BN(I,J,NF)+BS(I,J,NF)
      CALL  CONVEC(IN,JN,KN,A,AE,AW,AN,AS,I,J,NW)
      CE=AE+BE(I,J,NW)
      CW=AW+BW(I,J,NW)
      CN=AN+BN(I,J,NW)
      CS=AS+BS(I,J,NW)
      CWT=CE+CW+CN+CS
      CALL  SORCE(IN,JN,KN,A,SOURCE,I,J,NW,DPDZ,DPDTHA)
      SUM1=SOURCE+CE*A(I+1,J,NW)+CW*A(I-1,J,NW)+CN*A(I,J+1,NW)
      DEN=CWT-CS*G2+CS*G1*X2(J)*VP(I,J)/(ROW*DR*DR*CF)
      S2=(BE(I,J,NF)*A(I+1,J,NF)+BW(I,J,NF)*A(I-1,J,NF)+
     * BN(I,J,NF)*A(I,J+1,NF)+BS(I,J,NF)*A(I,J-1,NF))/CF
      SUM2=A(I,J-1,NF)-S2+FVZ/CF
      SUM3=(G1*SUM2/(ROW*DR*DR)+G3*A(I,J,NVZ))*CS
      SUM=SUM1+SUM3
      IF( DEN.EQ.0.0) GO TO 60
      Z=A(I,J,NW)
      A(I,J,NW)=SUM/DEN
      A(I,J,NW)=Z+RP(NW)*(A(I,J,NW)-Z)
60    CONTINUE
CC
CC
```

```
CC
      I=2
      J=JNM
      DR=R0-X2(N2-1)
      G1=6.*(3.*DR-2.*R0)/(5.*DR-4.*R0)
      G2=-2.*(DR-R0)/(5.*DR-4.*R0)
      G3=-PS*(3.*R0-2.*DR)*(3.*DR-2.*R0)/(DR*(5.*DR-4.*R0))
      G11=3.
      G22=-0.5
      DT=X2(J)*X1(2)
      HN=R0-X2(N2-1)
      HS=X2(J)-X2(J-1)
      DVZDR=((A(I,J+1,NVZ)-A(I,J,NVZ))*HS/HN+(A(I,J,NVZ)-
     * A(I,J-1,NVZ))*HN/HS)/(HN+HS)
      FVZ=PS*X2(J)*VP(I,J)*(X2(J)*DVZDR+2.*A(I,J,NVZ))
      CF=BE(I,J,NF)+BW(I,J,NF)+BN(I,J,NF)+BS(I,J,NF)
      CALL  CONVEC(IN,JN,KN,A,AE,AW,AN,AS,I,J,NW)
      CE=AE+BE(I,J,NW)
      CW=AW+BW(I,J,NW)
      CN=AN+BN(I,J,NW)
      CS=AS+BS(I,J,NW)
      CWT=CE+CW+CN+CS
      SUM1=CE*A(I+1,J,NW)+CS*A(I,J-1,NW)
      S1=BE(I,J,NF)*A(I+1,J,NF)+BW(I,J,NF)*A(I-1,J,NF)+
     * BN(I,J,NF)*A(I,J+1,NF)+BS(I,J,NF)*A(I,J-1,NF)
      S2=CF*A(I-1,J,NF)-S1+FVZ
      SUM2=CW*(G11*S2/(ROW*DT*DT*CF))
      S3=CF*A(I,J+1,NF)-S1+FVZ
      S4=G1*S3/(ROW*DR*DR*CF)
      S6=S4+G3*A(I,J,NVZ)
      SUM3=S6*CN
      CALL SORCE(IN,JN,KN,A,SOURCE,I,J,NW,DPDZ,DPDTHA)
      SUM=SUM1+SUM2+SUM3+SOURCE
      DEN=CWT-G22*CW-G2*CN+CN*G1*X2(J)*VP(I,J)/(ROW*DR*DR*CF)+
     * CW*G11*X2(J)*VP(I,J)/(ROW*DT*DT*CF)
      IF( DEN.EQ.0.0) GO TO 61
      Z=A(I,J,NW)
      A(I,J,NW)=SUM/DEN
      A(I,J,NW)=Z+RP(NW)*(A(I,J,NW)-Z)
CC
CC
CC
61    I=N1-1
      J=N2-1
      DR=R0-X2(N2-1)
      G1=6.*(3.*DR-2.*R0)/(5.*DR-4.*R0)
      G2=-2.*(DR-R0)/(5.*DR-4.*R0)
      G3=-PS*(3.*R0-2.*DR)*(3.*DR-2.*R0)/(DR*(5.*DR-4.*R0))
      G11=3.
      G22=-0.5
      DT=X2(J)*(X1(N1)-X1(N1-1))
      HN=X2(J+1)-X2(J)
      HS=X2(J)-X2(J-1)
      DVZDR=((A(I,J+1,NVZ)-A(I,J,NVZ))*HS/HN+(A(I,J,NVZ)-
```

```
     * A(I,J-1,NVZ))*HN/HS)/(HN+HS)
       FVZ=PS*X2(J)*VP(I,J)*(X2(J)*DVZDR+2.*A(I,J,NVZ))
       CF=BE(I,J,NF)+BW(I,J,NF)+BN(I,J,NF)+BS(I,J,NF)
       CALL  CONVEC(IN,JN,KN,A,AE,AW,AN,AS,I,J,NW)
       CE=AE+BE(I,J,NW)
       CW=AW+BW(I,J,NW)
       CN=AN+BN(I,J,NW)
       CS=AS+BS(I,J,NW)
       CWT=CE+CW+CN+CS
       SUM1=CW*A(I-1,J,NW)+CS*A(I,J-1,NW)
       S1=BE(I,J,NF)*A(I+1,J,NF)+BW(I,J,NF)*A(I-1,J,NF)+
     * BN(I,J,NF)*A(I,J+1,NF)+BS(I,J,NF)*A(I,J-1,NF)
       S2=CF*A(I+1,J,NF)-S1+FVZ
       SUM2=CE*G11*S2/(ROW*DT*DT*CF)
       S3=CF*A(I,J+1,NF)-S1+FVZ
       SUM3=(S3*G1/(ROW*DR*DR*CF)+G3*A(I,J,NVZ))*CN
       CALL  SORCE(IN,JN,KN,A,SOURCE,I,J,NW,DPDZ,DPDTHA)
       SUM=SUM1+SUM2+SUM3+SOURCE
       DEN=CWT-G22*CE-G2*CN+CN*G1*X2(J)*VP(I,J)/(ROW*DR*DR*CF)+
     * CE*G11*X2(J)*VP(I,J)/(ROW*DT*DT*CF)
       IF( DEN.EQ.0.0) GO TO 62
       Z=A(I,J,NW)
       A(I,J,NW)=SUM/DEN
       A(I,J,NW)=Z+RP(NW)*(A(I,J,NW)-Z)
CC
CC
CC
62     I=2
       J=2
       G1=36./5.
       G2=-4./5.
       G3=PS*12./5.
       DR=X2(2)
       G11=3.
       G22=-0.5
       DT=X2(J)*X1(2)
       HN=X2(J+1)-X2(J)
       HS=X2(J)-X2(J-1)
       DVZDR=((A(I,J+1,NVZ)-A(I,J,NVZ))*HS/HN+(A(I,J,NVZ)-
     * A(I,J-1,NVZ))*HN/HS)/(HN+HS)
       FVZ=PS*X2(J)*VP(I,J)*(X2(J)*DVZDR+2.*A(I,J,NVZ))
       CF=BE(I,J,NF)+BW(I,J,NF)+BN(I,J,NF)+BS(I,J,NF)
       CALL  CONVEC(IN,JN,KN,A,AE,AW,AN,AS,I,J,NW)
       CE=AE+BE(I,J,NW)
       CW=AW+BW(I,J,NW)
       CN=AN+BN(I,J,NW)
       CS=AS+BS(I,J,NW)
       CWT=CE+CW+CN+CS
       SUM1=CE*A(I+1,J,NW)+CN*A(I,J+1,NW)
       S1=BE(I,J,NF)*A(I+1,J,NF)+BW(I,J,NF)*A(I-1,J,NF)+
     * BN(I,J,NF)*A(I,J+1,NF)+BS(I,J,NF)*A(I,J-1,NF)
       S2=CF*A(I-1,J,NF)-S1+FVZ
       SUM2=CW*G11*S2/(ROW*DT*DT*CF)
       S3=CF*A(I,J-1,NF)-S1+FVZ
```

```
      SUM3=(S3*G1/(ROW*DR*DR*CF)+G3*A(I,J,NVZ))*CS
      CALL  SORCE(IN,JN,KN,A,SOURCE,I,J,NW,DPDZ,DPDTHA)
      SUM=SUM1+SUM2+SUM3+SOURCE
      DEN=CWT-G22*CW-G2*CS+CS*G1*X2(J)*VP(I,J)/(ROW*DR*DR*CF)
     * +CW*G11*X2(J)*VP(I,J)/(ROW*DT*DT*CF)
      IF( DEN.EQ.0.0)GO TO 63
      Z=A(I,J,NW)
      A(I,J,NW)=SUM/DEN
      A(I,J,NW)=Z+RP(NW)*(A(I,J,NW)-Z)
CC
CC
CC
63    I=N1-1
      J=2
      G1=36./5.
      G2=-4./5.
      G3=PS*12./5.
      DR=X2(2)
      G11=3.
      G22=-0.5
      DT=X2(J)*(X1(N1)-X1(N1-1))
      HN=X2(J+1)-X2(J)
      HS=X2(J)-X2(J-1)
      DVZDR=((A(I,J+1,NVZ)-A(I,J,NVZ))*HS/HN+(A(I,J,NVZ)-
     * A(I,J-1,NVZ))*HN/HS)/(HN+HS)
      FVZ=PS*X2(J)*VP(I,J)*(X2(J)*DVZDR+2.*A(I,J,NVZ))
      CF=BE(I,J,NF)+BW(I,J,NF)+BN(I,J,NF)+BS(I,J,NF)
      CALL  CONVEC(IN,JN,KN,A,AE,AW,AN,AS,I,J,NW)
      CE=AE+BE(I,J,NW)
      CW=AW+BW(I,J,NW)
      CN=AN+BN(I,J,NW)
      CS=AS+BS(I,J,NW)
      CWT=CE+CW+CN+CS
      SUM1=CW*A(I-1,J,NW)+CN*A(I,J+1,NW)
      S1=BE(I,J,NF)*A(I+1,J,NF)+BW(I,J,NF)*A(I-1,J,NF)+
     * BN(I,J,NF)*A(I,J+1,NF)+BS(I,J,NF)*A(I,J-1,NF)
      S2=CF*A(I+1,J,NF)-S1+FVZ
      SUM2=CE*G11*S2/(ROW*DT*DT*CF)
      S3=CF*A(I,J-1,NF)-S1+FVZ
      SUM3=(S3*G1/(ROW*DR*DR*CF)+G3*A(I,J,NVZ))*CS
      CALL  SORCE(IN,JN,KN,A,SOURCE,I,J,NW,DPDZ,DPDTHA)
      SUM=SUM1+SUM2+SUM3+SOURCE
      DEN=CWT-G22*CE-G2*CS+CS*G1*X2(J)*VP(I,J)/(ROW*DR*DR*CF)
     * +CE*G11*X2(J)*VP(I,J)/(ROW*DT*DT*CF)
      IF( DEN.EQ.0.0) GO TO 65
      Z=A(I,J,NW)
      A(I,J,NW)=SUM/DEN
      A(I,J,NW)=Z+RP(NW)*(A(I,J,NW)-Z)
CC
CC
CC    STREAM FUNCTION SUB CYCLE
65    DO 90 J=2,JNM
      DO 100 I=2,INM
      CALL  SORCE(IN,JN,KN,A,SOURCE,I,J,NF,DPDZ,DPDTHA)
```

```
      ANUM=BE(I,J,NF)*A(I+1,J,NF)+BW(I,J,NF)*A(I-1,J,NF)+
     * BN(I,J,NF)*A(I,J+1,NF)+BS(I,J,NF)*A(I,J-1,NF)+SOURCE
      ADNM=BE(I,J,NF)+BW(I,J,NF)+BN(I,J,NF)+BS(I,J,NF)
      IF(ANUM.EQ.0.0 .OR. ADNM.EQ.0.0) GO TO 100
      Z=A(I,J,NF)
      ZREF=(ABS(A(I,J+1,NF))+ABS(A(I,J-1,NF))+
     * ABS(A(I+1,J,NF))+ABS(A(I-1,J,NF)))/4.
      A(I,J,NF)=ANUM/ADNM
      IF(ZREF .EQ. 0.0) GO TO 2
      RSS(I,J,NF)=(A(I,J,NF)-Z)/ZREF
2     A(I,J,NF)=Z+RP(NF)*(A(I,J,NF)-Z)
      IF(ABS(RSS(I,J,NF)).GT.ABS(RSDU(NF)))RSDU(NF)=RSS(I,J,NF)
100   CONTINUE
90    CONTINUE
C
CC
CC    AXIAL VELOCITY SUB CYCLE
101   DO 110 J=2,JNM
      DO 120 I=2,INM
      CALL  SORCE(IN,JN,KN,A,SOURCE,I,J,NVZ,DPDZ,DPDTHA)
      CALL  CONVEC(IN,JN,KN,A,AE,AW,AN,AS,I,J,NVZ)
      CE=AE+BE(I,J,NVZ)
      CW=AW+BW(I,J,NVZ)
      CN=AN+BN(I,J,NVZ)
      CS=AS+BS(I,J,NVZ)
      ANUM=CE*A(I+1,J,NVZ)+CW*A(I-1,J,NVZ)+CN*A(I,J+1,NVZ)+
     * CS*A(I,J-1,NVZ)+SOURCE
      ADNM=CE+CW+CN+CS
      ZVZ(I,J)=A(I,J,NVZ)
      IF(ADNM.EQ.0.0)GO TO 120
      A(I,J,NVZ)=ANUM/ADNM
120   CONTINUE
110   CONTINUE
CC    CONSTRAIN VELOCITY FIELD TO UB
      CALL  BULK(IN,JN,KN,A,N1,N2,UBAR)
      DO 708 J=1,N2
      DO 708 I=1,N1
      A(I,J,3)=A(I,J,3)*UB/UBAR
708   CONTINUE
      DO 709 J=2,JNM
      DO 709 I=2,INM
      RSS(I,J,NVZ)=1.0-ZVZ(I,J)/A(I,J,NVZ)
      A(I,J,NVZ)=ZVZ(I,J)+RP(NVZ)*(A(I,J,NVZ)-ZVZ(I,J))
      IF(ABS(RSS(I,J,NVZ)).GT.ABS(RSDU(NVZ)))RSDU(NVZ)=RSS(I,J,NVZ)
709   CONTINUE
      IF(AL.EQ.0.0 .OR.  MOD(NITER,20).NE.0)
     * GO TO 102
      CALL  PSS(IN,JN,KN,A,N1,N2,DPDTHA)
102   CONTINUE
      RETURN
      END
CC    CALCULATE SOURCE TERMS
      SUBROUTINE SORCE(IN,JN,KN,A,SOURCE,I,J,K,DPDZ,DPDTHA)
      IMPLICIT REAL (A-H,O-Z)
```

```
      DIMENSION A(IN,JN,KN),DPDTHA(20,20)
      COMMON /CG/ X1(20),X2(20),VP(20,20)
      COMMON /CR/ NNF,FH,RO,AF,PS,AL,ROW,AMEW,NITER,BETA
      DATA NW,NF,NVZ /1,2,3/
      GO TO (1,2,3),K
CC    AXIAL VORTICITY
 1      HE=X2(J)*(X1(I+1)-X1(I))
        HW=X2(J)*(X1(I)-X1(I-1))
        HN=X2(J+1)-X2(J)
        HS=X2(J)-X2(J-1)
        DSDN=((A(I,J+1,NF)-A(I,J,NF))*HS/HN+(A(I,J,NF)-
     *       A(I,J-1,NF))*HN/HS)/(HS+HN)
        DSDNE=((A(I+1,J+1,NF)-A(I+1,J,NF))*HS/HN+(A(I+1,J,NF)-
     *        A(I+1,J-1,NF))*HN/HS)/(HN+HS)
        DSDNW=((A(I-1,J+1,NF)-A(I-1,J,NF))*HS/HN+(A(I-1,J,NF)-
     *        A(I-1,J-1,NF))*HN/HS)/(HN+HS)
        D2SDNT=((DSDNE-DSDN)*HW/HE+(DSDN-DSDNW)*HE/HW)/(HE+HW)
        DWDT=((A(I+1,J,NVZ)-A(I,J,NVZ))*HW/HE+(A(I,J,NVZ)-
     *       A(I-1,J,NVZ))*HE/HW)/(HE+HW)
        DWDN=((A(I,J+1,NVZ)-A(I,J,NVZ))*HS/HN+(A(I,J,NVZ)-
     *       A(I,J-1,NVZ))*HN/HS)/(HN+HS)
        D2SDN2=((A(I,J+1,NF)-A(I,J,NF))/HN-(A(I,J,NF)-
     *        A(I,J-1,NF))/HS)/(0.5*(HN+HS))
        S1= (DSDN+X2(J)*D2SDN2)/ROW-PS*(X2(J)*X2(J)*DWDN+2.*X2(J)*
     *      A(I,J,NVZ))
        S2=D2SDNT/ROW-PS*X2(J)*DWDT
        SPPW=PS*ROW*(DWDT*S1 -DWDN*S2*X2(J))
        SOURCE=VP(I,J)*SPPW
        SOURCE=-SOURCE*X2(J)
        GO TO 111
CC    STREAM FUNCTION
   2    HN=X2(J+1)-X2(J)
        HS=X2(J)-X2(J-1)
        DWDN=((A(I,J+1,NVZ)-A(I,J,NVZ))*HS/HN+(A(I,J,NVZ)-
     *       A(I,J-1,NVZ))*HN/HS)/(HN+HS)
        SPPS=PS*(X2(J)*DWDN+2.0*A(I,J,NVZ))-A(I,J,NW)
        SOURCE=VP(I,J)*SPPS
        SOURCE=-SOURCE*X2(J)
        GO TO 111
CC    AXIAL VELOCITY
3       SOURCE=VP(I,J)*(DPDZ+PS*DPDTHA(I,J))
        SOURCE=-SOURCE*X2(J)
 111    CONTINUE
        RETURN
        END
CC    SUBROUTINE FOR PRINTING THE VARIABLES
      SUBROUTINE PRINT(IN,JN,KN,A,N1,N2,NBEGIN,NTOTAL)
      IMPLICIT REAL (A-H,O-Z)
      DIMENSION A(IN,JN,KN)
      DO 10 NCODE=NBEGIN,NTOTAL
        GO TO (1,2,3,4,5),NCODE
CC      AXIAL VORTICITY
  1     PRINT 100
        GO TO 111
```

```
CC        STREAM FUNCTION
  2       PRINT 200
          GO TO 111
CC        AXIAL VELOCITY
  3       PRINT 300
          GO TO 111
CC        CIRCUMFERENTIAL VELOCITY
  4       PRINT 400
          GO TO 111
CC        RADIAL VELOCITY
  5       PRINT 500
  111     CONTINUE
          DO 20 J=1,N2
            PRINT 700,(A(I,J,NCODE),I=1,N1)
            PRINT 800,J
  20      CONTINUE
          PRINT 900,(I,I=1,7)
  10    CONTINUE
100     FORMAT('1',30X,'THE DISTRIBUTION OF AXIAL VORTICITY  ( 1/SEC )'
     * /'0',129X,'J'//)
200     FORMAT('1',30X,'THE DISTRIBUTION OF STREAM FUNCTION ( KG/M-S )'
     * /'0',129X,'J'//)
300     FORMAT('1',30X,'THE DISTRIBUTION OF AXIAL VELOCITY ( M/S )'/'0',
     * 129X,'J'//)
400     FORMAT('1',25X,'THE DISTRIBUTION OF CIRCUMFERENTIAL ',
     * 'VELOCITY ( M/S )'/'0',129X,'J'//)
500     FORMAT('1',30X,'THE DISTRIBUTION OF RADIAL VELOCITY ( M/S )'
     * /'0',129X,'J'//)
700     FORMAT('0',7E11.4)
800     FORMAT('+',129X,I2)
900     FORMAT('-','I',7X,7(I2,13X))
        RETURN
        END
CC      SUBROUTINE FOR CALCULATING CONVECTION TERMS
        SUBROUTINE  CONVEC(IN,JN,KN,A,AE,AW,AN,AS,I,J,K)
        IMPLICIT REAL (A-H,O-Z)
        DIMENSION A(IN,JN,KN)
        NF=2
CC        INTERIOR NODES
          G1PE=A(I+1,J-1,NF)+A(I,J-1,NF)-A(I+1,J+1,NF)-A(I,J+1,NF)
          G1PW=A(I-1,J+1,NF)+A(I,J+1,NF)-A(I-1,J-1,NF)-A(I,J-1,NF)
          G2PN=A(I+1,J+1,NF)+A(I+1,J,NF)-A(I-1,J+1,NF)-A(I-1,J,NF)
          G2PS=A(I-1,J-1,NF)+A(I-1,J,NF)-A(I+1,J-1,NF)-A(I+1,J,NF)
CC        COMPUTE AE, AW, AN, AS
          APP=1.0
          IF( K.EQ.NF )APP=0.0
          AE=APP*(G1PE+ABS(G1PE))/8.0
          AW=APP*(G1PW+ABS(G1PW))/8.0
          AN=APP*(G2PN+ABS(G2PN))/8.0
          AS=APP*(G2PS+ABS(G2PS))/8.0
          RETURN
          END
CC        SUBROUTINE FOR CALCULATING VELOCITY COMPONENTS
        SUBROUTINE  VELDIS(IN,JN,KN,A,N1,N2)
```

```
      IMPLICIT REAL (A-H,O-Z)
      DIMENSION A(IN,JN,KN)
      COMMON /CG/ X1(20),X2(20),VP(20,20)
      COMMON /CR/ NNF,FH,RO,AF,PS,AL,ROW,AMEW,NITER,BETA
      DATA NF,NVZ,NV1,NV2/2,3,4,5/
      JNM=N2-1
      INM=N1-1
      DO 20 J=2,JNM
        HN=X2(J+1)-X2(J)
        HS=X2(J)-X2(J-1)
        DO 30 I=2,INM
          HE=X2(J)*(X1(I+1)-X1(I))
          HW=X2(J)*(X1(I)-X1(I-1))
          DSDN=((A(I,J+1,NF)-A(I,J,NF))*HS/HN+(A(I,J,NF)-
     *          A(I,J-1,NF))*HN/HS)/(HN+HS)
          DSDT=((A(I+1,J,NF)-A(I,J,NF))*HW/HE+(A(I,J,NF)-
     *          A(I-1,J,NF))*HE/HW)/(HE+HW)
          A(I,J,NV1)=DSDN/ROW-PS*X2(J)*A(I,J,NVZ)
          A(I,J,NV2)=(-1.0)*DSDT/ROW
30      CONTINUE
20    CONTINUE
      RETURN
      END
CC    SUBROUTINE OUTPUT
      SUBROUTINE OUTPUT(N1,N2,NBEGIN,NTOTAL)
      IMPLICIT REAL (A-H,O-Z)
      COMMON /CP/ RSS(20,20,3),UB
      DO 10 NCODE=NBEGIN,NTOTAL
      GO TO (1,2,3), NCODE
1     PRINT 100
      GO TO 5
2     PRINT 200
      GO TO 5
3     PRINT 300
5     PRINT 360
      DO 70 J=1,N2
      PRINT 700,(RSS(I,J,NCODE), I=1,N1)
      PRINT 800, J
70    CONTINUE
10    CONTINUE
100   FORMAT(' ',54X,'AXIAL VORTICITY')
200   FORMAT(' ',54X,'STREAM FUNCTION')
300   FORMAT(' ',54X,'AXIAL VELOCITY')
360   FORMAT(' ',57X,'RESIDUAL')
700   FORMAT(' ',7E11.4)
800   FORMAT('+',129X,I2)
      RETURN
      END
CC    SUBROUTINE FOR CALCULATING CIRCUMFERENTIAL PRESSURE
CC    GRADIENT
      SUBROUTINE PSS(IN,JN,KN,A,N1,N2,DPDTHA)
      IMPLICIT REAL (A-H,O-Z)
      DIMENSION A(IN,JN,KN),DPDTHA(20,20)
      COMMON /CG/ X1(20),X2(20),VP(20,20)
```

```
      COMMON /CR/ NNF,FH,R0,AF,PS,AL,ROW,AMEW,NITER,BETA
      DATA NVZ,NV1,NV2/3,4,5/
      CALL  VELDIS(IN,JN,KN,A,N1,N2)
      INM=N1-1
      JNM=N2-1
      DO 65 J=2,JNM
      HN=X2(J+1)-X2(J)
      HS=X2(J)-X2(J-1)
      DO 75 I=2,INM
      HE=X2(J)*(X1(I+1)-X1(I))
      HW=X2(J)*(X1(I)-X1(I-1))
      DV1DR=((A(I,J+1,NV1)-A(I,J,NV1))*HS/HN+(A(I,J,NV1)-
     *       A(I,J-1,NV1))*HN/HS)/(HN+HS)
      DV1DR2=((A(I,J+1,NV1)-A(I,J,NV1))/HN-(A(I,J,NV1)-
     *        A(I,J-1,NV1))/HS)/(0.5*(HN+HS))
      DV2DT=((A(I+1,J,NV2)-A(I,J,NV2))*HW/HE+(A(I,J,NV2)-
     *       A(I-1,J,NV2))*HE/HW)/(HE+HW)
      DV1DT2=((A(I+1,J,NV1)-A(I,J,NV1))/HE-(A(I,J,NV1)-
     *       A(I-1,J,NV1))/HW)/(0.5*(HE+HW))
      DV1DT=((A(I+1,J,NV1)-A(I,J,NV1))*HW/HE+(A(I,J,NV1)-
     *       A(I-1,J,NV1))*HE/HW)/(HE+HW)
      S1=DV1DR/X2(J)-A(I,J,NV1)/(X2(J)*X2(J))+DV1DR2+2.0*
     *    DV2DT/X2(J)+(1.0+PS*PS*X2(J)*X2(J))*DV1DT2
      S2=X2(J)*A(I,J,NV2)*DV1DR+(A(I,J,NV1)+PS*X2(J)*A(I,J,NVZ))*
     *    X2(J)*DV1DT+A(I,J,NV1)*A(I,J,NV2)
      DPDTHA(I,J)=AMEW*X2(J)*S1-ROW*S2
75    CONTINUE
65    CONTINUE
      RETURN
      END
CC    SUBROUTINE FOR CALCULATING BOUNDARY VORTICITIES
      SUBROUTINE  BOUND(IN,JN,KN,A,N1,N2)
      IMPLICIT REAL (A-H,O-Z)
      DIMENSION A(IN,JN,KN)
      COMMON /CG/ X1(20),X2(20),VP(20,20)
      COMMON /CR/ NNF,FH,R0,AF,PS,AL,ROW,AMEW,NITER,BETA
      DATA NW,NF,NVZ/1,2,3/
CC    TUBE WALL
      J=N2
      INM=N1-1
      DR=R0-X2(N2-1)
      G1=6.*(3.*DR-2.*R0)/(5.*DR-4.*R0)
      G2=-2.*(DR-R0)/(5.*DR-4.*R0)
      G3=-PS*(3.*R0-2.*DR)*(3.*DR-2.*R0)/(DR*(5.*DR-4.*R0))
      DO 10 I=2,INM
      A(I,J,NW)=G1*(A(I,J,NF)-A(I,J-1,NF))/(ROW*DR*DR)+
     * G2*A(I,J-1,NW)+G3*A(I,J-1,NVZ)
10    CONTINUE
CC    FIN SURFACE
      I=1
      JNM=N2-1
      G1=3.
      G2=-0.5
      DO 20 J=2,JNM
```

```
      DT=X2(J)*X1(2)
      A(I,J,NW)=G1*(A(I,J,NF)-A(I+1,J,NF))/(ROW*DT*DT)+
     * G2*A(I+1,J,NW)
20    CONTINUE
CC
      I=N1
      DO 30 J=2,JNM
      DT=X2(J)*(X1(N1)-X1(N1-1))
      A(I,J,NW)=G1*(A(I,J,NF)-A(I-1,J,NF))/(ROW*DT*DT)+
     * G2*A(I-1,J,NW)
30    CONTINUE
CC    CENTER NODE
      N=N1/2
      G1=36./5.
      G2=-4./5.
      G3=PS*12./5.
      DR=X2(2)
      A(N,1,NW)=G1*(A(N,1,NF)-A(N,2,NF))/(ROW*DR*DR)+
     * G2*A(N,2,NW)+G3*A(N,2,NVZ)
      DO 40 I=1,N1
      A(I,1,NW)=A(N,1,NW)
40    CONTINUE
      RETURN
      END
CC    SUBROUTINE FOR CALCULATING WALL SHEAR STRESSES
      SUBROUTINE  SHEAR(IN,JN,KN,A,N1,N2,DPDZW,DUDR,DUDT1,DUDT2)
      IMPLICIT REAL(A-H,O-Z)
      DIMENSION A(IN,JN,KN),DUDR(20),DUDT1(20),DUDT2(20)
      COMMON /CG/ X1(20),X2(20),VP(20,20)
      COMMON /CR/ NNF,FH,RO,AF,PS,AL,ROW,AMEW,NITER,BETA
      COMMON /CX/ AREA,AVG,SUM1,SUM2,SUM3,AREA1,AREA2,AREA3,AVG1,AVG2,
     * AVG3
      NVZ=3
      NV1=4
      NV2=5
CC    CALCULATE VELOCITY GRADIENTS ON WALL
CC    TUBE WALL
      DR1=RO-X2(N2-1)
      DR2=X2(N2-1)-X2(N2-2)
      J=N2
      DO 10 I=1,N1
      DUDR(I)=ABS(A(I,J-2,NVZ)*DR1/(DR2*(DR1+DR2))-
     *  A(I,J-1,NVZ)*(DR1+DR2)/(DR1*DR2))
10    CONTINUE
      DUDR(1)=0.5*DUDR(2)
      DUDR(N1)=0.5*DUDR(N1-1)
CC    FIN SURFACE
      I=1
      DT1=X1(I+1)-X1(I)
      DT2=X1(I+2)-X1(I+1)
      DO 20 J=2,N2
      DTT1=DT1*X2(J)
      DTT2=DT2*X2(J)
      G1=ABS(A(I+1,J,NVZ)*(DTT1+DTT2)/(DTT1*DTT2)-
```

```
     * A(I+2,J,NVZ)*DTT1/(DTT2*(DTT1+DTT2)))
       G2=ABS(A(I+1,J,NV1)*(DT1+DT2)/(DT1*DT2)-
     * A(I+2,J,NV1)*DT1/(DT2*(DT1+DT2)))
       G3=ABS(A(I+1,J,NV2)*(DT1+DT2)/(DT1*DT2)-
     * A(I+2,J,NV2)*DT1/(DT2*(DT1+DT2)))
       DUDT1(J)=(1.+2.*AL*X2(J)/R0)*G1+AL*G2/R0+AL*G3/R0
20     CONTINUE
       DUDT1(N2)=0.5*DUDT1(N2-1)
CC
CC
       I=N1
       DT1=X1(I)-X1(I-1)
       DT2=X1(I-1)-X1(I-2)
       DO 30 J=2,N2
       DTT1=X2(J)*DT1
       DTT2=X2(J)*DT2
       G1=ABS(A(I-2,J,NVZ)*DTT1/(DTT2*(DTT1+DTT2))-
     * A(I-1,J,NVZ)*(DTT1+DTT2)/(DTT1*DTT2))
       G2=ABS(A(I-2,J,NV1)*DT1/(DT2*(DT1+DT2))-
     * A(I-1,J,NV1)*(DT1+DT2)/(DT1*DT2))
       G3=ABS(A(I-2,J,NV2)*DT1/(DT2*(DT1+DT2))-
     * A(I-1,J,NV2)*(DT1+DT2)/(DT1*DT2))
       DUDT2(J)=(1.+2.*AL*X2(J)/R0)*G1+AL*G2/R0+AL*G3/R0
30     CONTINUE
       DUDT2(N2)=0.5*DUDT2(N2-1)
CC
CC     CENTER NODE
       A1=0.5*DUDT1(2)
       A2=0.5*DUDT2(2)
       N=N1/2
       DR1=X2(2)
       DR2=X2(3)-X2(2)
       A3=ABS(A(N,2,NVZ)*(DR1+DR2)/(DR1*DR2)-A(N,3,NVZ)*
     * DR1/(DR2*(DR1+DR2)))
       AA=(A1+A2+A3)/3.
       DUDT1(1)=AA
       DUDT2(1)=AA
CC     INTEGRATE VELOCITY GRADIENTS USING TRAPEZOIDAL RULE
CC     TUBE WALL
       SUM1=0.
       INM=N1-1
       DO 40 I=1,INM
       SUM1=SUM1+(DUDR(I)+DUDR(I+1))*R0*(X1(I+1)-X1(I))/2.
40     CONTINUE
CC     FIN SURFACE
       SUM2=0.
       JNM=N2-1
       DO 50 J=1,JNM
       X2A=(X2(J)+X2(J+1))/2.
       RSQ=AL*X2A/R0
       SECG=SQRT(1.+RSQ*RSQ)
       SUM2=SUM2+(DUDT1(J)+DUDT1(J+1))*SECG*(X2(J+1)-X2(J))/2.
50     CONTINUE
CC
```

```
CC
      SUM3=0.
      DO 60 J=1,JNM
      X2A=(X2(J)+X2(J+1))/2.
      RSQ=AL*X2A/R0
      SECG=SQRT(1.+RSQ*RSQ)
      SUM3=SUM3+(DUDT2(J)+DUDT2(J+1))*SECG*(X2(J+1)-X2(J))/2.
60    CONTINUE
      SUM=SUM1+SUM2+SUM3
CC    TOTAL SURFACE AREA
      PI=3.14159
      IF(AL.EQ.0.0)GO TO 70
      AUG=SQRT(1.+AL*AL)
      AREA=2.*R0*(PI/NNF-BETA*AUG)+R0*AUG+R0*ALOG(AL+AUG)/AL
      AREA1=2.*R0*(PI/NNF-BETA*AUG)
      AREA2=0.5*(R0*AUG+R0*ALOG(AL+AUG)/AL)
      AREA3=AREA2
      GO TO 80
70    AREA=2.*R0*(PI/NNF-BETA)+R0*2.
      AREA1=2.*R0*(PI/NNF-BETA)
      AREA2=R0
      AREA3=R0
CC    AVERAGE VELOCITY GRADIENT
80    AVG=SUM/AREA
CC    WALL SHEAR STRESSES NORMALIZED BY AVERAGE VALUE
      DO 90 I=1,N1
      DUDR(I)=DUDR(I)/AVG
90    CONTINUE
      DO 100 J=1,N2
      DUDT1(J)=DUDT1(J)/AVG
      DUDT2(J)=DUDT2(J)/AVG
100   CONTINUE
      AVG=AVG*AMEW
      SUM1=SUM1*AMEW
      AVG1=SUM1/AREA1
      SUM2=SUM2*AMEW
      AVG2=SUM2/AREA2
      SUM3=SUM3*AMEW
      AVG3=SUM3/AREA3
CC    CALCULATE PRESSURE GRADIENT
      DPDZW=-NNF*SUM*AMEW/AF
      RETURN
      END

$ENTRY
```

APPENDIX F

IMPLICIT FORMULATION OF VORTICITY BOUNDARY CONDITION

Figure F.1 shows a typical node P surrounded by nodes N, S, E, W of which N is a boundary node. Vorticity boundary condition, equation (4.3), gives:

$$\omega_N = C_1 \left(\frac{\Psi_N - \Psi_P}{\rho n^2}\right) + C_2\, \omega_P + C_3\, V_{z,P}, \qquad (F.1)$$

where

$$C_1 = \frac{6(3n - 2r_o)}{(5n - 4r_o)},$$

$$C_2 = -\frac{2(n - r_o)}{(5n - 4r_o)},$$

and

$$C_3 = -\frac{\alpha}{r_o}\,\frac{(3r_o - 2n)\,(3n - 2r_o)}{n(5n - 4r_o)}.$$

Vorticity and stream function at node P are obtained from the successive substitution formula:

$$\omega_P = C_E^{\omega}\, \omega_E + C_W^{\omega}\, \omega_W + C_N^{\omega}\, \omega_N + C_S^{\omega}\, \omega_S + D^{\omega} \qquad (F.2)$$

$$\Psi_P = C_E^{\Psi}\, \Psi_E + C_W^{\Psi}\, \Psi_W + C_N^{\Psi}\, \Psi_N + C_S^{\Psi}\, \Psi_S + D^{\Psi} \qquad (F.3)$$

where

$$D^{\Psi} = -\, d^{\Psi}_{,P} \cdot V_P/\Sigma_{AB}. \qquad (F.4)$$

Substituting the appropriate value of $d^{\Psi}_{,P}$ from Section 3.4 gives:

$$D^{\Psi}_{,p} = \omega_P \, r'_P \, \frac{V_P}{\Sigma_{AB}} - F(V_z) \tag{F.5}$$

in which $F(V_z)$ is the part of the source term of stream function equation which is a function of V_z only. Thus,

$$F(V_z) = \frac{\alpha}{r_o} \, r'_P \, \left(r'_P \frac{\partial V_z}{\partial r'} + 2V_{z,P}\right) \frac{V_P}{\Sigma_{AB}} \quad . \tag{F.6}$$

Equation (F.5) can be combined with equation (F.3). When the resulting equation is substituted into equation (F.1), there results:

$$\omega_N = \frac{C_1}{\rho n^2} \left[\Psi_N - \{C^{\Psi}_E \Psi_E + C^{\Psi}_W \Psi_W + C^{\Psi}_N \Psi_N + C^{\Psi}_S \Psi_S + \right.$$

$$\left. + \omega_P r'_P \, \frac{V_P}{\Sigma_{AB}} - F(V_z)\}\right] + C_2 \, \omega_P + C_3 \, V_{z,P} \quad . \tag{F.7}$$

Substituting equation (F.7) into equation (F.2) and solving for ω_P, the final expression for ω_P is obtained as follows:

$$\omega_P = \frac{\sum_{i=E,W,S} C^{\omega}_i \, \omega_i + D^{\omega} + \frac{C^{\omega}_N C_1}{\rho n^2} \left[\Psi_N - \{ \sum_{i=E,W,N,S} C^{\omega}_i \, \Psi_i - F(V_z)\} + \right.}{\left. + C_3 \, V_{z,P}\right]}$$

$$1 + C^{\omega}_N \, \{\frac{C_1}{\rho n^2} \, \frac{r'_P \, V_P}{\Sigma_{AB}} - C_2\} \tag{F.8}$$

Similar expressions can be obtained for vorticity values for nodes on i=2, $2 \leq j \leq n2-1$; i=n-1, $2 \leq j \leq n2-1$ and j=2, $2 \leq i \leq n1-1$. However, it should be noted that the nodes (2,2), (2,n2-1), (n1-1,2), and (n1-1, n2-1) are surrounded by two boundary nodes and thus require special consideration while calculating the vorticity values. Nevertheless, the basic procedure of treating such nodes remains the same as already discussed.

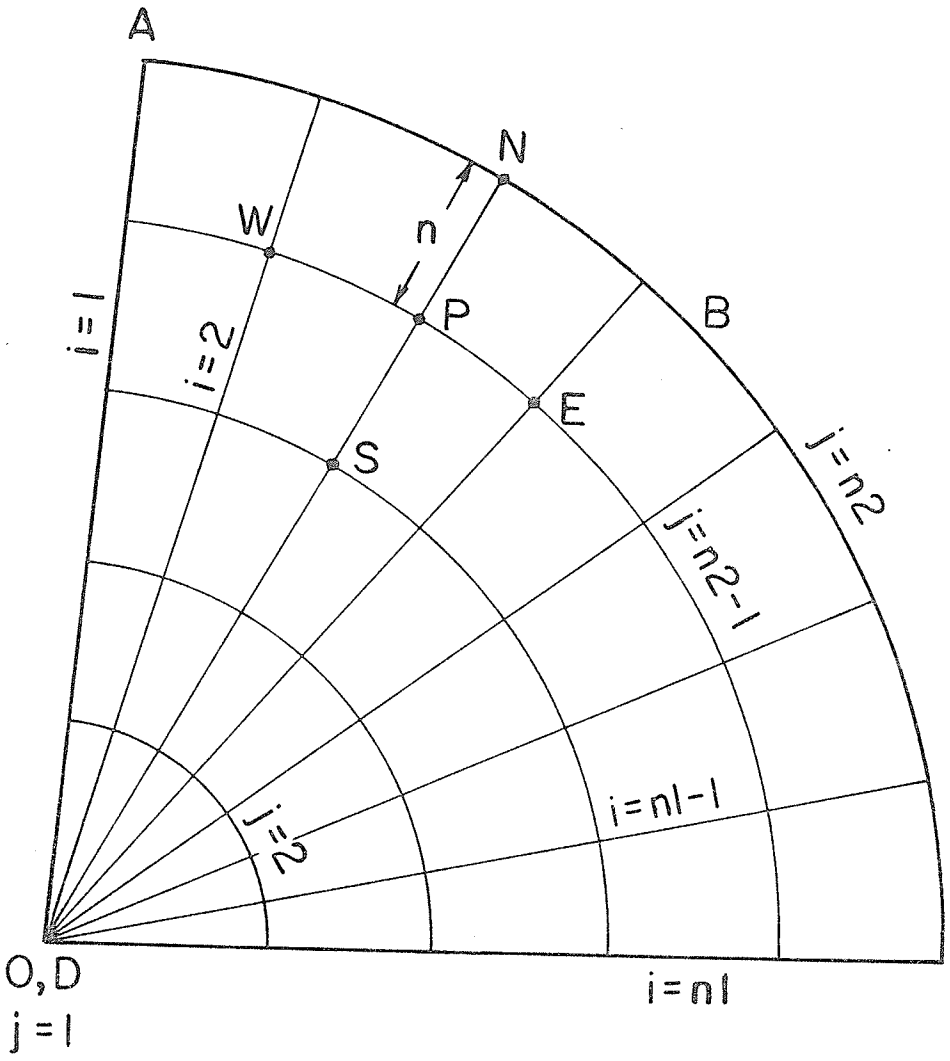

Figure F.1: Implicit Formulation of Vorticity Boundary Condition

TABLE 1

Effect of Grid Size on Predicted Values
of Friction Factor for Straight and Spiral Finned Tubes

Straight Fins						Spiral Fins					
M	$f_o Re$ due to [11]	Predicted Values of $f_o Re$ Grid Size				α	Re	Predicted Values of f/f_o Grid Size			
		11x11	13x13	15x15	17x17			11x11	13x13	15x15	17x17
4	87.820	86.510	86.761	86.946	87.087	0.3	1000	1.711	1.740	1.750	1.750
8	243.500	239.651	240.382	240.930	241.346	0.4	1000	1.802	1.860	1.906	1.935
12	545.900	536.160	537.780	539.104	540.118	0.5	1000	2.010	2.019	2.038	2.069

TABLE 2

Effect of Twist Ratio and Reynolds Number
on the Rate of Convergence for M = 4

Twist Ratio (α)	Reynolds Number (Re)	Maximum Residual in the Field			Relaxation Factor			Number of Interations required
		Vorticity (ω)	Stream Function (Ψ)	Axial Velocity (V_z)	Vorticity (ω)	Stream Function (Ψ)	Axial Velocity (V_z)	
0.1	1000	9.29×10^{-4}	-8.82×10^{-4}	6.45×10^{-5}	1.0	1.0	1.0	168
0.3	1000	-6.49×10^{-4}	-9.80×10^{-4}	-3.72×10^{-5}	0.4	0.6	1.0	665
0.5	1000	-5.56×10^{-4}	9.67×10^{-4}	6.68×10^{-5}	0.4	0.6	1.0	1143
0.4	100	9.45×10^{-4}	8.65×10^{-4}	-8.58×10^{-5}	1.0	1.0	1.0	113
0.4	500	-4.14×10^{-4}	9.80×10^{-4}	3.70×10^{-5}	1.0	1.0	1.0	448
0.4	1000	4.18×10^{-4}	9.49×10^{-4}	-3.43×10^{-5}	0.4	0.6	1.0	809

TABLE 3

Effect of Twist Ratio and Reynolds Number
on the Rate of Convergence for M = 8

Twist Ratio (α)	Reynolds Number (Re)	Maximum Residual in the Field			Relaxation Factor			Number of Iterations required
		Vorticity (ω)	Stream Function (Ψ)	Axial Velocity (V_z)	Vorticity (ω)	Stream Function (Ψ)	Axial Velocity (V_z)	
0.1	1000	-5.28×10^{-4}	-5.56×10^{-4}	-9.67×10^{-4}	1.0	1.0	1.0	119
0.3	1000	-9.45×10^{-4}	9.88×10^{-4}	6.06×10^{-5}	1.0	1.0	1.0	747
0.5	1000	9.81×10^{-4}	6.95×10^{-4}	-3.53×10^{-5}	0.4	0.6	1.0	1288
0.4	100	-9.05×10^{-4}	9.49×10^{-4}	-6.28×10^{-4}	1.0	1.0	1.0	104
0.4	400	9.96×10^{-4}	7.57×10^{-4}	-3.91×10^{-5}	1.0	1.0	1.0	157
0.4	1000	-9.92×10^{-4}	-8.67×10^{-4}	-2.09×10^{-5}	0.4	0.6	1.0	952

TABLE 4

Effect of Twist Ratio and Reynolds Number
on the Rate of Convergence for M = 12

Twist Ratio (α)	Reynolds Number (Re)	Maximum Residual in the Field			Relaxation Factor			Number of Iterations required
		Vorticity (ω)	Stream Function (Ψ)	Axial Velocity (V_z)	Vorticity (ω)	Stream Function (Ψ)	Axial Velocity (V_z)	
0.1	1000	2.59×10^{-4}	-5.63×10^{-4}	-9.52×10^{-4}	1.0	1.0	1.0	125
0.3	1000	9.14×10^{-4}	8.58×10^{-4}	2.02×10^{-5}	1.0	1.0	1.0	235
0.5	1000	-9.86×10^{-4}	-9.07×10^{-4}	3.91×10^{-5}	0.4	0.6	1.0	885
0.4	100	-9.75×10^{-4}	-9.67×10^{-4}	-7.27×10^{-4}	1.0	1.0	1.0	103
0.4	500	-3.60×10^{-4}	-9.94×10^{-4}	-7.63×10^{-4}	1.0	1.0	1.0	135
0.4	1000	9.73×10^{-4}	6.98×10^{-4}	-1.81×10^{-5}	0.4	0.6	1.0	620

TABLE 5

Friction Factor Values for Tubes With Straight Fins

M	Friction Factor times Reynolds Number ($f_o Re$)	
	Present Predictions	Due to Soliman and Feingold [11]
4	86.946	87.82
8	240.930	243.50
12	539.104	545.90

TABLE 6

Characteristics of the Flow at M = 4

[Based on the properties of air (ρ = 1.204 Kg/m^3, μ = 18.17 Pa.S) and r_o = 0.02 m].
Re = 10, $V_{z,m} = 0.4042 \times 10^{-2}$ m/s, $A_o = 0.693 \times 10^{-1}$ m^2/m length of the tube

α	$[\frac{V_z}{V_{z,m}}]_{max}$	$\frac{\alpha}{r_o}[\frac{\partial P_o/\partial\theta'}{d\bar{P}/dz'}]_{max}$	$[\frac{V_s}{V_{s,m}}]_{mean}$	$\frac{A_\alpha}{A_o}$	Average wall shear stress (N/m^2)			
					Tube Wall τ_{abc}	Fin Surface τ_{oa}	Fin Surface τ_{cd}	Overall τ_{av}
0.0	2.102	0	0	1.000	0.3149×10^{-4}	0.3158×10^{-4}	0.3148×10^{-4}	0.3151×10^{-4}
0.1	2.086	0.010	0.062	1.001	0.3242×10^{-4}	0.3458×10^{-4}	0.3497×10^{-4}	0.3378×10^{-4}
0.2	2.078	0.039	0.125	1.003	0.3316×10^{-4}	0.3793×10^{-4}	0.3882×10^{-4}	0.3618×10^{-4}
0.3	2.072	0.084	0.187	1.007	0.3372×10^{-4}	0.4161×10^{-4}	0.4302×10^{-4}	0.3872×10^{-4}
0.4	2.068	0.140	0.250	1.013	0.3410×10^{-4}	0.4559×10^{-4}	0.4751×10^{-4}	0.4138×10^{-4}
0.5	2.067	0.204	0.313	1.020	0.3429×10^{-4}	0.4981×10^{-4}	0.5229×10^{-4}	0.4416×10^{-4}

Re = 600 , $V_{z,m}$ = 0.2425 m/s

Table 6 - continued

0.0	2.102	0	0	1.000	0.1890×10^{-2}	0.1894×10^{-2}	0.1889×10^{-2}	0.1891×10^{-2}
0.1	2.036	0.011	0.063	1.001	0.2150×10^{-2}	0.2041×10^{-2}	0.2211×10^{-2}	0.2136×10^{-2}
0.2	1.963	0.053	0.130	1.003	0.2522×10^{-2}	0.2196×10^{-2}	0.2713×10^{-2}	0.2483×10^{-2}
0.3	1.905	0.125	0.199	1.007	0.2866×10^{-2}	0.2470×10^{-2}	0.3313×10^{-2}	0.2881×10^{-2}
0.4	1.858	0.215	0.269	1.013	0.3129×10^{-2}	0.2834×10^{-2}	0.3951×10^{-2}	0.3283×10^{-2}
0.5	1.802	0.311	0.338	1.020	0.3310×10^{-2}	0.3276×10^{-2}	0.4632×10^{-2}	0.3689×10^{-2}

Re = 1000 , $V_{z,m}$ = 0.4042 m/s

0.0	2.102	0	0	1.000	0.3149×10^{-2}	0.3158×10^{-2}	0.3148×10^{-2}	0.3151×10^{-2}
0.1	1.977	0.013	0.065	1.001	0.3960×10^{-2}	0.3313×10^{-2}	0.3921×10^{-2}	0.3770×10^{-2}
0.2	1.891	0.061	0.134	1.003	0.4941×10^{-2}	0.3782×10^{-2}	0.5084×10^{-2}	0.4647×10^{-2}
0.3	1.802	0.134	0.204	1.007	0.5613×10^{-2}	0.4503×10^{-2}	0.6248×10^{-2}	0.5475×10^{-2}
0.4	1.765	0.242	0.274	1.013	0.6067×10^{-2}	0.5385×10^{-2}	0.7478×10^{-2}	0.6280×10^{-2}
0.5	1.718	0.360	0.344	1.020	0.6373×10^{-2}	0.6423×10^{-2}	0.8795×10^{-2}	0.7100×10^{-2}

TABLE 7

Characteristics of the Flow at M = 8

[Based on the properties of air (ρ = 1.204 Kg/m^3, μ = 18.17 Pa.S) and r_o = 0.02 m].

Re = 10, $V_{z,m} = 0.4353 \times 10^{-2}$ m/s, $A_o = 0.536 \times 10^{-1}$ m^2/m length of the tube

α	$[\frac{V_z}{V_{z,m}}]_{max}$	$\frac{\alpha}{r_o}[\frac{\partial P_o / \partial \theta'}{d\bar{P}/dz'}]_{max}$	$[\frac{V_s}{V_{z,m}}]_{mean}$	$\frac{A_\alpha}{A_o}$	Average wall shear stress (N/m^2)			
					Tube Wall τ_{abc}	Fin Surface τ_{oa}	Fin Surface τ_{cd}	Overall τ_{av}
0.0	2.221	0	0	1.000	0.5234×10^{-4}	0.5255×10^{-4}	0.5235×10^{-4}	0.5242×10^{-4}
0.1	2.207	0.010	0.069	1.001	0.5454×10^{-4}	0.5850×10^{-4}	0.5963×10^{-4}	0.5792×10^{-4}
0.2	2.192	0.038	0.139	1.004	0.5637×10^{-4}	0.6526×10^{-4}	0.6782×10^{-4}	0.6397×10^{-4}
0.3	2.177	0.081	0.209	1.009	0.5780×10^{-4}	0.7281×10^{-4}	0.7690×10^{-4}	0.7059×10^{-4}
0.4	2.162	0.135	0.279	1.016	0.5883×10^{-4}	0.8113×10^{-4}	0.8678×10^{-4}	0.7775×10^{-4}
0.5	2.148	0.196	0.348	1.025	0.5947×10^{-4}	0.9017×10^{-4}	0.9740×10^{-4}	0.8544×10^{-4}

Re = 500 , $V_{z,m}$ = 0.2177 m/s

Table 7 - continued

0.0	2.221	0	0	1.000	0.2617×10^{-2}	0.2628×10^{-2}	0.2618×10^{-2}	0.2621×10^{-2}
0.1	2.176	0.010	0.070	1.001	0.2855×10^{-2}	0.2936×10^{-2}	0.3019×10^{-2}	0.2947×10^{-2}
0.2	2.132	0.041	0.141	1.004	0.3207×10^{-2}	0.3245×10^{-2}	0.3516×10^{-2}	0.3337×10^{-2}
0.3	2.098	0.093	0.213	1.009	0.3595×10^{-2}	0.3607×10^{-2}	0.4132×10^{-2}	0.3801×10^{-2}
0.4	2.028	0.160	0.285	1.016	0.3937×10^{-2}	0.4050×10^{-2}	0.4843×10^{-2}	0.4321×10^{-2}
0.5	1.975	0.232	0.358	1.025	0.4212×10^{-2}	0.4567×10^{-2}	0.5624×10^{-2}	0.4881×10^{-2}

Re = 1000 , $V_{z,m}$ = 0.4353 m/s

0.0	2.221	0	0	1.000	0.5233×10^{-2}	0.5255×10^{-2}	0.5235×10^{-2}	0.5242×10^{-2}
0.1	2.133	0.011	0.070	1.001	0.6272×10^{-2}	0.5811×10^{-2}	0.6174×10^{-2}	0.6063×10^{-2}
0.2	2.036	0.049	0.143	1.004	0.7830×10^{-2}	0.6523×10^{-2}	0.7583×10^{-2}	0.7249×10^{-2}
0.3	1.959	0.115	0.216	1.009	0.8918×10^{-2}	0.7570×10^{-2}	0.9234×10^{-2}	0.8531×10^{-2}
0.4	1.891	0.227	0.289	1.016	0.9575×10^{-2}	0.8799×10^{-2}	0.1103×10^{-1}	0.9832×10^{-2}
0.5	1.834	0.360	0.361	1.025	0.9994×10^{-2}	0.1014×10^{-1}	0.1297×10^{-1}	0.1118×10^{-1}

TABLE 8

Characteristics of the Flow at M = 12

[Based on the properties of air (ρ = 1.204 Kg/m^3, μ = 18.17 Pa.S) and r_o = 0.02 m].

Re = 10, $V_{z,m}$ = 0.4716×10^{-2} m/s, A_o = 0.484×10^{-1} m^2/m length of the tube

α	$[\frac{V_z}{V_{z,m}}]_{max}$	$\frac{\alpha}{r_o}[\frac{\partial P_o/\partial\theta'}{d\bar{P}/dz'}]_{max}$	$[\frac{V_s}{V_{z,m}}]_{mean}$	$\frac{A_\alpha}{A_o}$	Average wall shear stress (N/m^2)			
					Tube Wall τ_{abc}	Fin Surface τ_{oa}	Fin Surface τ_{cd}	Overall τ_{av}
0.0	2.317	0	0	1.000	0.7715×10^{-4}	0.8079×10^{-4}	0.8040×10^{-4}	0.8000×10^{-4}
0.1	2.310	0.009	0.072	1.001	0.8058×10^{-4}	0.9072×10^{-4}	0.9272×10^{-4}	0.8980×10^{-4}
0.2	2.296	0.036	0.145	1.004	0.8337×10^{-4}	0.1020×10^{-3}	0.1067×10^{-3}	0.1007×10^{-3}
0.3	2.278	0.077	0.218	1.010	0.8553×10^{-4}	0.1147×10^{-3}	0.1223×10^{-3}	0.1129×10^{-3}
0.4	2.256	0.121	0.291	1.018	0.8709×10^{-4}	0.1287×10^{-3}	0.1393×10^{-3}	0.1262×10^{-3}
0.5	2.233	0.187	0.362	1.028	0.8808×10^{-4}	0.1441×10^{-3}	0.1576×10^{-3}	0.1406×10^{-3}

Re = 500, $V_{z,m}$ = 0.2358 m/s

Table 8 - continued

0.0	2.317	0	0	1.000	0.3857×10^{-2}	0.4039×10^{-2}	0.4020×10^{-2}	0.4000×10^{-2}
0.1	2.295	0.010	0.072	1.001	0.4122×10^{-2}	0.4545×10^{-2}	0.4668×10^{-2}	0.4523×10^{-2}
0.2	2.252	0.038	0.146	1.004	0.4457×10^{-2}	0.5093×10^{-2}	0.5418×10^{-2}	0.5119×10^{-2}
0.3	2.188	0.085	0.219	1.010	0.4816×10^{-2}	0.5700×10^{-2}	0.6295×10^{-2}	0.5797×10^{-2}
0.4	2.175	0.144	0.293	1.018	0.5137×10^{-2}	0.6379×10^{-2}	0.7298×10^{-2}	0.6555×10^{-2}
0.5	2.139	0.210	0.365	1.028	0.5402×10^{-2}	0.7134×10^{-2}	0.8411×10^{-2}	0.7385×10^{-2}

Re = 1000, $V_{z,m}$ = 0.4716 m/s

0.0	2.317	0	0	1.000	0.7715×10^{-2}	0.8078×10^{-2}	0.8040×10^{-2}	0.8000×10^{-2}
0.1	2.265	0.013	0.073	1.001	0.8678×10^{-2}	0.9055×10^{-2}	0.9413×10^{-2}	0.9138×10^{-2}
0.2	2.192	0.041	0.147	1.004	0.1012×10^{-1}	0.1012×10^{-1}	0.1121×10^{-1}	0.1057×10^{-1}
0.3	2.125	0.080	0.220	1.010	0.1117×10^{-1}	0.1143×10^{-1}	0.1344×10^{-1}	0.1223×10^{-1}
0.4	2.037	0.164	0.292	1.018	0.1179×10^{-1}	0.1292×10^{-1}	0.1591×10^{-1}	0.1398×10^{-1}
0.5	1.951	0.293	0.364	1.028	0.1226×10^{-1}	0.1457×10^{-1}	0.1856×10^{-1}	0.1586×10^{-1}

TABLE 9

Predicted Values of the Ratio f/f_o for M = 4

$[f_o = 86.946/Re]$

α \ Re	10	20	50	100	200	350	600	1000
0.1	1.073	1.073	1.076	1.080	1.088	1.101	1.130	1.196
0.2	1.152	1.153	1.158	1.167	1.186	1.226	1.317	1.479
0.3	1.237	1.240	1.248	1.262	1.297	1.376	1.535	1.750
0.4	1.330	1.333	1.344	1.364	1.422	1.546	1.758	2.018
0.5	1.429	1.433	1.447	1.475	1.561	1.735	1.989	2.297

TABLE 10

Predicted Values of the Ratio f/f_o for M = 8

$[f_o = 240.930/Re]$

α \ Re	10	20	50	100	250	500	750	1000
0.1	1.106	1.106	1.107	1.109	1.114	1.125	1.139	1.158
0.2	1.225	1.226	1.228	1.232	1.245	1.278	1.329	1.388
0.3	1.359	1.360	1.364	1.370	1.394	1.464	1.556	1.642
0.4	1.507	1.509	1.514	1.523	1.560	1.675	1.800	1.906
0.5	1.671	1.673	1.680	1.691	1.747	1.909	2.062	2.186

TABLE 11

Predicted Values of the Ratio f/f_o for M = 12

$[f_o = 539.104/Re]$

α \ Re	10	20	50	100	250	500	750	1000
0.1	1.124	1.124	1.124	1.125	1.127	1.132	1.137	1.144
0.2	1.265	1.265	1.266	1.268	1.274	1.286	1.304	1.328
0.3	1.425	1.426	1.428	1.430	1.440	1.464	1.502	1.544
0.4	1.606	1.607	1.609	1.613	1.626	1.668	1.725	1.779
0.5	1.807	1.808	1.810	1.815	1.835	1.898	1.971	2.038

TABLE 12

Local Values of Axial Velocity
and Resultant Secondary Velocity
For Selected Values of M, α, and Re

$[V_z/V_{z,m}]$: M = 4, α = 0.1, Re = 10

Table 12(a)

r'/r_o \ θ'/θ_d	0.0	1/14	1/7	3/14	2/7	5/14	3/7	1/2	4/7	9/14	5/7	11/14	6/7	13/14	1.0
0.0	0.0	0.0	0.0	0.0	0.0	0.0	0.0	0.0	0.0	0.0	0.0	0.0	0.0	0.0	0.0
1/14	0.0	0.0318	0.0603	0.0848	0.105	0.119	0.128	0.131	0.128	0.120	0.105	0.0856	0.0610	0.0322	0.0
1/7	0.0	0.102	0.192	0.269	0.330	0.375	0.403	0.412	0.404	0.377	0.333	0.271	0.195	0.103	0.0
3/14	0.0	0.192	0.360	0.500	0.612	0.692	0.741	0.758	0.743	0.695	0.616	0.505	0.364	0.195	0.0
2/7	0.0	0.292	0.542	0.748	0.909	1.026	1.096	1.120	1.098	1.030	0.915	0.754	0.547	0.295	0.0
5/14	0.0	0.391	0.720	0.988	1.195	1.341	1.429	1.460	1.432	1.346	1.201	0.995	0.727	0.395	0.0
3/7	0.0	0.483	0.883	1.201	1.443	1.613	1.714	1.748	1.717	1.618	1.450	1.209	0.890	0.488	0.0
1/2	0.0	0.563	1.016	1.370	1.634	1.817	1.925	1.962	1.929	1.823	1.642	1.379	1.024	0.568	0.0
4/7	0.0	0.622	1.109	1.480	1.751	1.936	2.044	2.080	2.047	1.942	1.759	1.489	1.118	0.628	0.0
9/14	0.0	0.655	1.150	1.515	1.776	1.951	2.052	2.086	2.055	1.956	1.784	1.524	1.158	0.661	0.0
5/7	0.0	0.654	1.126	1.461	1.694	1.847	1.935	1.964	1.937	1.852	1.700	1.468	1.133	0.659	0.0
11/14	0.0	0.608	1.020	1.300	1.489	1.611	1.680	1.703	1.682	1.614	1.494	1.306	1.026	0.612	0.0
6/7	0.0	0.502	0.813	1.015	1.147	1.231	1.278	1.293	1.279	1.233	1.150	1.018	0.817	0.505	0.0
13/14	0.0	0.312	0.482	0.587	0.654	0.696	0.719	0.727	0.720	0.697	0.655	0.589	0.484	0.313	0.0
1.0	0.0	0.0	0.0	0.0	0.0	0.0	0.0	0.0	0.0	0.0	0.0	0.0	0.0	0.0	0.0

$[V_s/V_{z,m}]$: M = 4, α = 0.1, Re = 10

Table 12(a) - continued

r'/r_o \ θ'/θ_o	0.0	1/14	1/7	3/14	2/7	5/14	3/7	1/2	4/7	9/14	5/7	11/14	6/7	13/14	1.0
0.0	0.0	0.0	0.0	0.0	0.0	0.0	0.0	0.0	0.0	0.0	0.0	0.0	0.0	0.0	0.0
1/14	0.0	0.0005	0.0011	0.0017	0.0023	0.0027	0.0030	0.0032	0.0031	0.0028	0.0023	0.0017	0.0011	0.0005	0.0
1/7	0.0	0.0030	0.0060	0.0087	0.0109	0.0127	0.0137	0.0141	0.0137	0.0127	0.0110	0.0087	0.0060	0.0030	0.0
3/14	0.0	0.0080	0.0154	0.0216	0.0267	0.0303	0.0326	0.0334	0.0326	0.0305	0.0268	0.0218	0.0155	0.0081	0.0
2/7	0.0	0.0149	0.0279	0.0385	0.0467	0.0525	0.0560	0.0573	0.0562	0.0528	0.0470	0.0388	0.0281	0.0151	0.0
5/14	0.0	0.0228	0.0417	0.0566	0.0677	0.0755	0.0800	0.0816	0.0802	0.0758	0.0682	0.0571	0.0421	0.0231	0.0
3/7	0.0	0.0307	0.0551	0.0735	0.0869	0.0958	0.101	0.103	0.101	0.0963	0.0875	0.0743	0.0558	0.0311	0.0
1/2	0.0	0.0379	0.0666	0.0874	0.102	0.111	0.116	0.118	0.117	0.112	0.102	0.0882	0.0675	0.0385	0.0
4/7	0.0	0.0437	0.0751	0.0966	0.111	0.119	0.125	0.126	0.125	0.120	0.111	0.0974	0.0759	0.0443	0.0
9/14	0.0	0.0474	0.0794	0.100	0.113	0.120	0.124	0.126	0.124	0.120	0.113	0.100	0.0801	0.0480	0.0
5/7	0.0	0.0484	0.0787	0.0967	0.107	0.113	0.115	0.116	0.115	0.113	0.107	0.0970	0.0792	0.0489	0.0
11/14	0.0	0.0460	0.0720	0.0860	0.0932	0.0968	0.0984	0.0988	0.0983	0.0967	0.0932	0.0861	0.0723	0.0464	0.0
6/7	0.0	0.0392	0.0584	0.0673	0.0713	0.0730	0.0735	0.0736	0.0734	0.0728	0.0711	0.0672	0.0584	0.0393	0.0
13/14	0.0	0.0261	0.0363	0.0402	0.0416	0.0419	0.0500	0.0419	0.0419	0.0418	0.0414	0.0400	0.0362	0.0262	0.0
1.0	0.0	0.0	0.0	0.0	0.0	0.0	0.0	0.0	0.0	0.0	0.0	0.0	0.0	0.0	0.0

$[V_z/V_{z,m}]$: M = 4, α = 0.3, Re = 600

Table 12(b)

r'/r_o \ θ'/θ_o	0.0	1/14	1/7	3/14	2/7	5/14	3/7	1/2	4/7	9/14	5/7	11/14	6/7	13/14	0.0
0.0	0.0	0.0	0.0	0.0	0.0	0.0	0.0	0.0	0.0	0.0	0.0	0.0	0.0	0.0	0.0
1/14	0.0	0.0355	0.0670	0.0936	0.115	0.131	0.141	0.145	0.143	0.134	0.119	0.098	0.0705	0.0376	0.0
1/7	0.0	0.111	0.206	0.285	0.345	0.389	0.415	0.425	0.419	0.397	0.356	0.296	0.216	0.117	0.0
3/14	0.0	0.198	0.363	0.494	0.592	0.659	0.697	0.710	0.70	0.666	0.605	0.512	0.381	0.209	0.0
2/7	0.0	0.278	0.503	0.676	0.804	0.891	0.940	0.956	0.942	0.902	0.831	0.716	0.546	0.307	0.0
5/14	0.0	0.343	0.611	0.817	0.970	1.076	1.140	0.166	0.156	0.112	1.036	0.909	0.708	0.407	0.0
3/7	0.0	0.398	0.693	0.915	1.087	1.215	1.300	1.344	1.347	1.309	1.235	1.100	0.872	0.513	0.0
1/2	0.0	0.452	0.769	0.996	1.172	1.311	1.420	1.493	1.526	1.512	1.439	1.297	1.041	0.621	0.0
4/7	0.0	0.513	0.850	1.081	1.254	1.393	1.509	1.603	1.673	1.698	1.645	1.499	1.212	0.732	0.0
9/14	0.0	0.577	0.946	1.181	1.348	1.479	1.591	1.689	1.774	1.833	1.830	1.684	1.371	0.838	0.0
5/7	0.0	0.631	1.030	1.280	1.442	1.562	1.663	1.754	1.834	1.894	1.905	1.785	1.480	0.926	0.0
11/14	0.0	0.651	1.054	1.312	1.475	1.589	1.678	1.754	1.816	1.854	1.842	1.721	1.441	0.941	0.0
6/7	0.0	0.591	0.931	1.158	1.315	1.432	1.513	1.569	1.604	1.610	1.565	1.441	1.212	0.817	0.0
13/14	0.0	0.386	0.586	0.723	0.836	0.924	0.982	1.014	1.024	1.007	0.953	0.865	0.733	0.5065	0.0
1.0	0.0	0.0	0.0	0.0	0.0	0.0	0.0	0.0	0.0	0.0	0.0	0.0	0.0	0.0	0.0

$[V_s/V_{z,m}]$: M = 4, α = 0.3, Re = 600

Table 12(b) - continued

r'/r_o \ θ'/θ_o	0.0	1/14	1/7	3/14	2/7	5/14	3/7	1/2	4/7	9/14	5/7	11/14	6/7	13/14	0.0
0.0	0.0	0.0	0.0	0.0	0.0	0.0	0.0	0.0	0.0	0.0	0.0	0.0	0.0	0.0	0.0
1/14	0.0	0.0015	0.0032	0.0049	0.0064	0.0077	0.0086	0.0089	0.0087	0.0079	0.0067	0.0052	0.0034	0.0016	0.0
1/7	0.0	0.0084	0.0163	0.0232	0.0290	0.0336	0.0366	0.0381	0.0378	0.0357	0.0316	0.0256	0.0179	0.0092	0.0
3/14	0.0	0.0200	0.0374	0.0521	0.0642	0.0738	0.0805	0.0843	0.0849	0.0819	0.0747	0.0627	0.0457	0.0243	0.0
2/7	0.0	0.0321	0.0589	0.0816	0.100	0.116	0.128	0.136	0.139	0.137	0.129	0.113	0.0857	0.0472	0.0
5/14	0.0	0.0421	0.0759	0.105	0.130	0.153	0.171	0.184	0.192	0.194	0.188	0.171	0.136	0.0782	0.0
3/7	0.0	0.0514	0.0888	0.121	0.152	0.180	0.204	0.224	0.237	0.245	0.244	0.230	0.192	0.116	0.0
1/2	0.0	0.0631	0.103	0.136	0.169	0.201	0.230	0.255	0.274	0.287	0.291	0.282	0.246	0.158	0.0
4/7	0.0	0.0798	0.125	0.159	0.192	0.225	0.254	0.279	0.301	0.317	0.325	0.321	0.290	0.197	0.0
9/14	0.0	0.103	0.159	0.198	0.232	0.261	0.286	0.307	0.324	0.340	0.350	0.344	0.314	0.224	0.0
5/7	0.0	0.130	0.206	0.255	0.288	0.312	0.329	0.340	0.348	0.355	0.358	0.348	0.316	0.233	0.0
11/14	0.0	0.156	0.253	0.312	0.345	0.361	0.367	0.367	0.364	0.358	0.347	0.325	0.288	0.218	0.0
6/7	0.0	0.163	0.262	0.322	0.353	0.365	0.363	0.352	0.337	0.319	0.295	0.265	0.230	0.176	0.0
13/14	0.0	0.120	0.187	0.227	0.250	0.258	0.253	0.241	0.224	0.203	0.179	0.156	0.136	0.107	0.0
1.0	0.0	0.0	0.0	0.0	0.0	0.0	0.0	0.0	0.0	0.0	0.0	0.0	0.0	0.0	0.0

$[V_z/V_{z,m}]$: M = 4, α = 0.5 Re = 1000

Table 12(c)

r'/r_o \ θ'/θ_o	0.0	1/14	1/7	3/14	2/7	5/14	3/7	1/2	4/7	9/14	5/7	11/14	6/7	13/14	1.0
0.0	0.0	0.0	0.0	0.0	0.0	0.0	0.0	0.0	0.0	0.0	0.0	0.0	0.0	0.0	0.0
1/14	0.0	0.0509	0.0957	0.133	0.163	0.185	0.199	0.205	0.202	0.191	0.171	0.142	0.102	0.0547	0.0
1/7	0.0	0.144	0.266	0.364	0.437	0.488	0.517	0.526	0.518	0.494	0.448	0.378	0.280	0.153	0.0
3/14	0.0	0.230	0.416	0.560	0.665	0.735	0.773	0.783	0.770	0.736	0.678	0.587	0.449	0.254	0.0
2/7	0.0	0.292	0.515	0.687	0.815	0.904	0.955	0.972	0.960	0.921	0.861	0.763	0.605	0.355	0.0
5/14	0.0	0.344	0.585	0.759	0.893	0.999	1.075	1.110	1.109	1.076	1.019	0.923	0.755	0.460	0.0
3/7	0.0	0.399	0.649	0.814	0.941	1.048	1.138	1.205	1.233	1.222	1.171	1.083	0.909	0.575	0.0
1/2	0.0	0.459	0.722	0.873	0.987	1.086	1.176	1.257	1.321	1.352	1.332	1.253	1.079	0.704	0.0
4/7	0.0	0.539	0.822	0.965	1.062	1.142	1.219	1.297	1.373	1.442	1.487	1.435	1.268	0.848	0.0
9/14	0.0	0.648	0.963	1.107	1.179	1.230	1.284	1.347	1.419	1.497	1.577	1.615	1.470	1.005	0.0
5/7	0.0	0.782	1.142	1.280	1.315	1.336	1.370	1.418	1.478	1.550	1.630	1.703	1.643	1.152	0.0
11/14	0.0	0.915	1.326	1.405	1.416	1.430	1.455	1.495	1.543	1.600	1.664	1.718	1.656	1.218	0.0
6/7	0.0	0.926	1.282	1.374	1.398	1.416	1.440	1.476	1.516	1.558	1.599	1.618	1.513	1.113	0.0
13/14	0.0	0.634	0.875	0.986	1.018	1.026	1.039	1.068	1.100	1.133	1.158	1.144	1.021	0.742	0.0
1.0	0.0	0.0	0.0	0.0	0.0	0.0	0.0	0.0	0.0	0.0	0.0	0.0	0.0	0.0	0.0

$[V_s/V_{z,m}]$: M = 4, α = 0.5 Re = 1000

Table 12(c) - continued

θ'/θ_o / r'/r_o	0.0	1/14	1/7	3/14	2/7	5/14	3/7	1/2	4/7	9/14	5/7	11/14	6/7	13/14	1.0
0.0	0.0	0.0	0.0	0.0	0.0	0.0	0.0	0.0	0.0	0.0	0.0	0.0	0.0	0.0	0.0
1/14	0.0	0.0033	0.0067	0.0100	0.129	0.0153	0.0169	0.0177	0.0175	0.0163	0.0141	0.0110	0.0074	0.0036	0.0
1/7	0.0	0.0158	0.0296	0.0415	0.0513	0.0589	0.0644	0.0673	0.0676	0.0649	0.0589	0.0491	0.0356	0.0188	0.0
3/14	0.0	0.0312	0.0570	0.0790	0.0676	0.113	0.124	0.131	0.134	0.132	0.124	0.108	0.822	0.0455	0.0
2/7	0.0	0.0439	0.0778	0.107	0.134	0.158	0.177	0.192	0.200	0.202	0.197	0.179	0.144	0.0836	0.0
5/14	0.0	0.0582	0.0954	0.126	0.157	0.189	0.219	0.243	0.260	0.269	0.271	0.258	0.218	0.135	0.0
3/7	0.0	0.0778	0.116	0.142	0.173	0.210	0.248	0.283	0.310	0.330	0.340	0.338	0.302	0.20	0.0
1/2	0.0	0.102	0.141	0.164	0.195	0.235	0.276	0.315	0.350	0.379	0.400	0.410	0.388	0.276	0.0
4/7	0.0	0.135	0.180	0.207	0.242	0.281	0.318	0.352	0.384	0.415	0.448	0.469	0.464	0.355	0.0
9/14	0.0	0.184	0.248	0.293	0.333	0.363	0.385	0.406	0.426	0.449	0.481	0.517	0.524	0.423	0.0
5/7	0.0	0.258	0.363	0.434	0.464	0.475	0.479	0.482	0.488	0.499	0.520	0.552	0.569	0.464	0.0
11/14	0.0	0.369	0.536	0.589	0.596	0.591	0.581	0.572	0.565	0.563	0.570	0.583	0.572	0.465	0.0
6/7	0.0	0.458	0.641	0.676	0.668	0.653	0.636	0.623	0.609	0.596	0.587	0.575	0.527	0.406	0.0
13/14	0.0	0.366	0.505	0.540	0.530	0.510	0.495	0.486	0.476	0.466	0.451	0.420	0.355	0.263	0.0
1.0	0.0	0.0	0.0	0.0	0.0	0.0	0.0	0.0	0.0	0.0	0.0	0.0	0.0	0.0	0.0

$[V_z/V_{z,m}]$: M = 8, α = 0.1, Re = 10

Table 12(d)

r'/r_o \ θ'/θ_o	0.0	1/14	1/7	3/14	2/7	5/14	3/7	1/2	4/7	9/14	5/7	11/14	6/7	13/14	1.0
0.0	0.0	0.0	0.0	0.0	0.0	0.0	0.0	0.0	0.0	0.0	0.0	0.0	0.0	0.0	0.0
1/14	0.0	0.0098	0.0183	0.0253	0.0309	0.0348	0.0373	0.0381	0.0373	0.0350	0.0311	0.0256	0.0186	0.0100	0.0
1/7	0.0	0.0387	0.0719	0.0994	0.121	0.136	0.146	0.149	0.146	0.137	0.122	0.101	0.0731	0.0395	0.0
3/14	0.0	0.0861	0.159	0.220	0.268	0.303	0.324	0.331	0.325	0.305	0.271	0.223	0.162	0.0878	0.0
2/7	0.0	0.150	0.278	0.384	0.467	0.527	0.563	0.576	0.565	0.530	0.472	0.389	0.283	0.153	0.0
5/14	0.0	0.229	0.423	0.583	0.709	0.799	0.853	0.873	0.856	0.804	0.715	0.591	0.430	0.233	0.0
3/7	0.0	0.317	0.586	0.806	0.978	1.101	1.176	1.202	1.180	1.108	0.987	0.816	0.595	0.323	0.0
1/2	0.0	0.410	0.756	1.037	1.256	1.412	1.506	1.539	1.511	1.420	1.267	1.050	0.767	0.418	0.0
4/7	0.0	0.500	0.918	1.255	1.515	1.700	1.811	1.850	1.817	1.710	1.528	1.270	0.931	0.509	0.0
9/14	0.0	0.577	1.053	1.432	1.722	1.926	2.048	2.091	2.054	1.937	1.736	1.448	1.068	0.587	0.0
5/7	0.0	0.628	1.135	1.533	1.832	2.041	2.165	2.207	2.170	2.051	1.846	1.549	1.151	0.639	0.0
11/14	0.0	0.636	1.133	1.512	1.791	1.983	2.095	2.134	2.100	1.992	1.804	1.527	1.147	0.645	0.0
6/7	0.0	0.574	0.998	1.309	1.531	1.680	1.766	1.795	1.769	1.687	1.540	1.320	1.009	0.581	0.0
13/14	0.0	0.396	0.661	0.842	0.967	1.048	1.095	1.110	1.096	1.051	0.971	0.848	0.667	0.400	0.0
1.0	0.0	0.0	0.0	0.0	0.0	0.0	0.0	0.0	0.0	0.0	0.0	0.0	0.0	0.0	0.0

$[V_s/V_{z,m}]$: M = 8, α = 0.1, Re = 10

Table 12(d) - continued

θ'/θ_o / r'/r_o	0.0	1/14	1/7	3/14	2/7	5/14	3/7	1/2	4/7	9/14	5/7	11/14	6/7	13/14	1.0
0.0	0.0	0.0	0.0	0.0	0.0	0.0	0.0	0.0	0.0	0.0	0.0	0.0	0.0	0.0	0.0
1/14	0.0	0.00008	0.0001	0.0002	0.0003	0.0003	0.0003	0.0004	0.0003	0.0003	0.0003	0.0002	0.0002	0.00008	0.0
1/7	0.0	0.0006	0.0012	0.0017	0.0020	0.0024	0.0025	0.0026	0.0025	0.0023	0.0021	0.0017	0.0012	0.0006	0.0
3/14	0.0	0.0021	0.0039	0.0055	0.0067	0.0076	0.0082	0.0084	0.0083	0.0077	0.0068	0.0055	0.0039	0.0021	0.0
2/7	0.0	0.0048	0.0091	0.0127	0.0157	0.0178	0.0191	0.0195	0.0191	0.0179	0.0158	0.0129	0.0093	0.0049	0.0
5/14	0.0	0.0093	0.0174	0.0242	0.0297	0.0337	0.0361	0.0370	0.0362	0.0339	0.0300	0.0245	0.0177	0.0094	0.0
3/7	0.0	0.0155	0.0289	0.0401	0.0489	0.0554	0.0593	0.0606	0.0594	0.0557	0.0494	0.0406	0.0293	0.0157	0.0
1/2	0.0	0.0233	0.0432	0.0596	0.0723	0.0815	0.0870	0.0889	0.0873	0.0819	0.0729	0.0603	0.0438	0.0237	0.0
4/7	0.0	0.0321	0.0589	0.0806	0.0971	0.109	0.116	0.118	0.116	0.109	0.0980	0.0815	0.0598	0.0327	0.0
9/14	0.0	0.0408	0.0739	0.100	0.119	0.133	0.141	0.144	0.141	0.134	0.120	0.101	0.0750	0.0415	0.0
5/7	0.0	0.0477	0.0851	0.113	0.134	0.148	0.156	0.159	0.156	0.149	0.135	0.114	0.0862	0.0485	0.0
11/14	0.0	0.0509	0.0887	0.116	0.135	0.148	0.155	0.157	0.155	0.148	0.136	0.117	0.0898	0.0517	0.0
6/7	0.0	0.0478	0.0808	0.103	0.118	0.127	0.132	0.134	0.132	0.127	0.118	0.104	0.0816	0.0484	0.0
13/14	0.0	0.0351	0.0565	0.0694	0.0772	0.0818	0.0842	0.0850	0.0843	0.0820	0.0775	0.0698	0.0570	0.0357	0.0
1.0	0.0	0.0	0.0	0.0	0.0	0.0	0.0	0.0	0.0	0.0	0.0	0.0	0.0	0.0	0.0

$[V_z/V_{z,m}]$: M = 8, α = 0.3, Re = 500 Table 12(e)

r'/r_o \ θ'/θ_o	0.0	1/14	1/7	3/14	2/7	5/14	3/7	1/2	4/7	9/14	5/7	11/14	6/7	13/14	1.0
0.0	0.0	0.0	0.0	0.0	0.0	0.0	0.0	0.0	0.0	0.0	0.0	0.0	0.0	0.0	0.0
1/14	0.0	0.0107	0.0197	0.0272	0.0330	0.0372	0.0398	0.0408	0.0402	0.0379	0.0339	0.0282	0.0207	0.0113	0.0
1/7	0.0	0.0423	0.0781	0.107	0.130	0.147	0.157	0.161	0.159	0.150	0.134	0.112	0.0818	0.0447	0.0
3/14	0.0	0.0934	0.172	0.236	0.286	0.322	0.345	0.353	0.348	0.328	0.294	0.245	0.180	0.0986	0.0
2/7	0.0	0.161	0.295	0.404	0.488	0.548	0.585	0.598	0.589	0.557	0.500	0.417	0.307	0.169	0.0
5/14	0.0	0.238	0.436	0.595	0.715	0.800	0.850	0.868	0.853	0.807	0.726	0.609	0.451	0.248	0.0
3/7	0.0	0.319	0.581	0.788	0.944	1.052	1.114	1.134	1.113	1.053	0.951	0.801	0.597	0.332	0.0
1/2	0.0	0.394	0.713	0.964	1.152	1.282	1.358	1.381	1.357	1.286	1.166	0.988	0.743	0.416	0.0
4/7	0.0	0.458	0.822	1.108	1.326	1.481	1.574	1.609	1.587	1.509	1.375	1.174	0.888	0.501	0.0
9/14	0.0	0.515	0.916	1.224	1.460	1.636	1.755	1.814	1.807	1.732	1.588	1.362	1.036	0.588	0.0
5/7	0.0	0.569	1.000	1.324	1.571	1.758	1.893	1.977	2.001	1.949	1.798	1.546	1.177	0.669	0.0
11/14	0.0	0.607	1.060	1.398	1.649	1.836	1.972	2.061	2.098	2.065	1.931	1.670	1.276	0.731	0.0
6/7	0.0	0.588	1.021	1.350	1.591	1.767	1.891	1.966	1.989	1.947	1.818	1.579	1.225	0.723	0.0
13/14	0.0	0.439	0.734	0.954	1.130	1.268	1.362	1.408	1.405	1.350	1.240	1.077	0.849	0.519	0.0
1.0	0.0	0.0	0.0	0.0	0.0	0.0	0.0	0.0	0.0	0.0	0.0	0.0	0.0	0.0	0.0

$[V_s/V_{z,m}]$: M = 8, α = 0.3, Re = 500

Table 12(e) - continued

r'/r_o \ θ'/θ_o	0.0	1/14	1/7	3/14	2/7	5/14	3/7	1/2	4/7	9/14	5/7	11/14	6/7	13/14	1.0
0.0	0.0	0.0	0.0	0.0	0.0	0.0	0.0	0.0	0.0	0.0	0.0	0.0	0.0	0.0	0.0
1/14	0.0	0.0003	0.0005	0.0007	0.0009	0.0010	0.0011	0.0012	0.0011	0.0010	0.0009	0.0007	0.0005	0.0003	0.0
1/7	0.0	0.0020	0.0038	0.0054	0.0066	0.0075	0.0081	0.0083	0.0082	0.0077	0.0068	0.0056	0.0040	0.0021	0.0
3/14	0.0	0.0067	0.0125	0.0175	0.0214	0.0244	0.0262	0.0270	0.0266	0.0250	0.0223	0.0183	0.0133	0.0071	0.0
2/7	0.0	0.0153	0.0285	0.0396	0.0484	0.0550	0.0592	0.0609	0.0601	0.0568	0.0507	0.0420	0.0305	0.0165	0.0
5/14	0.0	0.0281	0.0521	0.0721	0.0881	0.0998	0.107	0.110	0.109	0.104	0.0934	0.0779	0.0571	0.0310	0.0
3/7	0.0	0.0443	0.0816	0.112	0.137	0.155	0.167	0.172	0.171	0.163	0.148	0.125	0.0929	0.0510	0.0
1/2	0.0	0.0619	0.113	0.155	0.188	0.213	0.230	0.239	0.239	0.230	0.212	0.182	0.137	0.0768	0.0
4/7	0.0	0.0791	0.142	0.193	0.235	0.268	0.292	0.305	0.308	0.299	0.279	0.244	0.189	0.108	0.0
9/14	0.0	0.0972	0.171	0.229	0.277	0.316	0.346	0.365	0.372	0.365	0.345	0.307	0.243	0.142	0.0
5/7	0.0	0.118	0.203	0.268	0.320	0.363	0.397	0.419	0.430	0.425	0.402	0.359	0.289	0.174	0.0
11/14	0.0	0.140	0.241	0.315	0.371	0.413	0.444	0.462	0.468	0.460	0.435	0.387	0.313	0.193	0.0
6/7	0.0	0.152	0.263	0.346	0.403	0.440	0.461	0.468	0.462	0.443	0.410	0.360	0.291	0.186	0.0
13/14	0.0	0.127	0.215	0.278	0.323	0.351	0.362	0.358	0.341	0.315	0.282	0.245	0.200	0.132	0.0
1.0	0.0	0.0	0.0	0.0	0.0	0.0	0.0	0.0	0.0	0.0	0.0	0.0	0.0	0.0	0.0

$[V_z/V_{z,m}]$: M = 8, α = 0.5, Re = 1000

Table 12(f)

θ'/θ_o / r'/r_o	0.0	1/14	1/7	3/14	2/7	5/14	3/7	1/2	4/7	9/14	5/7	11/14	6/7	13/14	1.0
0.0	0.0	0.0	0.0	0.0	0.0	0.0	0.0	0.0	0.0	0.0	0.0	0.0	0.0	0.0	0.0
1/14	0.0	0.0157	0.0289	0.0398	0.0483	0.0545	0.0583	0.0598	0.0589	0.0556	0.0498	0.0415	0.0304	0.0166	0.0
1/7	0.0	0.0614	0.113	0.155	0.188	0.212	0.227	0.232	0.229	0.217	0.194	0.162	0.119	0.653	0.0
3/14	0.0	0.131	0.241	0.329	0.397	0.445	0.474	0.484	0.477	0.452	0.407	0.341	0.252	0.138	0.0
2/7	0.0	0.212	0.386	0.524	0.627	0.698	0.739	0.752	0.738	0.699	0.632	0.533	0.397	0.221	0.0
5/14	0.0	0.286	0.516	0.696	0.830	0.921	0.971	0.985	0.965	0.915	0.831	0.707	0.534	0.300	0.0
3/7	0.0	0.343	0.611	0.818	0.976	1.089	1.154	1.176	1.155	1.096	1.001	0.8610	0.659	0.377	0.0
1/2	0.0	0.391	0.683	0.900	1.066	1.191	1.279	1.322	1.313	1.255	1.153	1.00	0.781	0.453	0.0
4/7	0.0	0.437	0.747	0.963	1.125	1.253	1.352	1.418	1.438	1.396	1.295	1.143	0.906	0.535	0.0
9/14	0.0	0.487	0.819	1.037	1.187	1.305	1.403	1.480	1.527	1.521	1.445	1.298	1.050	0.629	0.0
5/7	0.0	0.556	0.930	1.164	1.303	1.400	1.478	1.545	1.600	1.631	1.608	1.484	1.225	0.741	0.0
11/14	0.0	0.633	1.065	1.342	1.491	1.556	1.594	1.635	1.682	1.727	1.754	1.703	1.424	0.865	0.0
6/7	0.0	0.682	1.144	1.459	1.631	1.678	1.700	1.728	1.765	1.806	1.834	1.794	1.524	0.959	0.0
13/14	0.0	0.575	0.928	1.186	1.371	1.473	1.537	1.586	1.626	1.645	1.623	1.514	1.242	0.788	0.0
1.0	0.0	0.0	0.0	0.0	0.0	0.0	0.0	0.0	0.0	0.0	0.0	0.0	0.0	0.0	0.0

$[V_s/V_{z,m}]$: M = 8, α = 0.5, Re = 1000

Table 12(f) - continued

θ'/θ_o / r'/r_o	0.0	1/14	1/7	3/14	2/7	5/14	3/7	1/2	4/7	9/14	5/7	11/14	6/7	13/14	1.0
0.0	0.0	0.0	0.0	0.0	0.0	0.0	0.0	0.0	0.0	0.0	0.0	0.0	0.0	0.0	0.0
1/14	0.0	0.0006	0.0012	0.0018	0.0022	0.0025	0.0027	0.0028	0.0027	0.0026	0.0023	0.0018	0.0013	0.0007	0.0
1/7	0.0	0.0049	0.0092	0.0129	0.0158	0.0180	0.0195	0.0200	0.0198	0.0187	0.0166	0.0137	0.0099	0.0053	0.0
3/14	0.0	0.0155	0.0289	0.0401	0.0491	0.0558	0.0602	0.0620	0.0614	0.0582	0.0522	0.0434	0.0316	0.0171	0.0
2/7	0.0	0.0327	0.0604	0.0833	0.101	0.115	0.124	0.127	0.126	0.120	0.109	0.0922	0.0684	0.0375	0.0
5/14	0.0	0.0532	0.0968	0.133	0.161	0.182	0.197	0.203	0.203	0.195	0.180	0.155	0.118	0.0661	0.0
3/7	0.0	0.0731	0.130	0.176	0.214	0.244	0.266	0.278	0.280	0.272	0.255	0.225	0.176	0.102	0.0
1/2	0.0	0.0947	0.161	0.212	0.254	0.292	0.323	0.345	0.353	0.349	0.332	0.300	0.242	0.144	0.0
4/7	0.0	0.120	0.196	0.246	0.288	0.329	0.369	0.402	0.422	0.424	0.410	0.380	0.317	0.195	0.0
9/14	0.0	0.152	0.237	0.286	0.325	0.368	0.414	0.457	0.488	0.502	0.494	0.467	0.403	0.257	0.0
5/7	0.0	0.197	0.303	0.359	0.399	0.441	0.485	0.527	0.561	0.581	0.584	0.561	0.496	0.327	0.0
11/14	0.0	0.258	0.405	0.492	0.546	0.580	0.605	0.626	0.645	0.659	0.667	0.657	0.580	0.391	0.0
6/7	0.0	0.317	0.520	0.656	0.731	0.747	0.746	0.740	0.735	0.730	0.724	0.702	0.609	0.416	0.0
13/14	0.0	0.302	0.503	0.646	0.736	0.770	0.775	0.766	0.747	0.718	0.677	0.609	0.495	0.331	0.0
1.0	0.0	0.0	0.0	0.0	0.0	0.0	0.0	0.0	0.0	0.0	0.0	0.0	0.0	0.0	0.0

$[V_z/V_{z,m}]$: M = 12, α = 0.1, Re = 10 Table 12(g)

r'/r_o \ θ'/θ_o	0.0	1/14	1/7	3/14	2/7	5/14	3/7	1/2	4/7	9/14	5/7	11/14	6/7	13/14	1.0
0.0	0.0	0.0	0.0	0.0	0.0	0.0	0.0	0.0	0.0	0.0	0.0	0.0	0.0	0.0	0.0
1/14	0.0	0.0070	0.0129	0.0178	0.0216	0.0243	0.0259	0.0265	0.0260	0.0244	0.0218	0.0179	0.0131	0.0071	0.0
1/7	0.0	0.0276	0.0510	0.0701	0.0851	0.0958	0.102	0.105	0.103	0.0965	0.0860	0.0711	0.0519	0.0282	0.0
3/14	0.0	0.0619	0.114	0.157	0.191	0.215	0.229	0.234	0.230	0.216	0.193	0.159	0.116	0.0632	0.0
2/7	0.0	0.109	0.202	0.279	0.338	0.380	0.406	0.415	0.408	0.383	0.341	0.282	0.206	0.112	0.0
5/14	0.0	0.171	0.315	0.433	0.525	0.592	0.632	0.646	0.634	0.596	0.531	0.439	0.321	0.174	0.0
3/7	0.0	0.244	0.451	0.619	0.751	0.846	0.903	0.923	0.906	0.851	0.759	0.628	0.459	0.249	0.0
1/2	0.0	0.328	0.606	0.832	1.009	1.135	1.212	1.239	1.216	1.143	1.019	0.844	0.616	0.335	0.0
4/7	0.0	0.420	0.774	1.063	1.287	1.447	1.544	1.579	1.550	1.457	1.300	1.077	0.787	0.429	0.0
9/14	0.0	0.513	0.943	1.292	1.562	1.754	1.871	1.912	1.877	1.766	1.577	1.309	0.958	0.523	0.0
5/7	0.0	0.594	1.088	1.486	1.792	2.009	2.140	2.186	2.147	2.022	1.809	1.505	1.106	0.606	0.0
11/14	0.0	0.644	1.171	1.589	1.906	2.130	2.264	2.310	2.270	2.143	1.924	1.608	1.189	0.656	0.0
6/7	0.0	0.627	1.122	1.504	1.788	1.984	2.101	2.141	2.106	1.995	1.803	1.521	1.138	0.638	0.0
13/14	0.0	0.473	0.818	1.070	1.250	1.370	1.440	1.464	1.444	1.376	1.258	1.080	0.828	0.479	0.0
1.0	0.0	0.0	0.0	0.0	0.0	0.0	0.0	0.0	0.0	0.0	0.0	0.0	0.0	0.0	0.0

$[V_s/V_{z,m}]$: M = 12, α = 0.1, Re = 10

Table 12(g) - continued

θ'/θ_o / r'/r_o	0.0	1/14	1/7	3/14	2/7	5/14	3/7	1/2	4/7	9/14	5/7	11/14	6/7	13/14	0.0
0.0	0.0	0.0	0.0	0.0	0.0	0.0	0.0	0.0	0.0	0.0	0.0	0.0	0.0	0.0	0.0
1/14	0.0	0.00005	0.00009	0.00014	0.00017	0.00019	0.00021	0.00021	0.00021	0.00020	0.00017	0.00014	0.00010	0.00005	0.0
1/7	0.0	0.00041	0.00077	0.0011	0.0013	0.0015	0.0016	0.0016	0.0016	0.0015	0.0013	0.0011	0.00078	0.00042	0.0
3/14	0.0	0.0014	0.0026	0.0036	0.0043	0.0049	0.0052	0.0054	0.0053	0.0049	0.0044	0.0036	0.0026	0.0014	0.0
2/7	0.0	0.0033	0.0061	0.0084	0.0102	0.0116	0.0124	0.0126	0.0124	0.0116	0.0103	0.0085	0.0062	0.0033	0.0
5/14	0.0	0.0064	0.0118	0.0163	0.0199	0.0224	0.0240	0.0245	0.0241	0.0226	0.0201	0.0166	0.0120	0.0065	0.0
3/7	0.0	0.0109	0.0203	0.0280	0.0341	0.0385	0.0412	0.0421	0.0413	0.0388	0.0345	0.0284	0.0207	0.0112	0.0
1/2	0.0	0.0172	0.0319	0.0440	0.0535	0.0603	0.0645	0.0660	0.0647	0.0607	0.0540	0.0446	0.0324	0.0176	0.0
4/7	0.0	0.0252	0.0466	0.0641	0.0778	0.0877	0.0937	0.0958	0.0940	0.0883	0.0786	0.0650	0.0474	0.0257	0.0
9/14	0.0	0.0345	0.0636	0.0872	0.106	0.119	0.127	0.129	0.127	0.119	0.107	0.0884	0.0646	0.0352	0.0
5/7	0.0	0.0441	0.0806	0.109	0.132	0.148	0.158	0.161	0.158	0.149	0.134	0.111	0.0819	0.0450	0.0
11/14	0.0	0.0517	0.0932	0.126	0.150	0.167	0.177	0.180	0.177	0.168	0.151	0.127	0.0947	0.0527	0.0
6/7	0.0	0.0533	0.0941	0.125	0.147	0.162	0.171	0.174	0.171	0.163	0.148	0.126	0.0954	0.0542	0.0
13/14	0.0	0.0430	0.0732	0.0942	0.108	0.118	0.123	0.125	0.123	0.118	0.109	0.0950	0.0740	0.0436	0.0
1.0	0.0	0.0	0.0	0.0	0.0	0.0	0.0	0.0	0.0	0.0	0.0	0.0	0.0	0.0	0.0

$[V_z/V_{z,m}]$: M = 12, α = 0.3, Re = 500

Table 12(h)

r'/r_o \ θ'/θ_o	0.0	1/14	1/7	3/14	2/7	5/14	3/7	1/2	4/7	9/14	5/7	11/14	6/7	13/14	1.0
0.0	0.0	0.0	0.0	0.0	0.0	0.0	0.0	0.0	0.0	0.0	0.0	0.0	0.0	0.0	0.0
1/14	0.0	0.0074	0.0137	0.0187	0.0227	0.0255	0.0272	0.0279	0.0275	0.0260	0.0233	0.0195	0.0144	0.0079	0.0
3/14	0.0	0.0661	0.121	0.166	0.201	0.226	0.241	0.247	0.243	0.230	0.207	0.173	0.127	0.0702	0.0
2/7	0.0	0.116	0.213	0.292	0.353	0.397	0.424	0.434	0.428	0.405	0.364	0.304	0.224	0.124	0.0
5/14	0.0	0.179	0.328	0.449	0.542	0.609	0.650	0.666	0.657	0.621	0.558	0.467	0.345	0.190	0.0
3/7	0.0	0.253	0.462	0.631	0.761	0.854	0.910	0.931	0.917	0.868	0.781	0.654	0.484	0.267	0.0
1/2	0.0	0.333	0.607	0.828	0.996	1.115	1.187	1.213	1.193	1.129	1.017	0.853	0.632	0.350	0.0
4/7	0.0	0.414	0.754	1.025	1.232	1.377	1.464	1.494	1.469	1.389	1.253	1.054	0.784	0.435	0.0
9/14	0.0	0.489	0.889	1.207	1.449	1.621	1.725	1.763	1.736	1.643	1.485	1.252	0.935	0.522	0.0
5/7	0.0	0.557	1.005	1.358	1.629	1.826	1.953	2.008	1.987	1.889	1.712	1.448	1.084	0.607	0.0
11/14	0.0	0.609	1.092	1.468	1.756	1.968	2.112	2.187	2.188	2.101	1.912	1.618	1.213	0.680	0.0
6/7	0.0	0.617	1.096	1.470	1.753	1.692	2.103	2.178	2.184	2.110	1.936	1.650	1.249	0.710	0.0
13/14	0.0	0.498	0.863	1.145	1.362	1.523	1.627	1.675	1.665	1.593	1.458	1.252	0.963	0.564	0.0
1.0	0.0	0.0	0.0	0.0	0.0	0.0	0.0	0.0	0.0	0.0	0.0	0.0	0.0	0.0	0.0

$[V_s/V_{z,m}]$: M = 12, α = 0.3, Re = 500

Table 12(h) - continued

θ'/θ_o / r'/r_o	0.0	1/14	1/7	3/14	2/7	5/14	3/7	1/2	4/7	9/14	5/7	11/14	6/7	13/14	1.0
0.0	0.0	0.0	0.0	0.0	0.0	0.0	0.0	0.0	0.0	0.0	0.0	0.0	0.0	0.0	0.0
1/14	0.0	0.00017	0.00032	0.00044	0.00054	0.00061	0.00065	0.00067	0.00066	0.00062	0.00055	0.00045	0.00033	0.00018	0.0
1/7	0.0	0.0013	0.0024	0.0034	0.0041	0.0046	0.0050	0.0051	0.0050	0.0047	0.0042	0.0035	0.0026	0.0014	0.0
3/14	0.0	0.0044	0.0082	0.0113	0.0137	0.0154	0.0165	0.0169	0.0167	0.0157	0.0141	0.0117	0.0086	0.0047	0.0
2/7	0.0	0.0104	0.0191	0.0263	0.0319	0.0360	0.0385	0.0396	0.0390	0.0369	0.0330	0.0275	0.0202	0.0111	0.0
5/14	0.0	0.0199	0.0366	0.0504	0.0611	0.0689	0.0738	0.0758	0.0748	0.0708	0.0636	0.0530	0.0390	0.0214	0.0
3/7	0.0	0.0335	0.0616	0.0845	0.103	0.116	0.124	0.127	0.126	0.119	0.107	0.0896	0.0661	0.0363	0.0
1/2	0.0	0.0511	0.0938	0.129	0.156	0.176	0.189	0.194	0.192	0.182	0.164	0.138	0.102	0.0561	0.0
4/7	0.0	0.0720	0.132	0.180	0.218	0.246	0.264	0.272	0.269	0.256	0.232	0.196	0.146	0.0809	0.0
9/14	0.0	0.0947	0.172	0.235	0.284	0.321	0.345	0.356	0.354	0.338	0.308	0.262	0.198	0.111	0.0
5/7	0.0	0.118	0.212	0.287	0.347	0.392	0.423	0.439	0.438	0.421	0.386	0.332	0.253	0.144	0.0
11/14	0.0	0.142	0.252	0.337	0.404	0.454	0.489	0.509	0.511	0.494	0.454	0.391	0.300	0.173	0.0
6/7	0.0	0.157	0.277	0.369	0.439	0.489	0.521	0.537	0.535	0.514	0.473	0.408	0.316	0.186	0.0
13/14	0.0	0.141	0.245	0.323	0.381	0.420	0.440	0.444	0.432	0.407	0.369	0.319	0.250	0.152	0.0
1.0	0.0	0.0	0.0	0.0	0.0	0.0	0.0	0.0	0.0	0.0	0.0	0.0	0.0	0.0	0.0

$[V_z/V_{z,m}]$: M = 12, α = 0.5, Re = 1000 Table 12(i)

r'/r_o \ θ'/θ_o	0.0	1/14	1/7	3/14	2/7	5/14	3/7	1/2	4/7	9/14	5/7	11/14	6/7	13/14	1.0
0.0	0.0	0.0	0.0	0.0	0.0	0.0	0.0	0.0	0.0	0.0	0.0	0.0	0.0	0.0	0.0
1/14	0.0	0.0106	0.0194	0.0266	0.322	0.0363	0.0387	0.0397	0.0391	0.0369	0.0331	0.0276	0.0203	0.0112	0.0
1/7	0.0	0.0420	0.0771	0.106	0.128	0.144	0.154	0.157	0.155	0.146	0.131	0.109	0.0808	0.0444	0.0
3/14	0.0	0.0931	0.171	0.234	0.283	0.318	0.339	0.348	0.343	0.324	0.291	0.243	0.179	0.0983	0.0
2/7	0.0	0.160	0.294	0.402	0.485	0.545	0.581	0.595	0.586	0.554	0.498	0.416	0.307	0.169	0.0
5/14	0.0	0.237	0.434	0.591	0.712	0.797	0.848	0.866	0.852	0.805	0.725	0.608	0.451	0.249	0.0
3/7	0.0	0.312	0.567	0.771	0.928	1.038	1.104	1.127	1.108	1.047	0.944	0.795	0.593	0.329	0.0
1/2	0.0	0.375	0.677	0.914	1.098	1.232	1.317	1.352	1.334	1.264	1.144	0.968	0.727	0.407	0.0
4/7	0.0	0.428	0.763	1.021	1.219	1.368	1.473	1.529	1.527	1.460	1.327	1.128	0.852	0.481	0.0
9/14	0.0	0.468	0.825	1.095	1.300	1.458	1.575	1.650	1.672	1.622	1.487	1.272	0.968	0.551	0.0
5/7	0.0	0.496	0.865	1.142	1.354	1.518	1.643	1.732	1.774	1.749	1.628	1.406	1.083	0.6217	0.0
11/14	0.0	0.508	0.880	1.167	1.396	1.572	1.706	1.802	1.857	1.856	1.772	1.562	1.222	0.707	0.0
6/7	0.0	0.488	0.848	1.152	1.415	1.621	1.769	1.870	1.933	1.951	1.906	1.749	1.385	0.803	0.0
13/14	0.0	0.442	0.769	1.095	1.417	1.661	1.794	1.876	1.921	1.917	1.836	1.642	1.276	0.744	0.0
1.0	0.0	0.0	0.0	0.0	0.0	0.0	0.0	0.0	0.0	0.0	0.0	0.0	0.0	0.0	0.0

$[V_s/V_{z,m}]$: M = 12, α = 0.5, Re = 1000

Table 12(i) - continued

θ'/θ_o r'/r_o	0.0	1/14	1/7	3/14	2/7	5/14	3/7	1/2	4/7	9/14	5/7	11/14	6/7	13/14	1.0
0.0	0.0	0.0	0.0	0.0	0.0	0.0	0.0	0.0	0.0	0.0	0.0	0.0	0.0	0.0	0.0
1/14	0.0	0.0004	0.0007	0.0010	0.0013	0.0014	0.0015	0.0016	0.0015	0.0014	0.0013	0.0011	0.0008	0.0004	0.0
1/7	0.0	0.0031	0.0058	0.0080	0.0097	0.0110	0.0118	0.0121	0.0119	0.0112	0.0100	0.0083	0.0061	0.0033	0.0
3/14	0.0	0.0104	0.0191	0.0263	0.0319	0.0361	0.0387	0.0397	0.0392	0.0370	0.0332	0.0276	0.0202	0.0110	0.0
2/7	0.0	0.0236	0.0435	0.0598	0.0726	0.0820	0.0880	0.0904	0.0893	0.0846	0.0761	0.0635	0.0467	0.0255	0.0
5/14	0.0	0.0432	0.0792	0.109	0.132	0.149	0.160	0.164	0.163	0.154	0.139	0.117	0.0867	0.0477	0.0
3/7	0.0	0.0670	0.122	0.167	0.202	0.228	0.246	0.254	0.252	0.240	0.218	0.185	0.139	0.0773	0.0
1/2	0.0	0.0926	0.166	0.224	0.271	0.307	0.330	0.346	0.346	0.333	0.305	0.262	0.199	0.113	0.0
4/7	0.0	0.120	0.210	0.278	0.332	0.376	0.411	0.434	0.441	0.428	0.396	0.344	0.266	0.153	0.0
9/14	0.0	0.149	0.254	0.329	0.387	0.437	0.480	0.514	0.531	0.524	0.489	0.429	0.336	0.197	0.0
5/7	0.0	0.179	0.299	0.380	0.442	0.496	0.546	0.590	0.618	0.621	0.588	0.519	0.413	0.246	0.0
11/14	0.0	0.208	0.343	0.434	0.505	0.568	0.625	0.676	0.712	0.722	0.695	0.621	0.502	0.304	0.0
6/7	0.0	0.221	0.363	0.470	0.566	0.651	0.723	0.778	0.812	0.820	0.796	0.729	0.588	0.358	0.0
13/14	0.0	0.252	0.422	0.580	0.735	0.851	0.908	0.929	0.924	0.889	0.822	0.717	0.554	0.334	0.0
1.0	0.0	0.0	0.0	0.0	0.0	0.0	0.0	0.0	0.0	0.0	0.0	0.0	0.0	0.0	0.0

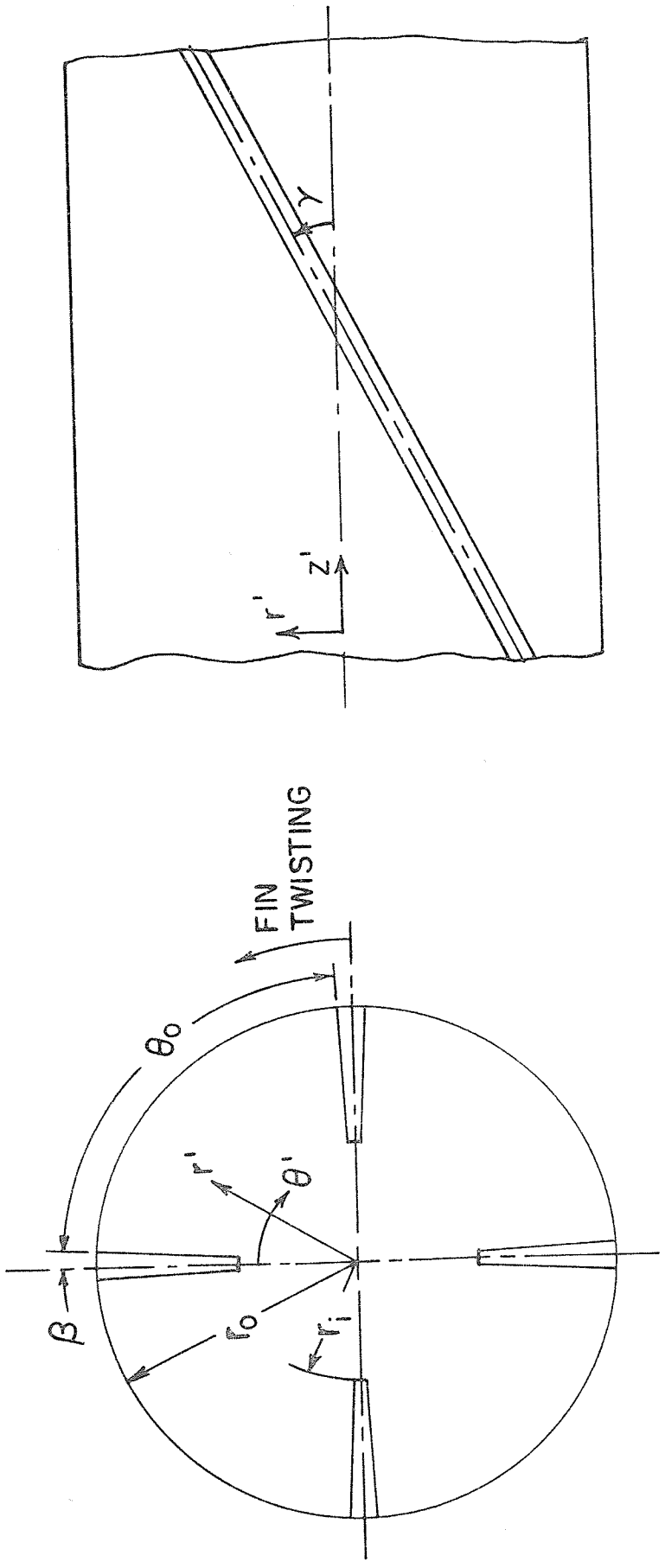

Figure 1: Internally Finned Tube Geometry and Coordinate System

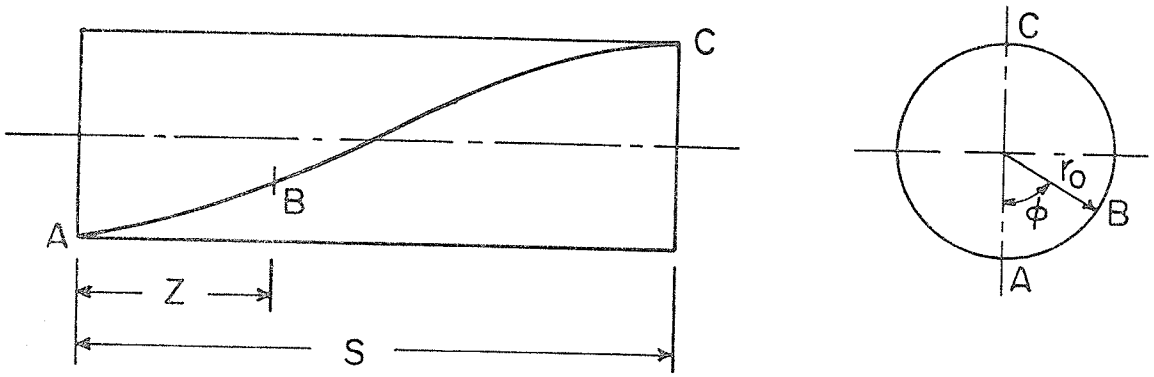

Figure 2: Illustration of the Twisted Fin Inside a Tube

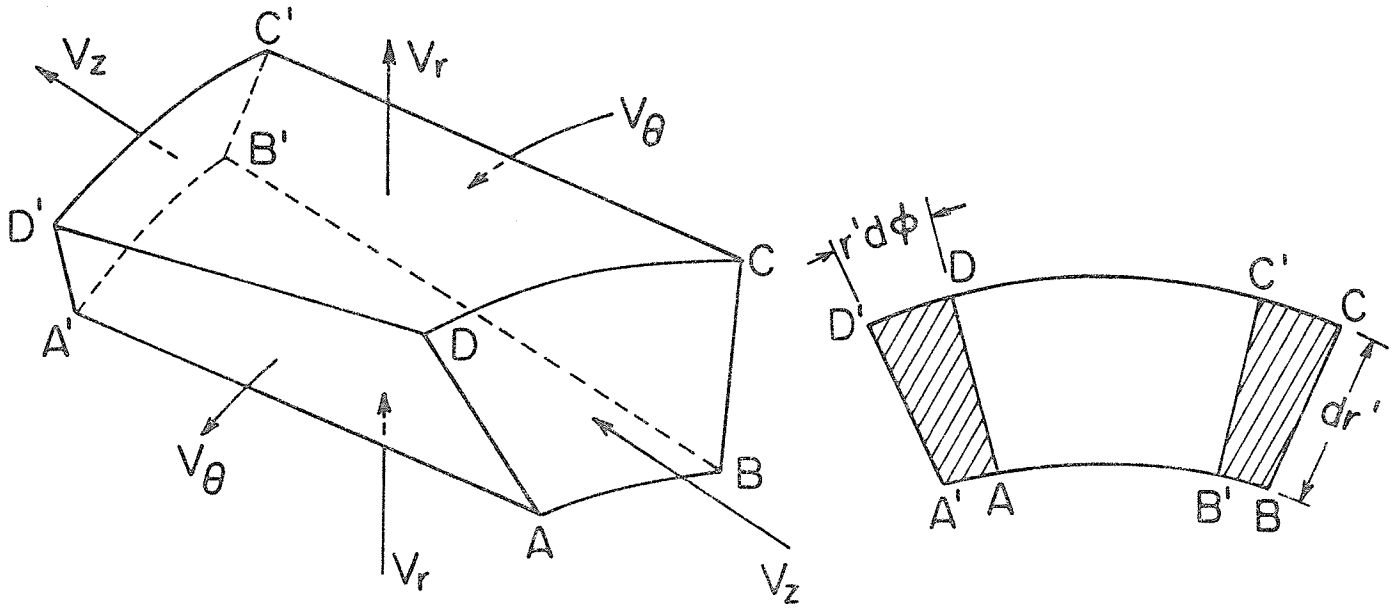

Figure 3: Twisted Control Volume and Its Projection on the r' - θ' Plane

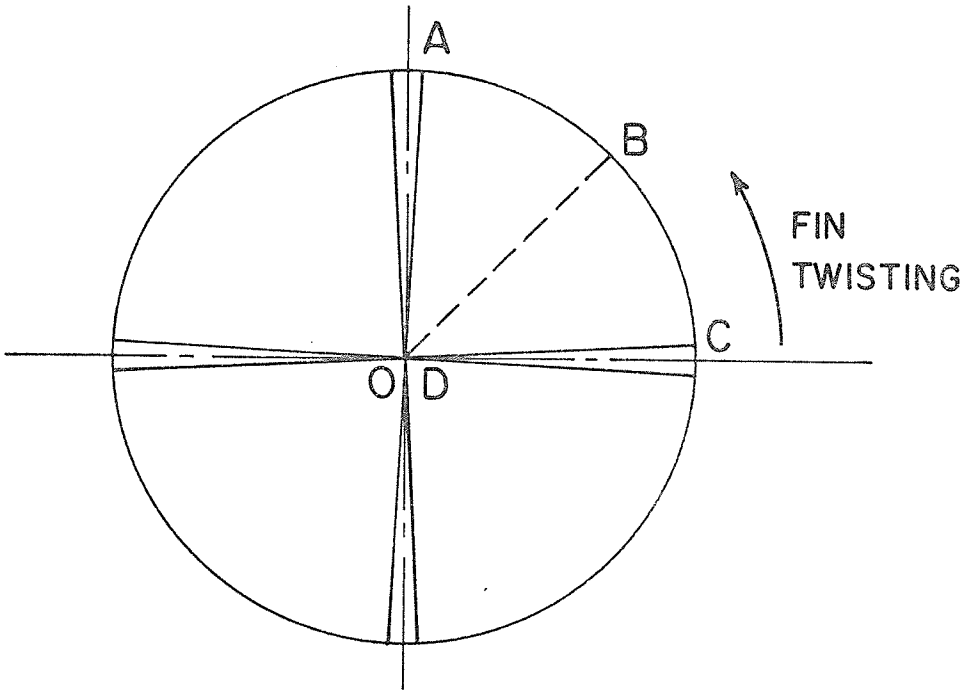

Figure 4: Domain of Interest

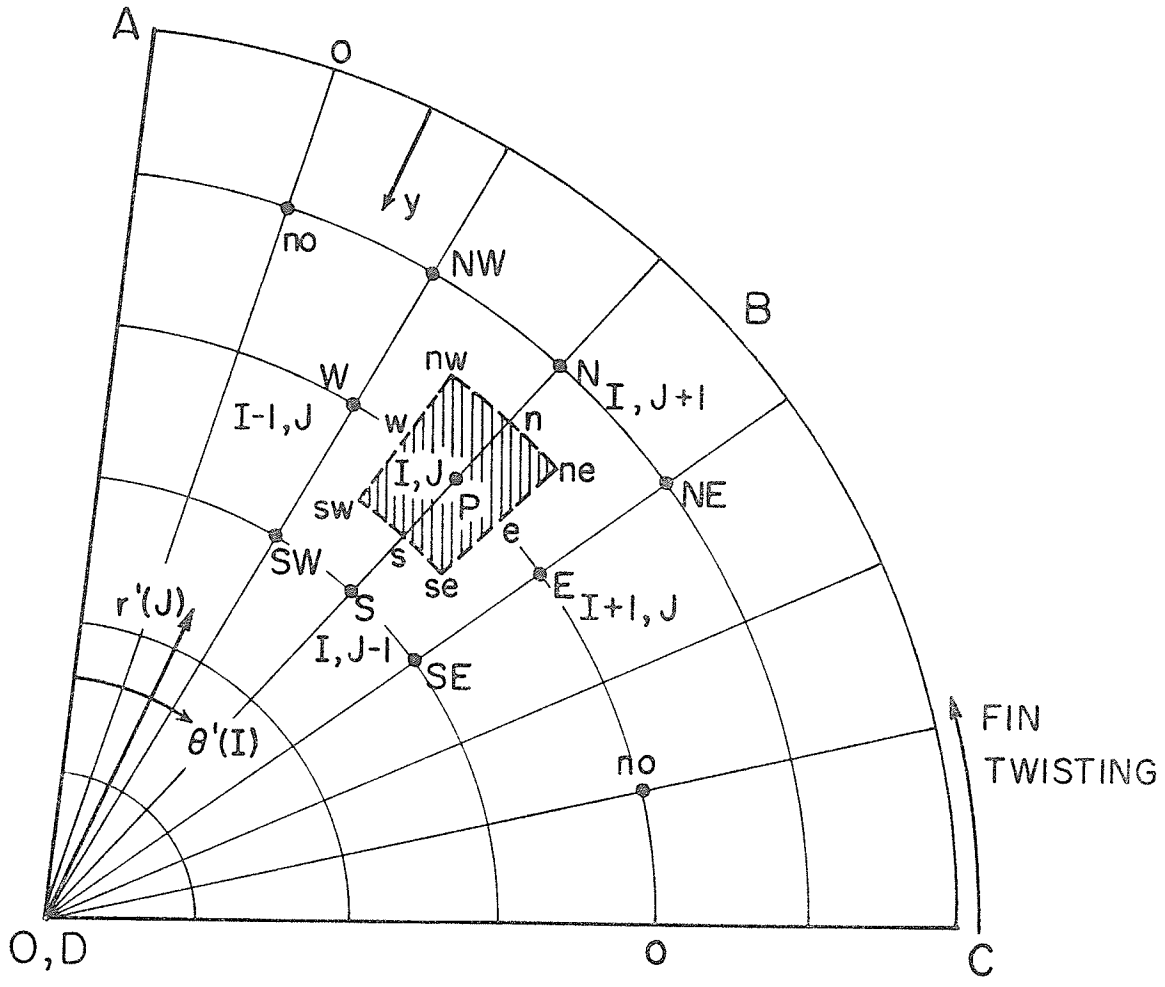

Figure 5: Illustration of the Finite-Difference Grid; the Dotted Lines Enclose the Control Volume

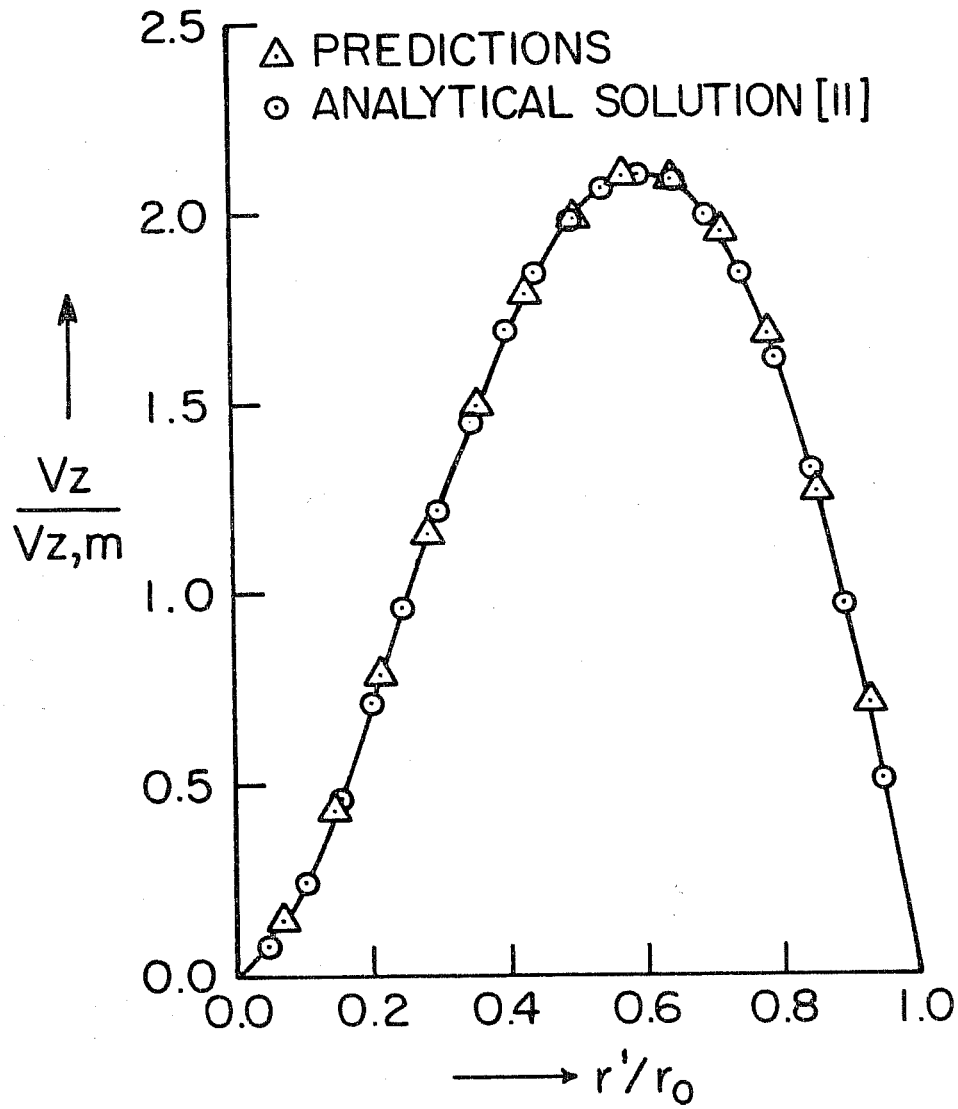

Figure 6: Comparison of Velocity Distribution at the Axis of Symmetry for M = 4 and α = 0

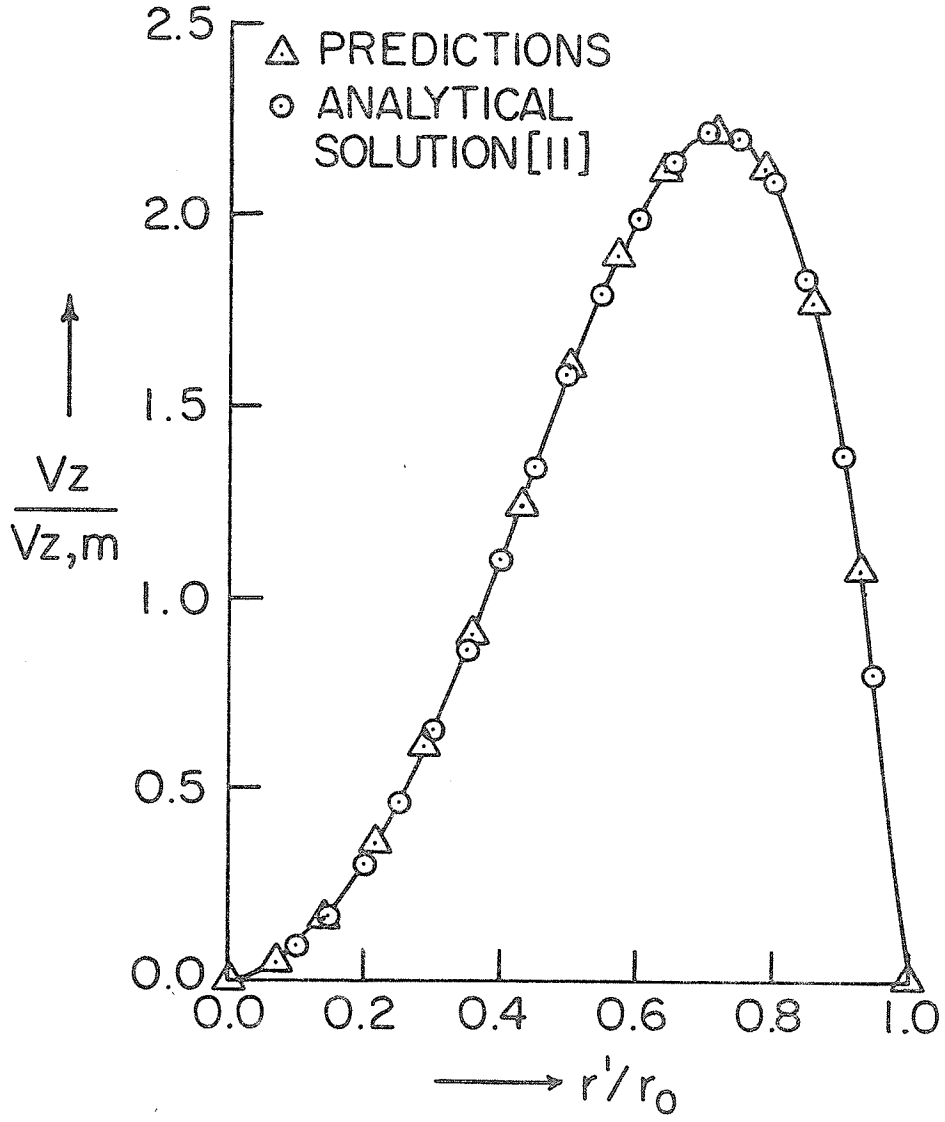

Figure 7: Comparison of Velocity Distribution at the Axis of Symmetry for M = 8 and α = 0

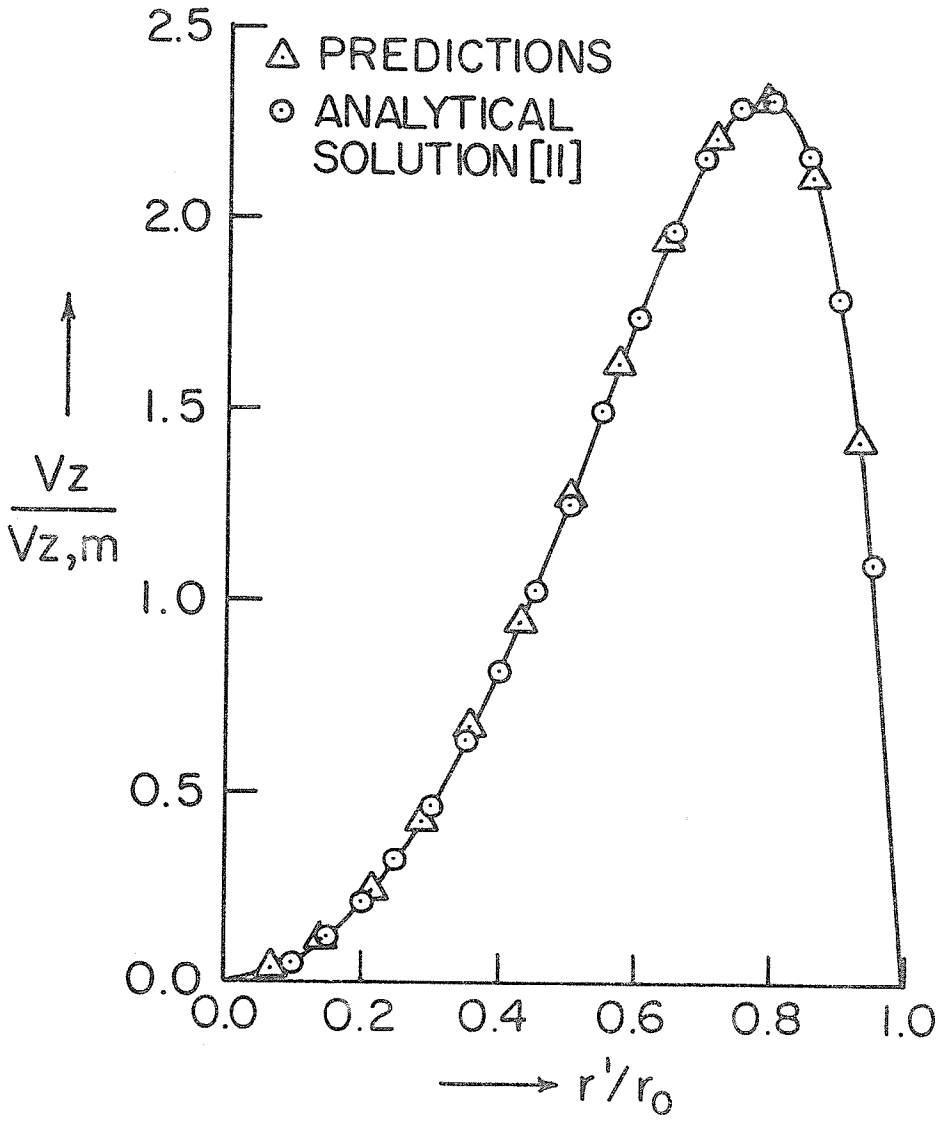

Figure 8: Comparison of Velocity Distribution at the Axis of Symmetry for M = 12 and α = 0

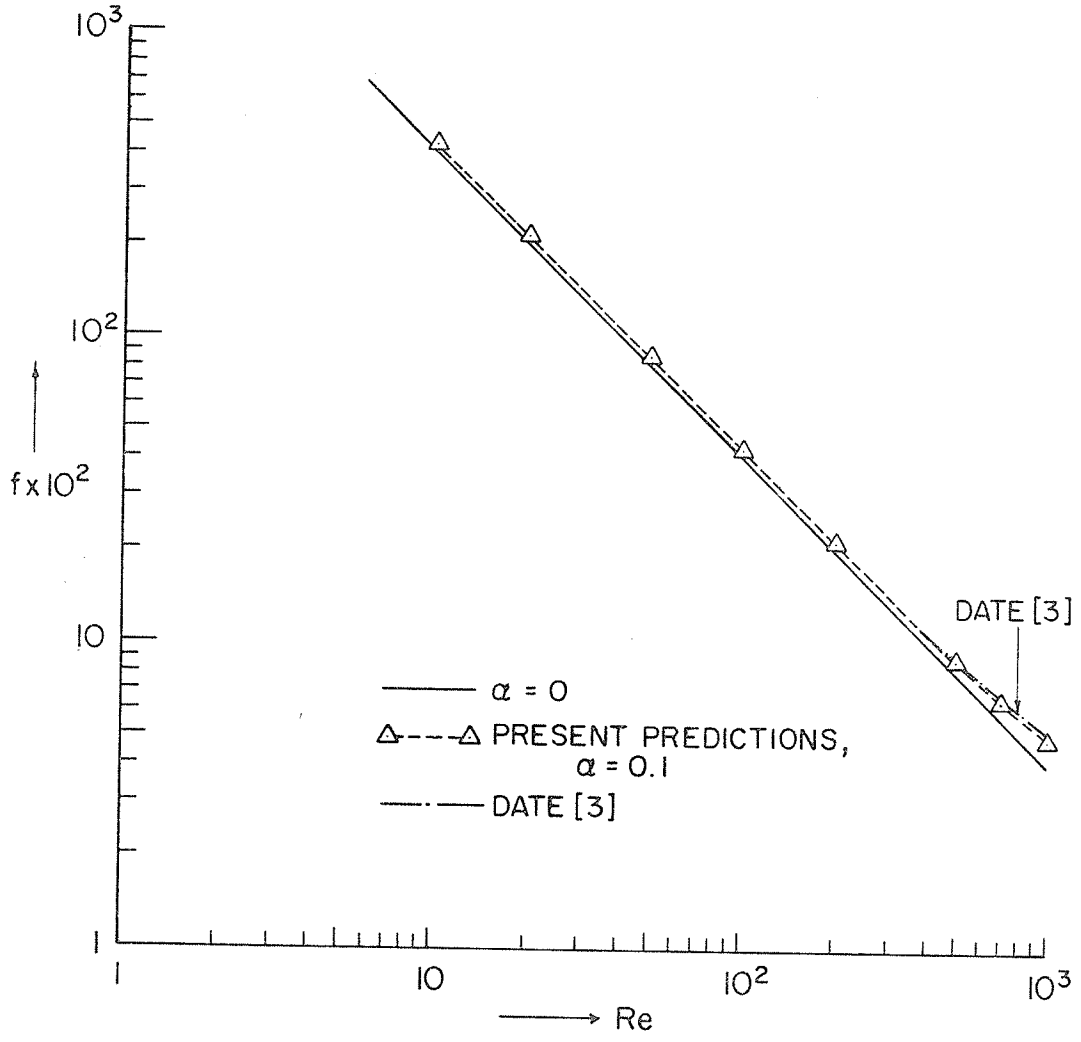

Figure 9: Comparison of Friction Factor Values for M = 2, β = 0, and α = 0.1

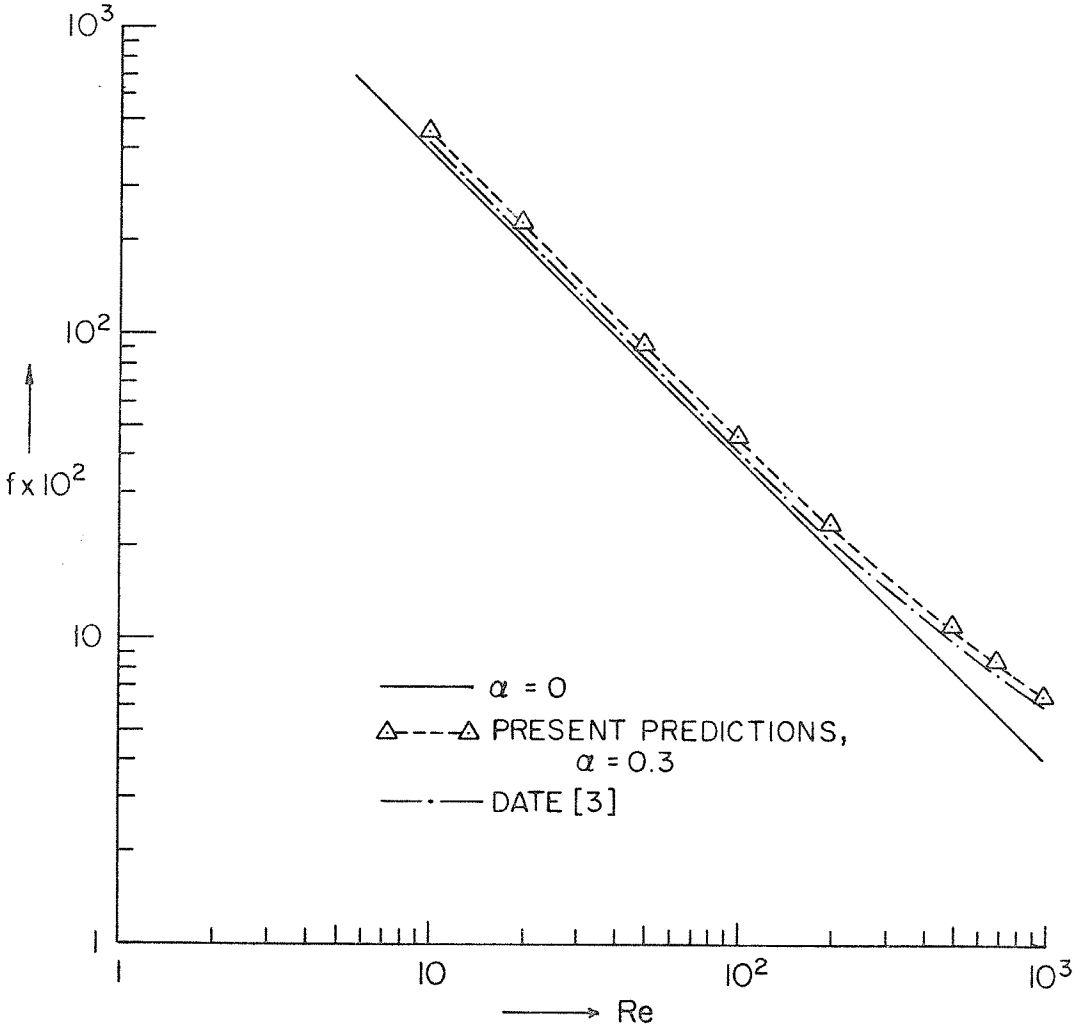

Figure 10: Comparison of Friction Factor Values for M = 2, $\beta = 0$, and $\alpha = 0.3$

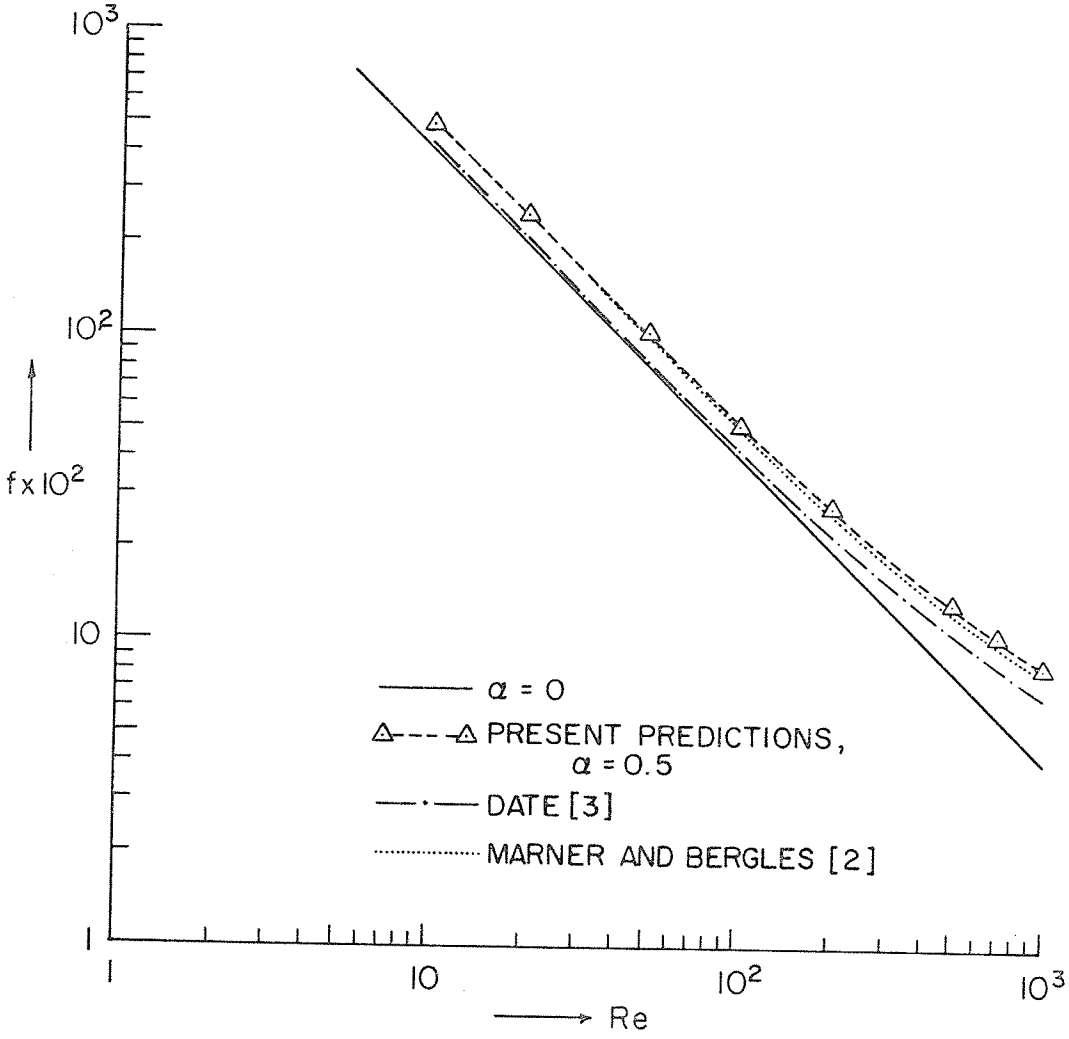

Figure 11: Comparison of Friction Factor Values for M = 2, $\beta = 0$, and $\alpha = 0.5$

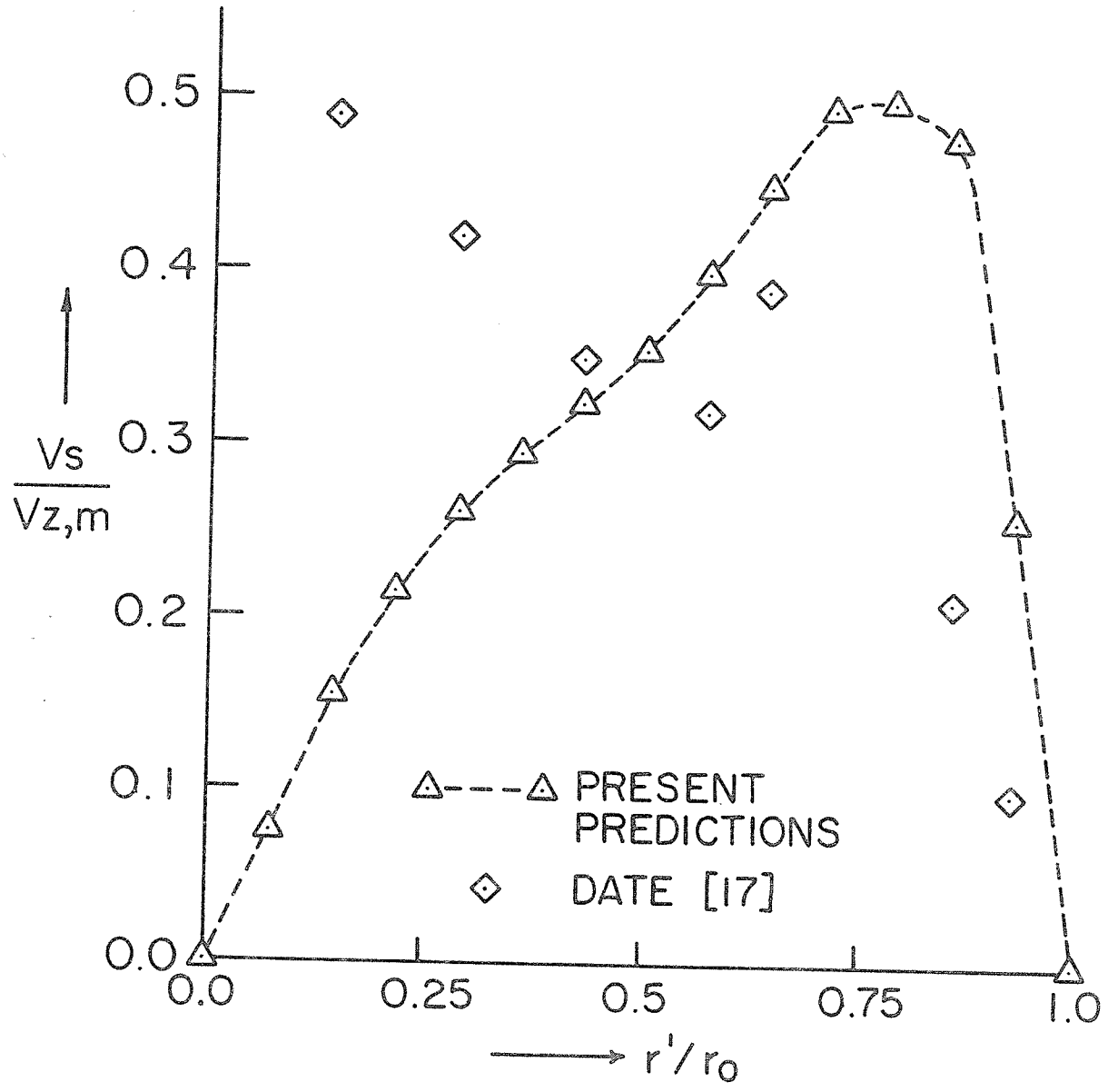

Figure 12: Comparison of Resultant Secondary Velocity Distribution at the Central Plane for M = 2, β = 0, α = 0.5, and Re = 515

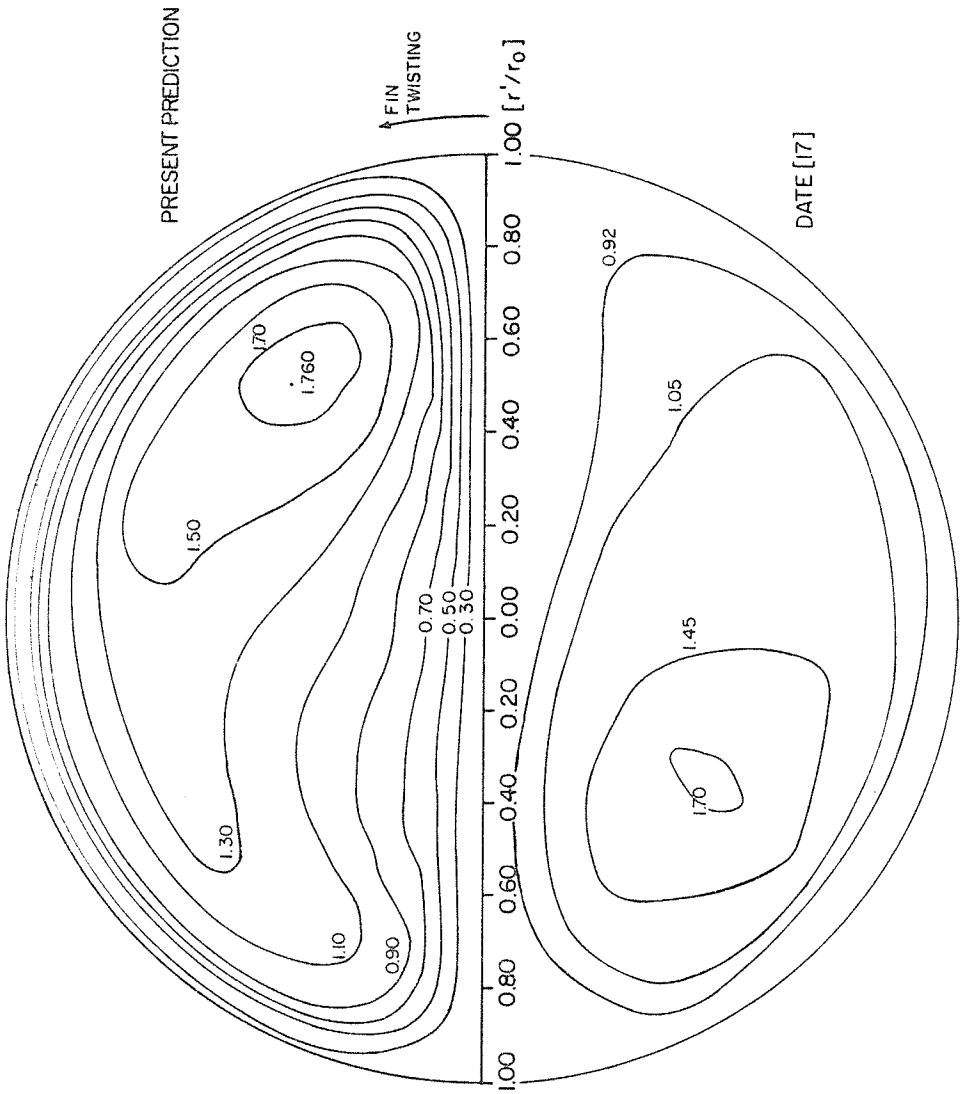

Figure 13: Comparison of Axial Velocity Profiles for M = 2, $\beta = 0$, $\alpha = 0.5$, and Re = 700

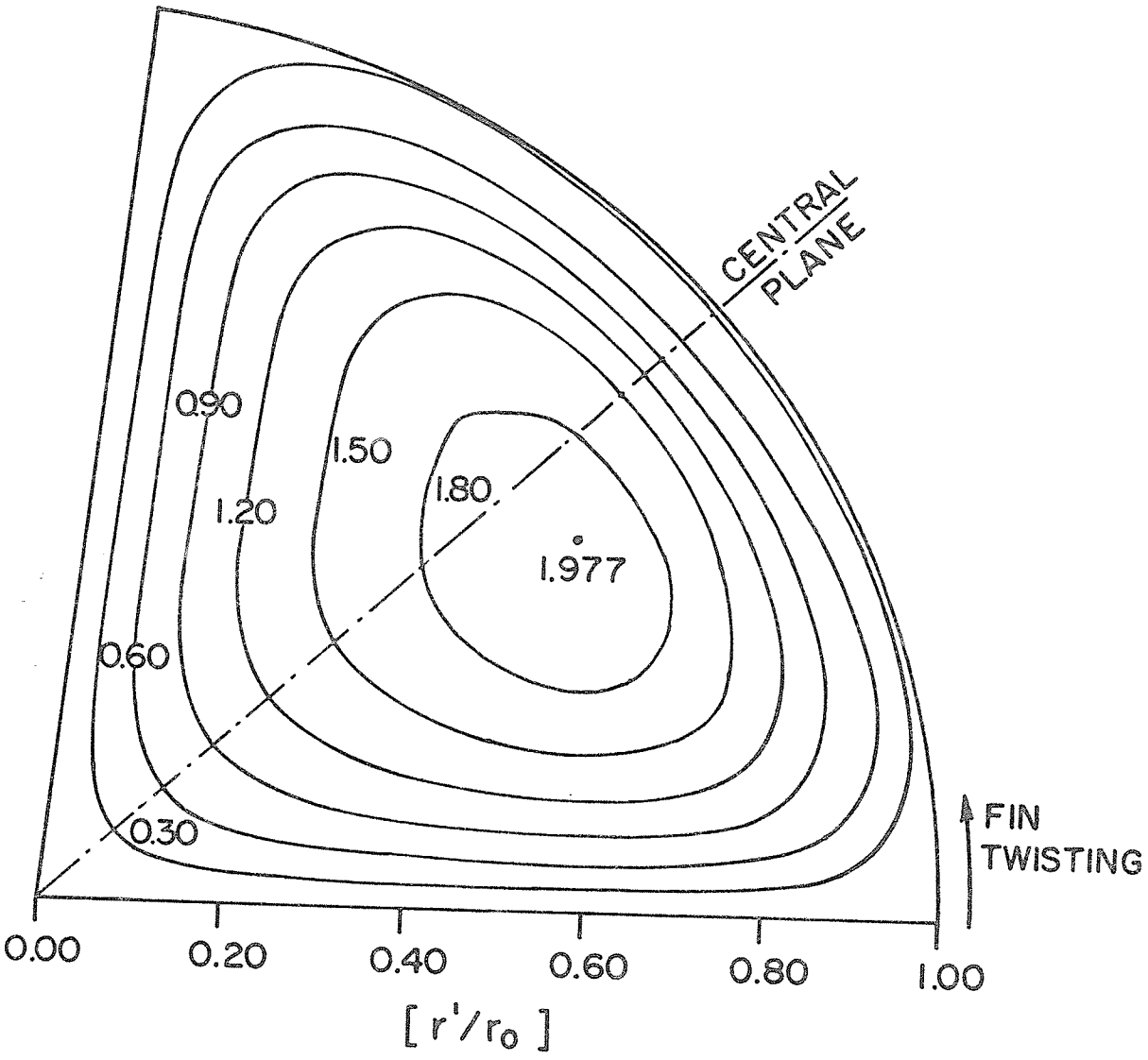

Figure 14: Predicted Axial Velocity $[V_z/V_{z,m}]$ Profiles for $M = 4$, $\alpha = 0.1$, and $Re = 1000$.

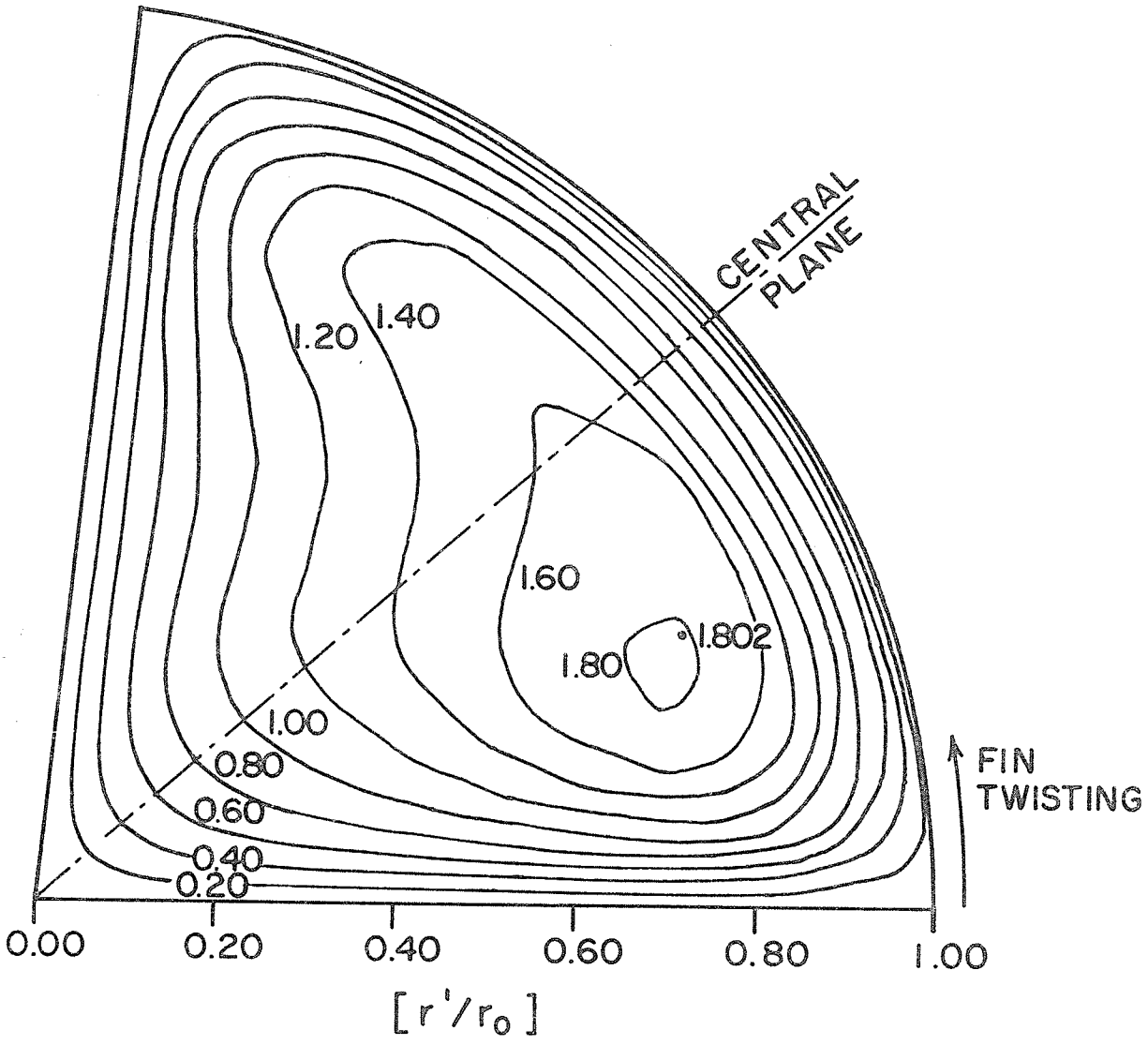

Figure 15: Predicted Axial Velocity Profiles for M = 4, α = 0.3, and Re = 1000

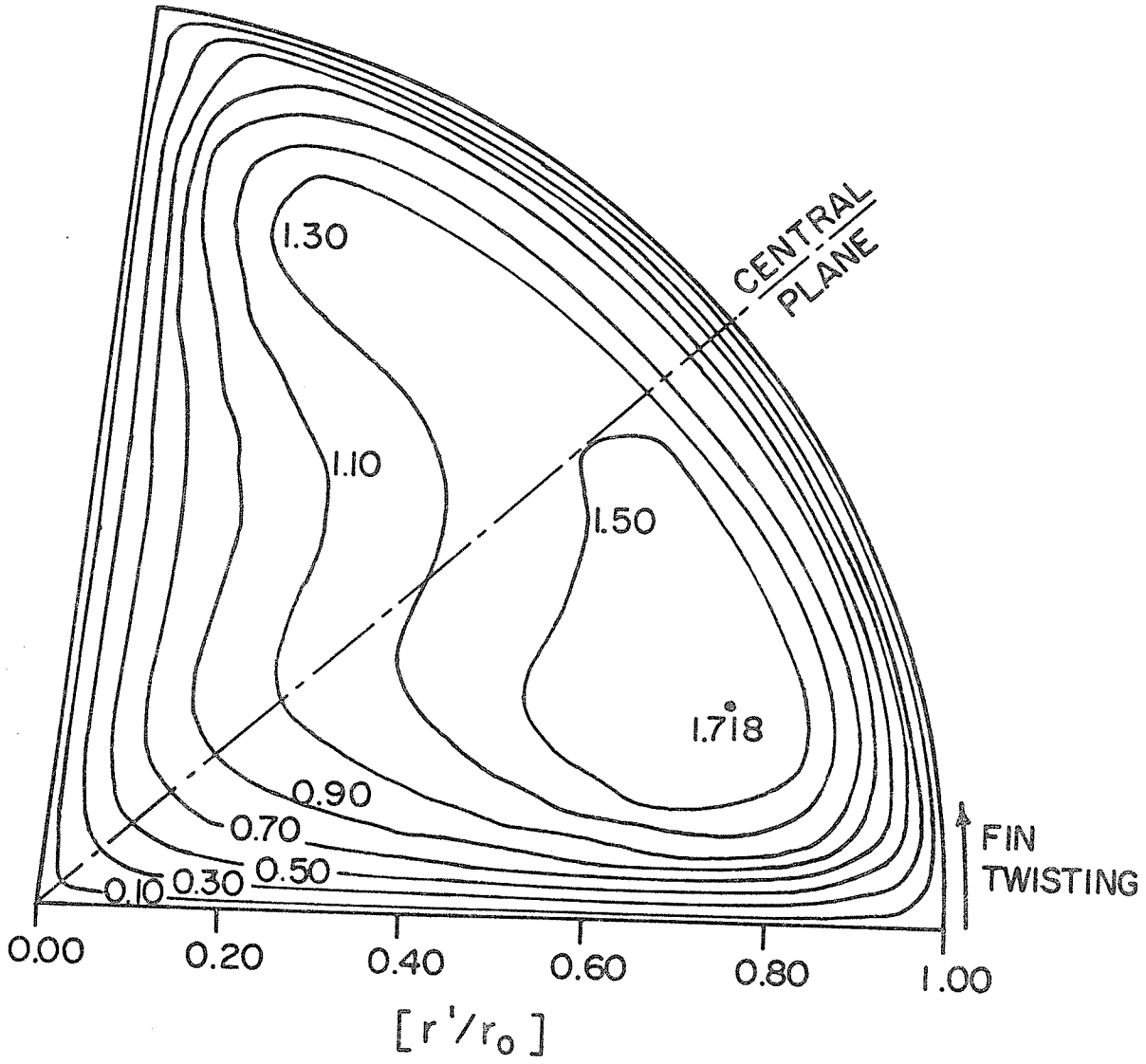

Figure 16: Predicted Axial Velocity $[V_z/V_{z,m}]$ Profiles for M = 4, α = 0.5, and Re = 1000.

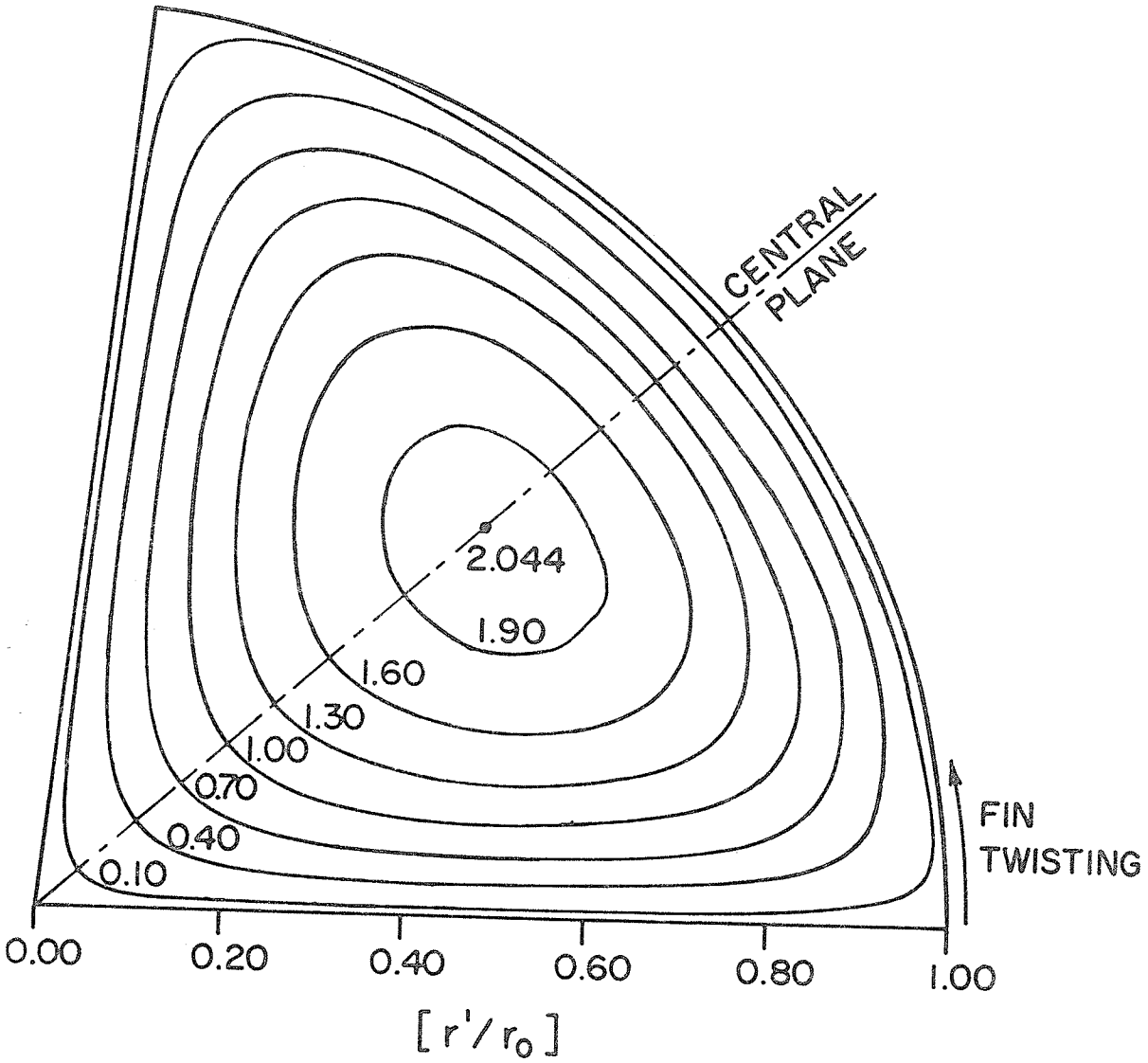

Figure 17: Predicted Axial Velocity $[V_z/V_{z,m}]$ Profiles for M = 4, α = 0.4, and Re = 100

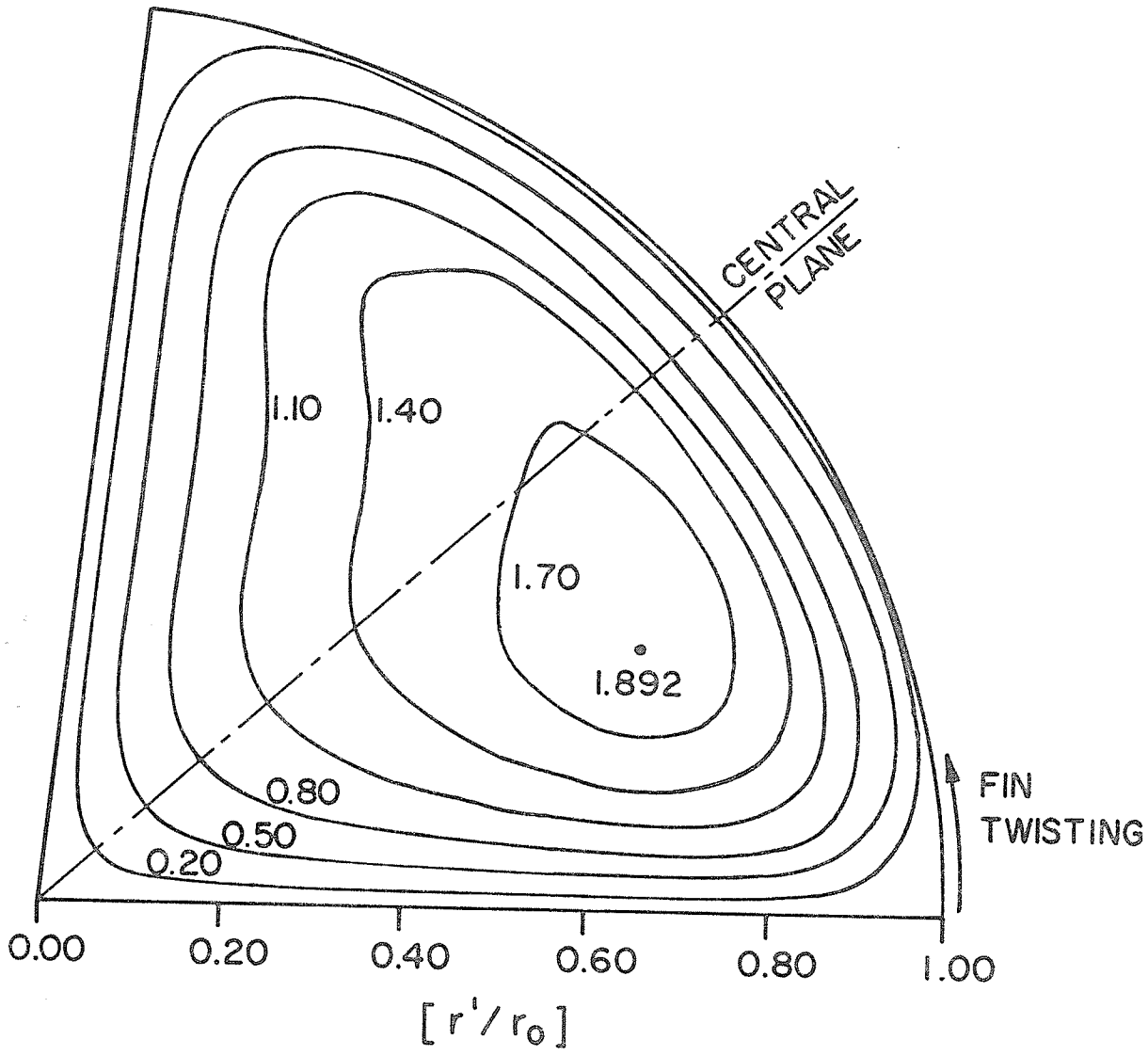

Figure 18: Predicted Axial Velocity $[V_z/V_{z,m}]$ Profiles for M = 4, α = 0.4, and Re = 500

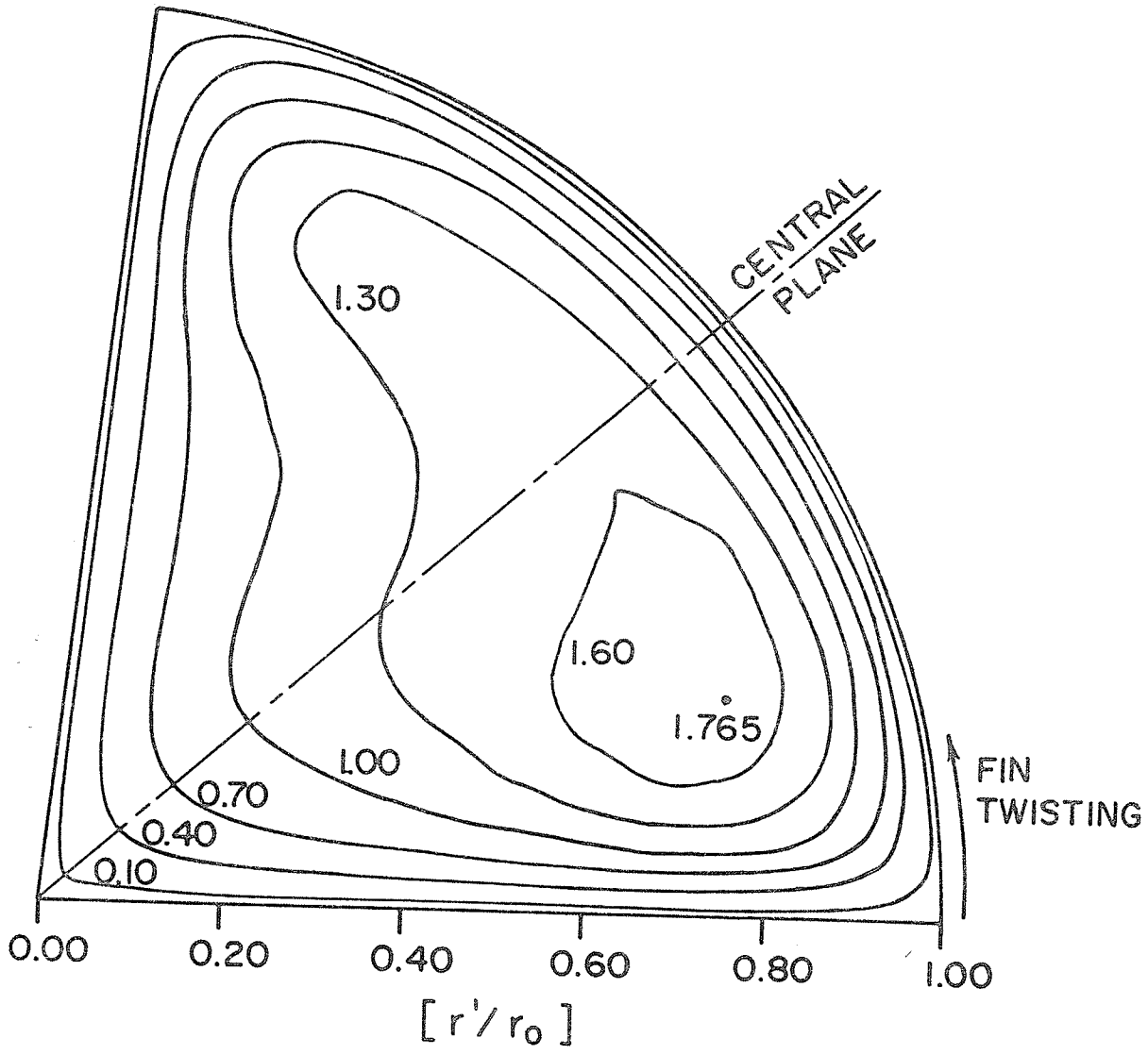

Figure 19: Predicted Axial Velocity $[V_z/V_{z,m}]$ Profiles for M = 4, α = 0.4, and Re = 1000

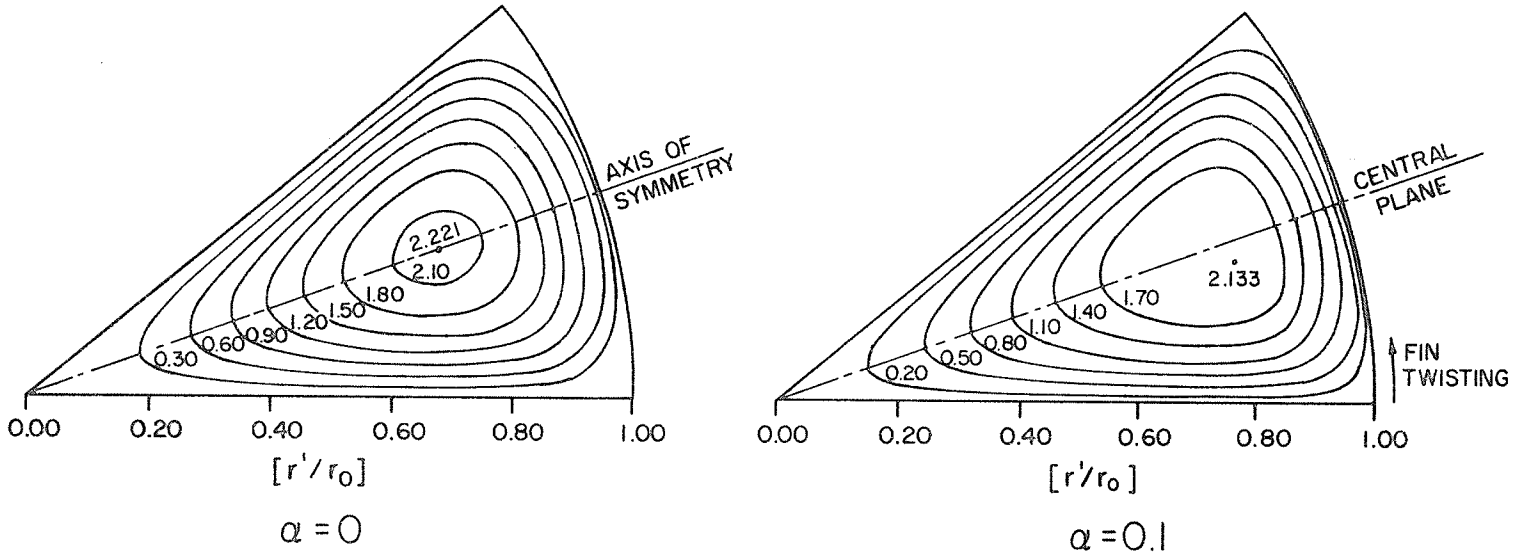

Figure 20: Effect of Twist Ratio (α = 0, 0.1) on Predicted Axial Velocity Profiles at M = 8 and Re = 1000

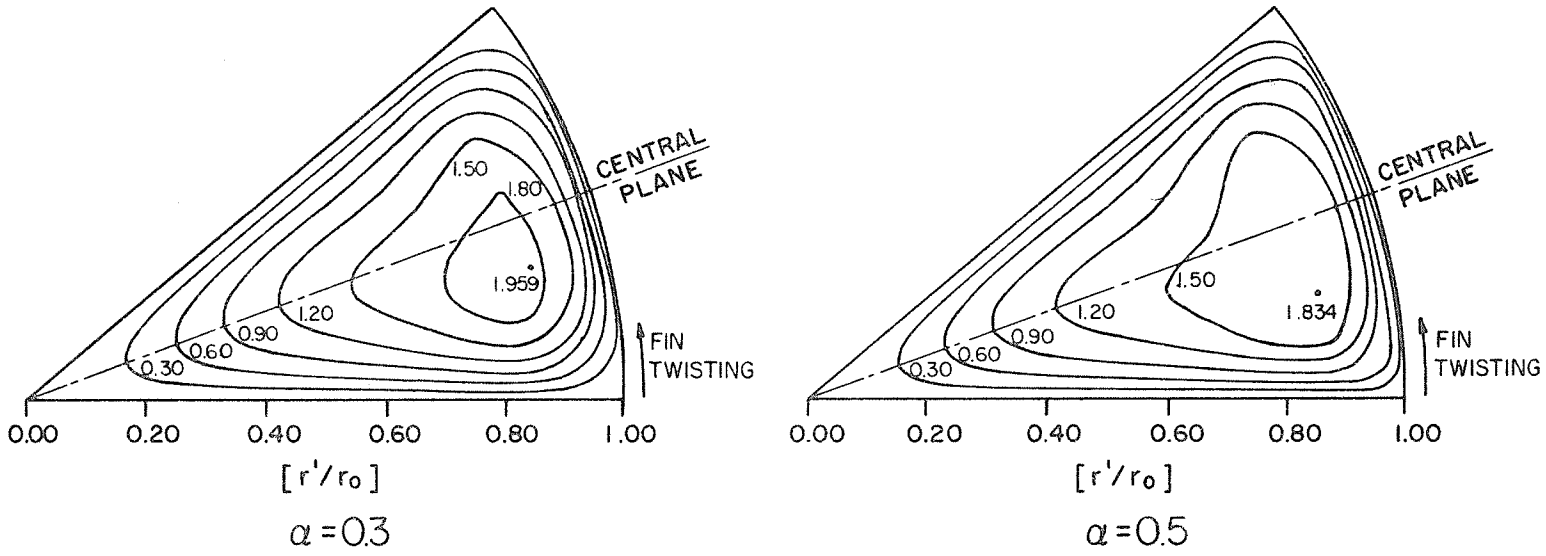

Figure 21: Effect of Twist Ratio (α = 0.3, 0.5) on Predicted Axial Velocity Profiles at M = 8 and Re = 1000

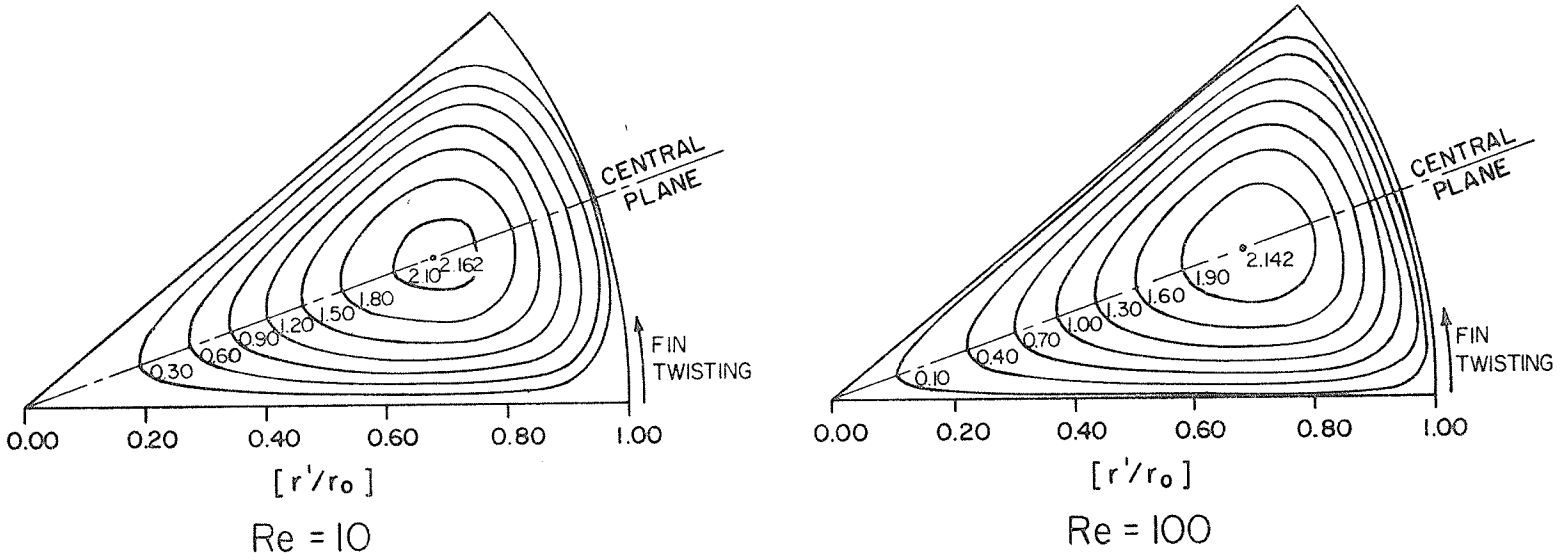

Figure 22: Effect of Reynolds Number (Re = 10,100) on Predicted Axial Velocity Profiles at M = 8 and α = 0.4

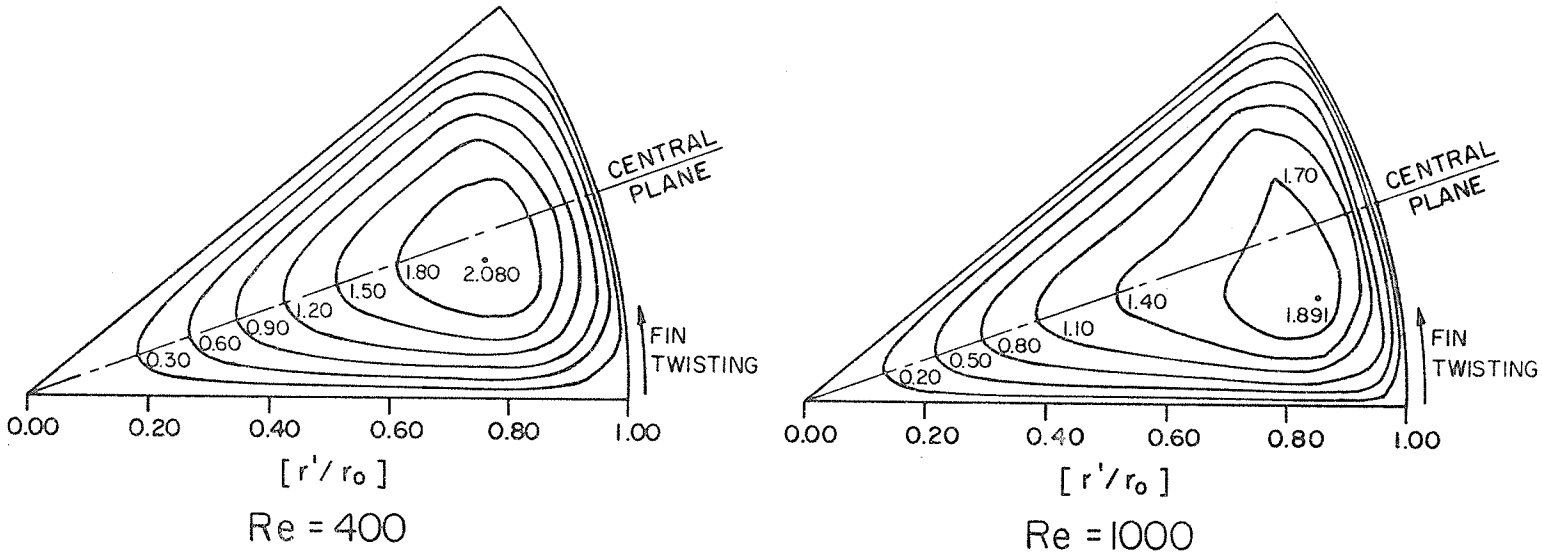

Figure 23: Effect of Reynolds Number (Re = 400,1000) on Predicted Axial Velocity Profiles at M = 8 and α = 0.4

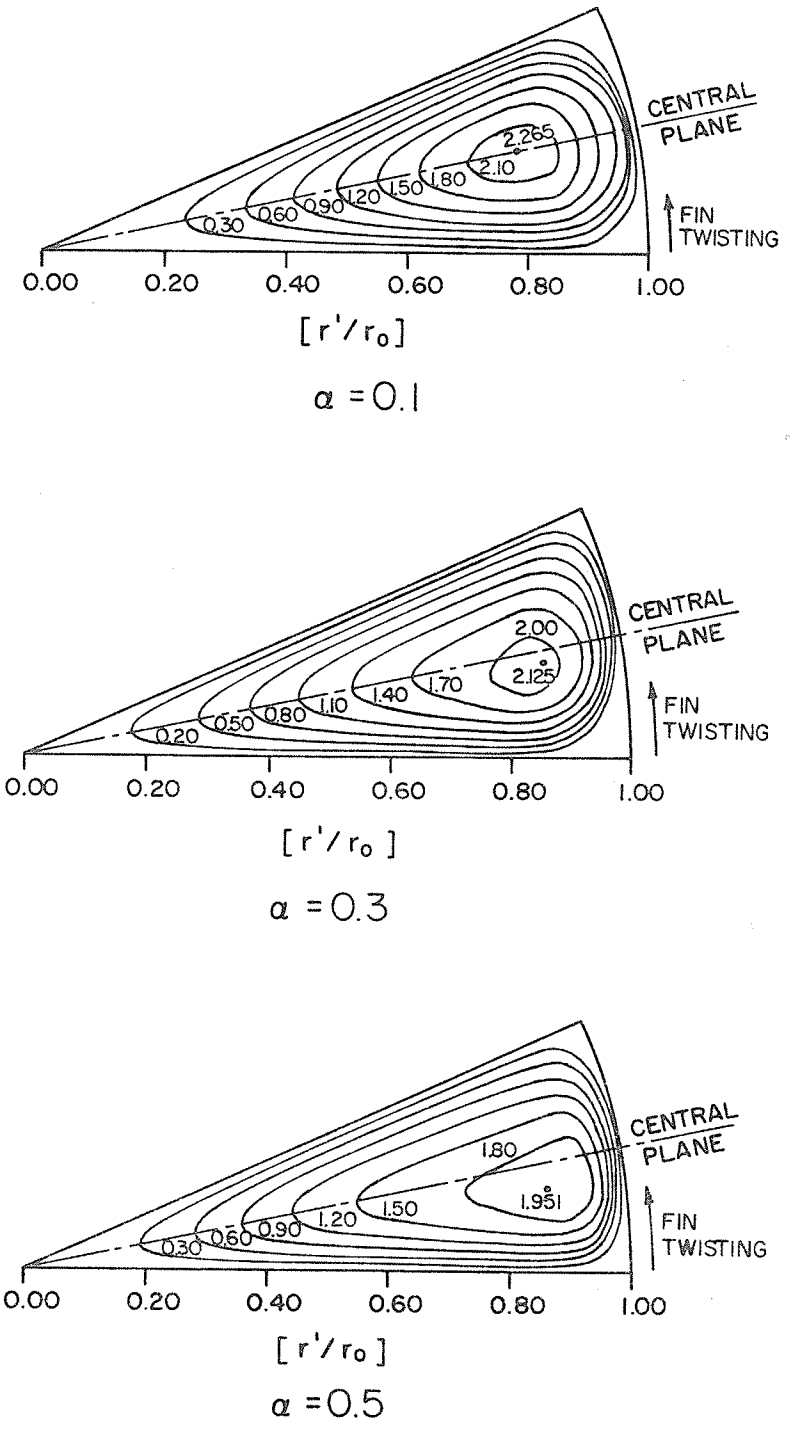

Figure 24: Effect of Twist Ratio on Predicted Axial Velocity Profiles at M = 12 and Re=1000

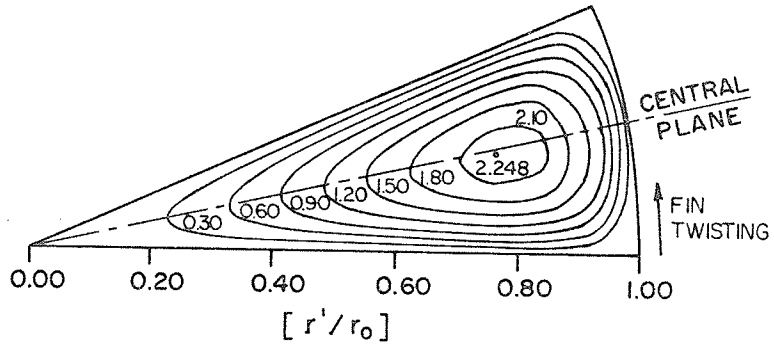

Re = 100

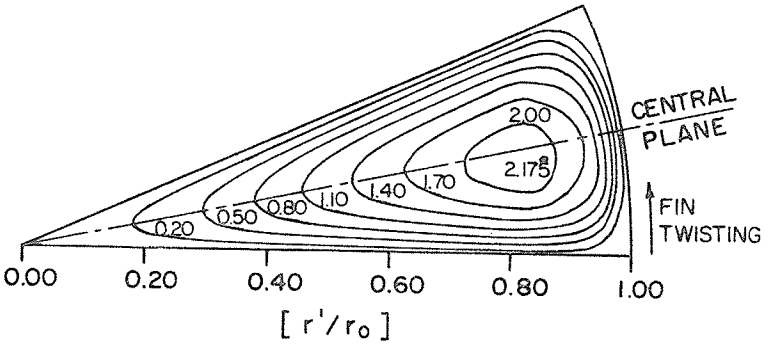

Re = 500

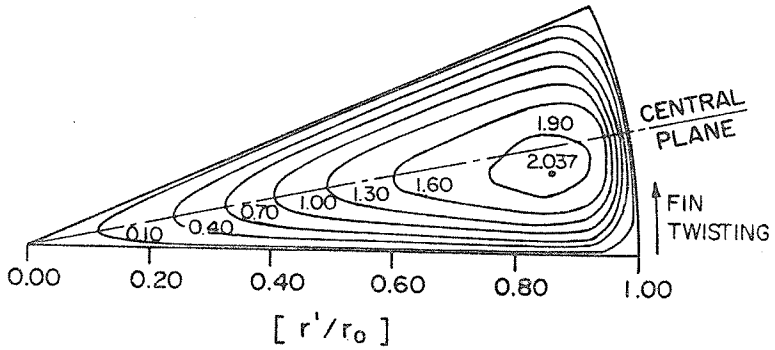

Re = 1000

Figure 25: Effect of Reynolds Number on Predicted Axial Velocity Profiles at M = 12 and α = 0.4

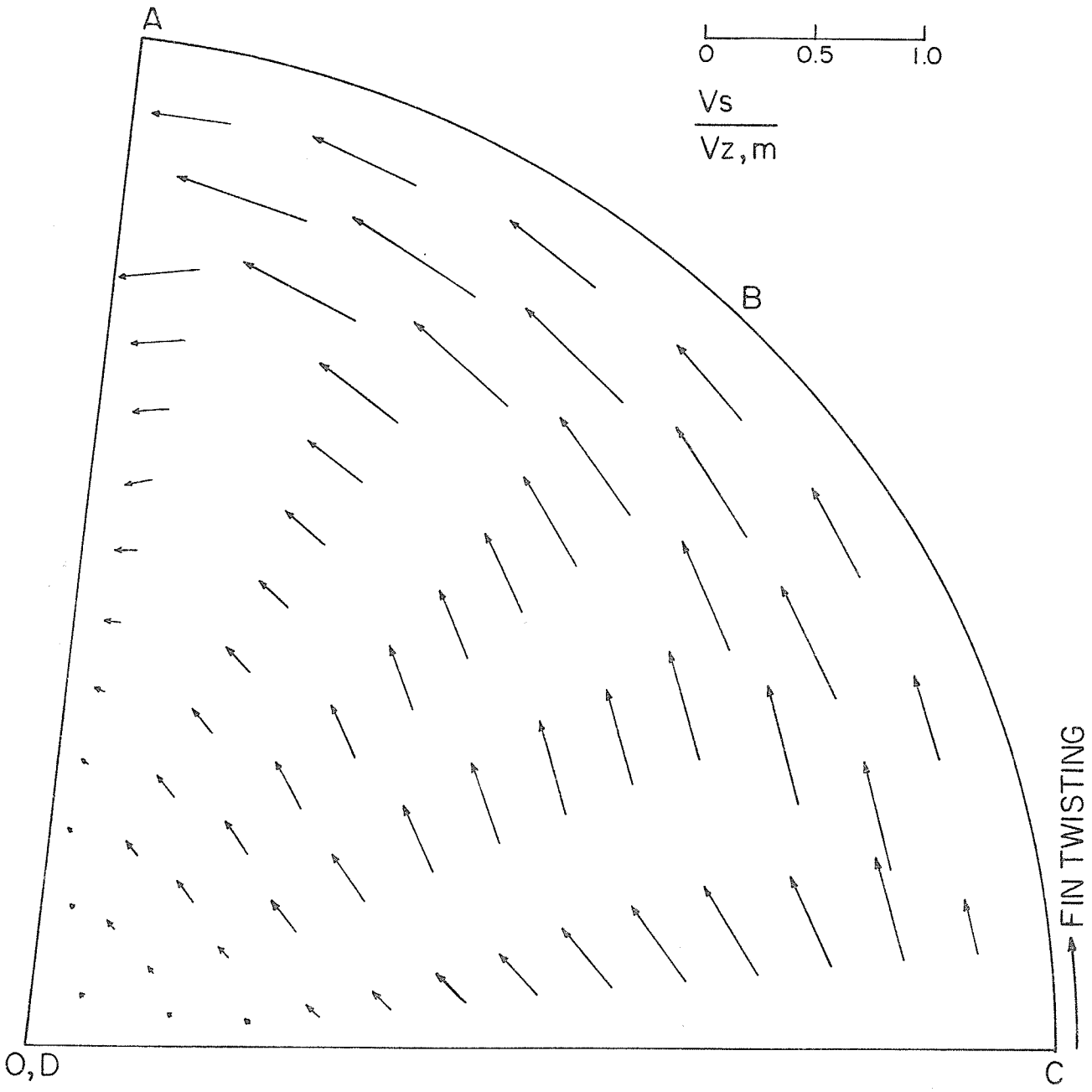

Figure 26: Predicted Resultant Secondary Velocity Distribution for M = 4, α = 0.5, and Re = 1000

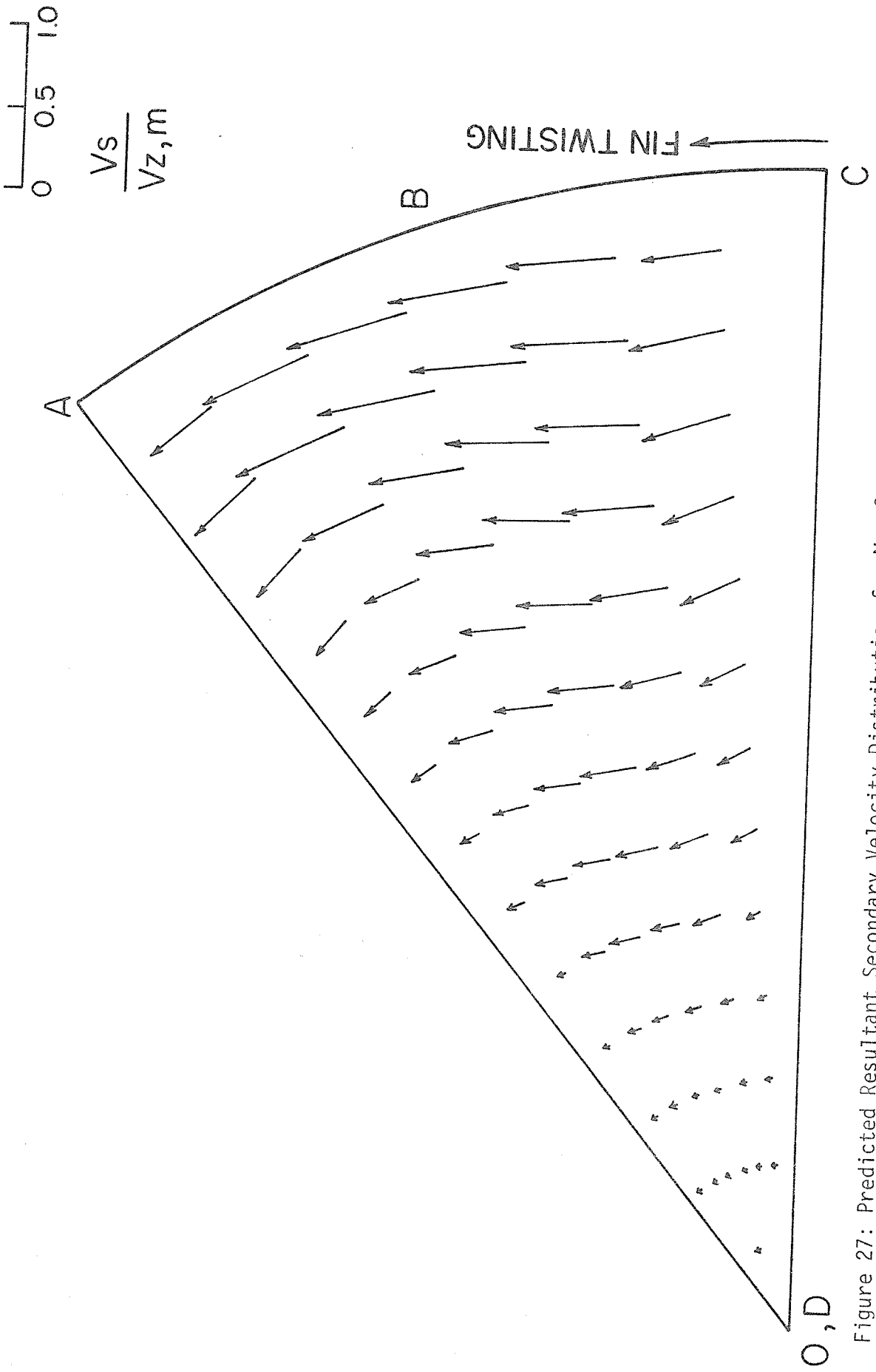

Figure 27: Predicted Resultant Secondary Velocity Distribution for M = 8, α = 0.5 and Re = 1000

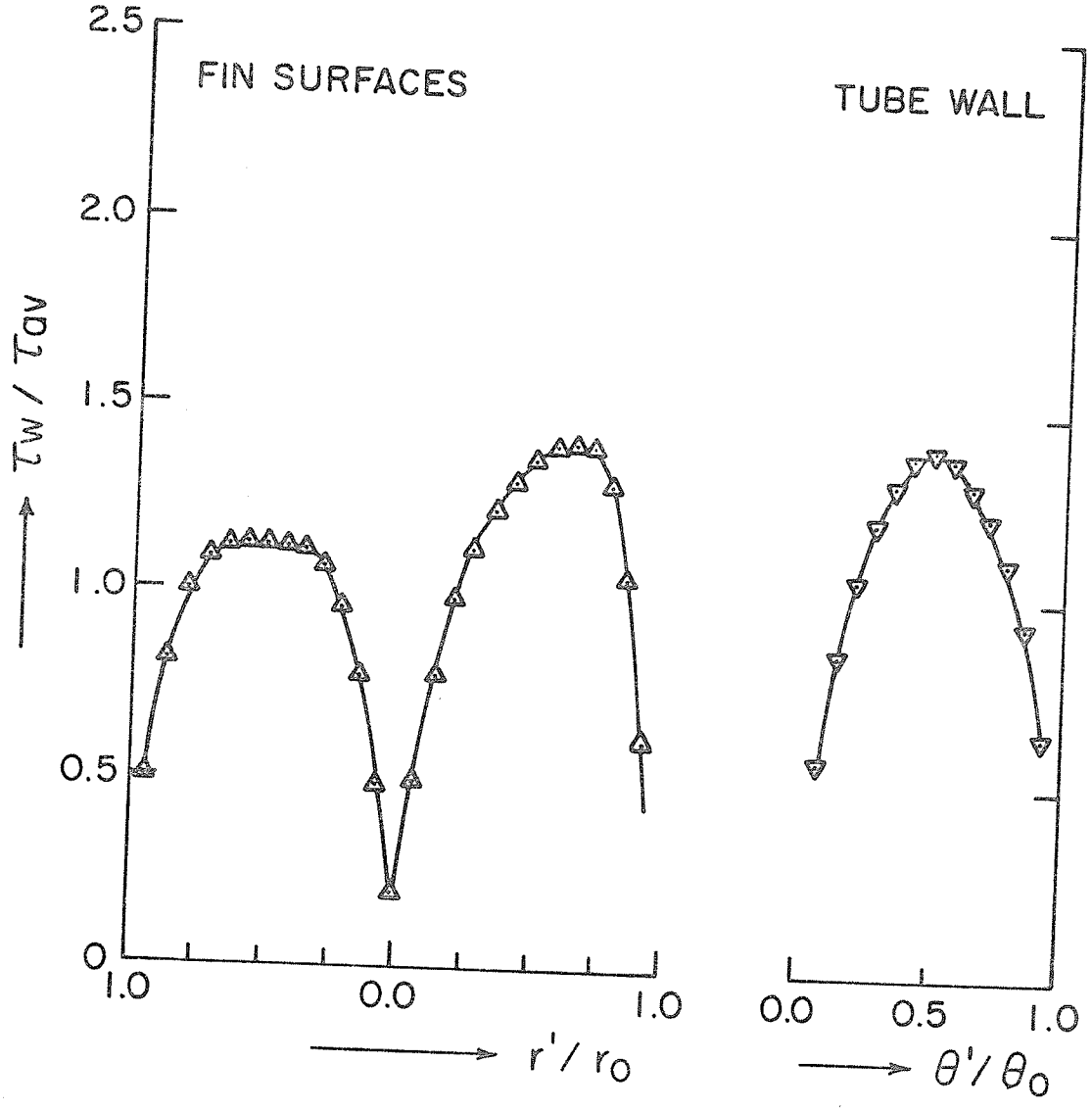

Figure 28: Distribution of Wall Shear Stress for M = 4, α = 0.1, and Re = 1000

$\tau_{av} = 0.3770 \times 10^{-2}$ N/m^2

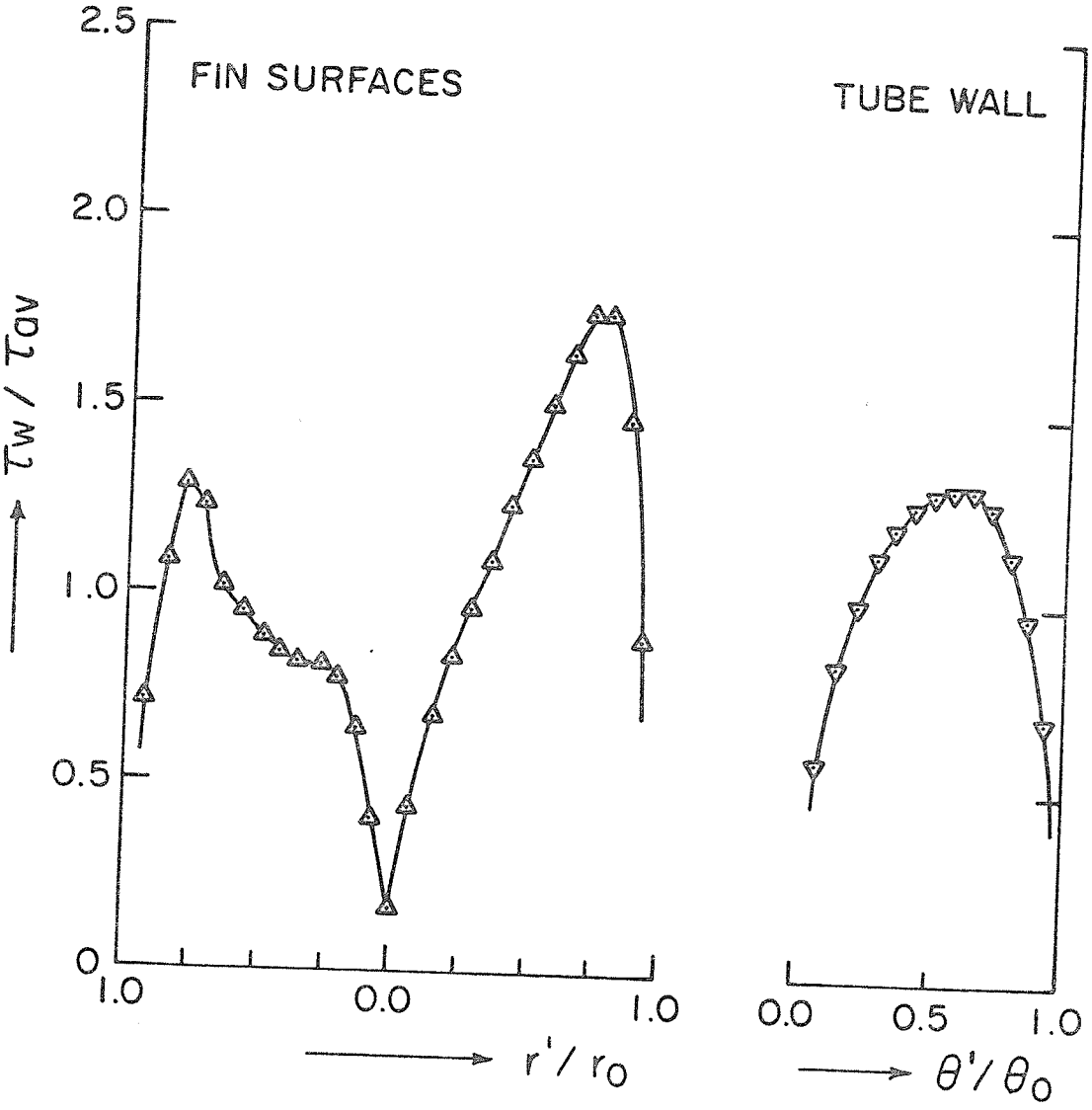

Figure 29: Distribution of Wall Shear Stress for M = 4, α = 0.3, and Re = 1000.

$\tau_{av} = 0.5475 \times 10^{-2}$ N/m^2

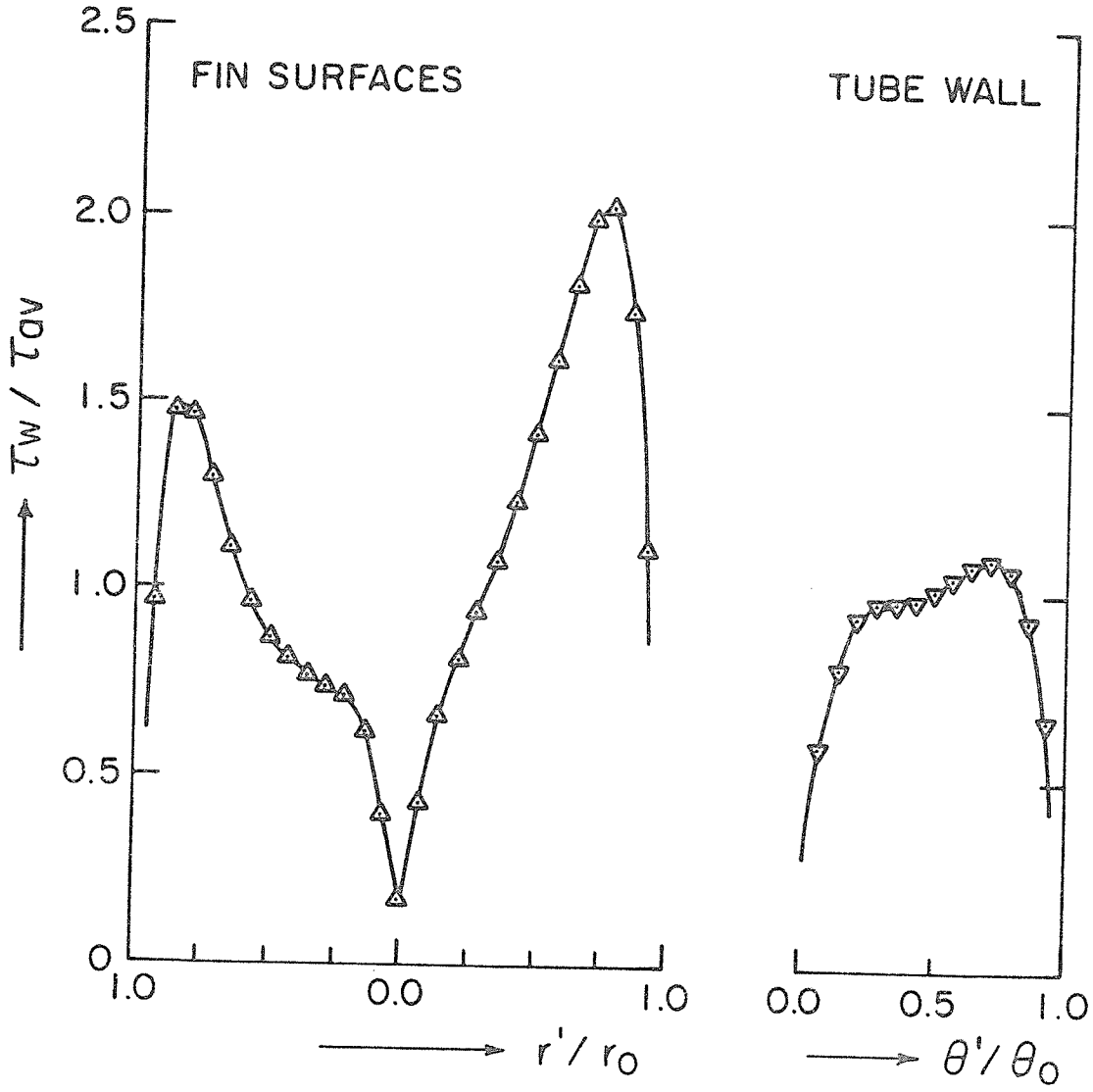

Figure 30: Distribution of Wall Shear Stress for M = 4, α = 0.5, and Re = 1000

$\tau_{av} = 0.7100 \times 10^{-2}$ N/m^2

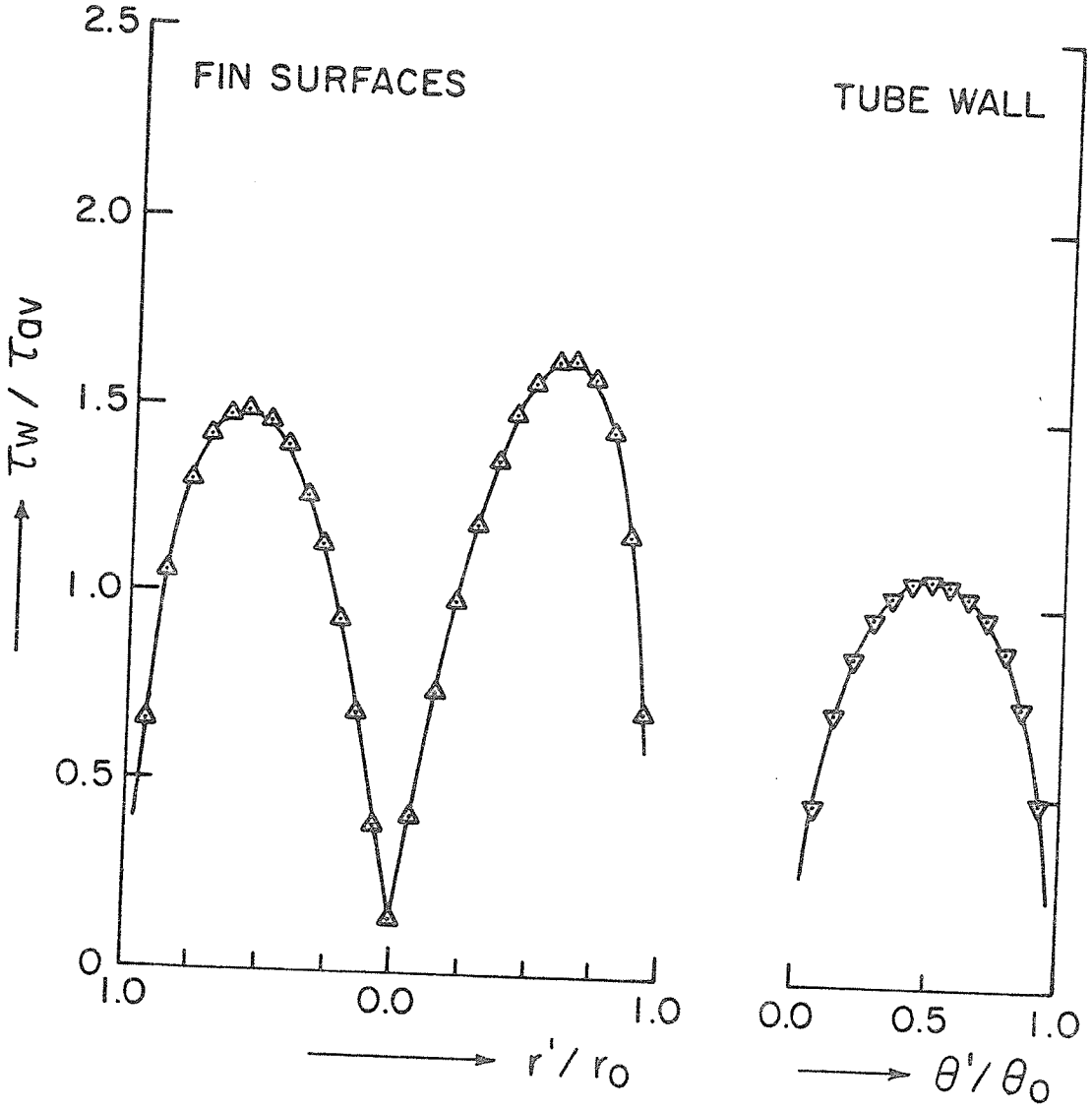

Figure 31: Distribution of Wall Shear Stress for M = 4, α = 0.4, and Re = 100

$\tau_{av} = 0.4246 \times 10^{-3}$ N/m^2

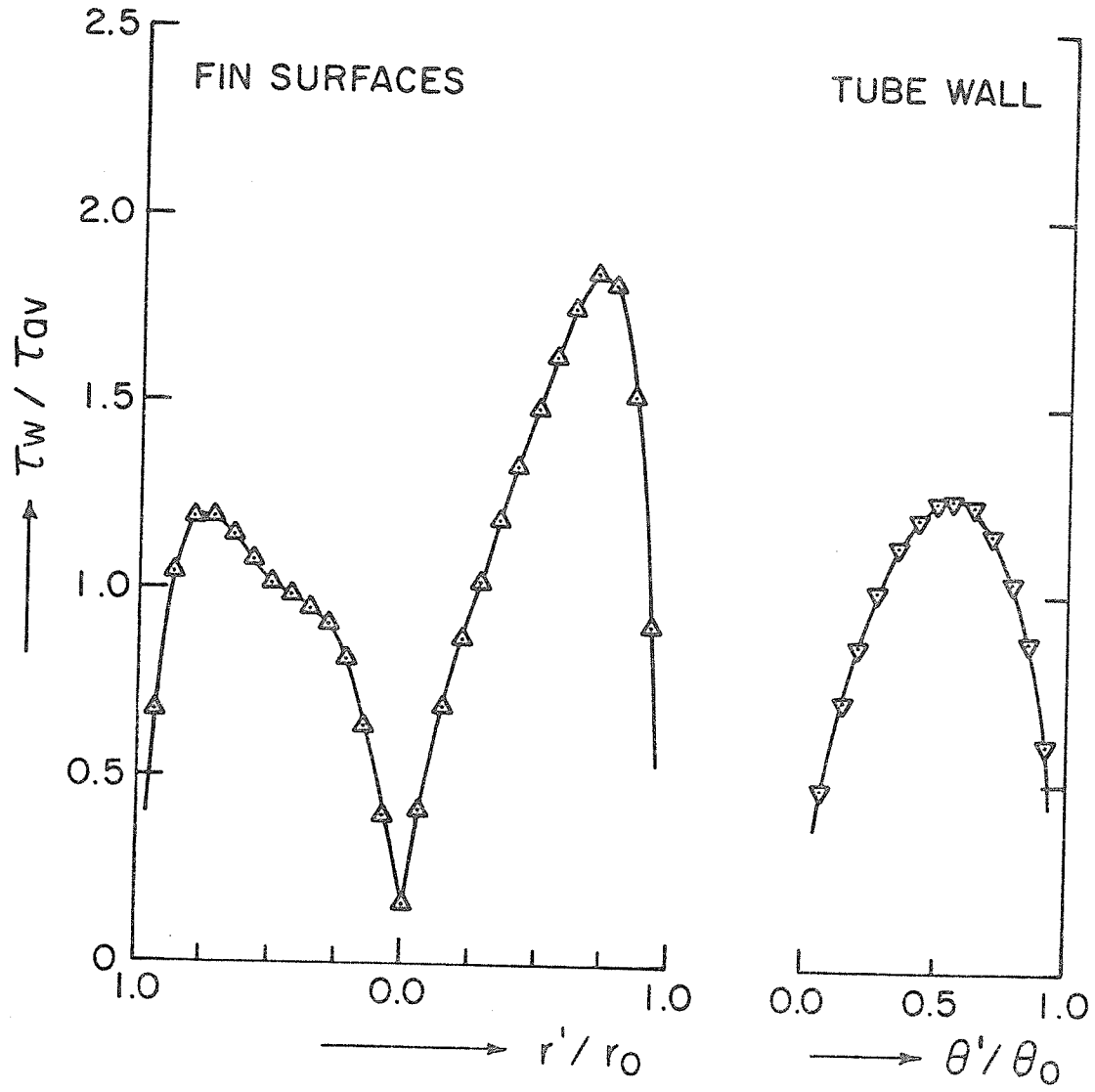

Figure 32: Distribution of Wall Shear Stress for M = 4, α = 0.4, and Re = 500

$\tau_{av} = 0.2610 \times 10^{-2}$ N/m^2

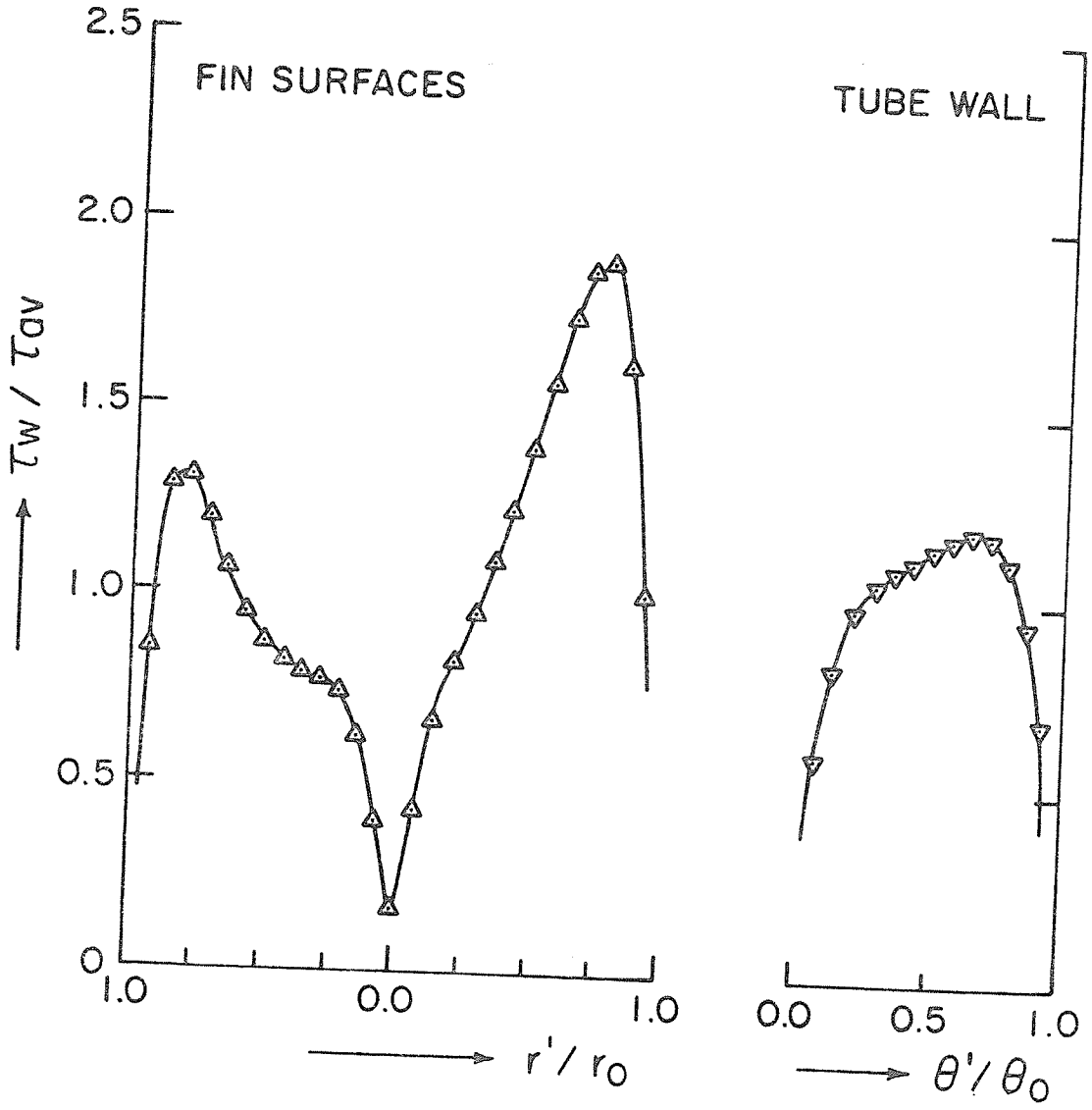

Figure 33: Distribution of Wall Shear Stress for M = 4, α = 0.4, and Re = 1000

$\tau_{av} = 0.6280 \times 10^{-2}$ N/m^2

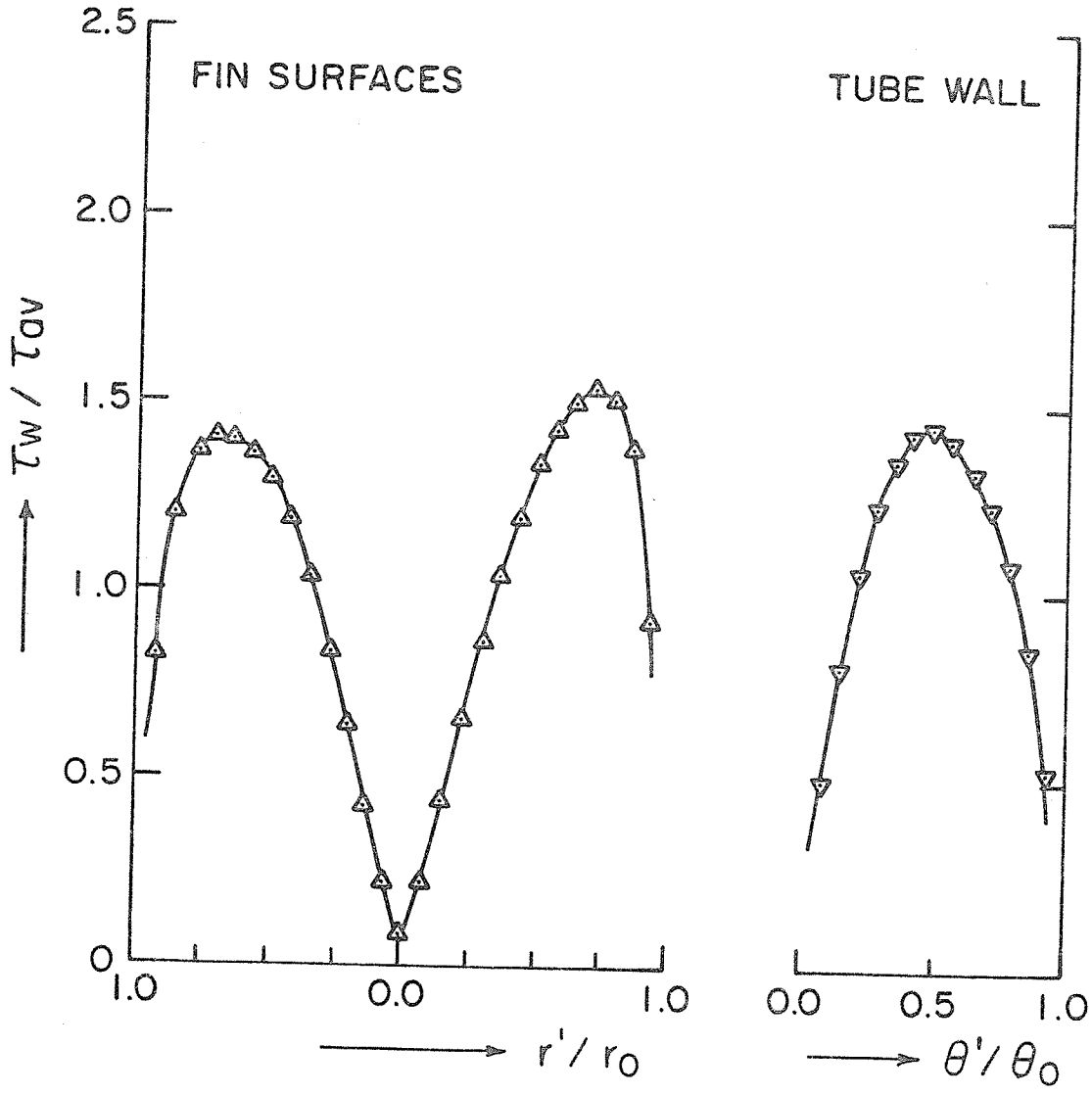

Figure 34: Distribution of Wall Shear Stress for M = 8, α = 0.1, and Re = 1000

$\tau_{av} = 0.6063 \times 10^{-2}$ N/m^2

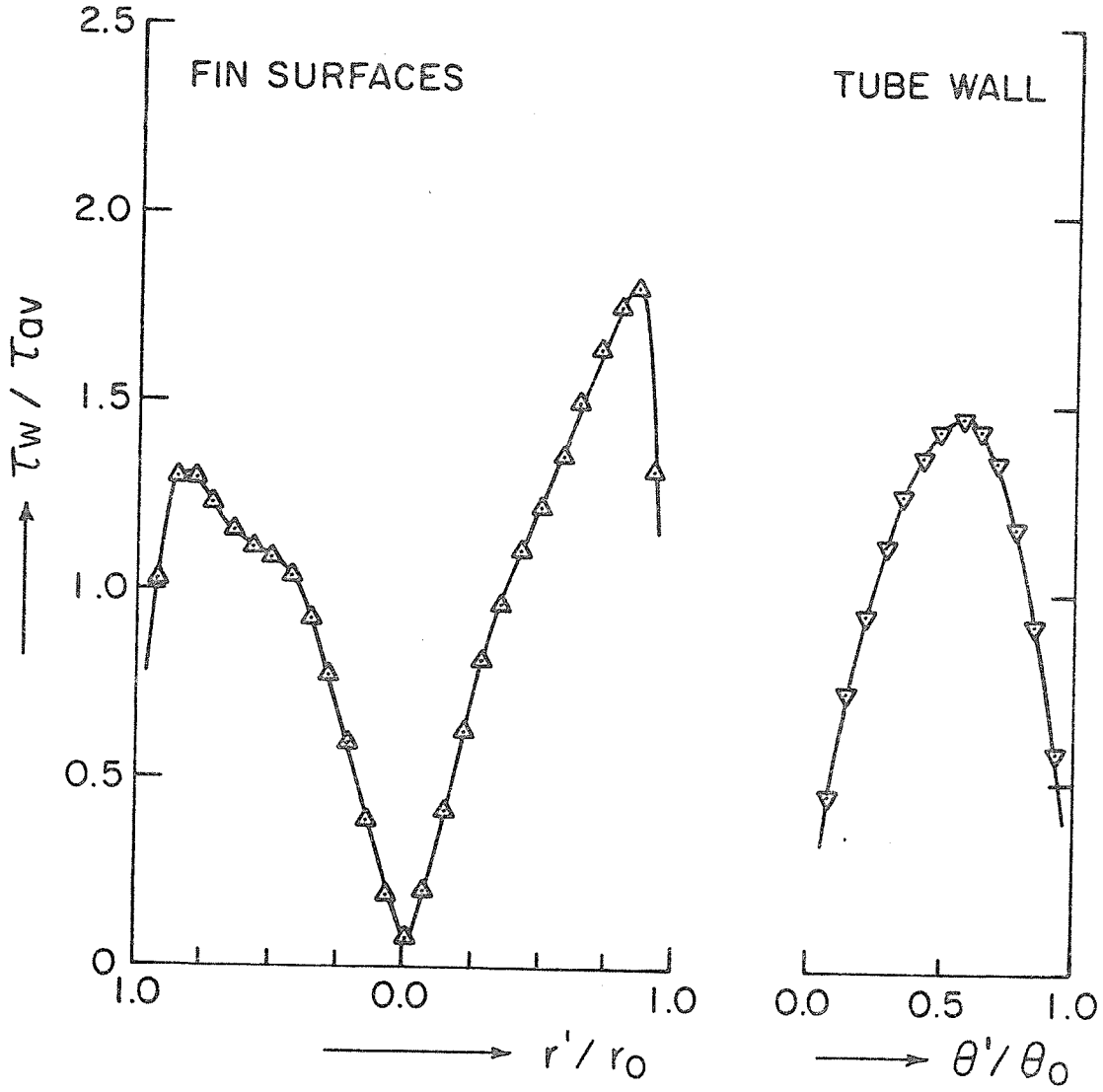

Figure 35: Distribution of Wall Shear Stress for M = 8, α = 0.3, Re = 1000

$\tau_{av} = 0.8531 \times 10^{-2}$ N/m^2

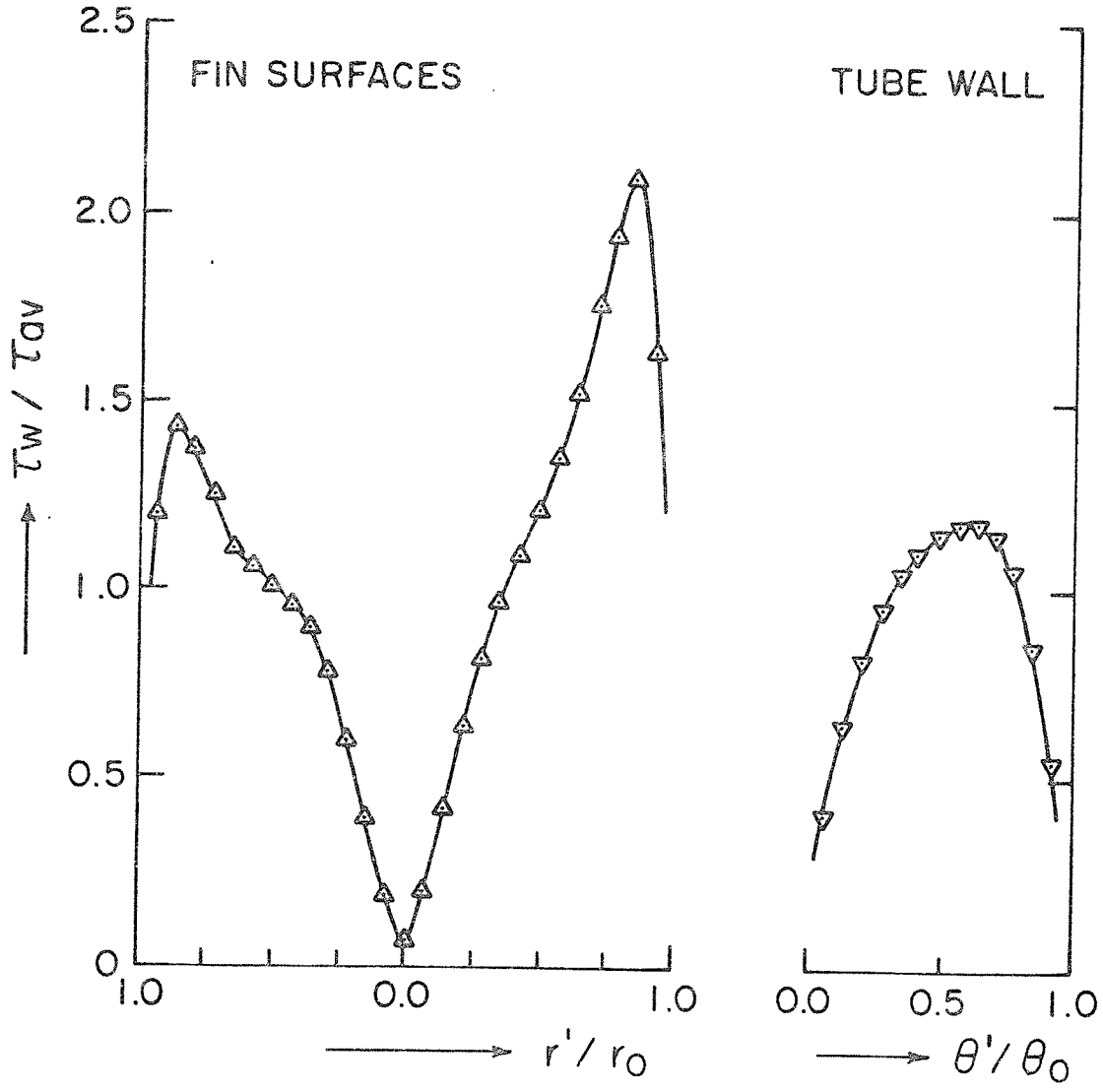

Figure 36: Distribution of Wall Shear Stress for M = 8, α = 0.5, and Re = 1000

$\tau_{av} = 0.1118 \times 10^{-1}$ N/m^2

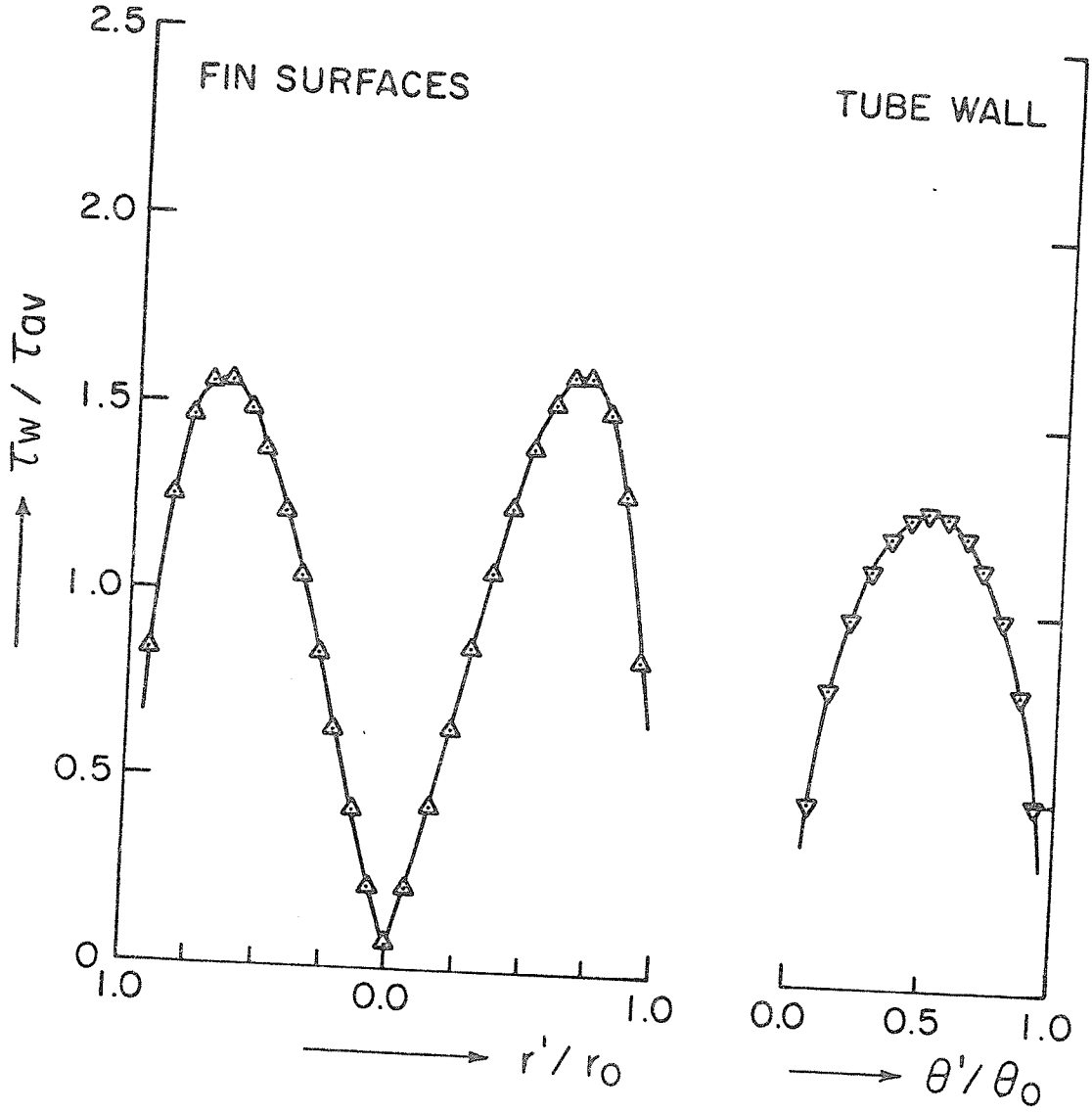

Figure 37: Distribution of Wall Shear Stress for M = 8, α = 0.1, and Re = 50

$\tau_{av} = 0.2899 \times 10^{-3}$ N/m^2

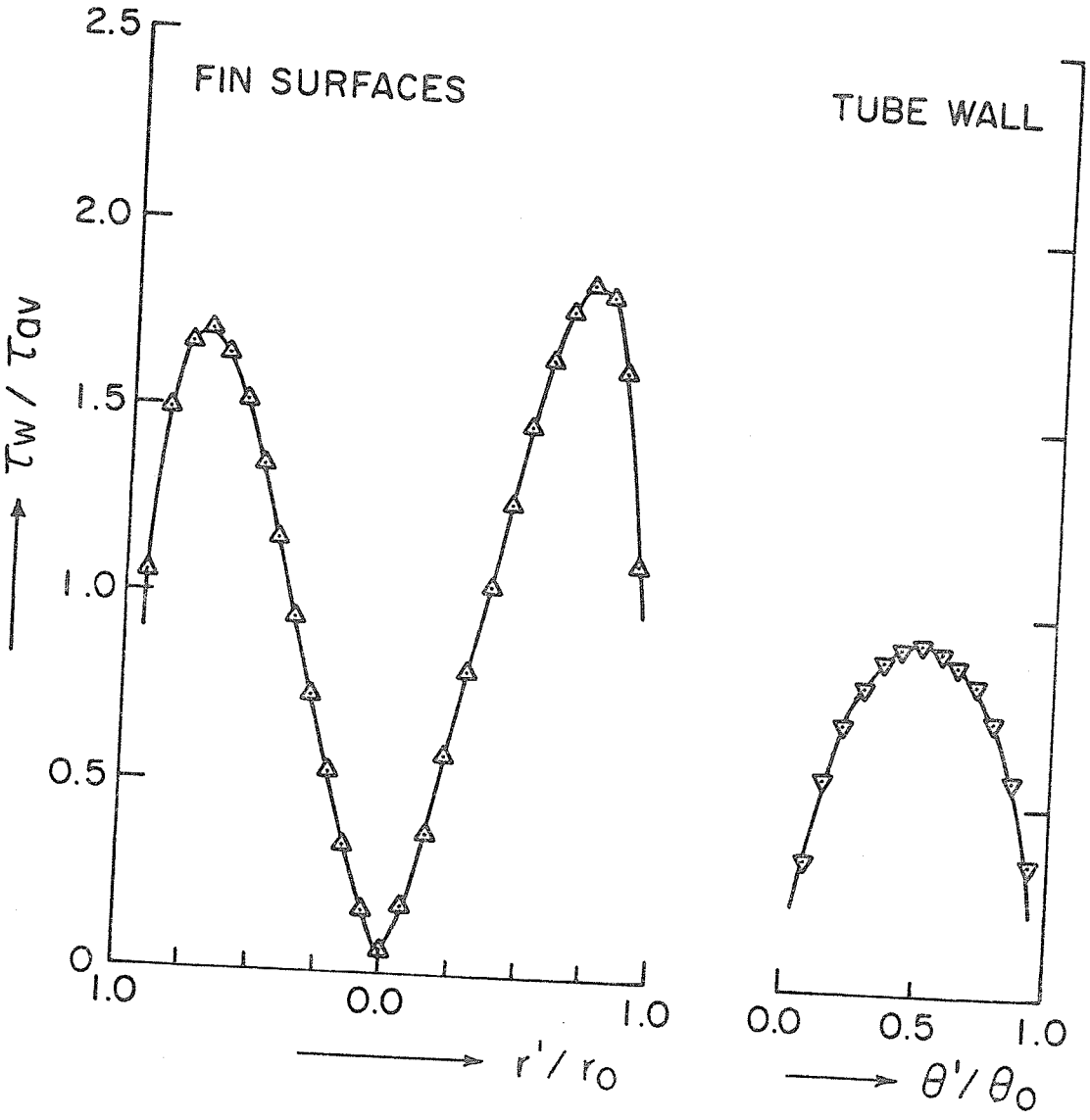

Figure 38: Distribution of Wall Shear Stress for M = 8, α = 0.5, and Re = 50

$\tau_{av} = 0.4294 \times 10^{-3}$ N/m^2

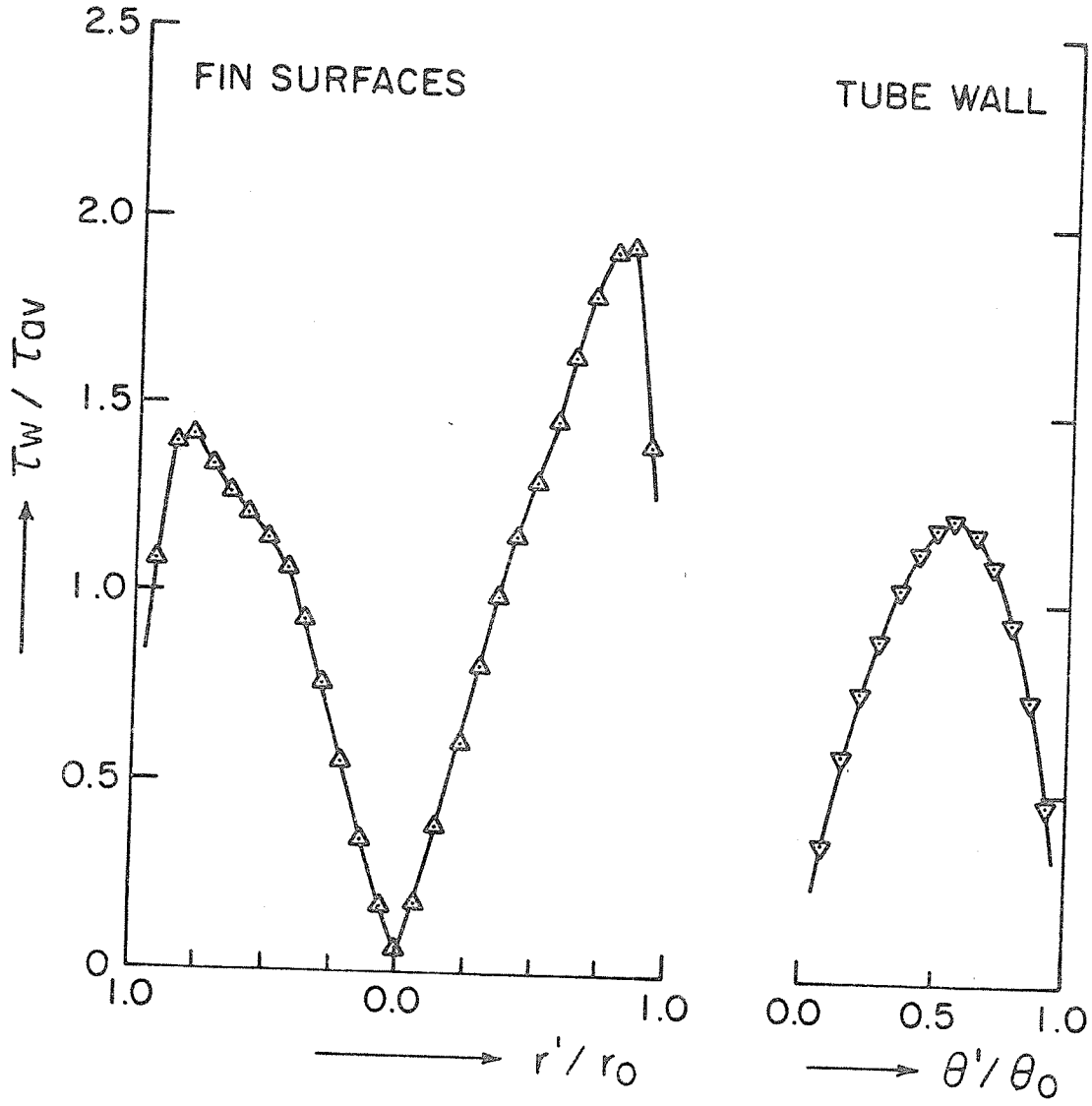

Figure 39: Distribution of Wall Shear Stress for M = 8, α = 0.5, and Re = 500

$\tau_{av} = 0.4881 \times 10^{-2}$ N/m^2

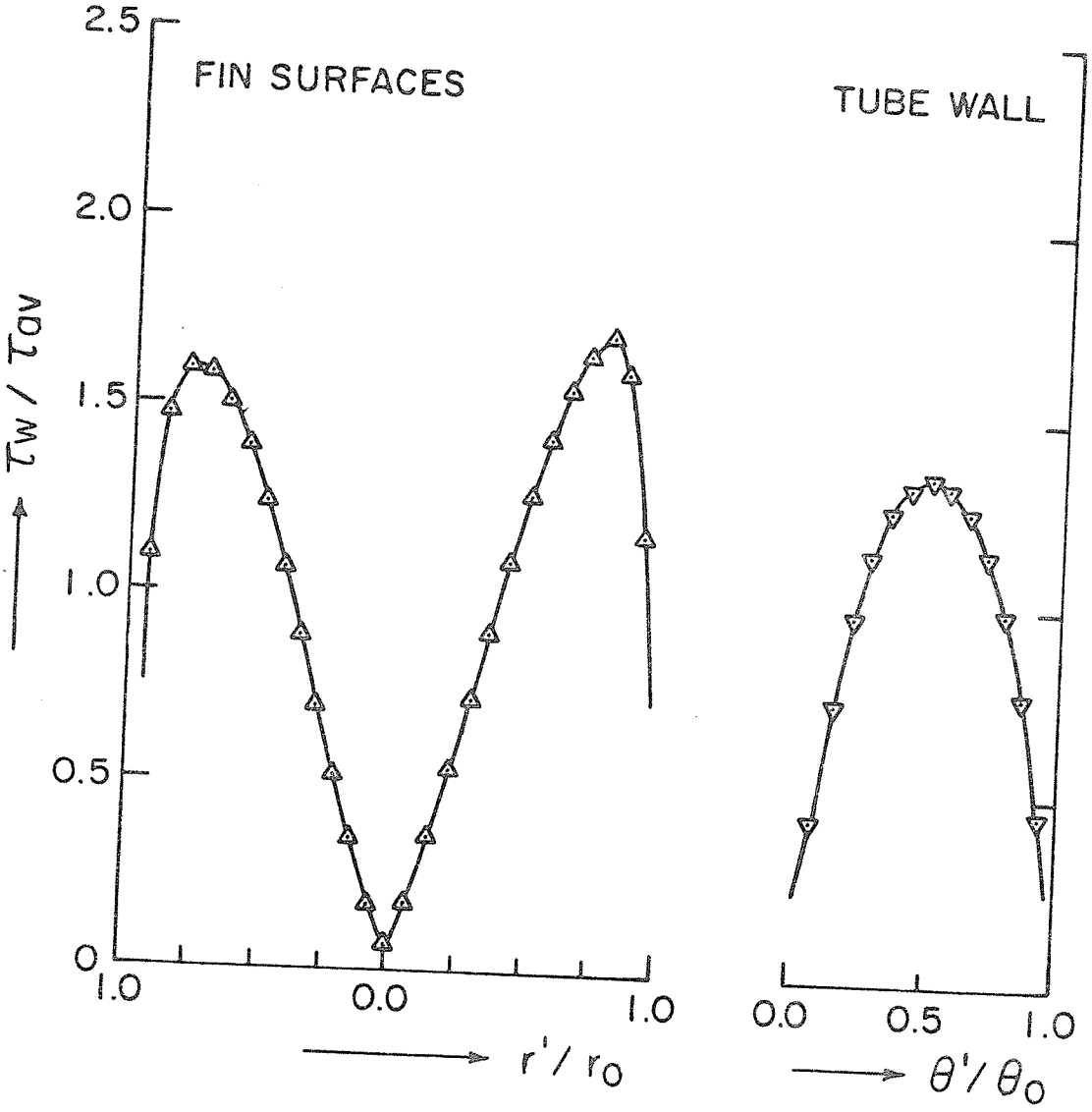

Figure 40: Distribution of Wall Shear Stress for M = 12, α = 0.1, and Re = 1000

$\tau_{av} = 0.9138 \times 10^{-2}$ N/m^2

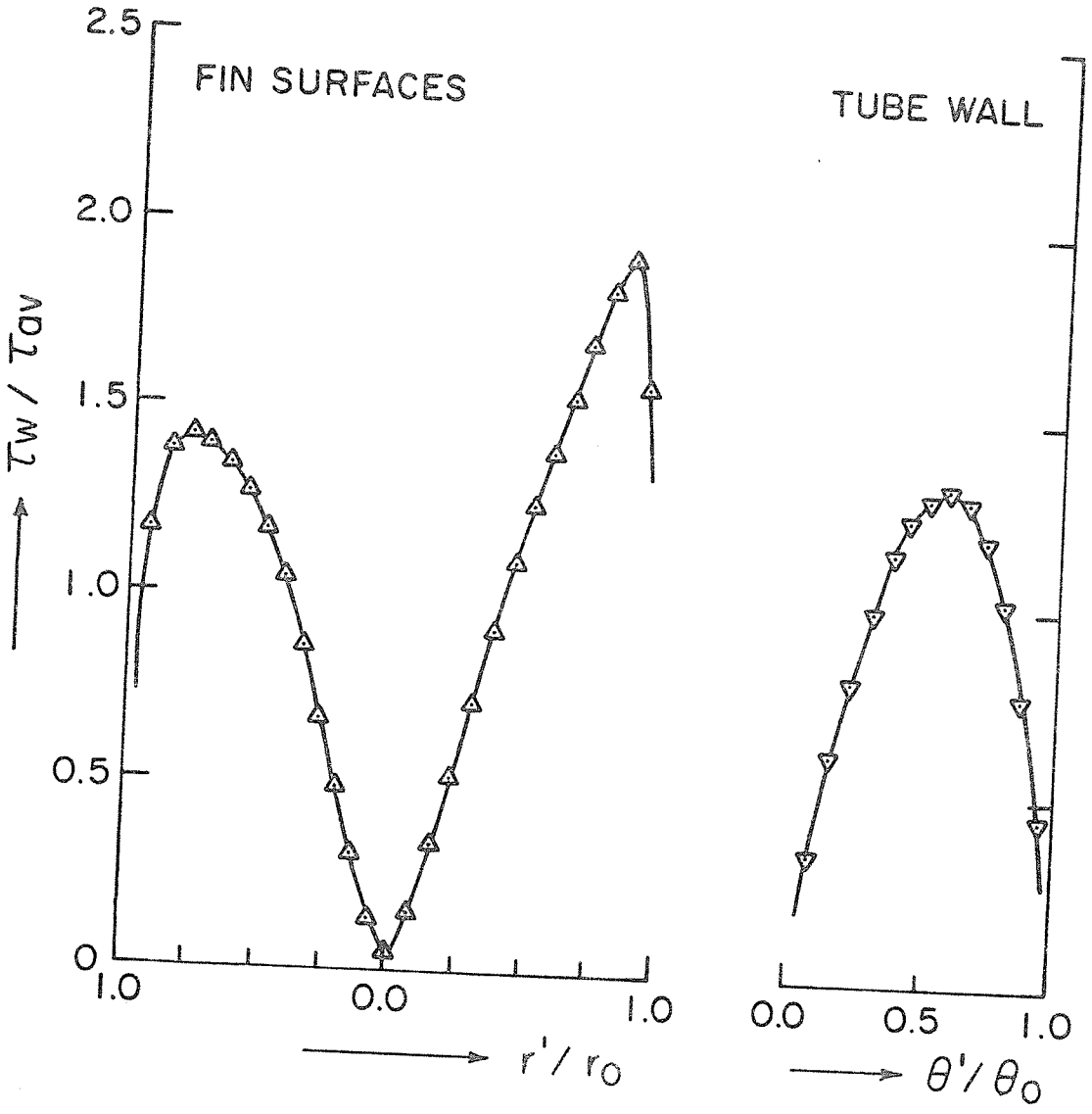

Figure 41: Distribution of Wall Shear Stress for M = 12, α = 0.3, and Re = 1000

$\tau_{av} = 0.1223 \times 10^{-1}$ N/m^2

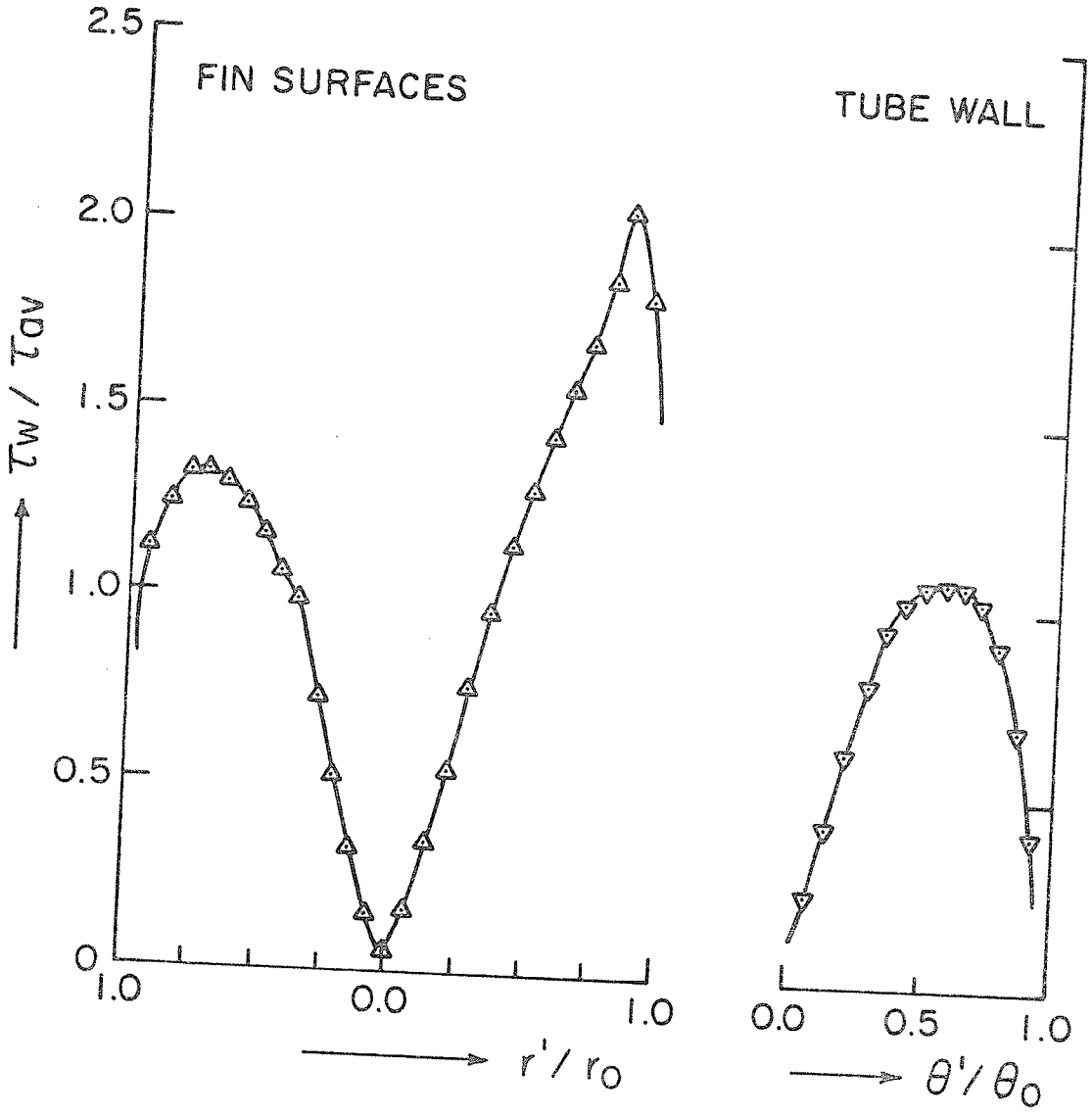

Figure 42: Distribution of Wall Shear Stress for M = 12, α = 0.5, and Re = 1000

$\tau_{av} = 0.1586 \times 10^{-1}$ N/m^2

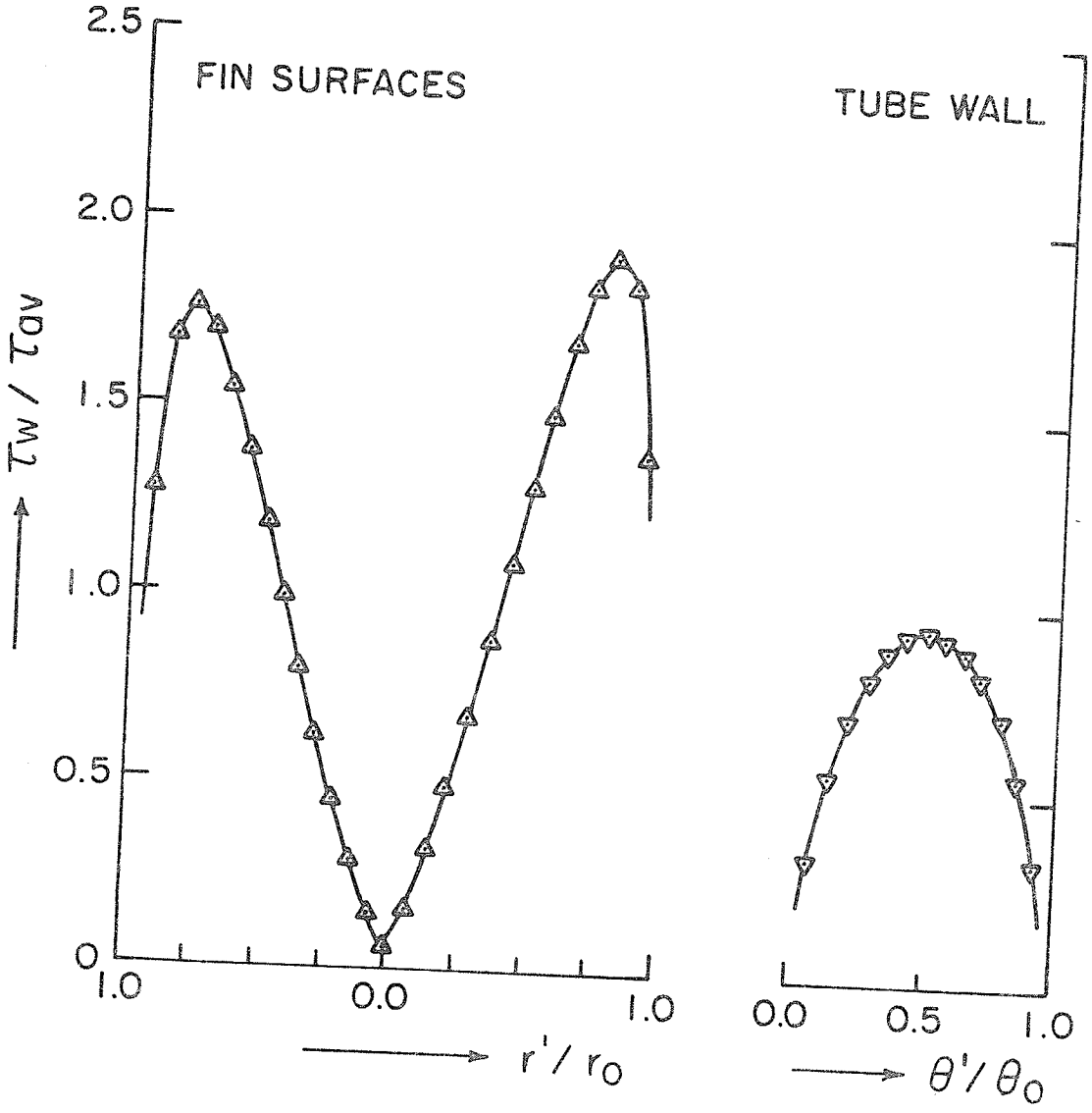

Figure 43: Distribution of Wall Shear Stress for M = 12, α = 0.4, and Re = 100

$\tau_{av} = 0.1270 \times 10^{-2}$ N/m^2

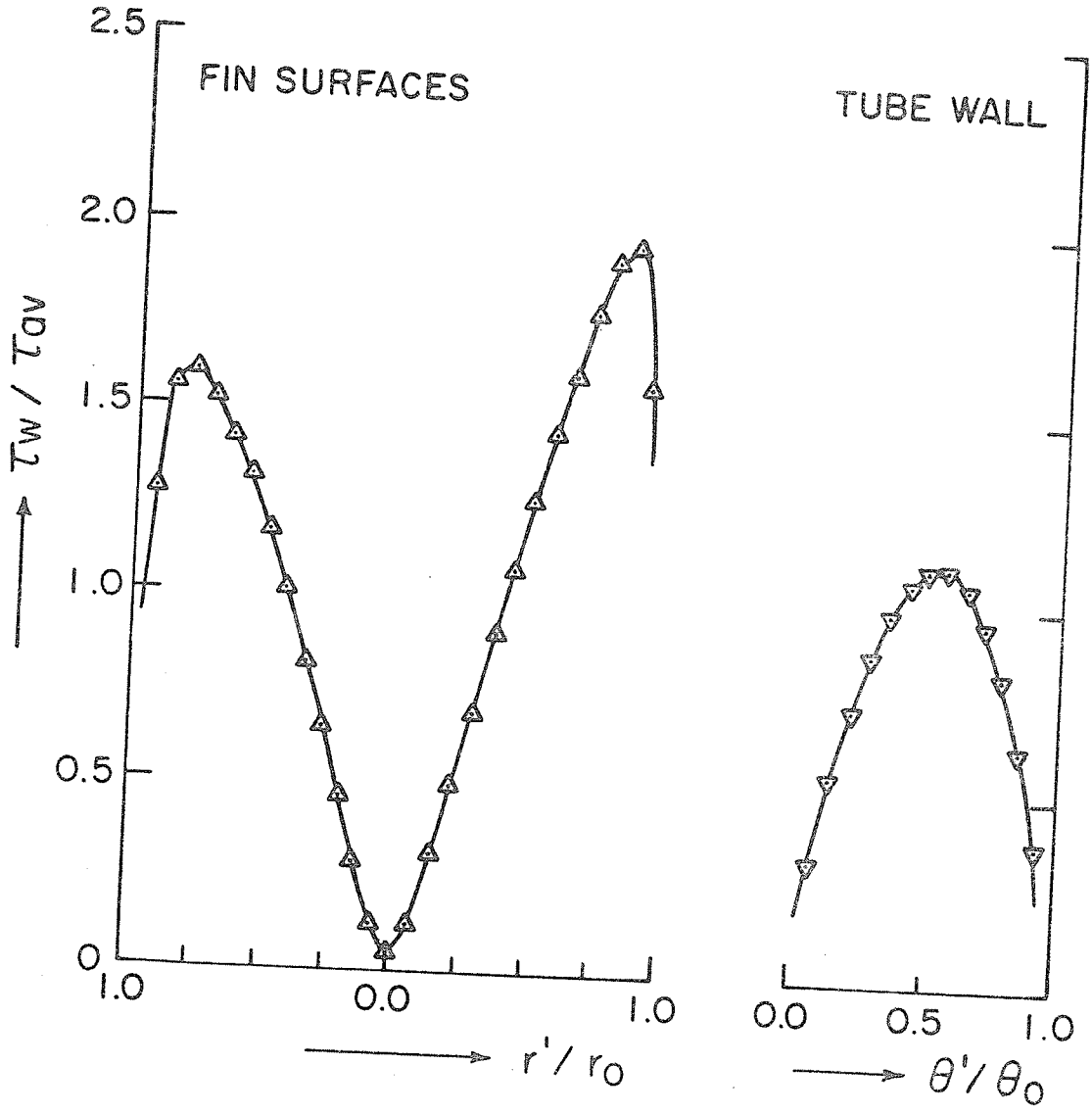

Figure 44: Distribution of Wall Shear Stress for M = 12, α = 0.4, and Re = 500

$\tau_{av} = 0.6555 \times 10^{-2}$ N/m^2

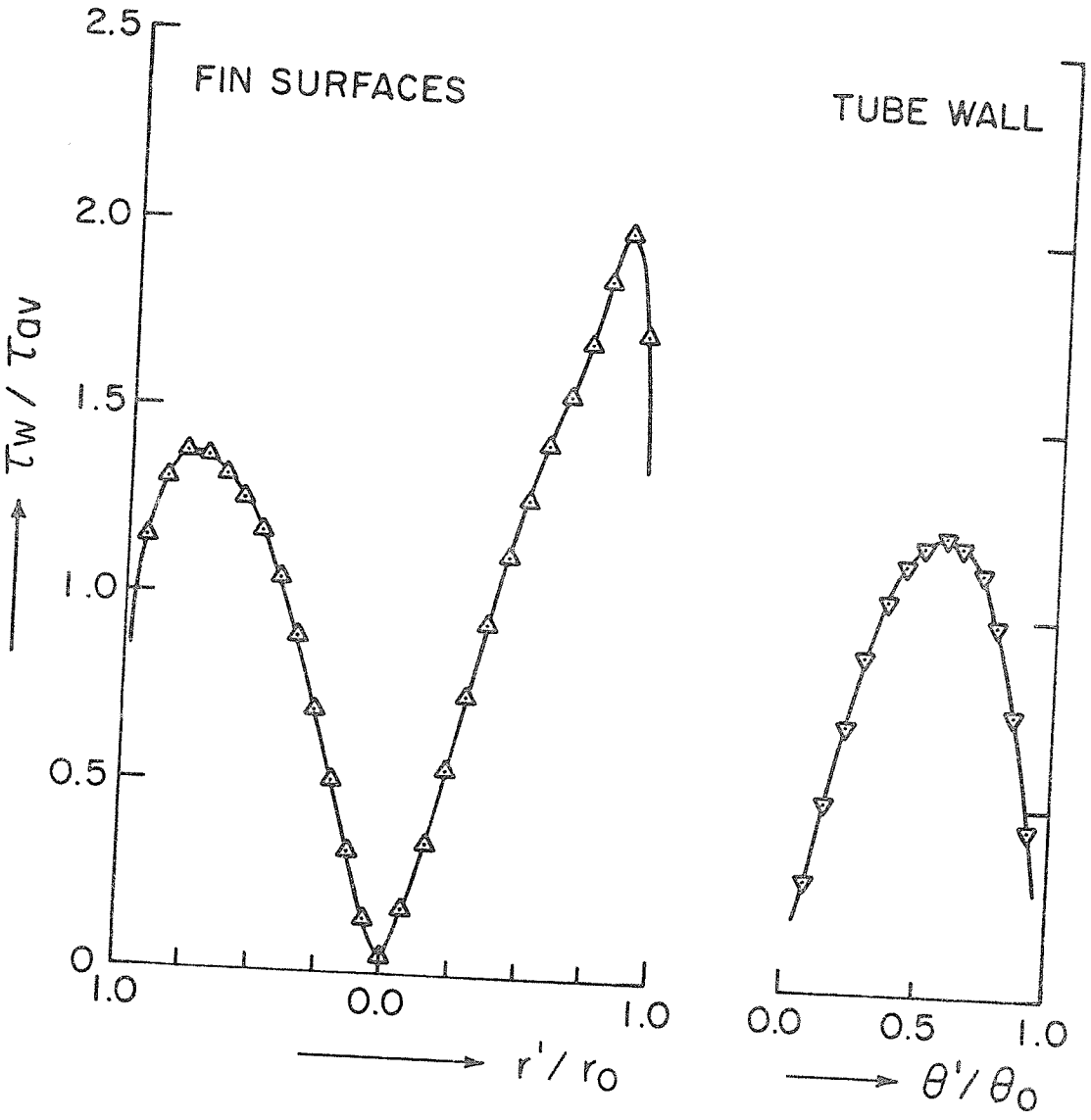

Figure 45: Distribution of Wall Shear Stress
For M = 12, α = 0.4, And Re = 1000
$\tau_{av} = 0.1398 \times 10^{-1}$ N/m^2

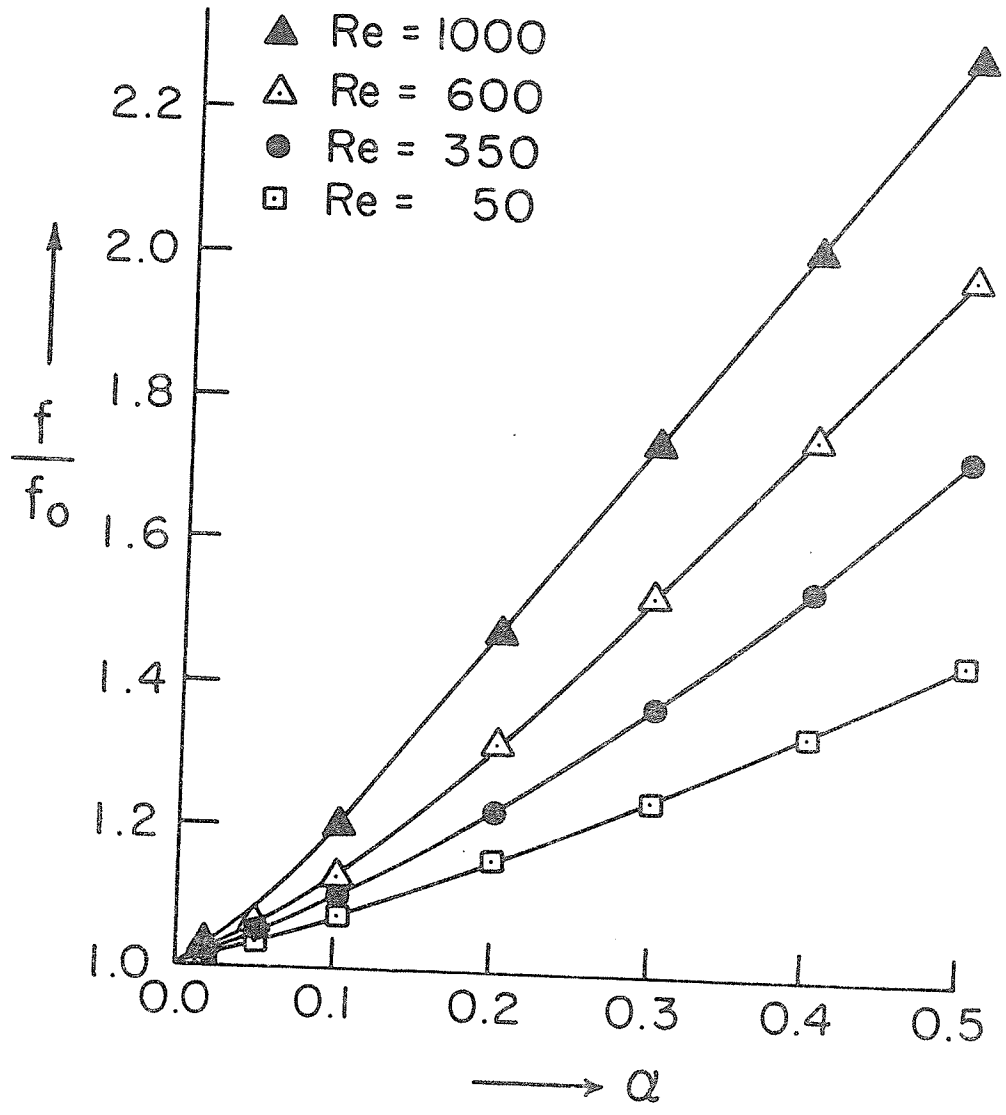

Figure 46: Effect of Twist Ratio On Friction Factor For M = 4

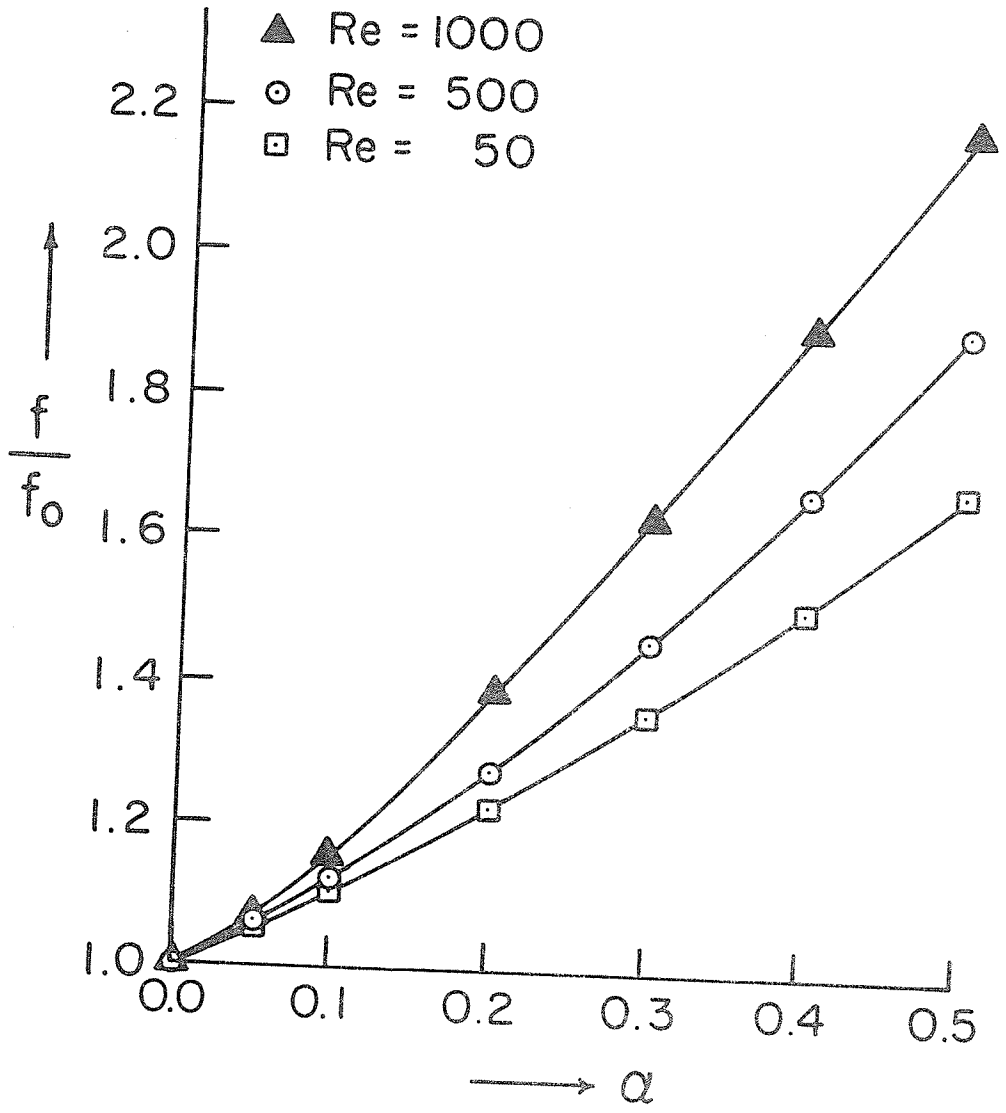

Figure 47: Effect of Twist Ratio on Friction Factor For M = 8.

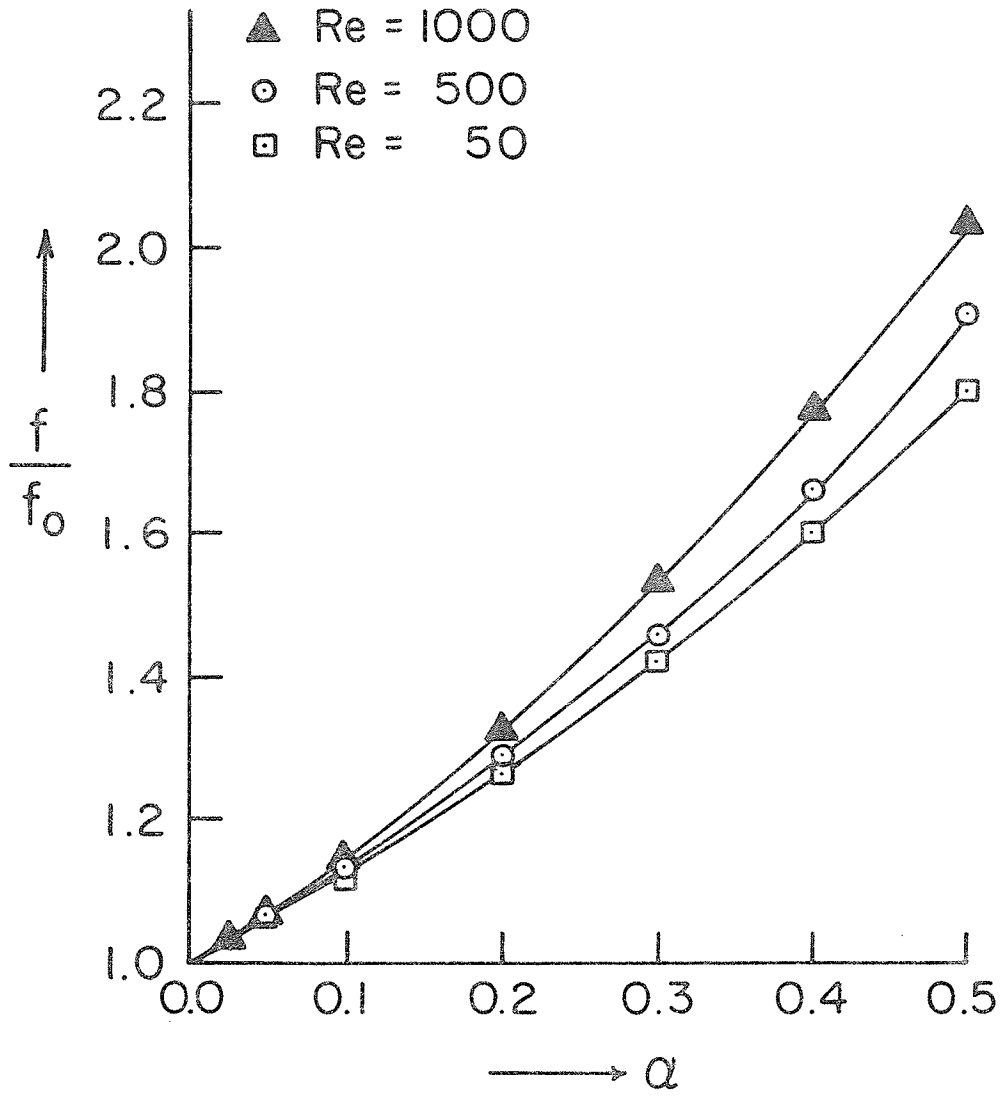

Figure 48: Effect of Twist Ratio On Friction Factor For M = 12

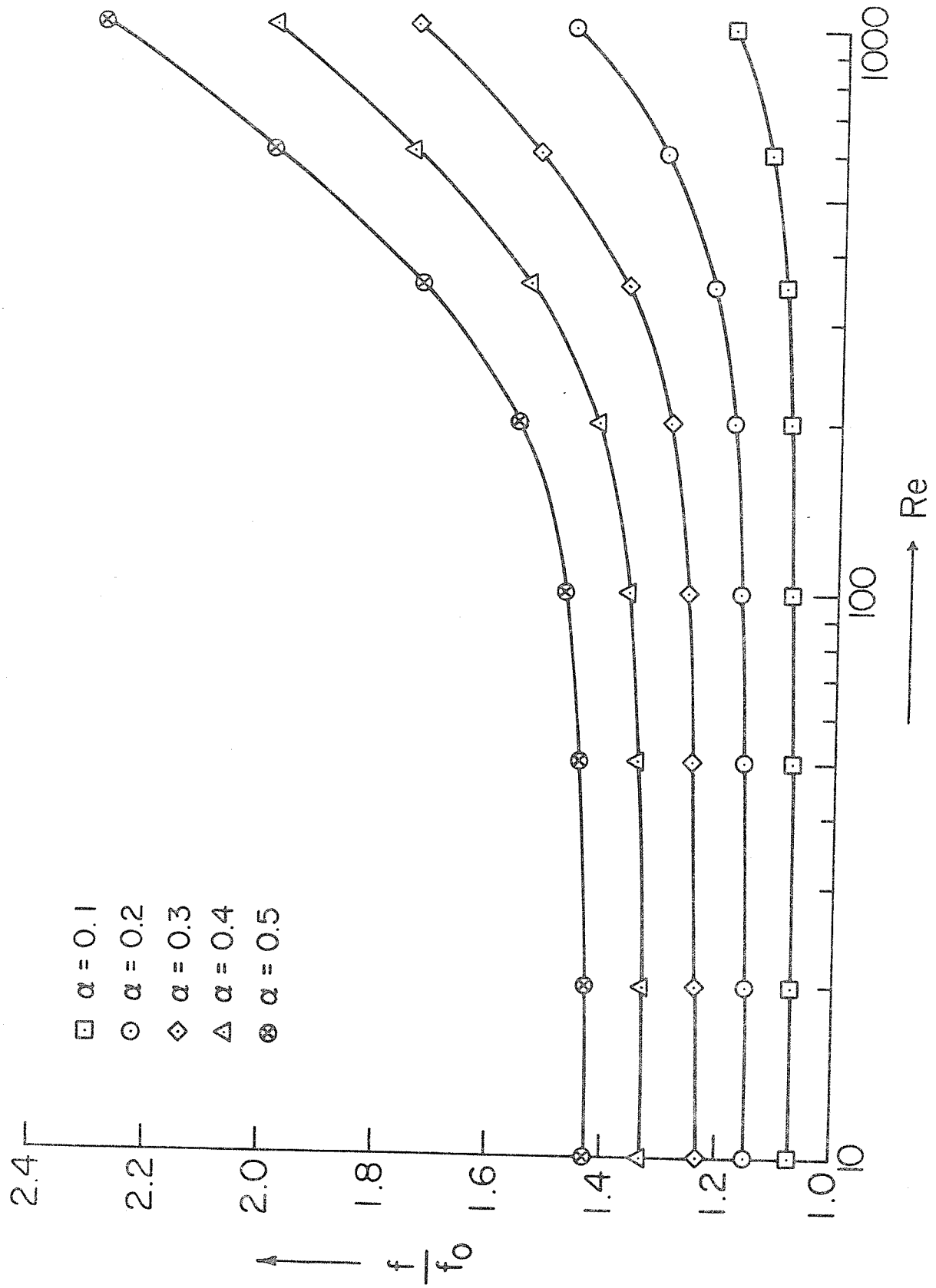

Figure 49: Effect of Reynolds Number On Friction Factor For M = 4.

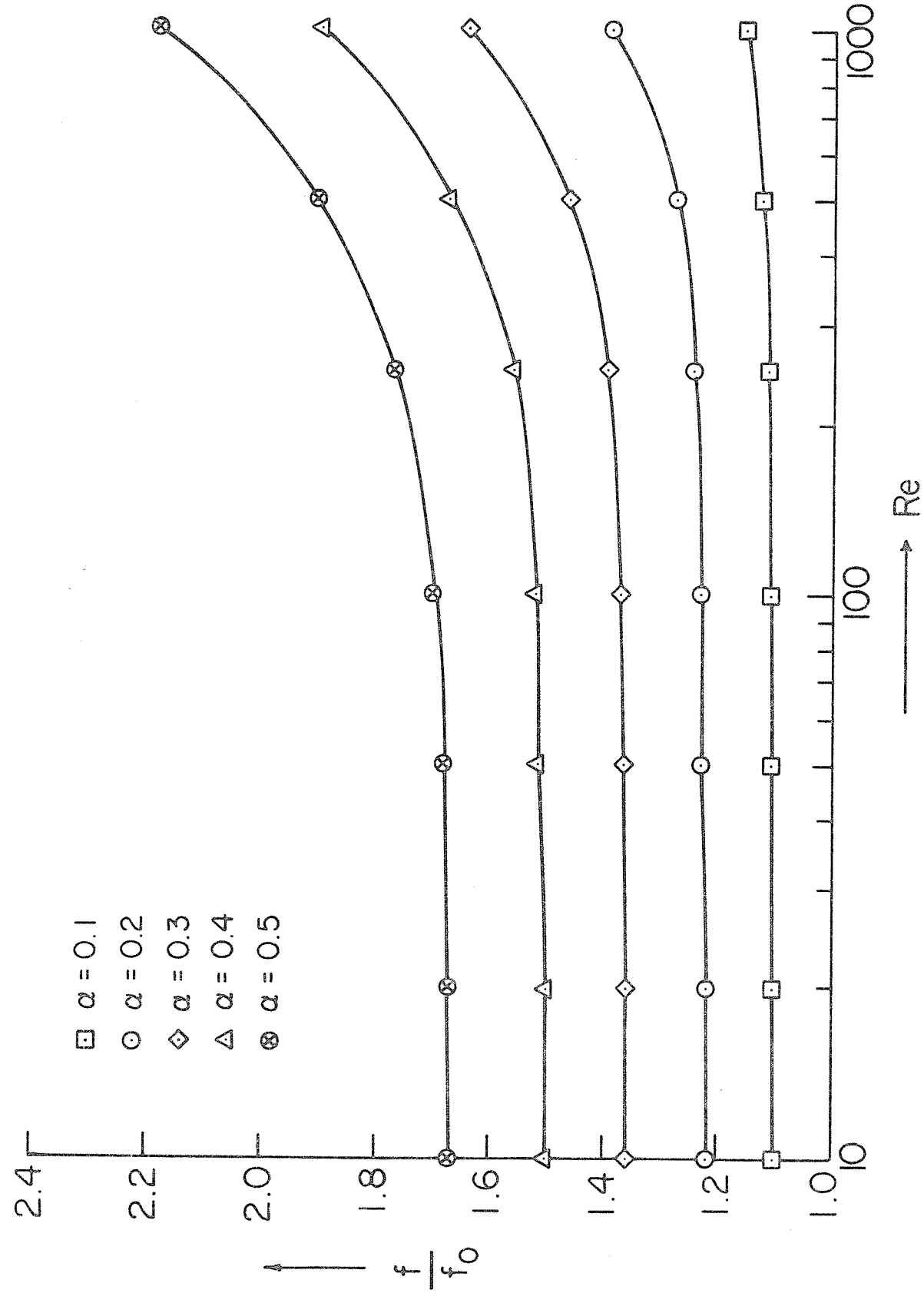

Figure 50: Effect of Reynolds Number On Friction Factor For M = 8.

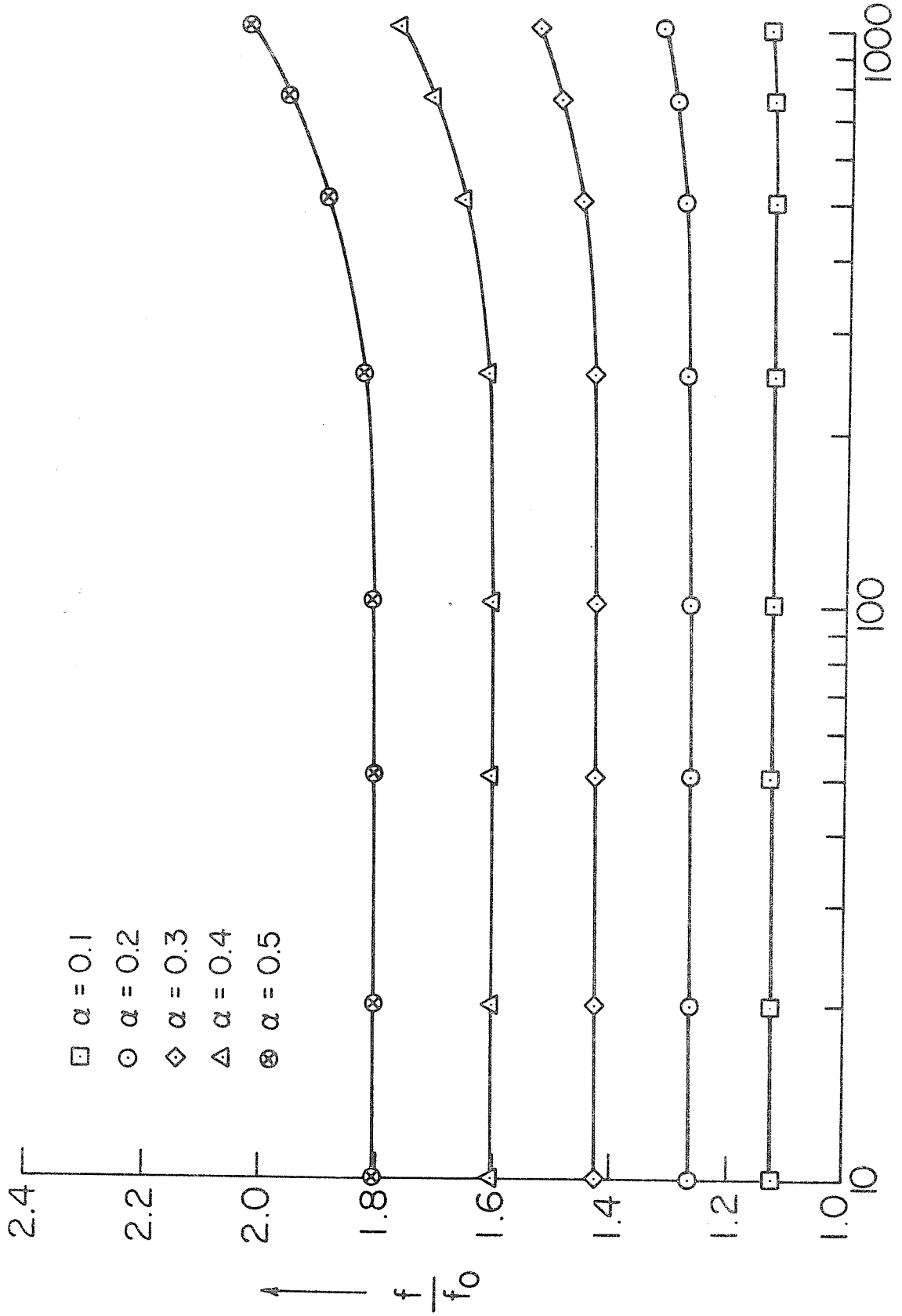

Figure 51: Effect Of Reynolds Number On Friction Factor For M = 12.